AD NUMBER

AD442305

NEW LIMITATION CHANGE

TO

Approved for public release, distribution unlimited

FROM

Distribution authorized to U.S. Gov't. agencies and their contractors; Administrative/Operational Use; JUL 1964. Other requests shall be referred to Arnold Engineering Development Center, Arnold AFB, TN 37389.

AUTHORITY

AEDC ltr dtd 20 Jul 1971

STORAGE HEATER DESIGN STUDY FOR THE HYPERSONIC TRUE TEMPERATURE TUNNEL

By

W. S. Hedrick, F. W. Larsen,
B. C. Lindahl, and D. G. DeCoursin

FluiDyne Engineering Corporation

AEDC-TDR-64-48

July 1964

Program Element 62410034/7778, Task 777805

Approved for public release; distribution unlimited.

(Prepared under Contract No. AF 40(600)-1039 by FluiDyne Engineering Corporation.)

ARNOLD ENGINEERING DEVELOPMENT CENTER

AIR FORCE SYSTEMS COMMAND

UNITED STATES AIR FORCE

NOTICES

Qualified requesters may obtain copies of this report from DDC, Cameron Station, Alexandria, Va. Orders will be expedited if placed through the librarian or other staff member designated to request and receive documents from DDC.

When Government drawings, specifications or other data are used for any purpose other than in connection with a definitely related Government procurement operation, the United States Government thereby incurs no responsibility nor any obligation whatsoever; and the fact that the Government may have formulated, furnished, or in any way supplied the said drawings, specifications, or other data, is not to be regarded by implication or otherwise as in any manner licensing the holder or any other person or corporation, or conveying any rights or permission to manufacture, use, or sell any patented invention that may in any way be related thereto.

STORAGE HEATER DESIGN STUDY FOR THE HYPERSONIC TRUE TEMPERATURE TUNNEL

By

W. S. Hedrick, F. W. Larsen,
B. C. Lindahl, and D. G. DeCoursin

FluiDyne Engineering Corporation

(The reproducibles used in the reproduction of this report were supplied by the authors.)

July 1964

AF - AEDC
Arnold AFS Tenn

References to named commercial products in this report are not to be considered in any sense as an endorsement of the product by the United States Air Force or the Government.

ABSTRACT

The results of a design study of a ceramic storage heater system for the Tripltee wind tunnel are presented. The heater is designed to supply 1500 lb/sec of air at 2000 psi and 3900°R for a period of 30 sec. Emphasis was placed on the application of improved refractory materials and shapes for the heat storage matrix to achieve a large reduction in total heater size and dust carry-over. Heating of the storage matrix with combustion products and the flow processes involved in pressurizing the heater were analyzed.

A heater design concept is presented and the advantages accruing from use of matrix elements specifically designed for this application are indicated. Procedures for procuring refractory elements having the requisite properties are outlined.

A second Tripltee design requirement is for 5000 lb./sec of air at 400 psi and 1600°R for 30 sec. The problem of achieving this flow condition by mixing hot air from the heater with cold air was studied and a design concept for a mixer developed.

PUBLICATION REVIEW

This report has been reviewed and publication is approved.

Donald J. Harney
Major, USAF
Chief, Special Projects Office
DCS/Civil Engineering

Donald R. Eastman, Jr.
DCS/Research

TABLE OF CONTENTS

LIST OF FIGURES

NOTATION

A	= area
A	= $\dot{m}_{noz}/\dot{m}_h$ -- Appendix F
A	= $a\ (2/\Delta R + 1/2)$ -- Appendix G
A^*	= nozzle throat area
A_f	= matrix face area
A_{fl}	= matrix flow area
B	= $1/\ell n\ (1 + \Delta R)$ -- Appendix G
C	= specific heat, solid
C_1	= $\left[\frac{(dp/dz)_h}{(dp/dz)_d}\right]^{1/2}$
D	= hole diameter
D_1, D_2, etc.,	= heater insulation diameters -- Appendix D
D_b	= bed diameter
D_h	= hydraulic diameter
D_t	= total duct diameter
E	= Young's modulus
E	= $hP\Delta\theta/2MC$ -- Appendix G
E_{lost}	= energy wasted through nozzle
F	= $hP\Delta z/2\dot{m}c_p$ -- Appendix G
F_{21}	= $\frac{\ell n\ (D_2/D_1)}{1-(D_1/D_2)}$ -- Appendix D
Gr	= $g\Delta T x^3 \rho_g/T\mu$ Grashof Number (perfect gas)
H	= hr_o/k = Biot Number
K_{cr}	= effective crack length coefficient
L	= ℓ/r_o = dimensionless length
M	= $\rho A_f \sigma$ = mass per unit length, matrix
Nu	= hD/k_g = Nusselt Number
P	= A_{ht}/ℓ = wetted perimeter
Pr	= $c_p\mu/k_g$ = Prandtl Number
Q	= heat flow per unit time
R	= r/r_o = dimensionless radius

R_g = gas constant

Re = $\rho_g u D/\mu$ = diameter Reynolds number

S = stress

S_r, S_t, S_z = stresses--radial, tangential, longitudinal

St = $h/c_p \rho_g u$ = Stanton Number

$\bar{T}$ = $(T - T_c)/(T_i - T_c)$ = dimensionless temperature

T = temperature

$\bar{T}$ = $V/\int_V \frac{1}{T} dV$ = effective temperature -- Appendix F

$\bar{T}_b$ = effective temperature in volume V_b

$\bar{T}_z$ = effective temperature in volume V_z

$\dot{T}$ = $\partial T/\partial \tau$ = temperature change per unit of dimensionless time -- Appendix H

T_{ex} = vessel exterior temperature

T_m = $(1/A)\int_A T dA$ = mean solid temperature -- Appendix H

T_{mix} = mixed mean temperature -- Appendix E

U = overall heat conductance coefficient

V = volume,

V = void volume -- Appendix F

V_b = void volume in bed and adjacent insulation

V_{bed} = total bed volume

V_z = void volume in bed and adjacent insulation between top and z location -- Appendix F

$\bar{z}$ = $\pi k z/\dot{m} c_p$ = dimensionless length

Z = z/r_o = dimensionless length -- Appendix G

a = $\Delta R^2/2\Delta\tau$ Appendix G

b = $\pi D_b u/\dot{m} c_p$

c_p = specific heat at constant pressure, gas

c_v = specific heat at constant volume, gas

e = 2.71828

f = friction factor

g = 32.2 ft/sec^2

h = heat transfer coefficient

h = $h_{conv} + h_{rad}$, = total heat transfer coefficient -- Appendix D

h_o = heat transfer coefficient without injection -- Appendix E

k = thermal conductivity, solid

k_g = thermal conductivity, fluid

ℓ = heater matrix length

m = mass of fluid, gas -- Appendix F

m = time increment number -- Appendix G

m_{lost} = mass of fluid wasted through nozzle

m^* = $\dfrac{\sqrt{\gamma g/R_g}}{\{(\gamma+1)/2\}^{\gamma/(\gamma-1)-1/2}}$ = choked flow parameter -- Appendix F

$\dot{m}$ = mass flow rate

$\dot{m}_{hole}$ = mass flow in one hole -- Appendix H

$\dot{m}_{in}$ = mass flow in -- Appendix F

$\dot{m}_{out}$ = mass flow out -- Appendix F

n = radius increment number -- Appendix G

p = pressure

p = length increment number -- Appendix G

q = heat flux

q = $\rho u^2/2g$ = dynamic pressure -- Appendices D & F

q_{loss} = insulation conduction heat flux

r = radius

r_o = $D/2$ = hole radius

s = hole spacing (center-to-center)

t = thickness

u = velocity

x = length variable

z = distance along heater matrix, measured from bottom

z = distance along heater matrix, measured from top -- Section 6 and Appendix F

α = $k/C\rho$ = thermal diffusivity

α = $(\rho u c_p)_{inj}/h_o$ -- Appendix E

α = $V_{cv}\,\bar{T}_b/V_b\,\bar{T}_{cv}$ -- Appendix F

α_{ex} = linear coefficient of thermal expansion

γ = c_p/c_v = ratio of specific heats or effective value

ϵ = strain (in/in) -- Appendix C

ϵ = thermal emissivity -- Appendix D

ϵ_t = eddy thermal diffusivity -- Appendix E

ζ = dummy variable -- Section 6

ζ = $\epsilon_t x / u r_j^2$ -- Appendix E

η = $hP\theta/CM$ = dimensionless time

η = r/r_j -- Appendix E

η_o = initial dimensionless time for non-constant initial T approximation -- Appendix B

$\dot{\eta}$ = final dimensionless time for non-constant initial T approximation -- Appendix B

η_f = dimensionless run time $(\dot{\eta} - \eta_o)$

θ = time

μ = viscosity

ν = Poisson's ratio

ξ = $hPz/c_p \dot{m}$ = dimensionless length

ξ_o = effective upstream dimensionless length for non-constant initial T approximation -- Appendix B

$\dot{\xi}$ = effective downstream dimensionless length for non-constant initial T approximation -- Appendix B

ξ_ℓ = dimensionless bed length $(\dot{\xi} - \xi_o)$

ρ = density, solid

ρ = density, fluid -- Appendices E and F

ρ_{bulk} = bulk density of matrix

σ = $1/R_a^2$ = matrix porosity

σ = material porosity -- Appendix C

σ = $.173 \times 10^{-8}$ BTU/(hr ft^2 $^oR^4$) = Stephan - Boltzman constant -- Appendix D

τ = $\theta\alpha/r_o^2$ = Fourier Number, dimensionless time

ϕ = $(T - T_{mix})/(T_h - T_{mix})$ -- Appendix E

SUBSCRIPTS

a	outside boundary of tube, (adiabatic)
amb	ambient
c	entering air, bottom, (cold)
$\mathbb{C}$	center line
conv	convective -- Appendix D
cr	crack
cv	control volume
d	steady state, (design)
ex	exterior, expansion
f	final
g	fluid, (gas)
h	top of bed, (hot)
ht	heat transfer surface
i	initial
inj	secondary flow injection
ins	insulation
j	jet boundary
ℓ	at $z = \ell$
max	maximum
noz	nozzle
o	hole surface
rad	radiative -- Appendix D
shell	pressure vessel wall
t	total
z	at z

INTRODUCTION

This study was undertaken to establish design criteria for an intermittent, thermal energy storage type of air heater. This heater is an element in the air supply system of the Hypersonic True Temperature Tunnel, hereinafter referred to as Tripltee, (or TTT).

The performance specification which is basic to this study is appended as Appendix A. It can be summarized briefly as follows:

	Mach 7	Mach 4
Design flow	1500 lb/sec.	5000 lb/sec.
Design pressure	2000 psia	400 psia
Design temperature	3900° R	1600° R

In addition, emphasis was placed on three operational characteristics:

Minimum dust formation
Wide range of operating temperatures
Minimum loss of stored air while bringing heater on line.

Since the heater would necessarily be very large and costly, it was evident that another requirement would be lowest cost consistent with the required performance and operational characteristics. The cost of such a heater is largely in the refractories, secondly in the pressure vessel and only affected (in capacities such as this) moderately by auxiliary equipment. In general, the size and cost are related, so that a smaller volume of the heater system would tend to reduce cost. Not only would there be this trend, but reductions in volume would tend to reduce the number of individual vessels. This would reduce the cost of interconnecting ductwork, isolation valves, etc. Another benefit would accrue if the number of vessels could be reduced. Experience has shown that the (refractory lined) connecting ductwork from heater to wind tunnel is a primary source of dust and that a considerable temperature drop is virtually unavoidable with such ductwork. Reduction in the number of heaters should reduce the length of duct from any heater to the nozzle. Thus, a derivative requirement placed on the study was that the heater have as small a volume as possible and that as few vessels as possible be used.

The first operational characteristic might have been stated as minimum dust carry-over. To establish whether the criterion should be minimum dust carry-over or minimum dust formation, a calculation was made of minimum dust

particle size to avoid carry-over as a function of mass flow per unit area of the matrix cross-section. The results appear in Fig. 1. It is apparent that for the range of material densities of interest, the minimum size particle to avoid carry-over will be quite large unless the mass flow per unit area is vanishingly small. Even at a mass flow per unit area of 1 pound per second per square foot (corresponding to about twenty, 12 ft O.D. vessels) all particles smaller than 3 to 4 thousandths inch will be carried over. Since our experience indicates that many particles smaller than this are generated in a conventional, pebble bed heater, it is apparent that the criterion must be minimum dust formation.

The specification of Appendix A requires that the heater system study be based primarily on "state of the art" development of storage heater systems. It was assumed that the requirement permitted complete flexibility of approach so long as the basic concept of storage of thermal energy by heating a matrix of storage/heat transfer material was adhered to. However, it was assumed that insofar as materials and processes were concerned, "state of the art" meant already demonstrated performance, precluding any consideration of fundamental development.

The outline of the study then resolved into:

A. Analytic study of the storage heater to determine influence of several geometric and material-property-dependent parameters on the heater volume required to achieve the specified performance,

B. Survey of refractory manufacturers to establish feasible geometries and material properties for matrix elements,

C. Survey of manufacturers of large, high pressure vessels to establish economic implications of, and fabrication limitations on vessel size,

D. Study of the insulation requirements as determined by vessel temperature and reheat considerations,

E. Study of a mixer to achieve Mach 4 design conditions without compromising heater design for Mach 7 operation,

F. Study of pressurization of heater to determine allowable operating pressure drop,

G. Synthesis of preliminary designs based on A through F, and

H. Determination of work remaining before finalization of heater specification and design.

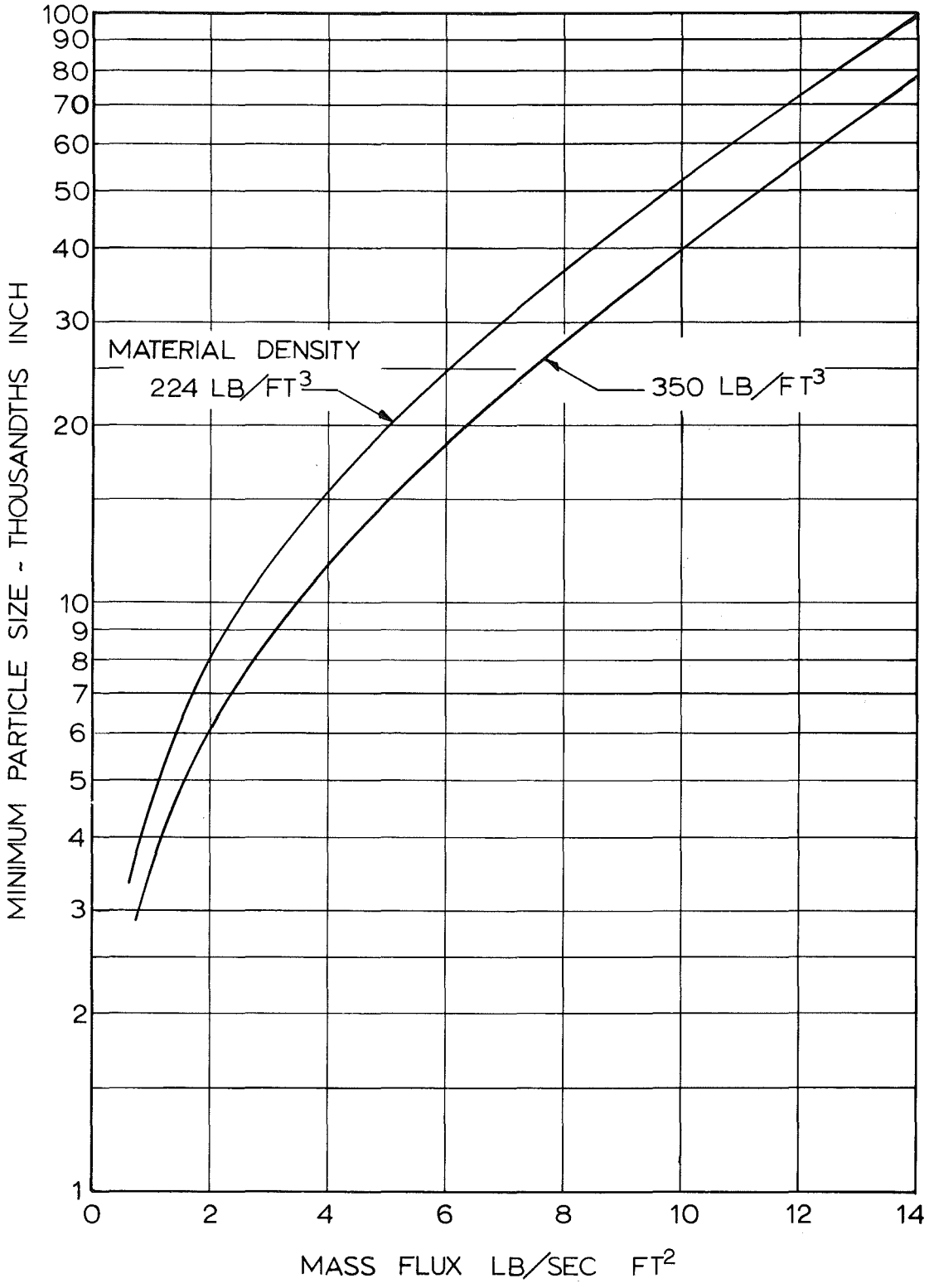

Fig. 1 Minimum Particle Size to Avoid Dust Carryover

1. PRELIMINARY THERMAL ANALYSIS

As the first step in this study, it was desired to establish the effects of various parameters on the size and proportions of a storage heater. Much of the rest of the study would be given direction thereby. Therefore, a simplified model of the heater was examined.

The basic concept of a storage heater is simple. A mass of material which is uniformly porous is heated. Then, the fluid to be heated is passed through the porous heat storage matrix. The fluid extracts heat from the matrix. If the matrix is heated uniformly, the first elements of fluid are likely to leave at a temperature very nearly equal to the matrix temperature. Subsequent amounts of fluid will leave at very slightly lower, but practically equal, temperatures for some period of time. Then will begin an increasingly rapid drop in fluid discharge temperature. Finally, the fluid discharge temperature reaches some tolerable lower limit and the heater must be regenerated, or reheated, before it can again be ready to deliver fluid at the required temperature level. This process is illustrated graphically in Fig. 2. The whole matrix is at a uniform temperature initially. It will be noted that as more and more heat is extracted from the matrix, the temperature distribution along the axis of the matrix parallel to the flow tends toward a fixed shape which moves toward the discharge end. This axial distribution of matrix temperature may be thought of as a "wave front".

It is evident that the amount of heat extracted from the matrix at any given point along its axis is proportional to the difference between the initial and final matrix temperature. This leads to the conclusion that the greatest amount of heat would be extracted from a matrix which was heated initially to a uniform temperature along the entire length. It also leads to the conclusion that the length of the temperature "wave front" should be as short as possible relative to the matrix length in order that the largest proportion of stored energy may be extracted.

Analytical treatment of the storage heater has been carried out by several men. Ref. 1 considers the problem in detail. Various analytic approaches are described there, including an analysis due to Hausen which is used here. This analysis groups certain quantities in two nondimensional parameters which together define the temperature distribution and the performance of the heater. Certain assumptions are implicit in the simple form of this analysis which we wish to consider at this point. They are:

a. Temperature within the heat storage matrix is uniform at any axial location, i.e., lateral

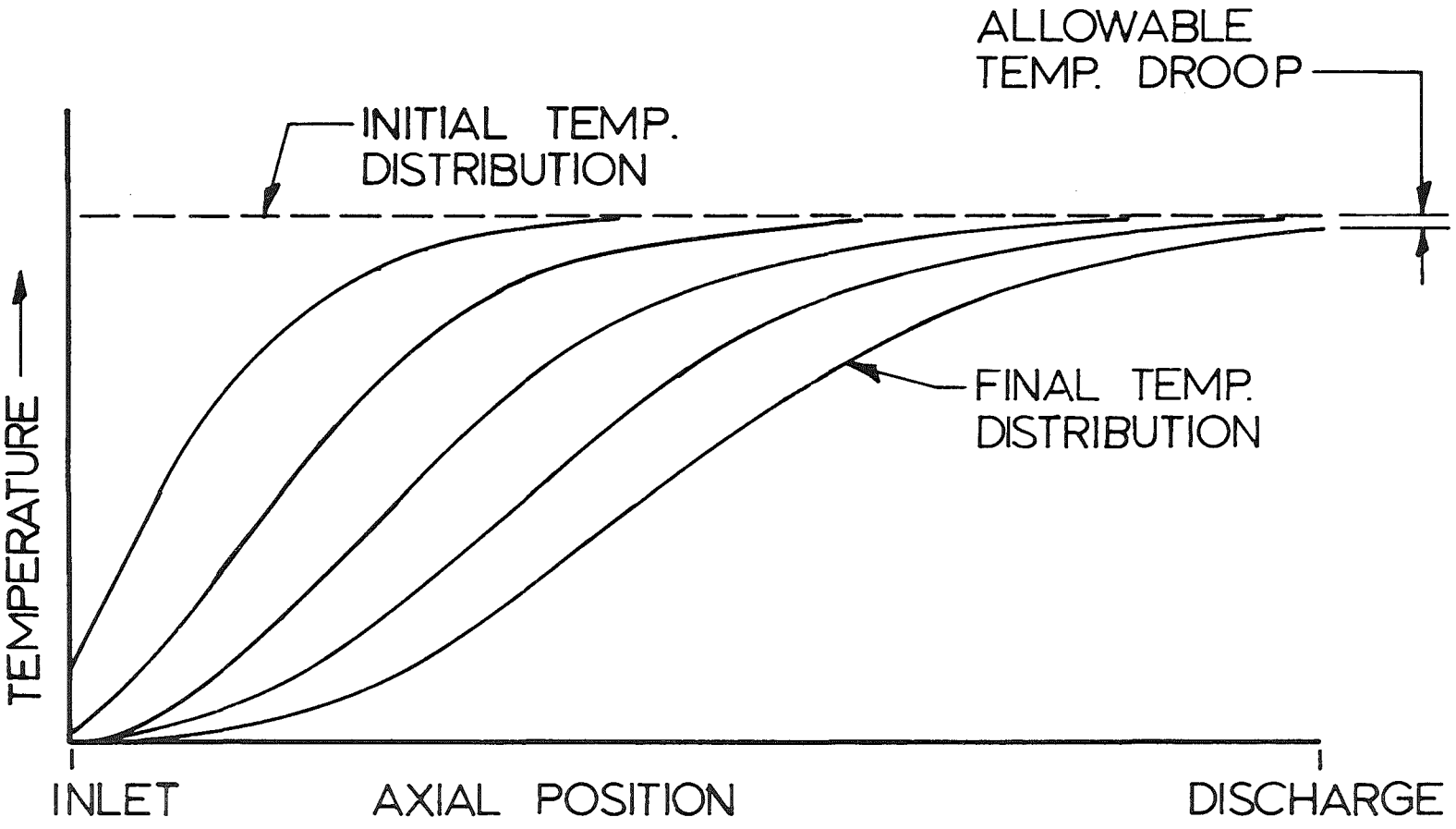

Fig. 2 Characteristic Temperature Distribution in a Storage Heater

thermal conductivity is infinite.

b. There is no heat flow in the matrix material in the axial direction, i.e., axial thermal conductivity is zero.

Assumption a is reasonable when the lateral dimensions of the matrix elements (between flow surfaces) are small or when the conductivity is high. For most ceramic materials the error due to this assumption becomes appreciable when the lateral thickness of the element is about 1/4 inch or greater. Assumption b is reasonable for almost all ceramic materials, since their thermal conductivity is low. Thus, this simplified analysis is very useful for preliminary investigation of the effects of different factors on heater volume.

The two parameters which define the conditions within the heater are:

a. Time related (η) and

b. Axial position related (ξ).

These parameters are defined as

$$\eta = \frac{hP}{CM}\,\Theta$$

$$\xi = \frac{hP}{c_p \dot{m}}\,z$$

Particular values of these two parameters determine values of a dimensionless temperature which is defined as

$$T = \frac{T - T_c}{T_i - T_c}$$

This dimensionless temperature is shown for values of η and ξ in Fig. 3a and 3b, representing the temperature of the gas and the matrix, respectively. This figure was prepared from tabulated values appearing in Ref. 1, pp. 287, 288, and additional calculations made for this report.

Not only does Fig. 3 permit the estimation of the temperature of the gas or the matrix, but it enables the effect on matrix volume of variations in geometric and material parameters to be assessed. The volume of the matrix is equal to the product of its length and the total face area.

HAUSEN RESULTS

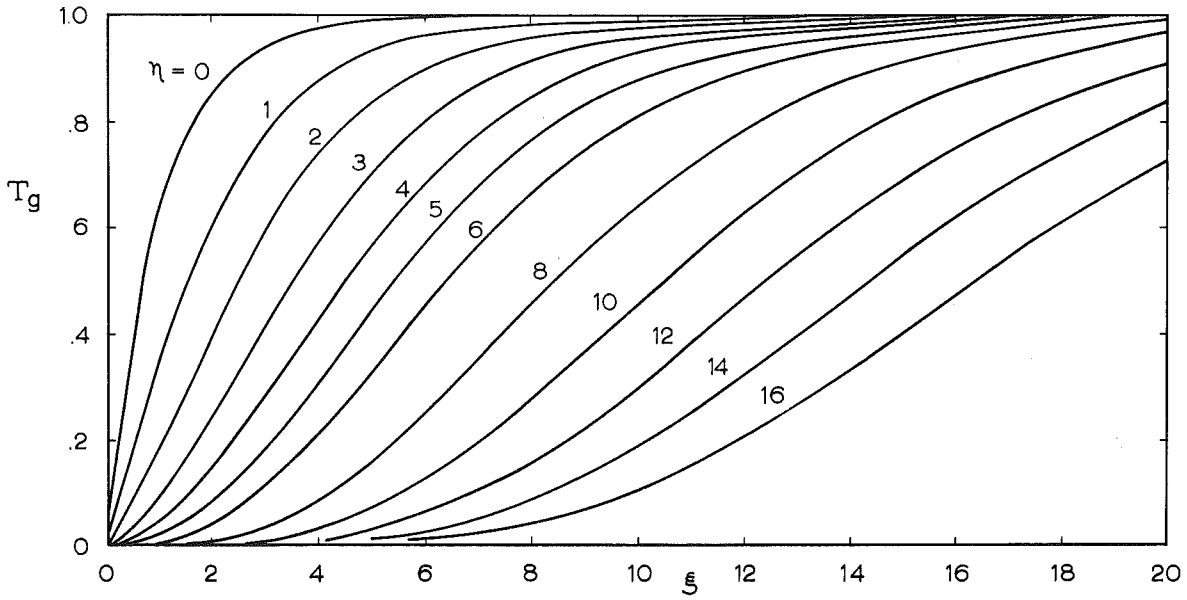

Fig. 3a Fluid Temperature in Regenerative Heater

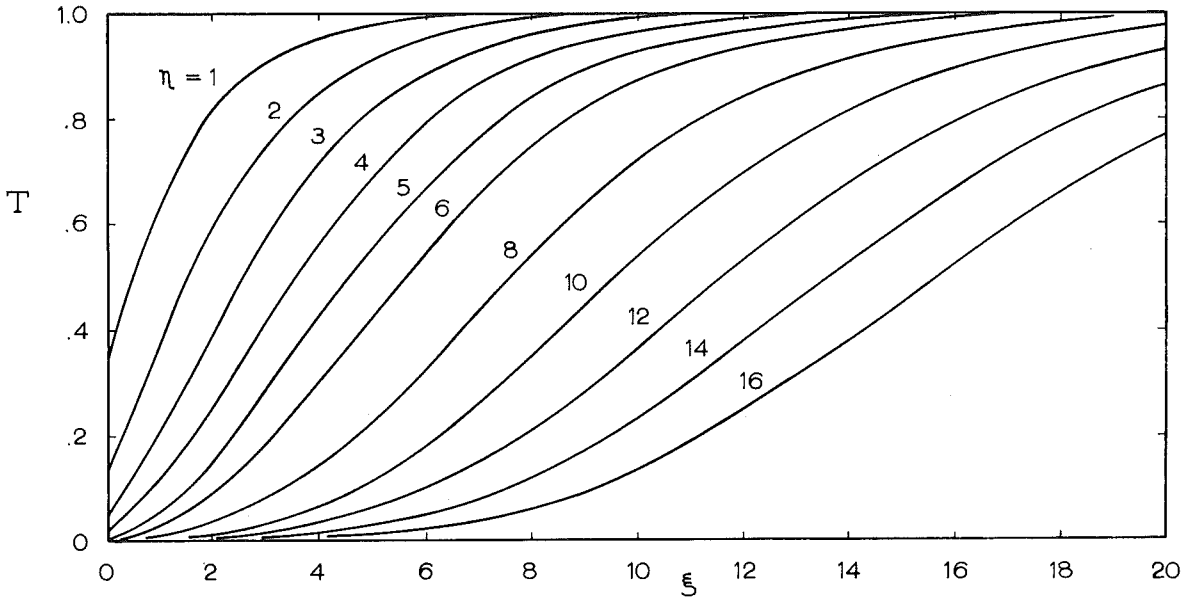

Fig. 3b Solids Temperature in Regenerative Heater

$$V_{bed} = A_f \ell$$

The mass of matrix material per unit length is proportional to the face area.

$$M = \rho_{bulk} A_f$$

so that the volume may be written as

$$V_{bed} = \frac{M}{\rho_{bulk}} \ell$$

Substituting for M and ℓ in the definitions of η_f and ξ_ℓ, one obtains

$$V_{bed} = \frac{c_p \dot{m} \theta_f}{C \rho_{bulk}} \frac{\xi_\ell}{\eta_f}$$

This result indicates that the volume of the matrix is proportional to ratio of the heat capacity of all the gas passing through in one run to the heat capacity per unit volume of the matrix. This might be likened to an ideal matrix volume which yields all of its stored heat to the gas. The volume is also proportional to the ratio $\frac{\xi_\ell}{\eta_f}$.

As was indicated earlier in this section, the end of the run is usually defined as the reduction of the gas discharge temperature to a tolerable lower limit. This would correspond to a specific value of T_g for the gas. Referring to Fig. 3a, it is evident that for any value of T_{gf}, the ratio ξ_ℓ/η_f is a minimum (corresponding to minimum matrix volume) when ξ_ℓ is large. The value of η_f will also tend to be large.

It is noteworthy that the foregoing results indicate that the proportions of the heater matrix (length to diameter ratio) do not affect the volume in this simplified analysis. To be sure, the desirable large value of ξ_ℓ may be achieved by increasing the length, ℓ. However, note that for a given value of matrix volume the face area of the matrix must be decreased proportionately. This means

that the heat transfer area per unit length, P, will be reduced in proportion to the increase in the length. Therefore ξ_ℓ does not, in fact, depend on heater proportions for this analysis.

The only geometric parameters which may be modified to increase ξ_ℓ would be the heat transfer area per unit volume of the matrix which should be large. A large value of gas-to-solid heat transfer coefficient h is also desirable. Evidently a matrix having many flow passages of relatively small cross-sectional dimensions is optimum. This geometry tends to increase pressure drop in the matrix, so that pressure drop could be a limiting factor.

The selection of a pressure drop criterion depends on the configuration of the heater. Most storage heaters have been so oriented that the flow is vertically upward through the matrix. In this case the matrix material is normally restrained only by gravity, so that the criterion for pressure drop becomes flotation of the matrix elements (lifting of the elements as the pressure drop exceeds their weight).

In order to establish the size range for the Tripltee heater, and to assess in a preliminary way the effect of various parameters, calculations have been made using this simple thermodynamic analysis with initially uniform matrix temperature. These calculations appear in Appendix B. The results of the calculation indicate that, for the range of geometric parameters of interest, geometry of the matrix elements does not exert a strong effect on matrix volume. However, material selection does have a substantial effect.

The analysis just described is seriously unrealistic in one particular: the assumption of an initially uniform temperature of the matrix. The extremely rapid cooling of the matrix elements in the inlet section would certainly cause fracture from thermally induced stresses. These are proportional to temperature differences developed within the matrix element. Since heat must flow from the interior of the matrix element, the temperature gradient will depend on the rate of heat extraction, and the temperature difference will vary directly with the thickness of the element normal to the direction of flow.

Referring to Fig. 3b, it is evident that the rate of change of matrix temperature with time at any point along its length decreases with increasing time. In fact, it can be shown that the rate of change of matrix temperature with time is (approximately) proportional to the value of the rate of change of matrix temperature with length. An analysis of these considerations is found in Appendix H. Thus, if one assumes that the initial temperature distribution is

given by the distribution for a specified value of η, it will be possible to calculate the volume while limiting the thermal stress (by limiting the value of the temperature ramp slope, dT/dz).

Calculations of matrix volume for a nonuniform initial temperature of the matrix are reported in Appendix B. These are carried out for a fixed (and arbitrary) value of matrix temperature ramp slope (dT/dz) equal to 200°F per foot. These calculations are less accurate than those for the initially uniform temperature case, but they should indicate reasonably well the size of the matrix. Within the accuracy of these calculations, the effects of matrix element geometry on the required matrix volume are not large, nor is the effect of material properties very great. There is a substantial increase in required volume due to the nonuniform temperature distribution. In fact this effect indicates that the primary factor determining matrix volume will be thermal stress resistance and the resultant value of temperature ramp slope in the matrix. The steeper the ramp the smaller will be the heater volume.

The volume of the matrix is indicated to be about 1500 cubic feet, and the face area about 100 square feet. These results indicate that it is possible that the heater may comprise a single vessel. This result is most favorable since it would certainly minimize cost and also minimize the length of duct work. This latter result reduces heat loss and minimizes the contribution of a major source of dust in most heater installations.

The question of matrix element geometry should be considered in some detail. There are two configurations now in use. These are spheres and cored brick. An example of a cored brick shape is shown in Fig. 4.

The cored brick shape was developed in order to minimize stresses which tend to limit the performance and increase the size of storage heaters. The temperature at which the matrix material must be held is so high that its bearing strength (creep limited) is quite low. Spheres have very small contact area, so that bearing stresses rise quite rapidly with increasing depth in the matrix. The result is that the high matrix temperatures can be permitted to exist for only a short distance in the matrix. As just demonstrated , this results in a requirement for a large heater volume or else for a large face area (so that the length of high matrix temperature can be large compared to the overall length). For large capacity heaters the required face area becomes so large that several vessels must be used.

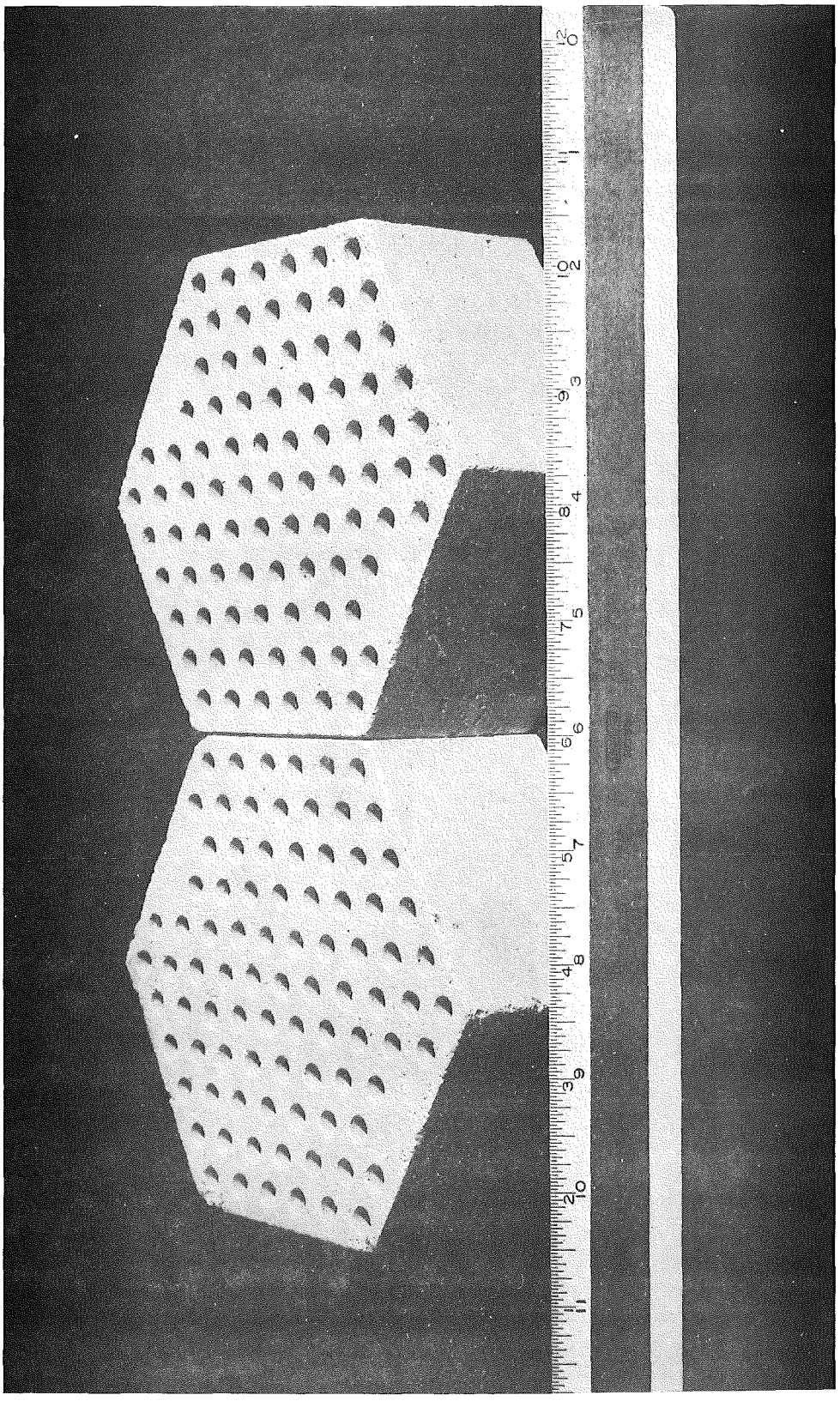

Fig. 4 Cored Brick

Another adverse aspect of spheres is the relatively large pressure drop which they cause. This is shown by Fig. 5 in which the mass velocity to develop a pressure gradient one half that corresponding to flotation at the hot end (normally the top) of the matrix is plotted as a function of hole diameter for cored brick and sphere diameter. The pressure drop for the spheres is based on the data of Ref. 2. It is seen that, for equal heat transfer area per unit volume, the permissible mass velocity is more than four times as great for the cored brick as for the spheres. That is, the pressure drop for the spheres would be about fourteen times as great for the same mass velocity as it is for the cored brick. The pressure drop across a matrix of spheres varies as the 1.9 power of the mass velocity.

This preliminary thermal analysis of the Tripltee air heater indicates thatit will probably comprise one vessel with a heat storage matrix of cored brick. It also indicates that thermal stress resistance will be the most critical single factor in determining the volumeof the matrix. It is then necessary to establish the fabrication and economic feasibility of the requisite vessel and to determine the feasibility of procuring matrix material of requisite thermal stress resistance.

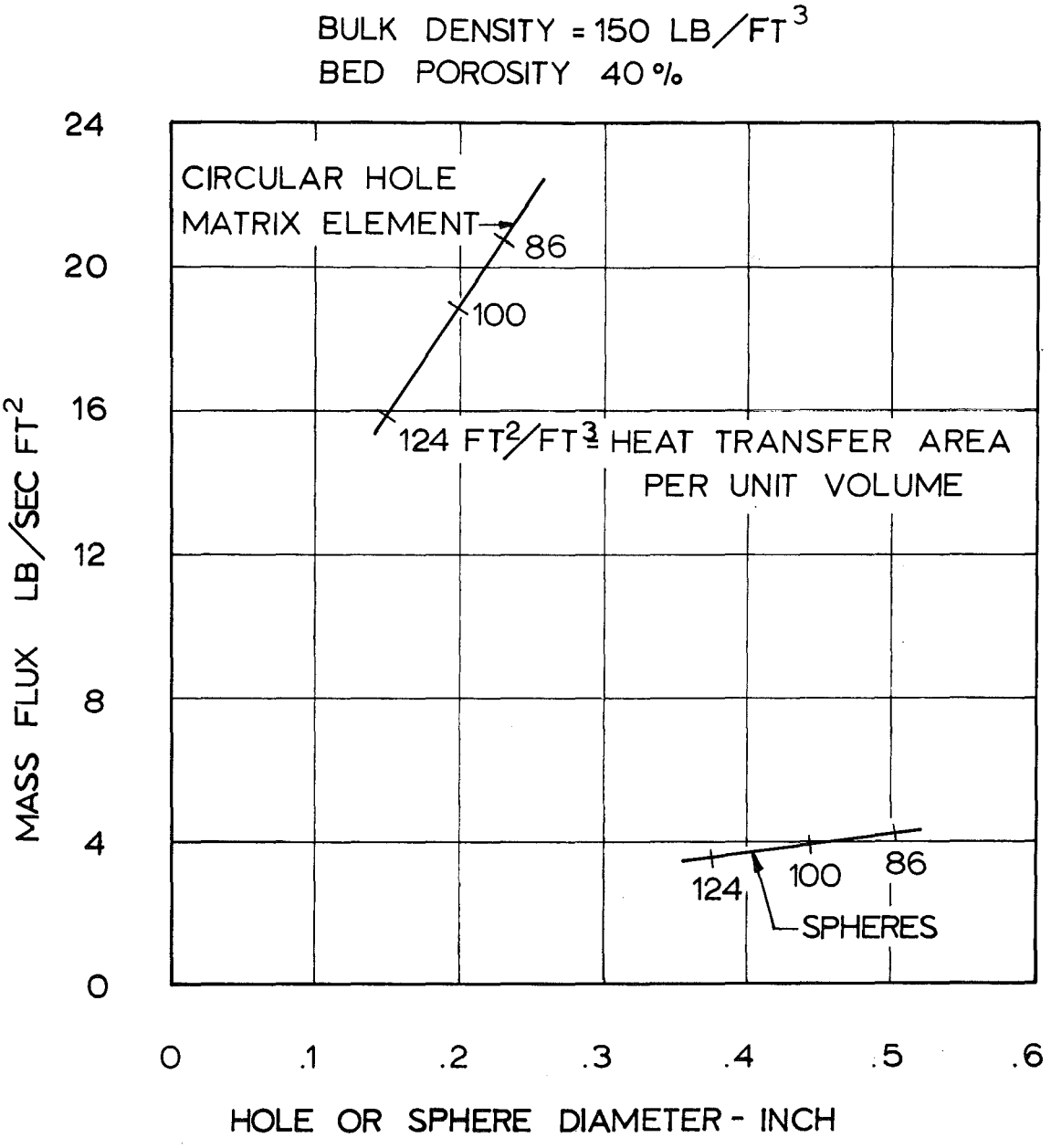

Fig. 5 Estimated Allowable Mass Flux

2. HEATER VESSEL

A study was undertaken to determine the fabrication and economic feasibility of a pressure vessel of sufficient capacity to contain the matrix volume indicated in the thermal analysis. Preliminary estimates indicated that the insulation thickness might be about 1 foot or somewhat less. For the minimum probable matrix face area (A_f) indicated by Fig. 12B, Appendix B (67 ft^2), the corresponding vessel inside diameter would be about 11 feet. The maximum probable matrix area indicated by Fig. 12B, Appendix B, is about 130 ft^2 (s/D of 1.7 and D of .15 in.). The corresponding vessel inside diameter would be about 15 feet. Accordingly three configurations of vessel were considered, one vessel comprising three 6-1/2 feet inside diameter cylinders joined by a sphere (design A), one vessel of 15 feet inside diameter (design B), and one vessel of 11 feet inside diameter (design C). These three configurations are illustrated by Figs. 6, 7, and 8. The first and second configurations yield face areas of about 130 ft^2. The third yields a face area of about 65 ft^2, so that one such vessel is suitable for the minimum face area matrix while two such vessels would be suitable for maximum face area matrix.

The consideration of multiple vessels, in light of the requirement for a "fixed" condition of the heater with respect to the rest of the facility, focused attention on the problem of vessel supports. The thermal expansion of a "complex" of heater vessels may be expected to present some design problems if undue stresses in the vessels and manifolding are to be avoided.

Expansion joints in the manifolding, appropriately placed and anchored offer an apparent solution. However, the large duct sizes, about 6 feet I.D., and the requirement for refractory linings complicate this procedure.

An alternative solution is to fix a carefully selected point in the heater system and permit the rest of the structure to move with respect to that point on some type of flexible support.

Clearly, a single vessel minimizes the problem of accommodating expansion.

In design of the vessel, first thought was given to ASME code specifications for allowable stresses, 4:1 on ultimate strength. For vessels with a diameter over 12 feet, plate thicknesses are so great that material homogeneity and available plate size introduce economic limitations. The application of non-code stresses, 3:1 or 2:1 on ultimate, offers relief here and may be acceptable when

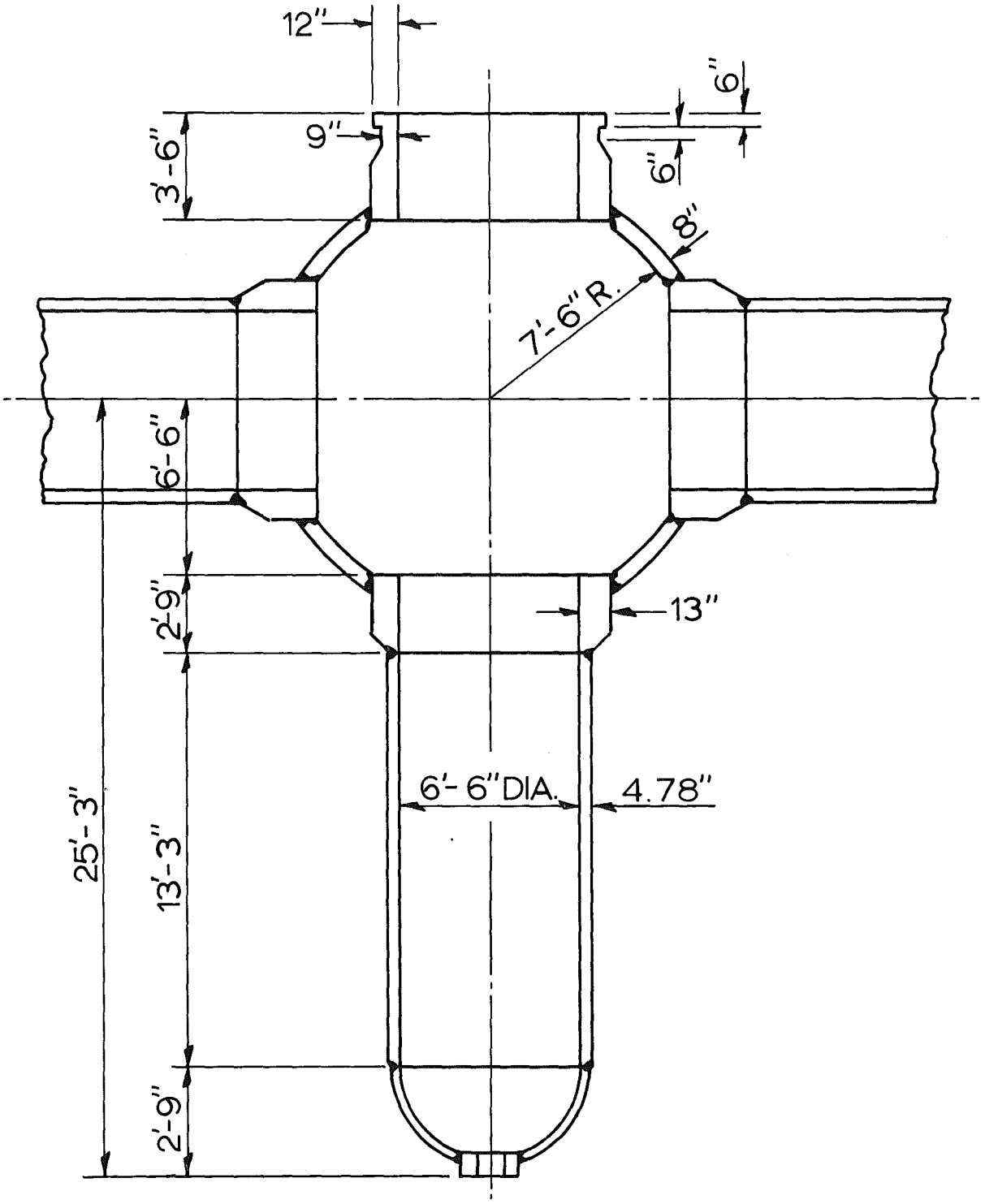

Fig. 6 Heater Vessel Design A

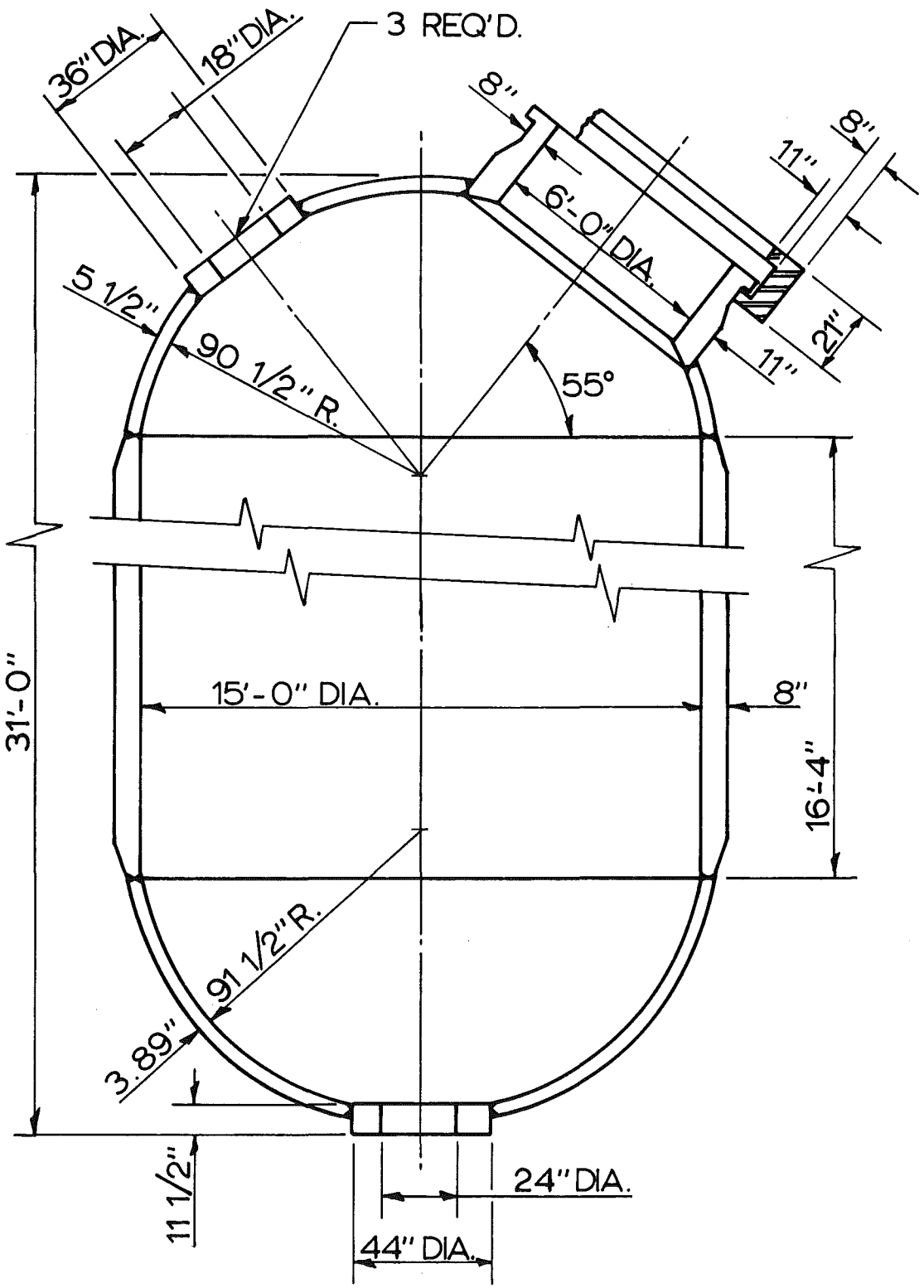

Fig. 7 Heater Vessel Design B

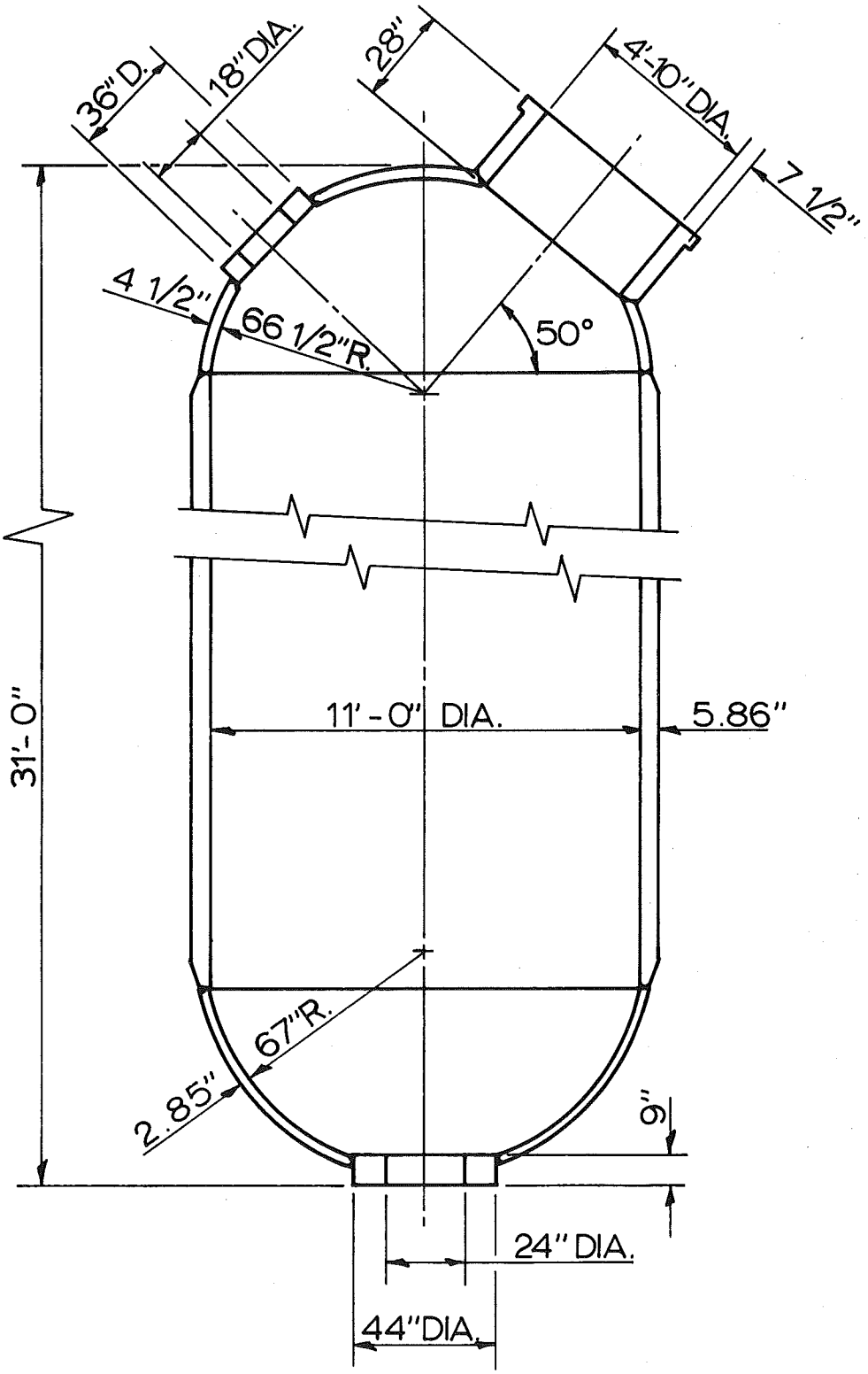

Fig. 8 Heater Vessel Design C

nuclear power codes are adopted. The requirement for more detailed analysis would be an accompanying penalty.

The patented Multilayer construction is not economically competitive for service conditions below 3000 psi and is limited to an O.D. of 10 feet by existing machinery. Banded construction appears to offer no outstanding advantage in this particular application.

The range of materials available for construction of a large heater vessel is not wide. Carbon steel boiler plate, (ASTM Spec A212), is a material worthy of first consideration because of its availability, forming, and welding properties. HY80, a federal specification material used in submarine construction, offers the advantages of an 80,000 psi yield material together with availability, established welding techniques and a considerable background in fabrication experience. It is more expensive and more difficult to work than A212. Depending on economic factors and development of fabrication experience, Mar-aging steels may offer a significant advantage. Yield strengths are close to ultimate strengths, both over 200,000 psi in 1/2 inch thick plates. This steel works very much like HY80 and the welding techniques that have been developed are currently being applied to rocket engine cases.

A filament wound structure, specifically a fiberglass reinforced plastic, may be applicable to this service when the facility is finally designed. Current winding facilities of one fabricator are limited to 13 foot diameter by 35 foot length vessels but extension to larger sizes may be expected since the technique offers advantages in weight saving and fabrication ease over steel in very large sizes. Curing the resins in thick selections, field fabrication possibilities and the enlargement of current machinery are considered to be engineering problems within the state of the art. Approximate costs are $.65 to $3.51/lb for glass, $2.00/lb for resin and conversion runs $2.00 to $3.00/lb of furnished vessel.

Shop fabrication is limited by shipping considerations rather than by technique or equipment. Conventional rail shipments are accepted up to 12.5 foot envelope diameter and about 50 foot length for a single car. These limits can be extended by using idle cars ahead and behind the load to give about 70 foot length, and by special rail car that carries the load only inches from the track to approach a diametral limit of 15 feet. Such a car is extant, a patented design by Newport News Shipbuilding & Dry Dock Co. Frequently, too, exceptions to size and weight limits can be arranged with the railroads when a design is firm and the transport problems real. Meeting at the engineering level between the

fabricator and the railroad is advised as the only suitable means of negotiating extensions and exceptions. The maximum load figure approaches 200 tons and a 15 foot diameter. In such diameters, design length would probably be under 50 feet.

Field fabrication was considered as a means of reaching vessel diameters beyond the shipping limits noted above. It is generally accepted that field fabrication of a vessel for this service implies the establishment of a complete field shop. Fabrication stress relief and weld inspection can all be carried out successfully in the field; but, increased labor rates, longer construction times and the logistics of a field operation may increase the cost of a given vessel over shop fabrication. Field fabrication is usually considered only when requirements cannot be satisfied by a shop fabricable design.

In the light of this information on fabrication and shipping limitations, the three designs to be considered are seen to cover both shop and field fabrication; design C most economically being a shop fabricated vessel while B probably must be field fabricated. Design A combines shop fabrication of large elements with field assembly of these elements into the final vessel.

The three designs were studied by Chicago Bridge and Iron Company. Careful studies of the structural and fabrication aspects were made which enabled cost estimates to be prepared. The cost of designs A and B are for the finished vessels only, at the site. The cost of design C is that of the finished vessels before shipment to site. These cost estimates are:

Design	Approximate Weight	Estimated Cost
A	535,000 lbs.	$450,000
B	426,000 lbs.	500,000
C (2 vessels)	574,000 lbs.	470,000

The cost per pound of the shop fabricated vessels (A and C) is about $.85, while the field erection required with the large diameter vessel of design B increased the cost per pound to about $1.16. The reduction in the amount of material required for the large vessel largely offsets the increased fabrication cost rate, so that there is no significant difference between the three designs in terms of cost per unit of matrix face area. It is obvious that a single large vessel will be appreciably more economical if shop fabricated. Certainly the question of transport deserves most careful attention, since the cost of a single, shop fabricated vessel appears likely to be more than $120,000 less than multiple vessels or a single field fabricated vessel.

It is clear that the most economical overall solution, in terms of vessel and installation cost, will be a single vessel, even if field fabrication is required. This follows because of the great simplification in ducting, allowance for expansion, etc. It is also clear that it is entirely feasible to plan on a single vessel for this heater if the matrix face area can be of the value estimated in the preliminary analysis. This depends largely on questions related to thermal stress.

3. REFRACTORY MATERIALS

The preliminary analysis has revealed the importance of the matrix temperature ramp slope in determining heater volume. Need for a matrix temperature ramp and its slope are related to the thermal stress resistance of the matrix material. If material cracking and the resulting dust are to be avoided, the thermal resistance properties of potential matrix materials will be of major importance.

The creation of dust is clearly a case of mechanical material failure such that small pieces are separated from a matrix element. Thus, minimization of dust requires making the probability of mechanical failure on either a micro- or macroscale small. Mechanical failure results from unsupportable stresses. All stresses must therefore be kept below some tolerable level. Bearing loads and net fluid-on-solid forces are not high in the cored brick design. Therefore, macroscale failure will depend on thermal stresses. Microscale failure can result in the loss of small particles from matrix surfaces. Failure of this type may result from thermal stresses, abrasion, or concentrated loads acting on corners, etc. It seems likely that the factor controlling microscale fracture at surfaces will be the surface condition. The degree to which a surface is smooth and firm will indicate to what extent its microstructure is continuous. The great hardness, chemical stability, and substantial strength of oxide ceramics should virtually preclude loss of small particles from a smooth surface in a relatively static application such as this.

To determine what performance might be expected from oxide refractories, a literature survey was made. The results of this survey are given in Appendix C. Briefly this survey revealed that two highly refractory materials appeared to be well suited to this application. They are zirconia and magnesia. However, it was also established that truly adequate properties would likely require higher material density than is common in the refractory brick industry. This requirement derives from both thermal stress resistance and the surface condition considerations. In fact, it appears at least possible that a density of more than 90% of theoretical will be essential. Higher densities, say about 95%, would be still better.

In addition to high density, the data obtained by the literature survey indicated that high purity is certainly desirable, and that purities of greater than 99% may be required.

While both zirconia and magnesia appear to be suitable in this application, each has a characteristic which could

disqualify the material. It will be necessary to establish by test results that their potentially deleterious characteristics will not adversely affect the operation of the Tripltee heater.

The undesirable characteristic of zirconia results from a change in crystalline structure from monoclinic to tetragonal. This crystallographic transformation is accompanied by a large volume change which appears superficially as an inversion (in slope) of the thermal expansion curve. The transformation of the individual crystallite is not simultaneous, of course, so that extreme stresses are set up in the zirconia piece and cracks develop.

It is customary to suppress this transformation by adding small amounts (up to 10%) of calcia to the zirconia. This causes the crystalline structure to assume a third (cubic) form which is (presumably) stable. Experience with commercially available zirconia has suggested that the "stabilization" of zirconia in this way is not necessarily permanent, since thermal cycling always results in gradual deterioration of the material and formation of dust.

Work now in progress suggests that high purity zirconia may be able to withstand long term thermal cycling without becoming "destabilized". If this can be demonstrated conclusively, it is likely that zirconia will be satisfactory as a material for matrix elements.

Magnesia has been reported to have a relatively high vapor pressure. It is rather common to encounter the opinion that it will vaporize rapidly at temperatures in excess of, say, 3200°F. Such is actually the case when the magnesia is heated in a vacuum or in some kinds of reducing atmospheres (e.g., carbon vapor from electric arc). In the case of vaporization in a reducing situation, the process appears to be that of reduction of magnesia to magnesium which vaporizes readily (see Ref. 3). However, magnesia has been used in regenerative heaters for nitrogen fixation for extended periods of time at temperatures in excess of 4000°F without evidence of excessive vaporization (Ref. 4). It has also been used in a pebble bed air heater at the NASA Ames Research Center at similar temperatures. As long as excess oxygen is present, no evidence of vaporization has been noted. It appears probable then that high purity magnesia will not vaporize materially at temperatures of interest so long as there is some finite (but as yet undefined) oxygen vapor pressure.

In order to determine the production and economic feasibility of the kind of material desired for the matrix, a survey questionnaire was made up and submitted to all of the

manufacturers who appeared to be at all qualified to produce material of a suitable type. This questionnaire (in two parts) and the covering letter is included in Appendix C.

All manufacturers (twenty) acknowledged the inquiry. The list of their names appears in Appendix C. Nine manufacturers have indicated that they feel able to supply suitable matrix elements in either zirconia or magnesia. Since two manufacturers have yet to submit final replies to this inquiry, the number of potential suppliers might reach eleven. Those replying favorably are:

a. Zirconia matrix elements:
   Harbison-Walker Refractories Co.
   Minnesota Mining & Manufacturing Co.
   Zirconium Corporation of America

b. Magnesia matrix elements:
   Coors Porcelain Company
   Kaiser Refractories
   Minneapolis-Honeywell

c. Both zirconia and magnesia matrix elements:
   Laboratory Equipment Corporation
   National Beryllia Corporation
   Norton Company .

Without exception those replying favorably indicated that the desired properties are within the present state of the art and therefore feasible. However, ceramic properties are extremely sensitive to production processes. Consequently, all manufacturers stated that it would be necessary to carry out some trials to establish the production process that would economically produce the desired shapes with the desired properties.

The replies indicated that the probable techniques for production of the two shapes would be cold pressing followed by sintering for the cored brick, and extrusion or pressing for the tubular shape. The probability of achieving high density appears greater for the tube than for the cored brick.

In view of the pronounced variation in material properties with production processes, it is clear that tests will have to be made on material prepared specifically for this application in order to realistically establish material properties for use in the final heater design. Since trials will be necessary on the part of manufacturers to establish the correct technique and process details before production of even a test batch of matrix elements can be undertaken, it is quite unlikely that material properties can be established without purchase of at least small lots of material. The manufacturers are not in a position to assuredly produce material to specification.

It is recommended that small lots (several hundred pounds) of matrix elements be procured from several manufacturers and that these elements be tested, both by laboratory tests to establish the basic mechanical and physical properties of the material, and by bench tests under simulated heater operation. On the basis of these tests, material and shape specifications and dimensional tolerances could be established. These could provide the basis for procurement of matrix elements for either a pilot heater or the Tripltee heater itself.

4. INSULATION

INSULATION REQUIREMENTS

In order to prevent the pressure vessel containing the heat storage matrix from becoming too hot, some insulation must be provided. An approach using no insulation (in the usual sense), was considered (air cooling behind a radiation shield), but the indications were unfavorable in terms of safety and reliability.

The analytical work to determine the required insulation thickness and cooling is summarized in Appendix D. This analysis deals primarily with free convection and radiation cooling of the heater vessel, inasmuch as this is the simplest method available.

Results based on the use of an insulation liner with thermal resistance comparable to commercially available insulating zirconia (150 lb/ft^3) are plotted in Fig. 9. The strong influence of insulation thickness on heater size is apparent. In this calculation the influence of insulation thickness on the volume in the vessel domes above and below the bed is not included but the trends are qualitatively similar. The effect of changing insulation thickness is greatest at small diameters, but even with a vessel I.D. of 12 ft, an increase in insulation thickness from 1 to 2 ft increases the ratio of heater vessel volume to bed volume from 1.5 to 2.2. As the insulation thickness decreases, the vessel temperature rises. Thus, if the vessel is permitted to operate at higher temperatures, a significant reduction in total vessel volume for a given bed volume requirement can be achieved, with the concomitant reduction in cost. The vessel temperatures required are not excessive, e.g., they do not exceed the ASME code limit. One foot of insulation in a 12 ft I.D. vessel will give a maximum vessel temperature of 500°F.

A further conclusion from Fig. 9 is that cooling of the vessel by free convection and radiation is adequate. Water cooling is not required.

The results of Fig. 9 apply directly to a zirconia heat storage bed. In the case of a magnesia bed, at least a portion of the insulation liner would be magnesia. A comparable analysis for magnesia insulation was not made because of the lack of thermal conductivity data for low density (insulating) magnesia. The thermal conductivity of magnesia is greater than that of zirconia, therefore more insulation would be required. To keep the thickness to a minimum, the cooler layer could be a low density alumina, zirconia, or Fiberfrax (a fibrous alumina - silica material). Application

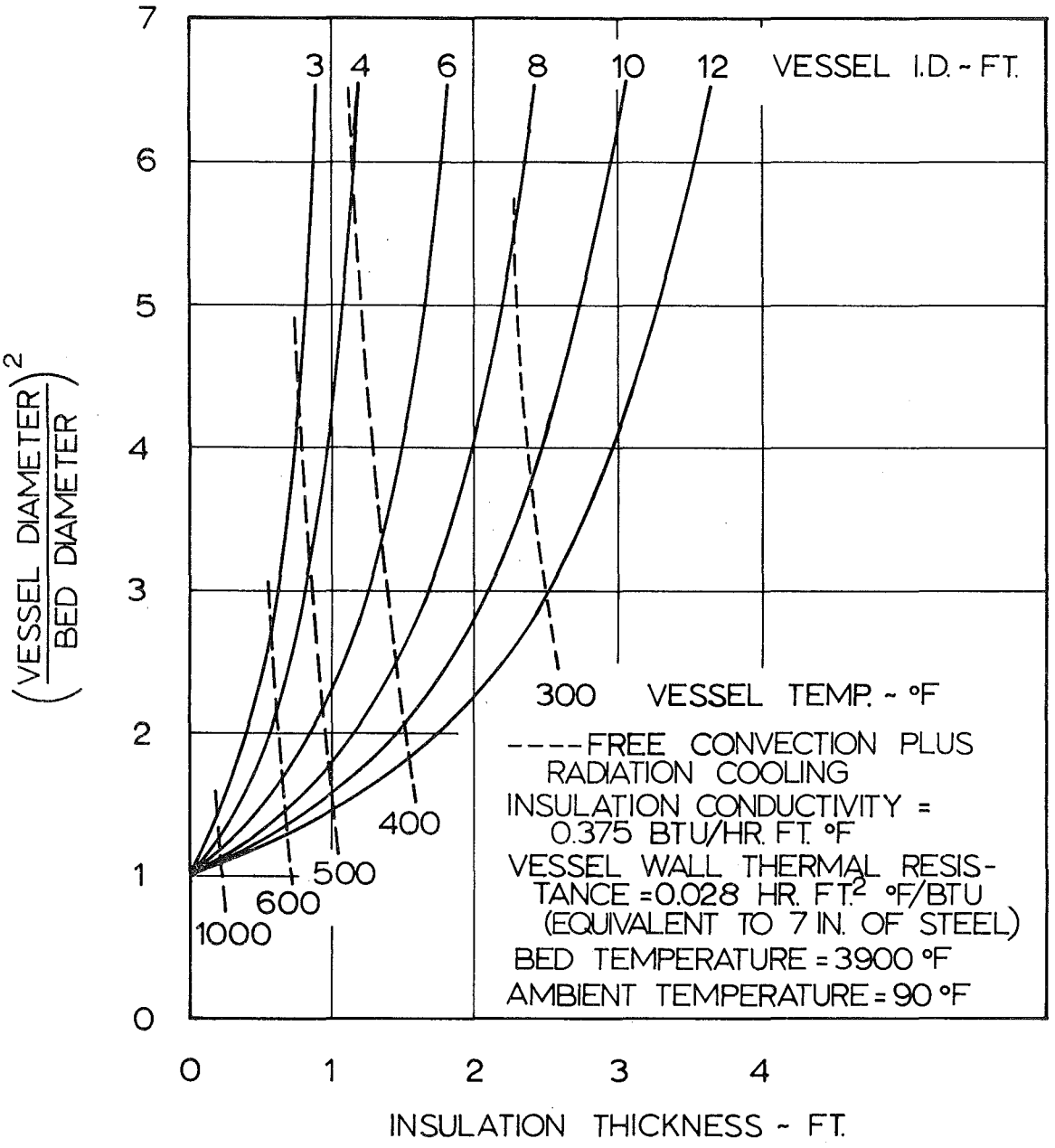

Fig. 9 Effect of Temperature on Vessel Size

of corrugated ceramics may also be feasible. At the present time it is estimated that a magnesia bed would require a 50% thicker insulation layer than a zirconia bed.

If it became necessary to limit the heater vessel temperature to values below 500°F, an alternate to providing thicker insulation would be additional cooling of the vessel by forced air flow. Substantial reductions in vessel temperature are possible through increased cooling, as shown in the Appendix Fig. 1D.

AIR FLOW THROUGH INSULATION

Air flow through the insulation can have an important influence in reducing the air discharge temperature from the heater for a given bed temperature. The air in the insulation is at lower temperatures than that in the bed; therefore the density is greater, and a given volumetric flow can depress the final temperature by a significant amount in some cases. Both the bed and the insulation around the bed experience the same overall pressure difference from inlet to outlet. They in effect form parallel flow channels. Consequently, the relative resistance to flow between these two channels is of primary importance in determining the importance of this effect. Cored brick have an advantage over pebbles in this respect, since they give less pressure drop at the same flow rates. Another factor of importance is the ratio of insulation cross section area to bed area. This ratio decreases as vessel diameter increases, and therefore the problem is not as severe in large heaters.

An estimate of the effect of bypass flow is presented in Fig. 10, for cored bricks of different hole diameters, but at a fixed value of porosity. The ordinate can also be interpreted as the difference between the bed temperature required with bypass flow and that required if there were no bypass flow, to produce a given air discharge temperature. The effect of hole diameter shown is due to the greater flow resistance of small holes.

The advantage of permitting high vessel temperatures (500 to 600°F), in reducing insulation thickness for cooling by free convection and radiation has been discussed above (Fig. 9). In addition to reducing the vessel size, bypass flow is also reduced. An example of this is shown in Fig. 10 for a 12 ft I.D. vessel. It is obvious that the influence of bypass flow can be reduced to negligible proportions.

In summary, this aspect of the study demonstrates that high vessel temperatures in conjunction with commercially available insulation materials should be adequate to allow

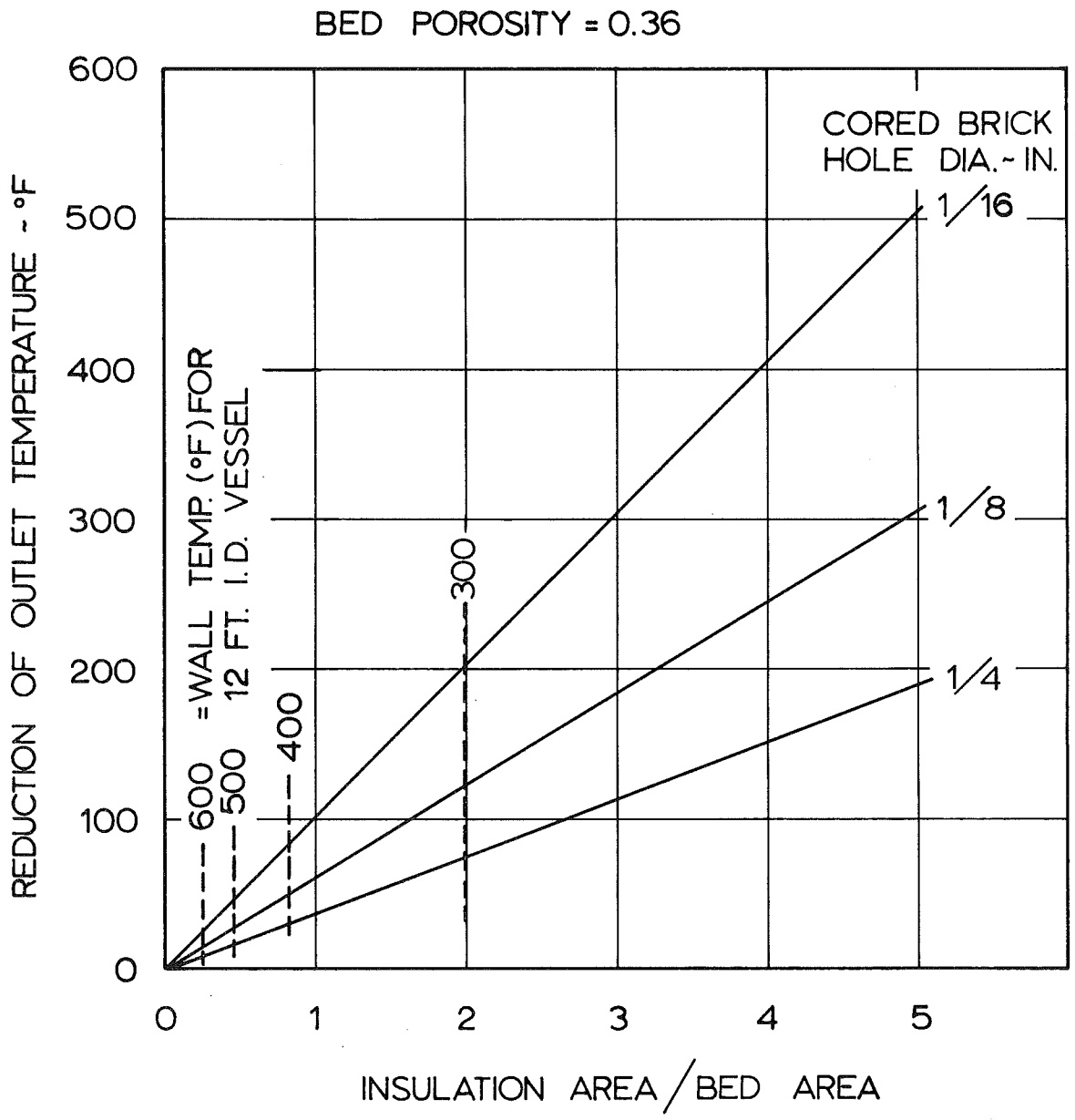

Fig. 10 Effect of Bypass Flow Through Insulation on Outlet Gas Temperature

a thin insulation liner. Such a thin liner will prove superior to a thicker liner both with regard to heater vessel volume and insulation bypass flow. Also, internal cooling is neither necessary nor desirable. However, in view of the fact that some dust originates in the insulation, great care should be exercised in the selection of insulation to minimize such dust formation.

5. MIXER

GENERAL REQUIREMENTS

The proposed test facility has two primary design points:

		Mach 7	Mach 4
Stagnation pressure, psia	=	2000	400
Stagnation temperature, ^{o}R	=	3900	1600
Mass flow rate, lb/sec	=	1500	5000
Approx. throat dia., in.	=	11	35

A single storage heater system is not compatible with direct operation at both of these design points; therefore, an alternate means of providing the low temperature high mass flow condition is required. Since the thermal energy is the same in the two flow conditions, it appears desirable to supply the Mach 4 nozzle by mixing cold air from the storage reservoir with hot air from the heater. A mixer is not required with the Mach 7 nozzle because a reasonable temperature range can be obtained by varying the heater temperature. Therefore, the following discussion is directed to the problem of a mixer for use with the Mach 4 nozzle.

Preliminary estimates (from AEDC) indicate that the Mach 7 nozzle will be 25 ft longer than the Mach 4 nozzle. With the heater and test cabin in fixed locations, this difference in length could be used for a mixer which is installed only when using the Mach 4 nozzle. Inasmuch as the mixer pressure and temperature requirements are not compatible with Mach 7 operation, the replacement of the Mach 7 nozzle with a Mach 4 nozzle - mixer combination is particularly suitable. The downstream end of the mixer would act as the stilling chamber for the nozzle. Adopting a minimum area ratio of 4 from the mixer to the nozzle throat gives a preliminary estimate of mixer diameter as 6 ft. The corresponding velocity at $1600^{o}R$ is 260 fps.

RELATION TO HEATER AND AIR RESERVOIR

Maximum utilization of the energy storage capability of the heater requires that the hot air be at the highest possible temperature. In this case the Mach 4 design point is attained by mixing 3600 lb/sec of ambient air ($70^{o}F$) with 1400 lb/sec at $3900^{o}R$. If the heater is sized for the Mach 7 design conditions, this hot air flow rate will be available only at high pressures, near the design level of 2000 psi, due to bed flotation limits.

As discussed earlier, the mass flow capability of the heater is ultimately limited by bed flotation, with a further limitation being thermal stress fracture of the refractories, thermal stresses increasing with flow rate. The

bed flotation limits may be used to estimate flow rates available at off design operating conditions, viz.,

$$\mathring{m} \propto (p/T)^{1/2} A_f$$

where A_f is the face area of the heater bed. We are interested here only in operation at the maximum temperature of 3900°R. Therefore, with the bed designed to deliver 1500 lb/sec at 2000 psi, a flow rate of 1400 lb/sec would require $p \geq 1740$ psi. Discharge of this air to the mixer (at 400 psi) would require a choked throat, approximately the size of the Mach 7 throat, between the heater and the mixer.

The heater backpressure requirement means the air storage reservoir cannot be blown down to a pressure level near the 400 psi mixer pressure. However, it is not necessary that the entire reservoir be limited by the heater pressure level requirement. A significant reduction in reservoir capacity is possible by dividing the total air storage, with suitable valves, so that the cold air and hot air to the mixer are drawn from separate reservoirs. In this way the reservoir supplying cold air to the mixer can be blown down to a low pressure level, approaching the mixer pressure of 400 psia.

The possibility of reducing the air storage volume by increasing the heater diameter was briefly investigated. Increasing the heater bed area A_f would permit passage of the 1400 lb/sec flow at a lower pressure level. This, in turn, would permit extraction of a greater fraction of the stored air thereby reducing the air storage volume needed. For heater pressures in the range 1000 to 2000 psi the increase in heater cost offsets the decrease in air storage cost. Above this pressure range the total system cost increased. Hence, there is no cost advantage to oversizing the heater, with respect to the Mach 7 design point, in order to reduce air storage requirements at the Mach 4 design point.

MIXER CONFIGURATION

The preceding discussion has established the desired size of the mixer at 6 ft diameter by no more than 25 ft long. Attention was initially focused on the possibility of performing the mixing with a simple coaxial stream arrangement. As discussed in Appendix E, investigation of this concept led to the conclusion that sufficient mixing (± 5 percent variation in temperature) could not be obtained in 25 feet.

Although sufficient mixing cannot be generated with the coaxial arrangement, the necessary mixing is readily attainable with more sophisticated devices. The major problem in building such a device is the high temperature of the hot flow. All surfaces exposed to temperatures on the order of 3900°R must be cooled or fabricated of heat and oxidation resistant materials.

In order to improve the rapidity with which the two streams mix there are at least two basic approaches that can be used. The first would be to increase, by turbulence generators, etc., the effective lateral energy conductance; (lower limit is the thermal diffusivity). Secondly, one can divide the hot and cold streams into a number of smaller streams and thus reduce the lateral distances across which the streams must mix. A mixer concept, which is shown in Fig. 11, was developed to indicate this approach to providing adequate mixing.

The mixer and the heater backpressure nozzle form a single unit. The nozzle and mixer flow passages are sized to provide subsonic mixer exit velocities and to cause the cold flow static pressure to be higher than the hot flow static pressure throughout most of the device. Cooling is provided by using this pressure difference to transpiration cool the surfaces exposed to hot flow. In the upstream part of the nozzle where such a favorable pressure difference does not exist between the low pressure cold air and the hot flow, high pressure cold air is provided and passed through the walls. The amount of high pressure air needed for this purpose will be about 5 percent of the hot flow.

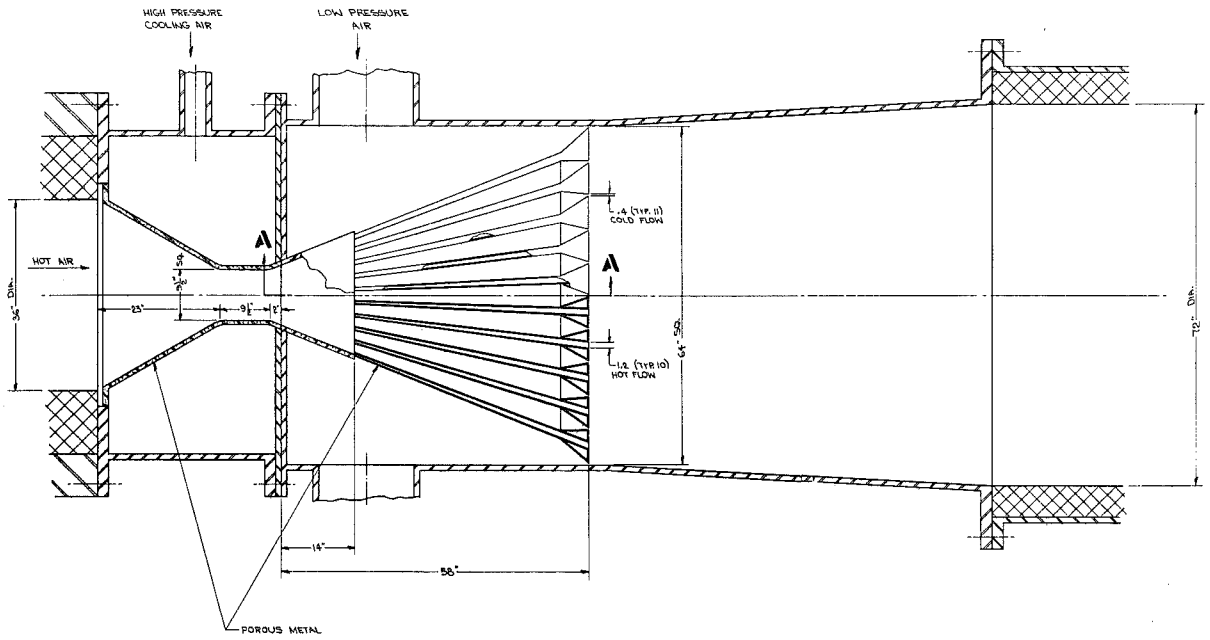

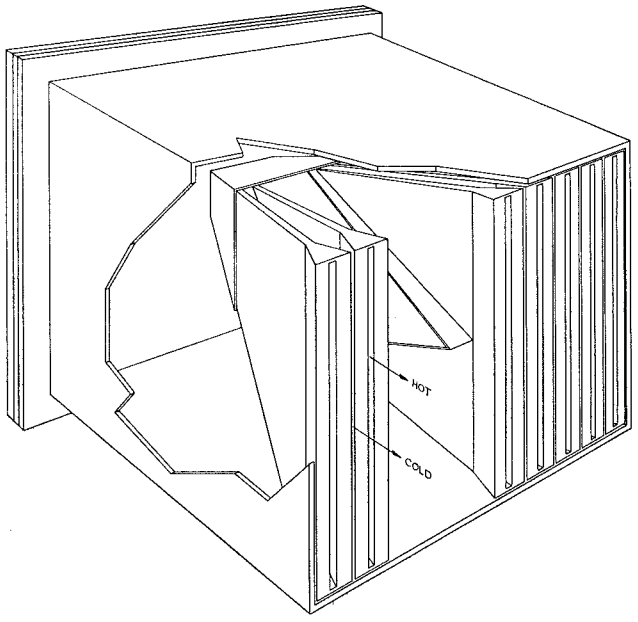

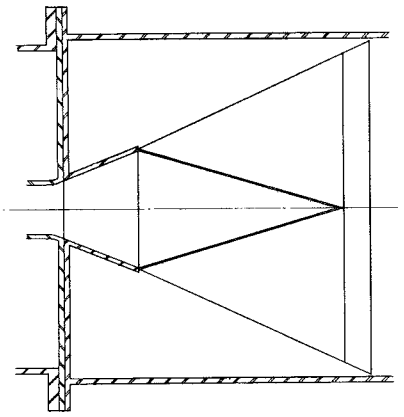

SECTION A-A

Fig. 11 Mach 4 Mixer Concept

6. REGENERATOR

REHEAT ANALYSIS

Heating of the heat storage material comprising the heater bed will be accomplished by passing combustion products, supplied by a burner, through the matrix in the reverse flow direction. The specification requires that the reheat period not exceed 5 hours between maximum energy extraction runs. Since the product of tunnel mass flow and run time is approximately equal to the product of reheat mass flow and reheat time, a reheat mass flow of at least 2.5 lb/sec will be necessary between runs of 30 second duration at 1500 lb/sec, simply to replace the heat extracted.

Of more concern, however, is the shape of the temperature distribution obtained. The preferred distribution is sketched in Fig. 12. It consists of a uniform temperature

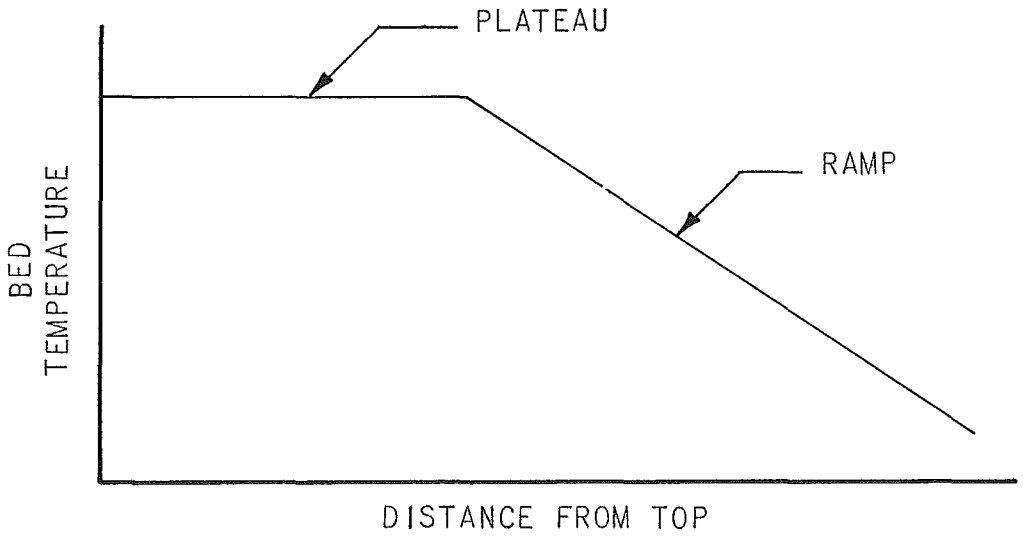

Fig. 12 Preferred Temperature Distribution

at the top of the bed, below which the temperature varies linearly to a low value at the bottom of the bed. The basis for this selection is discussed in Sections 1 and 8. Briefly, a long uniform temperature region and a steep temperature ramp at the air inlet end increases bed efficiency and reduces the total bed volume required. The slope of the temperature ramp is limited by thermal stresses in the matrix. The critical thermal stresses are those across the thickness of the web, due to the temperature difference between the

inside of the web and the hole surface. These stresses increase with both mass flow per unit area and axial temperature gradient (see Appendix H). Because of the thermal stress - temperature ramp relationship, the preferred bed temperature distribution at the inlet end is linear, with the slope at the maximum permissible value. Variation from a linear ramp will increase bed length while still subjecting part of the refractories to the design value of thermal stress.

The bed temperature at the air inlet end must be kept within certain bounds. A low temperature limit is established by the requirement that, within the heater, water vapor not be condensed from the combustion products. Upper limits are imposed by thermal stress levels produced when the cold air impinges on the hot bed matrix, and by temperature limitations on the bed support structure and exhaust piping.

Summarizing these requirements, it is the purpose here, to describe a method of reheating the heat storage bed to a temperature distribution having the following characteristics.

a. Temperature at bottom within desired limits,

b. Linear "Ramp", sloped at the maximum allowable gradient,

c. Rather uniform temperature "plateau" at the top and,

d. Temperature uniform over any horizontal cross section.

Since the running and reheating mass flows differ greatly in magnitude, the formulation of the present problem has significant differences from that of the high mass flow running situation. The model used in analyzing the reheating problem is described as follows.

a. Gases enter top of bed at constant temperature with equal mass flow in all holes.

b. Local fluid temperature and bed temperature are equal.

c. Heat is lost at the periphery of the bed due to the overall heat transfer driving force of local temperature minus ambient temperature.

d. Longitudinal conduction is negligible.

Heat loss at the periphery is limited by the overall heat conductance coefficient, U, at each location along the bed. This conductance coefficient depends upon the insulation lining around the bed and the heat transfer

coefficient at the outer surface of the vessel. For a cylindrical wall, the conductance is

$$U = \frac{2}{D_b\left[\frac{1}{h\,r_{ex}} + \left\{\frac{\ln (r_{out}/r_{in})}{k}\right\}_1 + \left\{\frac{\ln (r_{out}/r_{in})}{k}\right\}_2 + \cdots\right]}$$

where D_b = bed diameter

h = heat transfer coefficient, including free convection and radiation

k = thermal conductivity

r_{ex} = exterior radius of pressure vessel

r_{in} = inner radius of layer

r_{out} = outer radius of layer

and the number subscripts refer to the concentric layers of insulation.

The simplest design for the insulation would consist of one which is invarient with length. In such a design, the coefficient U is approximately constant along the entire length of the bed. Assuming that the conductivity of the bed material in the transverse direction is infinite, we can write the following ordinary differential equation for steady state conditions.

$$\frac{\partial T}{\partial z} = -\frac{\pi D_b U}{\dot{m} c_p}(T - T_{amb})$$

where T = local temperature

T_{amb} = ambient temperature

$\dot{m}$ = mass flow

c_p = specific heat, fluid

z = distance from top of bed

Imposing the condition of a fixed temperature T_h at $z = 0$, and constant U, the solution is

$$T = T_{amb} + (T_h - T_{amb}) e^{-bz} \qquad (1)$$

where $b = \pi U D_b / \dot{m} c_p$

Since b varies inversely with mass flow, higher mass flows tend to produce a more uniform temperature along the length of the bed.

Some of the problems associated with the reheat process are best explained with an example. For this purpose we consider heating the bed from a cold, or relatively low temperature condition, to that required for maximum temperature operation. To produce a temperature distribution approximating that shown in Fig. 12, a two-step heating schedule is used. First, the bed is heated with a low mass flow rate for a long period of time, such that near steady state conditions are reached. Then a higher mass flow rate is used for a few hours, which causes the high temperature to penetrate the bed to the desired depth.

The differential equation describing the unsteady reheat process with the same assumptions as those resulting in the previous differential equation, except for the time dependance consideration is:

$$\frac{\partial T}{\partial z} = - \frac{\pi D_b U}{\dot{m} c_p} (T - T_{amb}) - \frac{MC}{\dot{m} c_p} \frac{\partial T}{\partial \theta}$$

The boundary conditions with constant U are:

$$T = T_h \quad \text{at} \quad z = 0 \quad \text{and} \quad \text{all} \quad \theta > 0$$

$$T = T_{amb} + (T_h - T_{amb}) e^{-b_o z} \quad \text{at} \quad \theta = 0$$

where
- $b = \pi D_b U / \dot{m} c_p$ for large mass flow $\dot{m}$
- $b_o = \pi D_b U / \dot{m}_o c_p$ for low mass flow $\dot{m}_o$
- C = specific heat of solid
- M = mass of solids per unit length of bed
- θ = time

The solution is:

$$T = T_{amb} + (T_h - T_{amb}) f\left(z - \frac{\dot{m} c_p}{MC}\theta\right) e^{-bz} \qquad (2)$$

where the function f is given by

$$f(\xi) = e^{(b-b_o)\xi} \qquad \text{for } \xi > 0$$

$$f(\xi) = 1 \qquad \text{for } \xi \leq 0$$

A distribution obtained with 490 lb/hr low mass flow followed by 18,000 lb/hr for a period of 3 hours, both flows entering bed at 3700°F, is shown in Fig. 13. The final temperature distribution after the high mass flow heating is essentially the low mass flow distribution shifted downstream by the amount $\dot{m}c_p\theta/MC$.

This heating schedule has approximated the desired shape (Fig. 12) except for a curved rather than linear ramp. The axial temperature gradient varies from 100°F/ft at 15 ft to 300°F/ft at 3 ft. As discussed earlier, a curved temperature ramp requires a larger bed than a linear ramp, and therefore is to be avoided.

In general, the temperature decrease along the length of the bed is due to heat loss through the insulation lining to the surroundings. The exponential shape (Eqs. 1 and 2) is produced in the case where the insulation conductance is constant along the bed. This leads to lower vessel temperatures at the bottom of the bed and reduced heat loss there. To produce a linear, rather than an exponential, distribution therefore requires increased heat loss from the lower portions of the bed. A simple and practical method of achieving such a result is to vary the thermal conductivity of the insulation along the bed, conductivity increasing as one moves from top to bottom. In the ideal case, the insulation conductivity could be varied so as to produce a uniform shell temperature when the bed temperature distribution is that needed for a maximum heat extraction run. This would tend to produce a linear temperature ramp because the heat loss from the vessel to its ambient surroundings would be uniform.

Reheating of the bed after completion of a run will be a process whose details depend on several factors, such as:

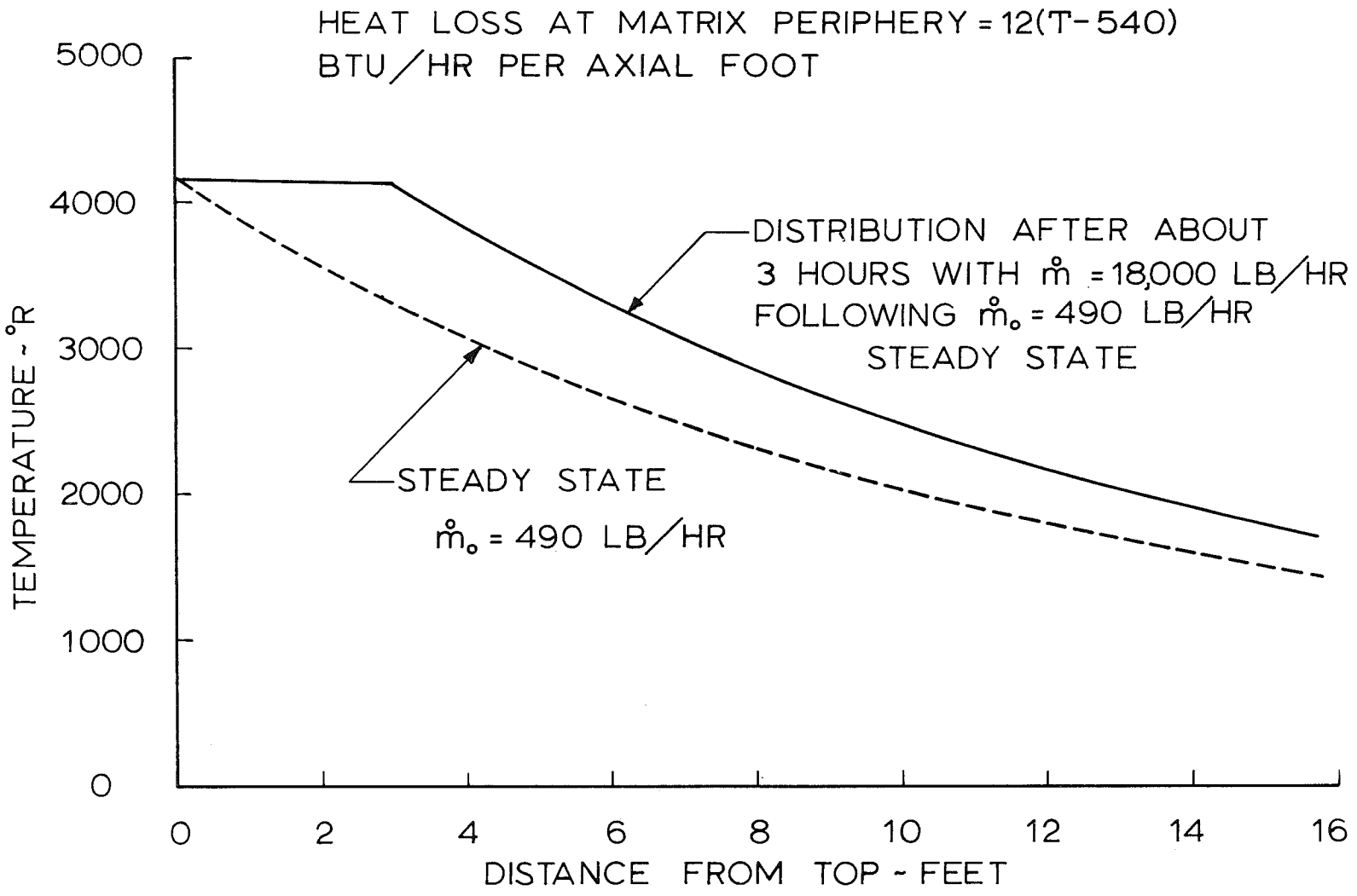

Fig. 13 Heater Matrix Axial Temperature Distribution after Reheat

a. Time available between heater runs,

b. Flow conditions needed next run, and

c. The temperature field existing in the heater after the last run.

For example, if another run is desired quickly, at the same flow conditions, the heater would be reheated with a high mass flow. This high mass flow would be the same as that used in the second phase of heating a bed from a cold start.

On the other hand, if the time between runs is long, the procedure would be to reheat at low mass flow with conditions such that at steady state the desired heater ramp temperature slope would be obtained and the top of the heater bed would be at its final desired value. Within a few hours of the actual run, the mass flow would be increased and the desired flat temperature plateau produced.

In general, the "idle" or standby reheat flow would be selected to produce the desired bed temperature ramp slope and temperature level corresponding to that anticipated for the next run.

Many variations in reheat procedure will produce the same end results. This is an area where actual experience will play a significant role in determining optimum procedures.

Another feature of the reheat temperature profile which requires careful design consideration is the initial bed temperature at the cold air inlet. In the example of Fig. 13 this temperature is 1300°F for a bed depth of 15 ft. If the bed were composed entirely of refractory material, the cold air impinging on refractories at this temperature would cause thermal stress fracture, and subsequent degradation of the lower portion of the bed. Two methods of eliminating this problem have been studied.

The first method applies to the use of refractory materials (thermal stress limited) throughout the bed. It involves limiting the temperature at the bottom of the bed to a value low enough to prevent failure of the refractories due to thermal shock. The relationships to be used in setting this limit are developed in Appendix H. In this case the temperature could not exceed roughly 300°F. Furthermore the bed temperature is to vary linearly in the axial direction. The approach mentioned above, of using insulation with varying thermal conductivity, would not be sufficient by itself to maintain such low temperatures. In addition, some other means of heat removal would have to be introduced.

Water cooling the grate used to support the heat storage bed is a possible approach.

The second method involves use of a thermal stress resistant material in the lower portion of the bed, preferably a metal. A ductile material would eliminate the need for very low temperatures at the air inlet. Hence, the bottom of the bed could be operated at temperatures in the vicinity of 1500°F, or even higher. The maximum length of the metal matrix will depend on the overall temperature distribution in the bed. Also, the metal matrix should be designed to have approximately the same volumetric specific heat as the adjacent ceramic matrix. A variation in the heat capacity per unit volume can be made by changing the bed porosity (hole diameter). With the same heat capacities in metal and ceramic, a smooth temperature distribution will be produced at the interface during reheating. Otherwise it is possible to develop high local axial gradients which increase thermal stresses in the ceramics. Detailed analysis of this approach might indicate the desirability of minimizing axial heat conduction in the metal. This could be accomplished by preventing complete surface-to-surface contact between the metal elements, with ridges or bosses, for example.

The analysis thus far has treated the bed as having infinite thermal conductivity in the radial direction. Therefore the temperature distribution has been uniform across the bed. We now investigate the effect of finite thermal conductivity to determine the nonuniformity of temperature in the radial direction. The equation for steady state heat conduction in cylindrical coordinates, applied to this problem, is

$$\frac{\partial}{\partial r}\left(r k \frac{\partial T}{\partial r}\right) = \frac{\dot{m} c_p r}{A_f} \frac{\partial T}{\partial z}$$

where A_f is the cross section area of the bed, and r is the radial distance from the center of the bed.

The presence of holes in the bed will influence its effective conductivity. Since the temperatures are high, considerable heat transfer by radiation across the holes will take place. In fact, at the highest temperatures, the radiation is so large that the effective heat transfer across the holes by radiation is greater than that by thermal conduction through the material itself. In the cooler region at the bottom of the bed, the effective conductivity is less than that of the material. For simplicity in this analysis the effective conductivity is taken equal to the

material conductivity and constant. This reduces the equation to

$$\frac{\partial^2 T}{\partial r^2} + \frac{1}{r}\frac{\partial T}{\partial r} - \frac{\dot{m} c_p}{k A_f}\frac{\partial T}{\partial z} = 0$$

The boundary conditions are

$$T = T_h \qquad \text{at} \qquad z = 0$$

$$k\frac{\partial T}{\partial r} = -q_{loss} \qquad \text{constant at} \qquad r = \frac{D_b}{2}$$

where q_{loss} is the heat flux at the periphery of the bed. The solution is, (see Ref. 8, pages 203, 328 and 329).

$$T = T_h - \frac{D_b q_{loss}}{k}\left[Z + \left(\frac{r}{D_b}\right)^2 - \frac{1}{8} - \sum_{n=1}^{\infty} e^{-\beta_n^2 Z}\left\{\frac{J_o\left(\frac{2r}{D_b}\beta_n\right)}{\beta_n^2 J_o(\beta_n)}\right\}\right]$$

where $Z = \pi k z/\dot{m} c_p$

J_o = Bessel function of first kind of order zero

J_1 = Bessel function of first kind of order one

and β_n = nth root of $J_1(\beta) = 0$, (note: $\beta n > 0$)

Using this equation, the distribution for a typical low mass flow condition has been calculated. In this calculation, a linear temperature ramp was assumed, i.e., the average temperature across the heater varies linearly in the temperature ramp portion of the distribution.

The results are presented as a plot of temperature versus radius with length a parameter in Fig. 14. It is evident from this plot that the radial conduction losses, with a low mass flow, cause a large radial temperature variation. Furthermore, this variation still exists in the bed after the final high mass flow heating period is terminated. A typical distribution when the bed is in this state is illustrated by Fig. 15. From this plot it is clear that the axial temperature gradient approaching the plateau from below will be

HEAT LOSS AT BED PERIPHERY = 44,000 $\frac{BTU}{HR\ FT}$

RADIAL CONDUCTIVITY IN BED = 3.0 $\frac{BTU}{HR\ FT^{\circ}F}$

REHEAT MASS FLOW = 490 $\frac{LB}{HR}$, UNIFORM OVER CROSS SECTION

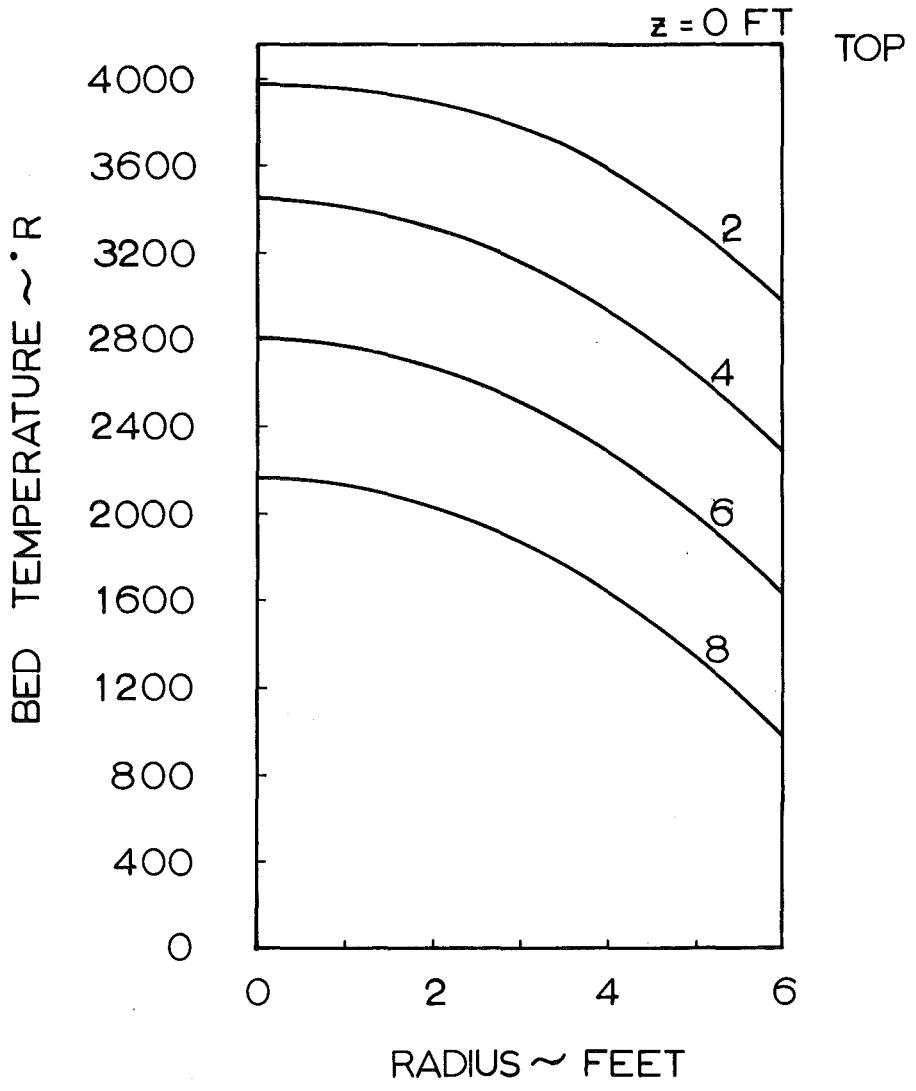

Fig. 14 Steady State Radial Bed Temperature Distribution

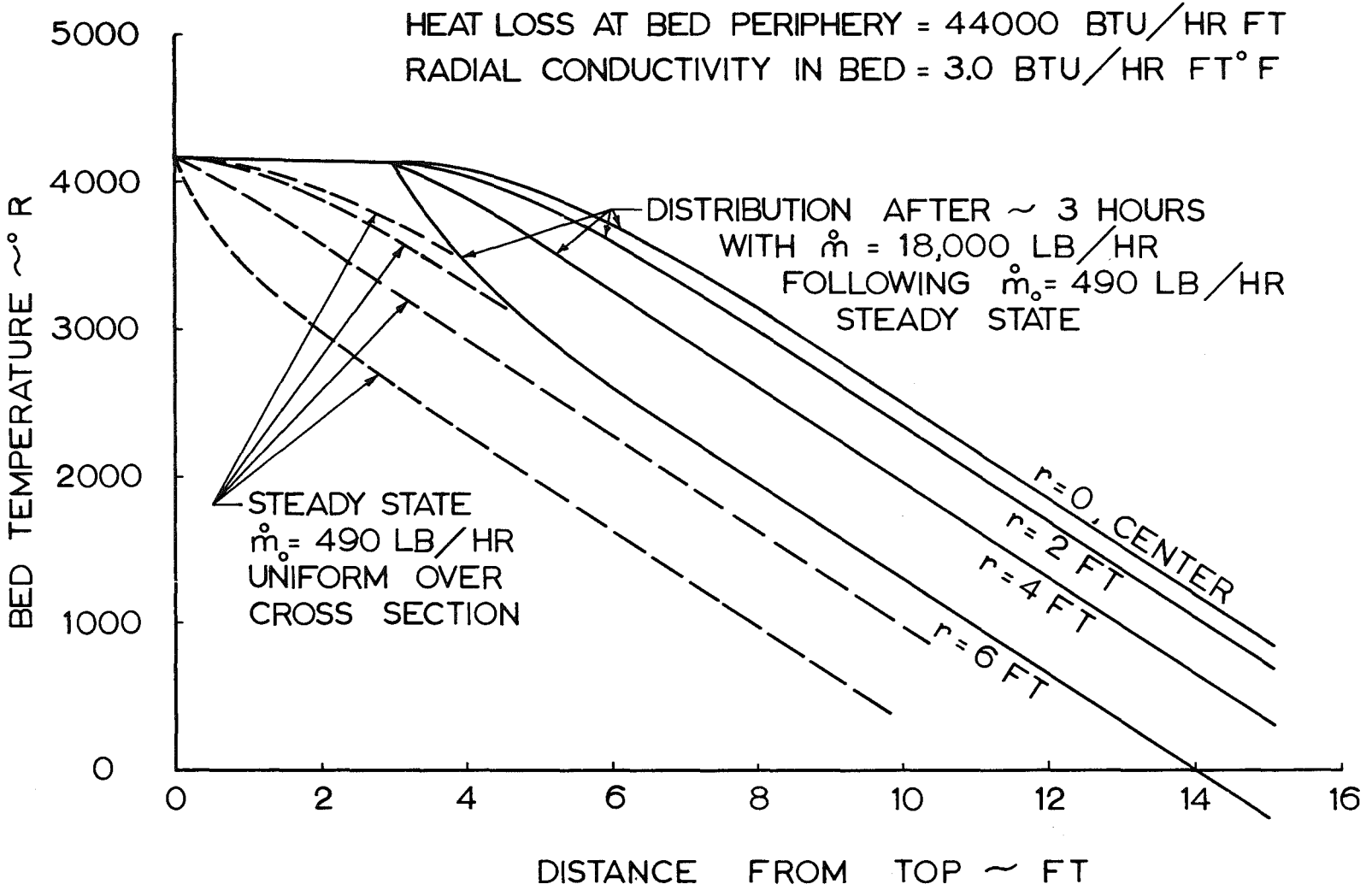

Fig. 15 Heater Matrix Temperature Distribution

excessive in the outer region of the bed. Running with such a distribution would cause high thermal stress in that region.

Thus the nonuniform radial distribution of temperature creates two problems. The energy storage capacity is reduced for a given maximum bed temperature, and regions of high thermal stress are introduced in the bed. The use of a cored brick bed, or any bed consisting of parallel holes, provides what appears to be a simple solution. The combustion gas flow could be restricted to a narrow annular region at the periphery of the bed. This would restrict the heat input to this annulus, giving a steady state temperature distribution with smaller radial gradients in the bed. Such a flow restriction would be used only during low heating rates, full cross sectional flow being required when a high rate is used for final heating. This can be accomplished by having two separate plenums under the grate on which the bed rests.

Two nozzles would therefore be used at the bottom of the pressure vessel, one communicating with the annular plenum, the other communicating with the circular plenum in the center.

The results of this analysis may be summarized as follows.

1. The insulation liner should be designed with its thermal conductance increasing toward the bottom of the bed, in order to achieve a linear ramp in the temperature distribution.
2. The thermal stress problem at the air inlet to the bed may be solved by providing additional cooling, e.g., possibly with a cooled grate, or by using a metal matrix in the lower portion of the bed.
3. A uniform radial distribution of temperature in the bed can be produced by heating with gas flow near the periphery of the bed. This can be done by providing an annular exit for the combustion gases at the bottom of the bed.

BURNER

The burner provides the combustion gases for heating the ceramic storage bed. Several general requirements for the burner system may be stated. It should provide a wide range of flow rates and temperatures to permit good control over the complete heating and reheating process. Clean combustion is absolutely essential; the presence of carbon in the combustion products has a deleterious effect on the refractories. Direct flame impingement on refractories should be avoided because of the resulting thermal stresses which would cause refractory breakup and dusting.

A single burner or multiple burners can be used, depending on the range available with a single burner, preheating requirements for downstream ducting, and the details of the heater system operation. It is not necessary at this time to specify the number of burners, however, a general design concept which will satisfy the requirements set out above is needed.

To assure clean combustion, we first specify a 100% premix design. To reduce refractory dusting, the combustion chamber will be water cooled metal rather than refractory lined. Excess air must be available to permit combustion product temperatures below 1000°F. Such values are necessary when heating the bed from a cold temperature condition.

The problem of cooling and structural strength at elevated temperature are greatly relieved by designing the burner to be removed before the heater is pressurized. In this way the burner does not have to withstand the high operating pressure and can be made of relatively thin material which is more easily cooled.

These features are incorporated into the design sketched in Fig. 16. The required range of combustion gas flow was

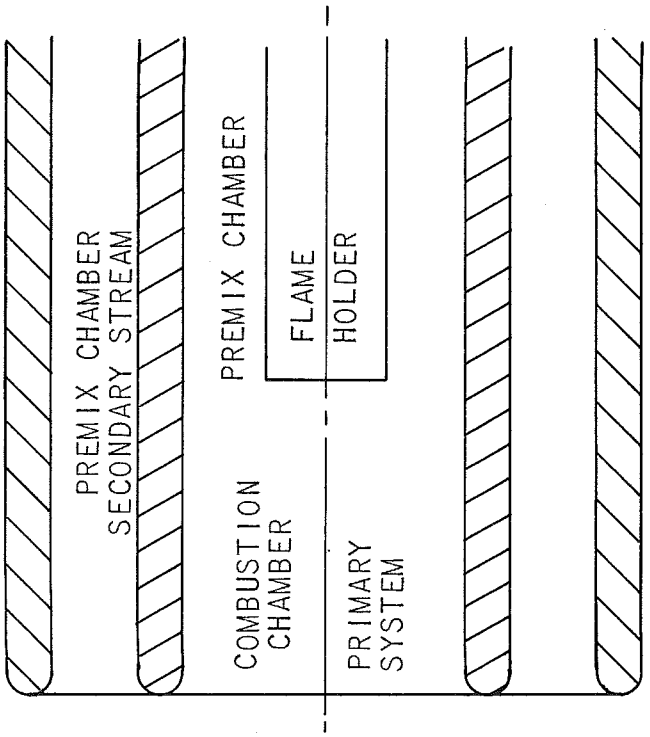

Fig. 16 Burner Concept

estimated at 0.11 to 5.0 lb/sec. Flashback data from tests with FluiDyne's premix burner together with flashback and blowoff information from Refs. 4 and 5 were used in establishing feasibility of this design concept. The overall length of the burner would be roughly 4 feet and the outside diameter about 7 inches. The fuel was assumed to be natural gas or propane, with oxygen enrichment required at the higher temperatures.

Referring to Fig. 16, the center or primary stream burns to completion within the cooled combustion chamber, with mass flows from .1 to 1.0 lb/sec permissible. Very low temperatures can be produced by added air through the secondary flow passage.

In order to reach high mass flows at high temperatures, additional air, oxygen, and fuel is added to the secondary stream, in the range 0.5 to 5.0 lb/sec. (The lower flow limit is determined by flashback.) The secondary stream reacts in the heater dome, which has been preheated to a high temperature with the primary stream. Having the dome refractories hot insures the combustion process will not be quenched by radiation losses.

A second design concept is sketched in Fig. 17. This

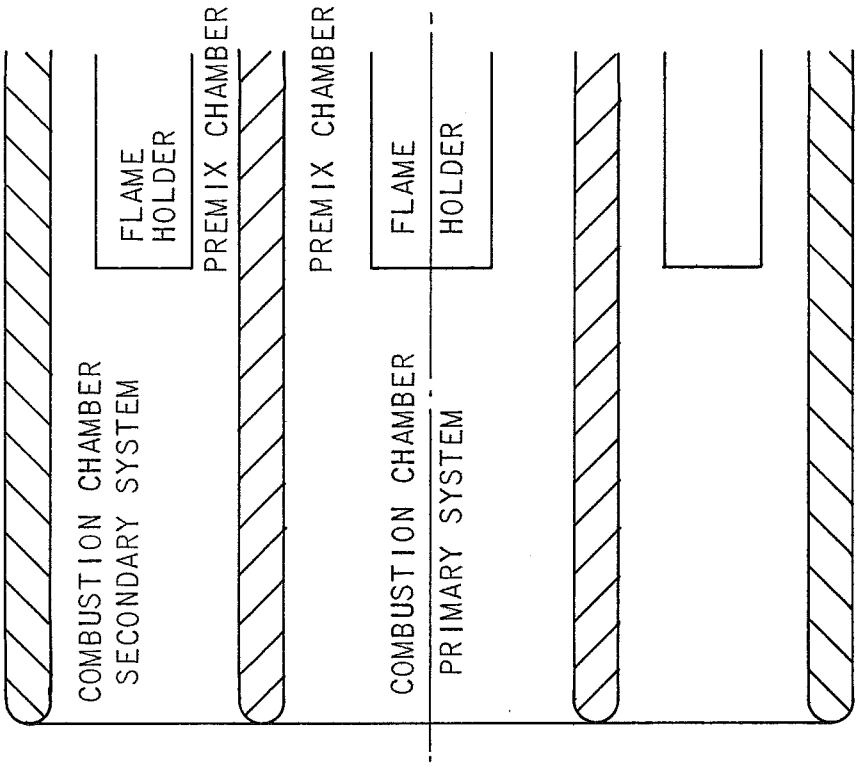

Fig. 17 Alternate Burner Concept

is the same general configuration as Fig. 16, but provides a combustion chamber for the secondary flow. The secondary flow is an annulus with an annular flameholder. This provides control of the combustion process, which is not the case when combustion occurs in the dome region. In this way, circulation of incomplete combustion products over refractories would be avoided. The purpose of two combustion chambers, rather than one large chamber, is to reduce the cold surface area seen by the flame at low flow rates and thus reduce radiation temperature losses which can be large.

7. START-STOP EFFECTS

The method used in bringing the heater system up to pressure can seriously affect the size and design of the heater system (and other tunnel components), and/or the heater design can dictate the procedures used to start the facility. The purpose of our analysis has been to describe with enough quantitative adequacy the starting processes so as to permit an evaluation of the interaction between these procedures and tunnel component design, with emphasis on the heater system.

A device whose inclusion or exclusion plays an important role in both operational procedure and design is the hot valve, i.e., a shut-off valve between the heater and the nozzle. Perhaps the most important potential value of the hot valve is in the sizing of the heater. With a hot valve, savings of stored air, vacuum capacity, and heater stored energy are possible. Also, the heater is not necessarily depressurized between runs, permitting successive runs without reheating. However, a hot valve is not quite as attractive as it first may seem. One finds that the compressive temperature rise of the gas above the bed is a maximum with a hot valve. This could lead to material thermal degragation problems. In addition, if a fairly flat temperature-time relationship is desired during the data taking phase of the tunnel tests, one must wait for the compressive temperature rise to decay, once the valve is opened (see Appendix Fig. 4F). During this period, significant quantities of air and energy, approaching and perhaps even exceeding those losses without a hot valve, are flowing out the nozzle. The temperature rise and the corresponding decay can be reduced by introducing part of the cold air directly into the heater dome, probably through the burner port. However, this technique can also be applied to the no-hot valve situation to produce longer run times and/or reduce the bed volume.

With a hot valve there is no advantage to rapid pressurization. Thus, the heater can be designed upon steady state requirements alone. For instance, if the factor limiting mass velocity is bed flotation, only the pressure gradient situation at steady state is analyzed. Without a hot valve, or cold air bypass, a lower steady state pressure gradient is required, since in order to reach the steady state pressure the steady state pressure gradient will be exceeded during the starting process.

The start-stop study considered primarily the problems and procedures connected with heater operation without a hot valve. This is a necessary prerequisite to the evaluation of hot valve advantages and disadvantages as well. The results

obtained permit eventual quantitative evaluation of the two methods of operation, i.e., with or without a hot valve.

During the pressurization process the gas temperature in the dome region of the heater and the temperature of the gas expended from the heater rise above the quasi-steady state value. The magnitude of the rise depends on the specific heater design, initial pressure, and pressurization rate. Fig. 1F (in Appendix F) illustrates the effect of the latter two, since the pressurization rate is related to the value of C_1. The hot valve case yields a temperature rise factor of $\gamma-1$ (= .25 in Fig. 1F) over the steady state value. γ is the effective ratio of specific heats, (that γ which best describes the process). Since the air in the dome region of the heater loses heat to the refractories and through the shell, the effective γ is always less than that for air under adiabatic conditions.

The compression temperature rise decreases the time and mass expended during the pressurization process, (see Fig. 2F) but causes other less desirable effects which were qualitatively discussed with regard to the hot valve. These effects include the flow and energy losses occurring during decay of the compressive temperature rise (premising the need for a flat temperature versus time curve during the data run) and overheating of the refractories (Figs. 2F and 4F).

Another phenomena is the variation of the axial mass flow rate as one moves through the heater. This happens only during start or stop operation when the pressure level is changing, (ignoring secondary effects). This phenomena becomes of importance with regard to bed flotation and thermal shock considerations. Because of the void volume distribution in the heater and the fact that more mass must increasingly be stored in all void volumes as the pressure rises, the mass flow is a maximum at the heater inlet and a minimum at the heater outlet. This effect must be considered with respect to avoiding bed flotation. Similarly, thermal stress problems, which are most severe in the lower regions of the bed, with a linear bed temperature ramp will be aggravated by flows in excess of those occurring during steady state operation. Fig. 3F presents the results of an analysis of this flow distribution phenomena.

Ordinarily the heater is depressurized to atmospheric pressure. Methods for calculating the mass expended during this process and corresponding times are presented in Appendix F.

8. HEATER SIZE REQUIREMENTS

It has been established that the storage heater for the Tripltee probably can comprise a single, large vessel. The properties of refractory materials suitable for this application have been estimated. The probable values of insulation thickness have been established. The reheating process has been analyzed, and it has been established that adequate control over this process can be exercised to insure that desired temperature distributions can be attained.

It is now necessary to carry out the final analysis of the matrix to determine the probable volume and proportions of the heater. The influence of material choice and material density should be established by this analysis. A feasible general arrangement of the heater should be evolved.

The thermal analysis used to estimate the matrix performance is described in Appendix G. Basically, it is a finite difference solution of the problem considered by the Hausen analysis. It is set up to take into account the finite lateral conductivity of this material. It also permits analysis of arbitrary initial temperature profiles. Variable (with temperature) fluid and matrix properties may be included in the analysis, however, constant values were used in obtaining the present results. The computations were carried out on a digital computer.

Combinations of matrix geometry and physical properties for final analysis were selected for the two materials of interest, zirconia and magnesia. Two values of density were selected for each material. The lower value in each case corresponds to a density which is presently being attained in commercial production of refractory brick and related shapes. The higher value, 95% of theoretical density, represents that which is being attained by the technical ceramics industry in shapes similar to the tubular shape shown in Appendix C.

Minimum volume of the matrix is achieved when the rate of heat extraction is as high as possible (see Section 1). This will be limited by pressure drop and by the thermal stress associated with the temperature difference in the matrix elements needed to cause heat flow to the surface. For a fixed value of thermal stress, equal to one half of the estimated stress for fracture, the value of the matrix temperature rise per unit length was calculated for hole sizes and spacing combinations that would yield a pressure drop about 0.3 of that which would float the elements at the top of the matrix. (See Appendix G for discussion of this analysis.) The final selection of hole size and spacing was based on considerations of minimum web thickness for the

ɔred brick shape and minimum wall thickness for the tubular nape.

The variation with time of the temperature distribution n the matrix was calculated for five combinations of mate- ial, density, hole size and spacing, matrix diameter, and nitial temperature distribution. These are shown in Figs. 18 through 22. The length of the matrix is defined as that which results, after 35 seconds, in a temperature droop of the discharge air equal to about 10% of its initial (absolute) temperature. Temperature-time curves are presented in Figs. 24 through 28. The resulting maximum value of mean-to-hole surface temperature difference is also shown.

The matrix volumes indicated by these calculations are tabulated below.

Material	Density	Matrix Diameter (feet)	Hole Diameter (inch)	Hole Spacing (inch)	Matrix Length (feet)	Matrix Volume (cu.ft)
ZrO_2	75%	10.5	.212	.312	53.3	4600
ZrO_2	95%	10.5	.15	.23	15.5	1340
MgO	88%	12	.194	.294	15.1	1700
MgO	95%	12	.15	.23	9.9	1120
MgO	95%	10.5	.17	.25	12.7	1100

Although its effect is somewhat masked by matrix dimensional differences, the bed volume differences displayed in the above table come about more through material density variations than any other factor. Next in importance is the choice of material with magnesia appearing to have a slight advantage.

An interesting and encouraging result is the volume for the 88% dense magnesia. Should the properties of this material equal or exceed those estimated for this calculation, it would mean that refractory brick practice would be suitable for the Tripltee matrix elements. However, note that the calculations indicate a further, very substantial reduction in volume should be possible by the use of the more dense material.

The indicated differences between mean and hole surface temperatures are all excessive near the inlet end of the matrix. This is due to the high temperature at the inlet end. The resultant thermal stresses would be completely unacceptable. Another calculation was carried out for the 88% dense magnesia matrix assuming that the inlet bed temperature was reduced to about 160°F (from 1200°F), while continuing the

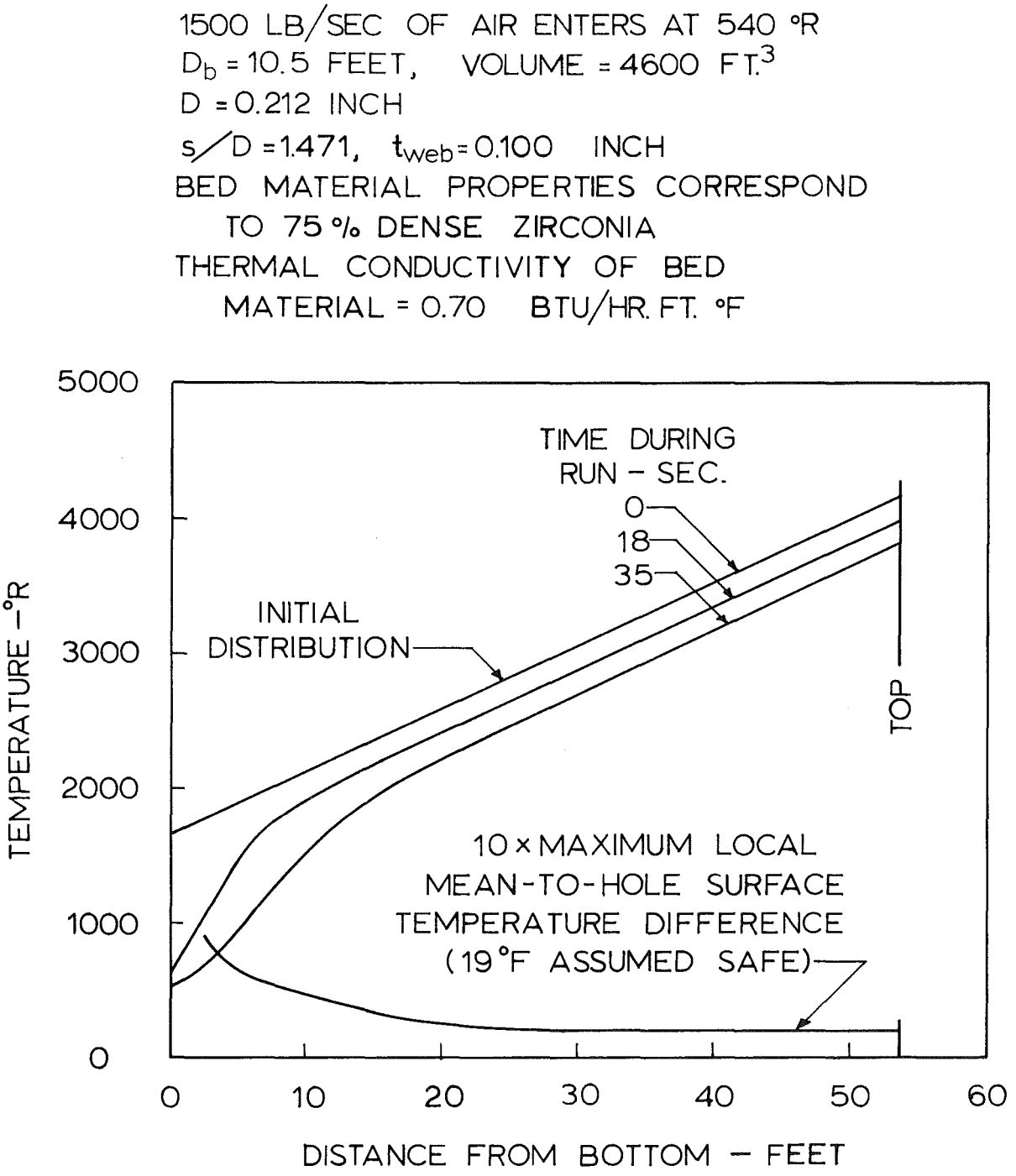

Fig. 18 Effect of Run on Matrix Temperature Distribution and Local Solid Temperature Differences

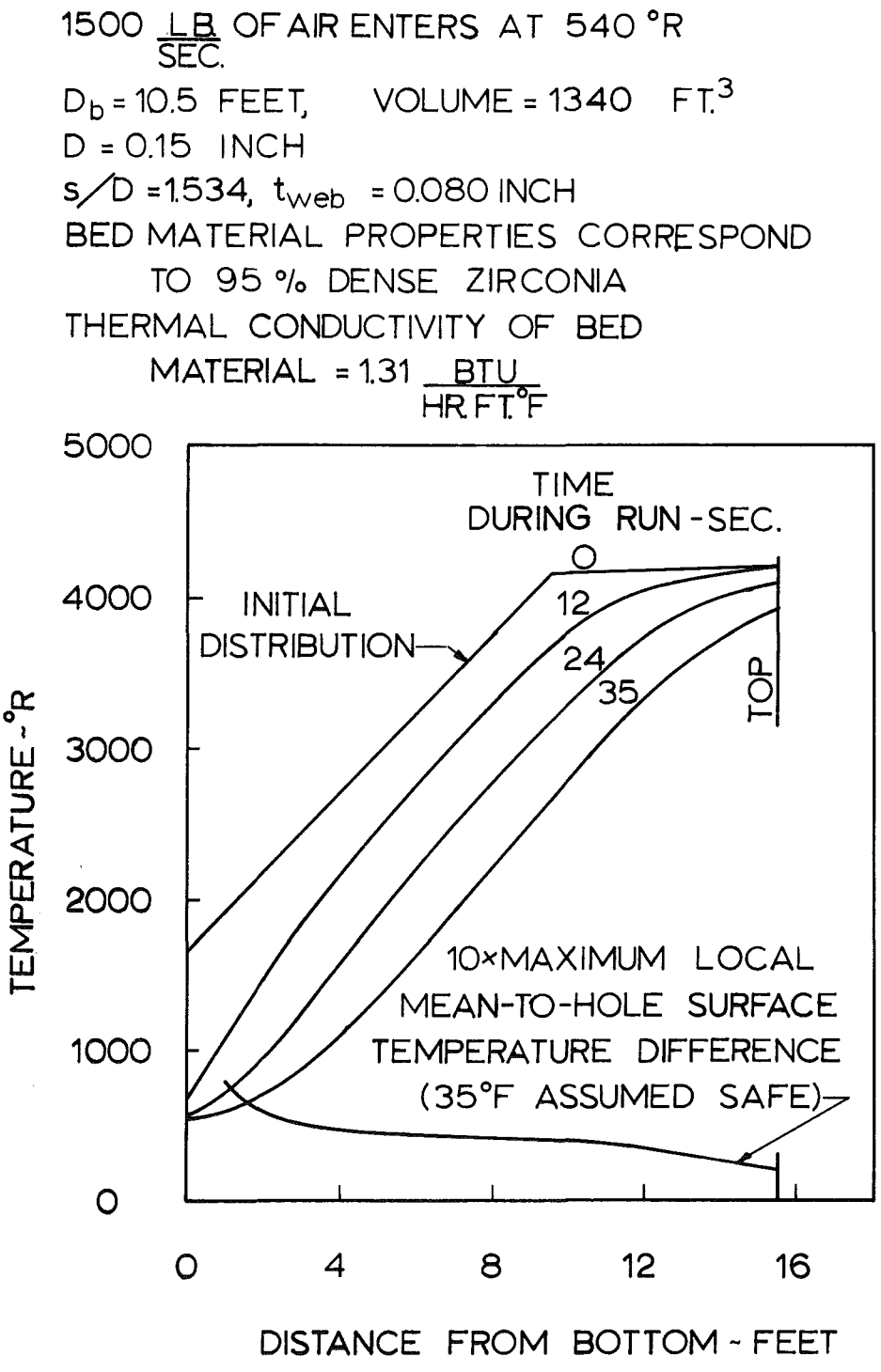

Fig. 19 Effect of Run on Matrix Temperature Distribution and Local Solid Temperature Differences

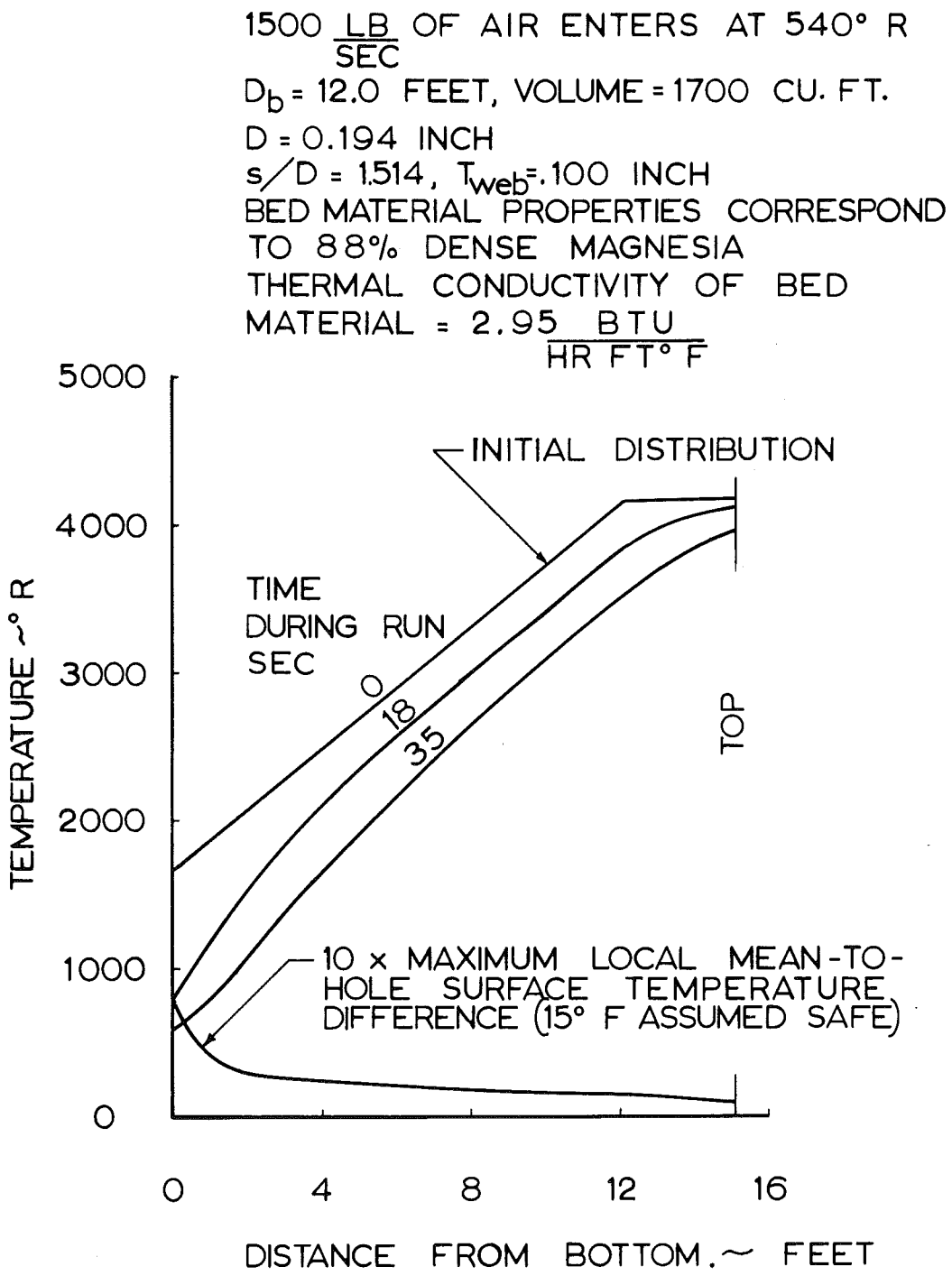

Fig. 20 Effect of Run on Matrix Temperature Distribution and Local Solid Temperature Differences.

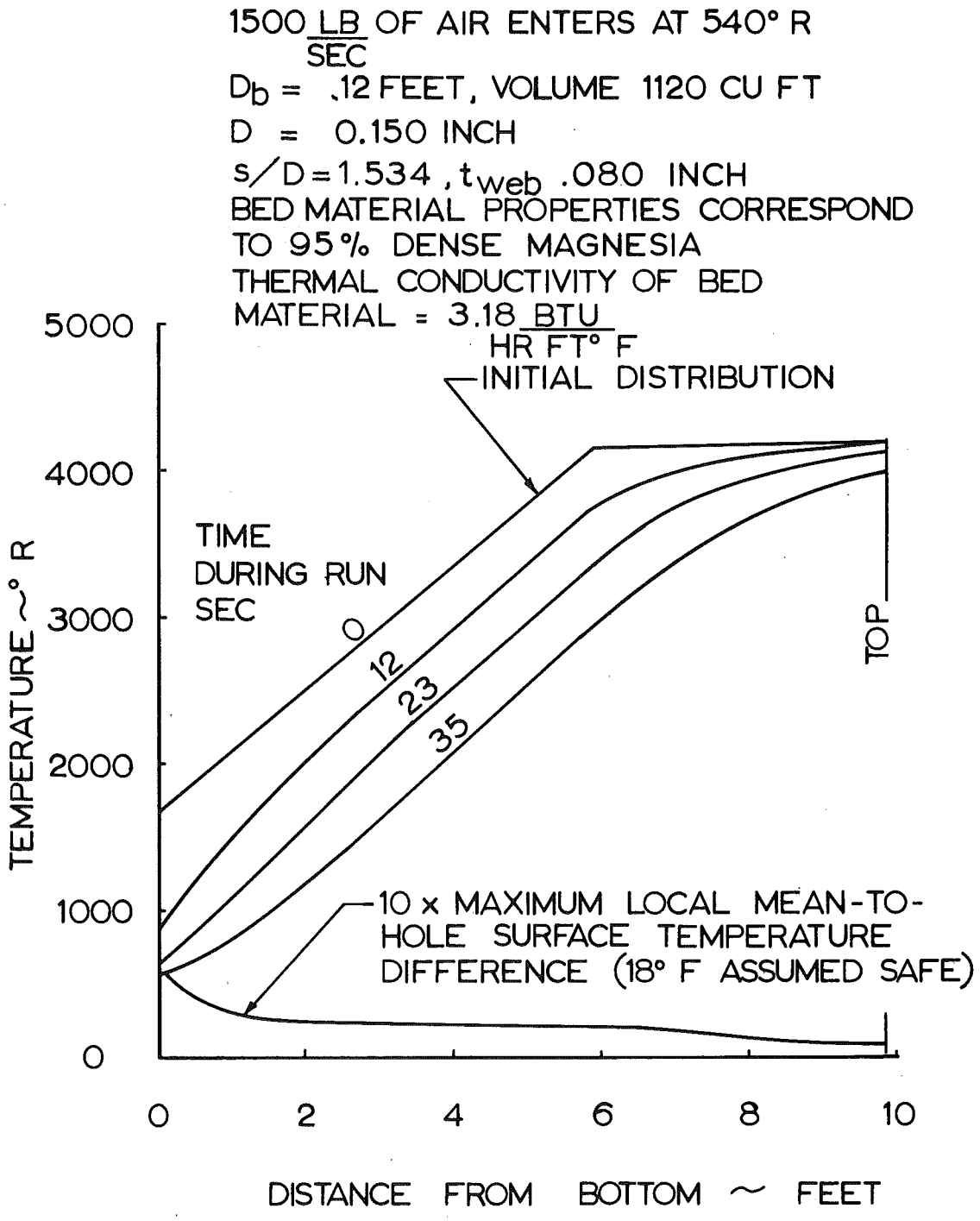

Fig. 21 Effect of Run on Matrix Temperature Distribution and Local Solid Temperature Differences

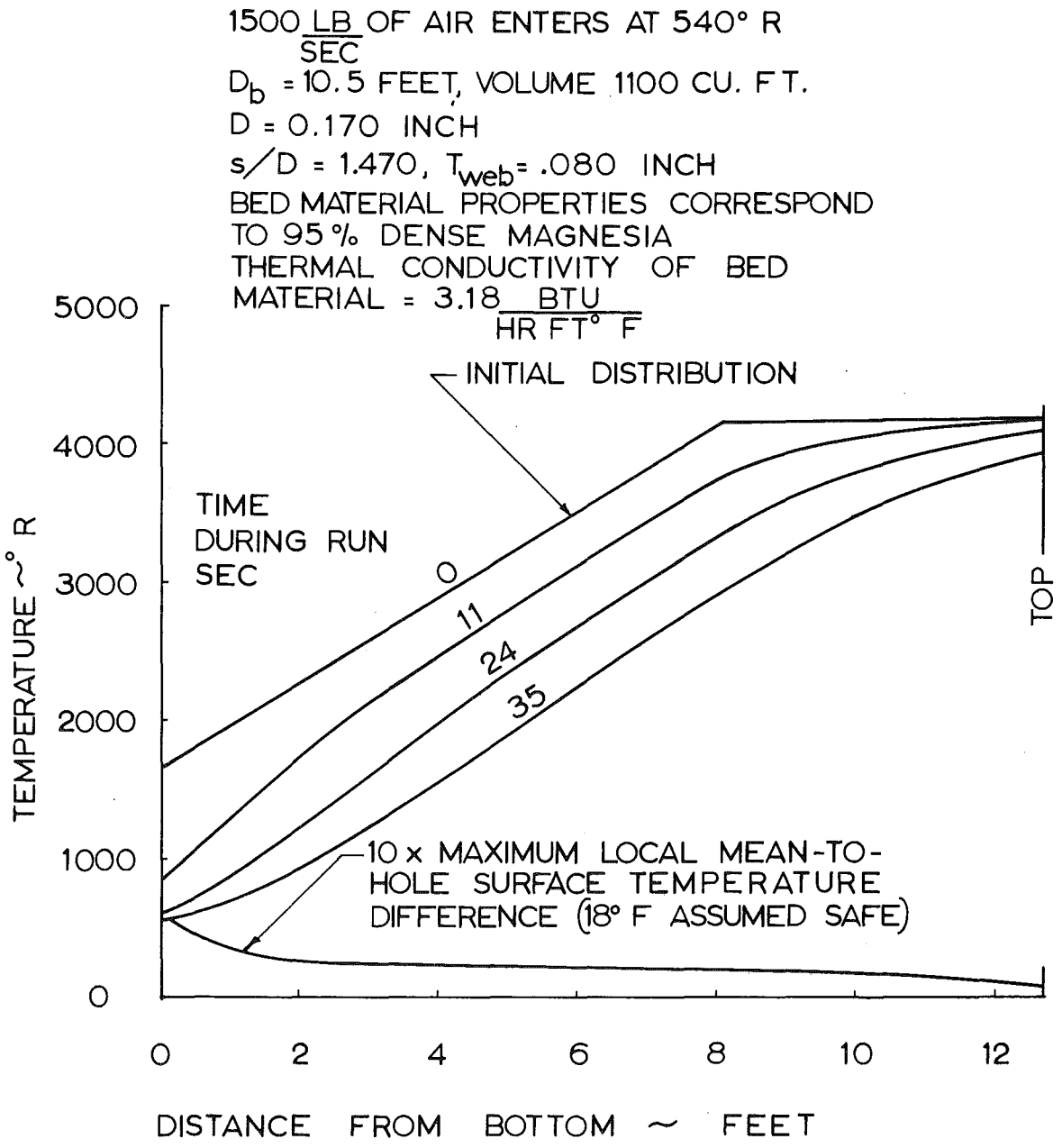

Fig. 22 Effect of Run on Matrix Temperature Distribution and Local Solid Temperature Differences

1500 LB/SEC OF AIR ENTERS AT 540 °R
D_b=12 FEET, VOLUME = 2280 FT.^{3}
D=0.194 INCH
s/D=1.514, t_{web}=0.100 INCH
BED MATERIAL PROPERTIES CORRESPOND TO 88 % DENSE MAGNESIA
THERMAL CONDUCTIVITY OF BED MATERIAL = 2.95 BTU/HR. FT. °F

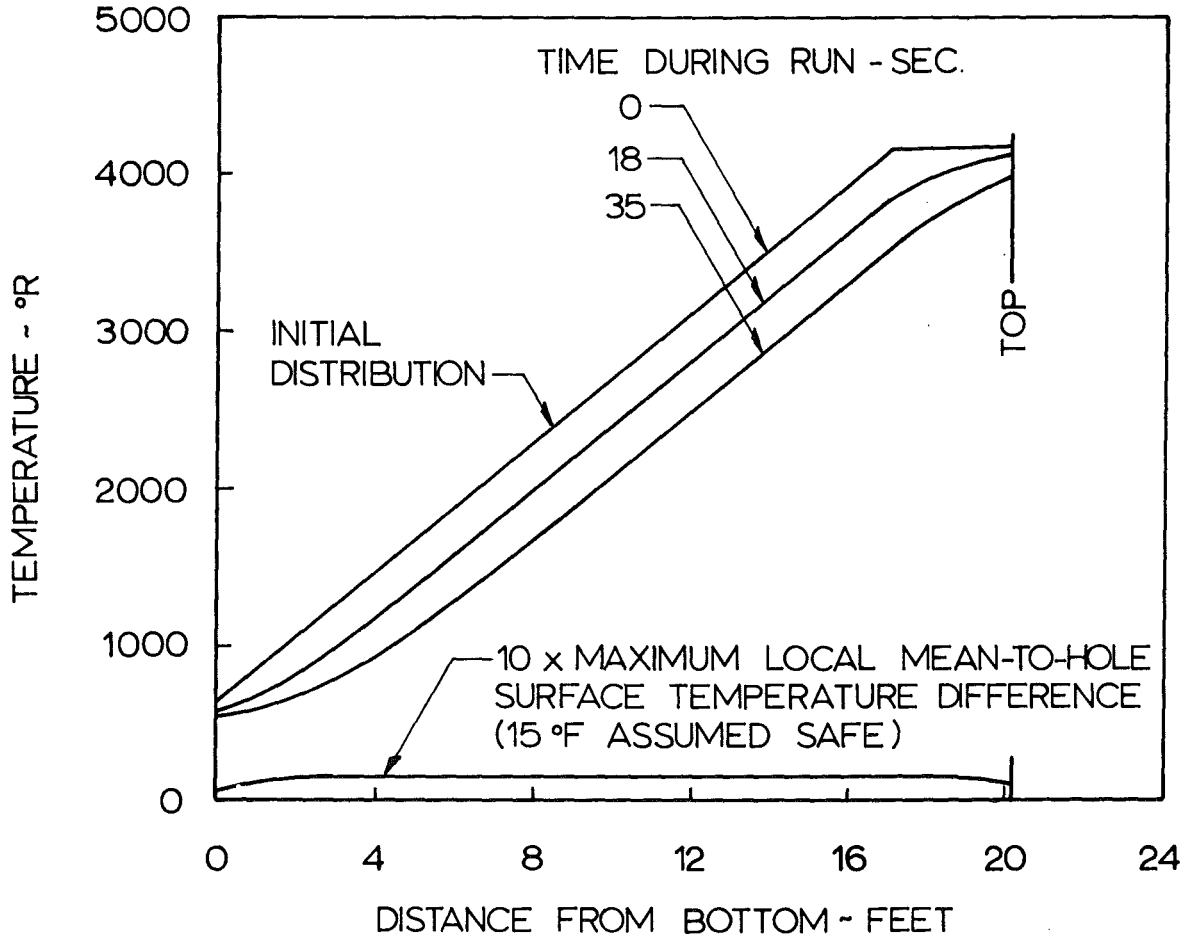

Fig. 23 Effect of Run on Matrix Temperature Distribution and Local Solid Temperature Differences

1500 LB/SEC OF AIR ENTERS AT 540 °R
D_b = 10.5 FEET, VOLUME = 4600 FT^3
D = .212 INCH
s/D = 1.471, t_{web} = .100 INCH
BED MATERIAL PROPERTIES CORRESPOND TO 75% DENSE ZIRCONIA

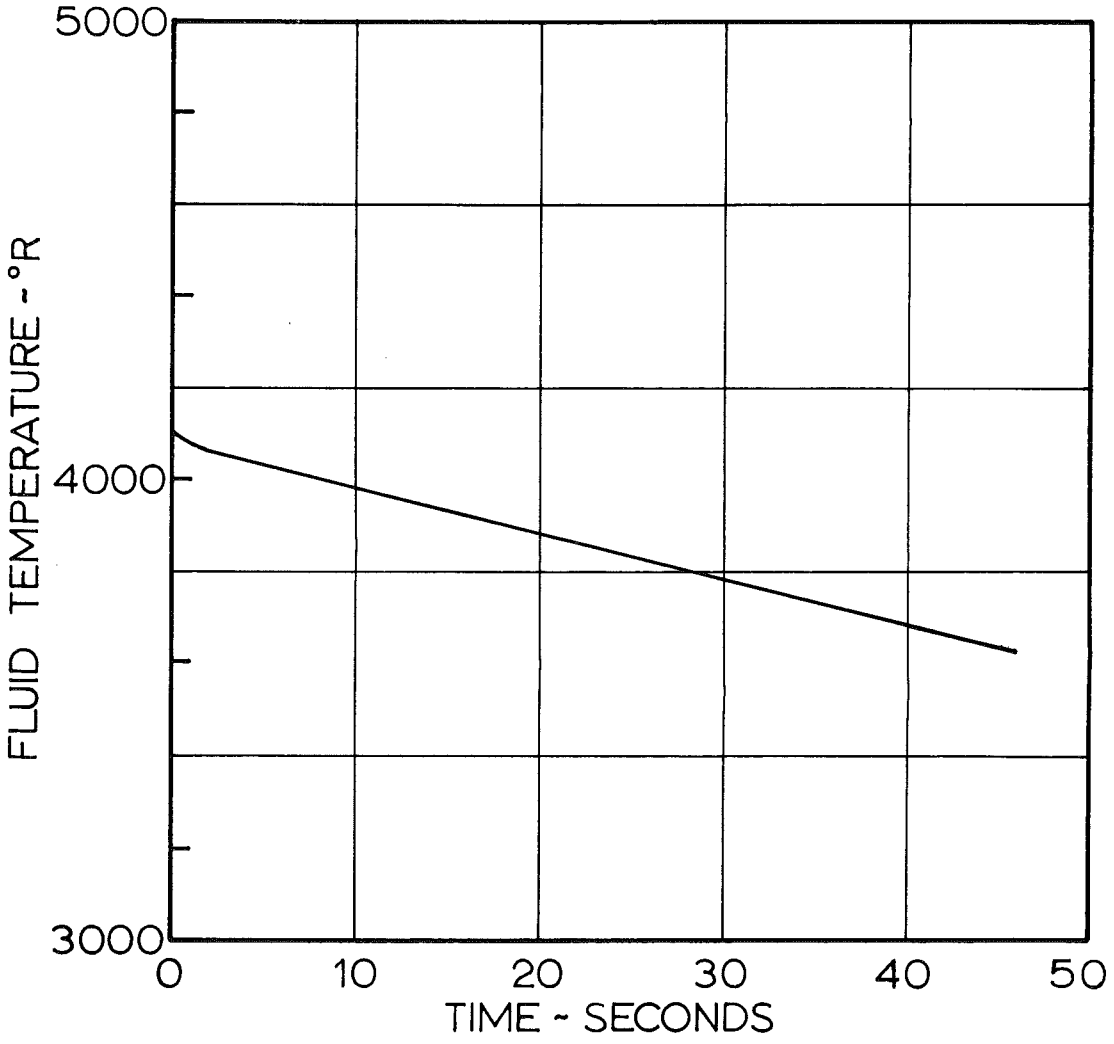

Fig. 24 Matrix Exit Air Temperature History

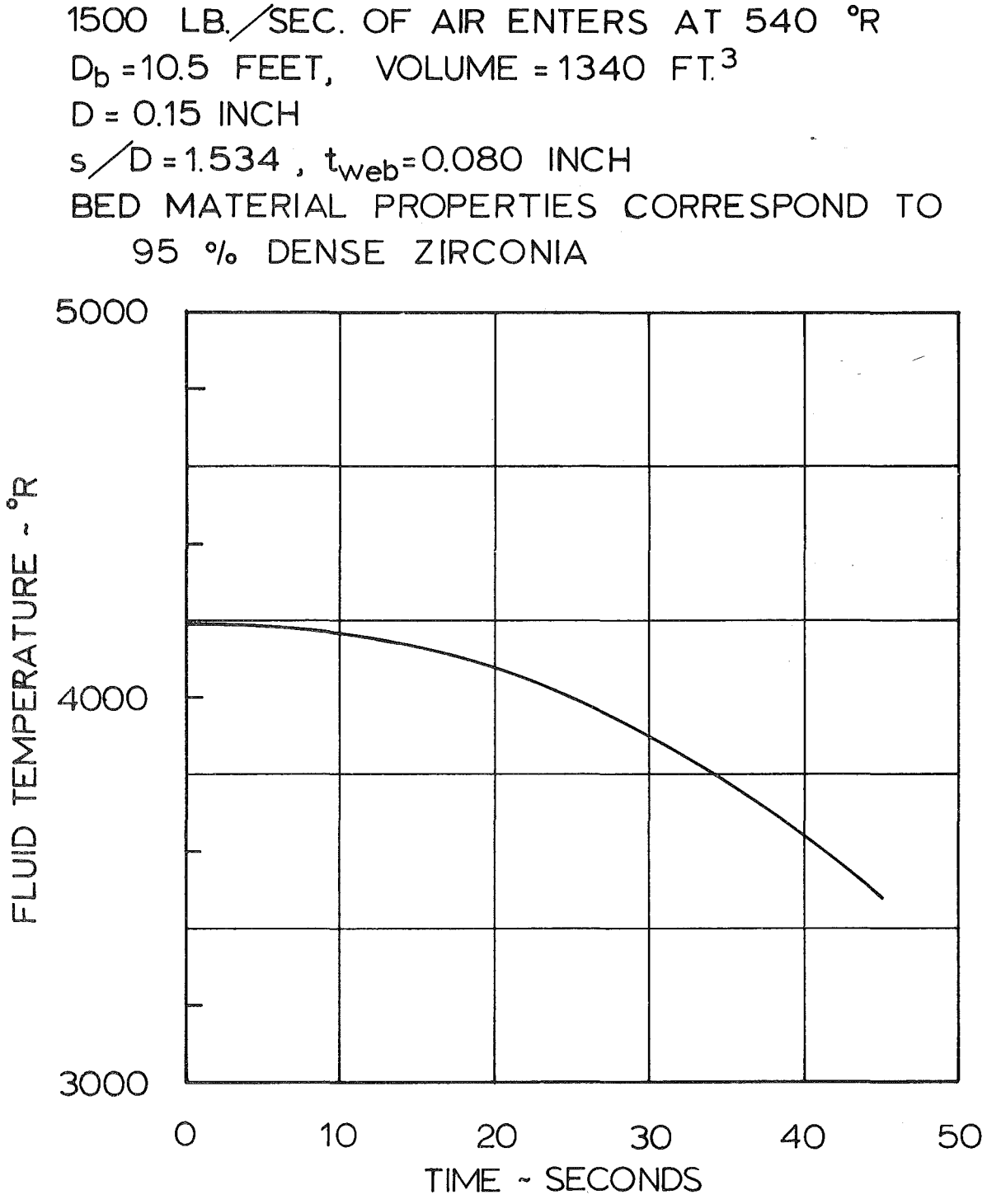

Fig. 25 Matrix Exit Air Temperature History

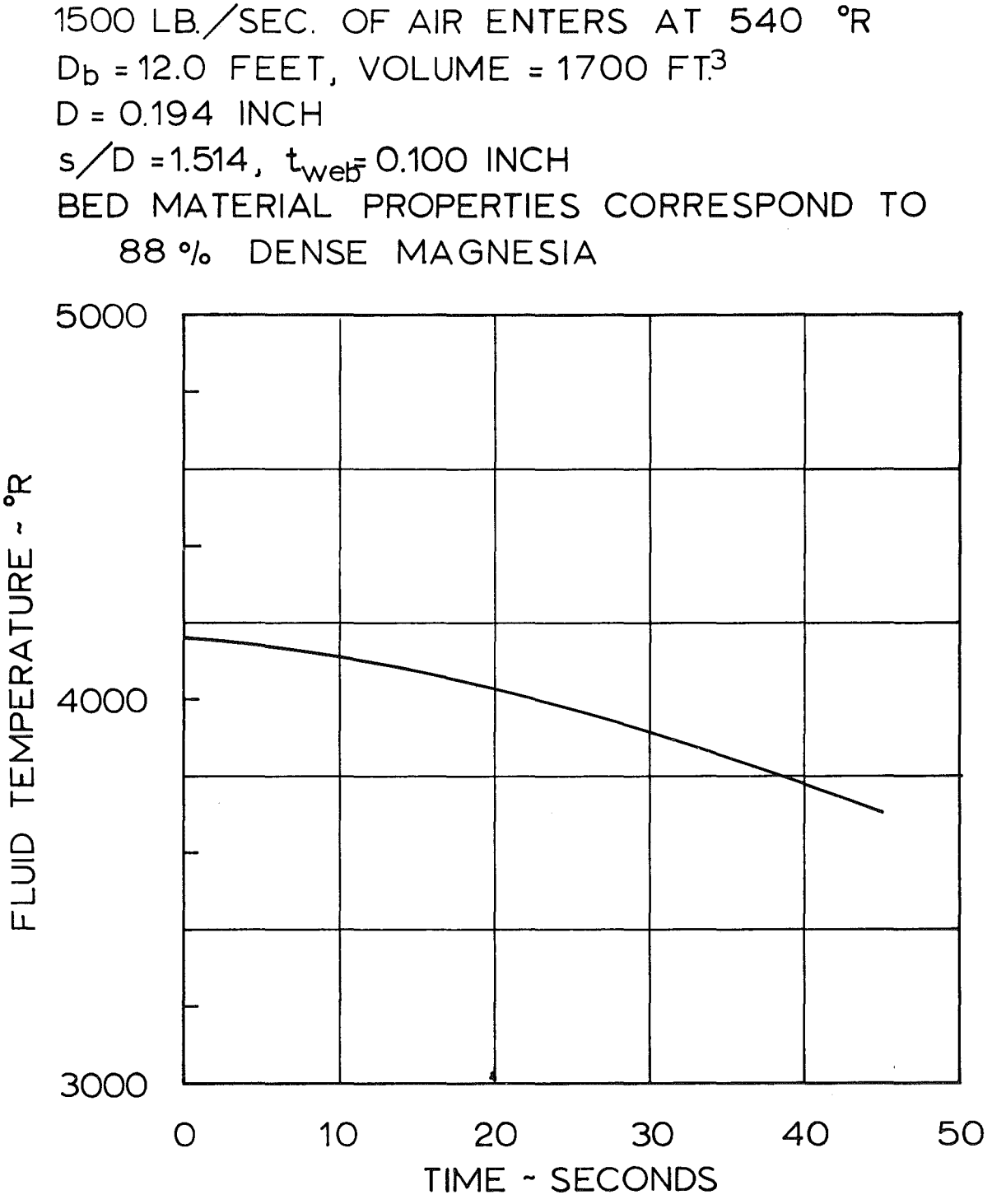

Fig. 26 Matrix Exit Air Temperature History

1500 LB/SEC OF AIR ENTERS AT 540 °R
D_b = 12.0 FEET, VOLUME = 1120 FT^3
D = .150 INCH
s/D = 1.534, t_{web} = .080 INCH
BED MATERIAL PROPERTIES CORRESPOND TO 95% DENSE MAGNESIA

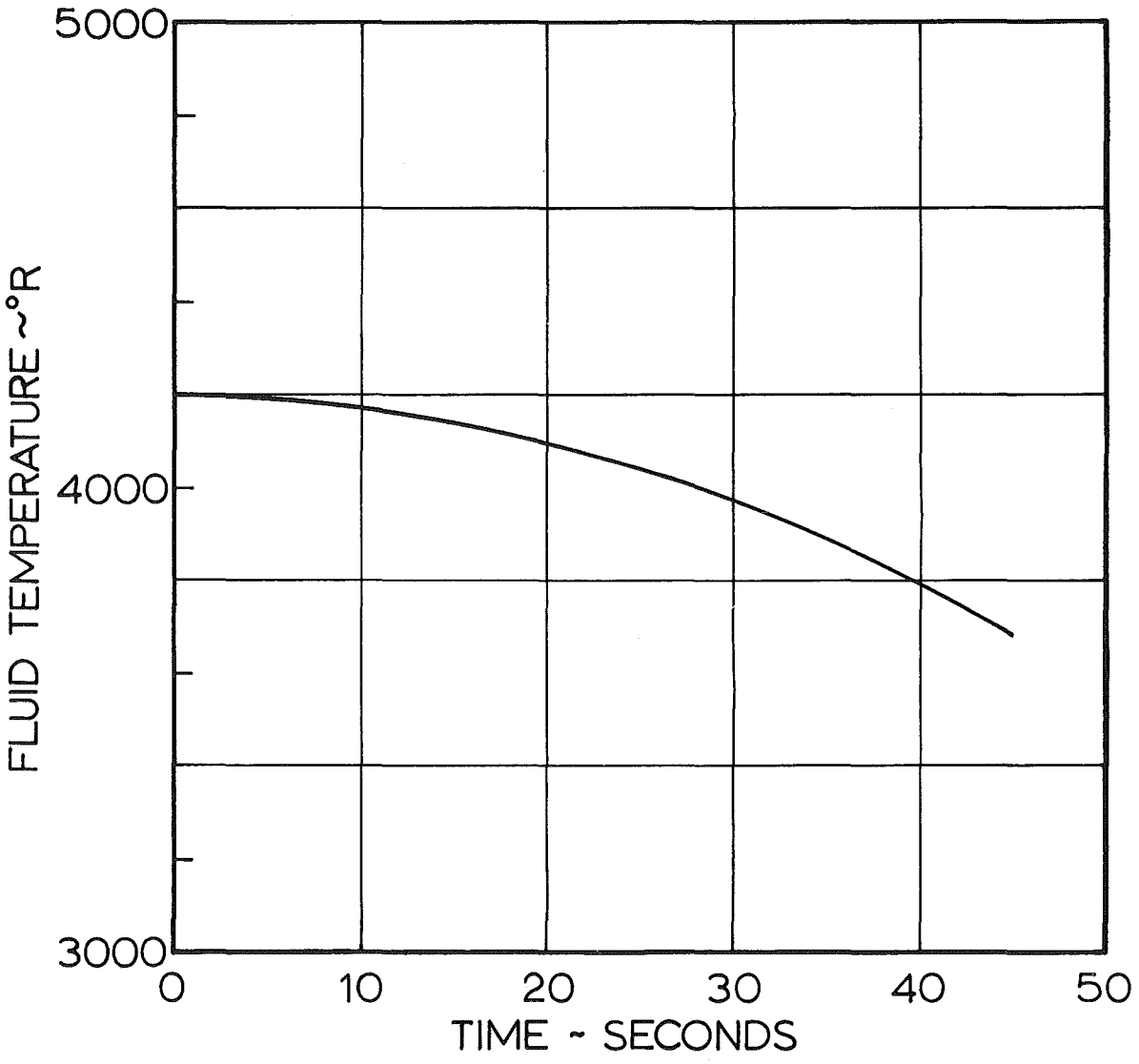

Fig. 27 Matrix Exit Air Temperature History

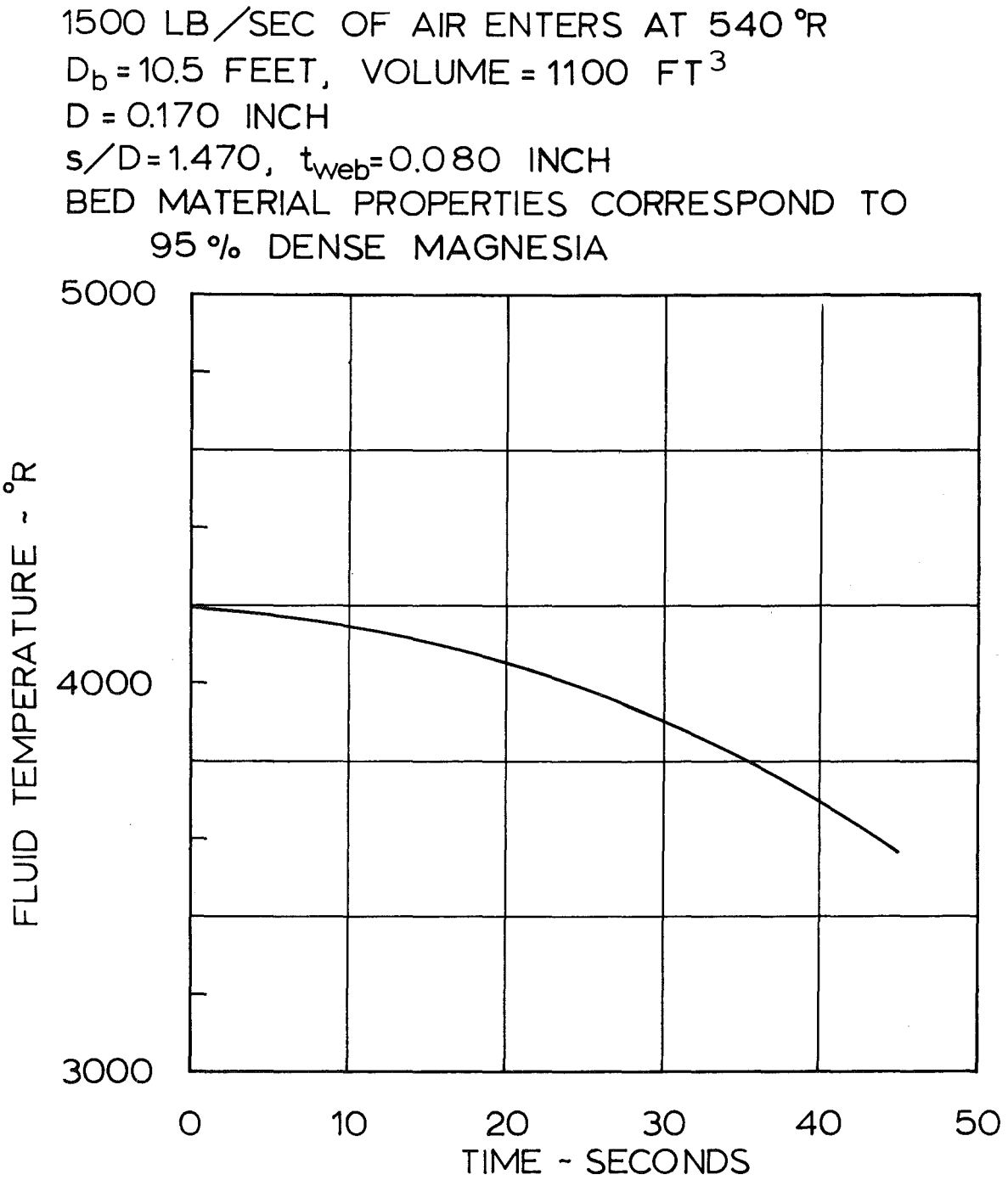

Fig. 28 Matrix Exit Air Temperature History

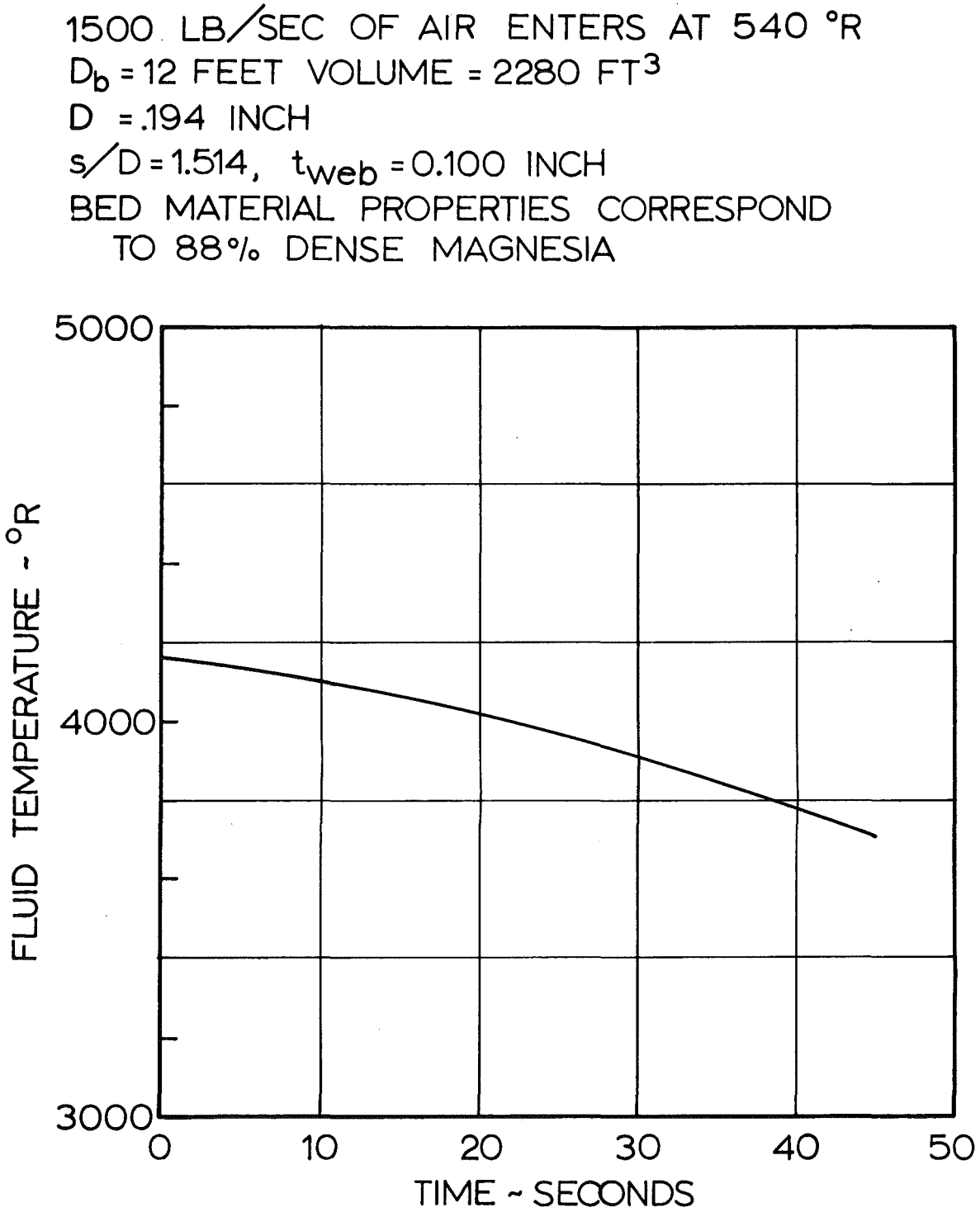

Fig. 29 Matrix Exit Air Temperature History

same slope of the temperature ramp. The results are shown in Figs. 23 and 29. The maximum mean-to-hole surface temperature difference is now everywhere acceptable, in fact, the inlet temperature could be increased somewhat. The increase in heater length amounts to about 5 feet, the volume becoming approximately 2300 cubic feet. The inlet-end temperature could be somewhat higher than indicated. The actual volume increase would then be somewhat less, perhaps 20 to 25%. Although calculations have not been carried out for the other combinations of material density, etc., the volumetric increase will be a similar percentage of the values indicated in the tabulation.

These calculations emphasize again the critical importance of thermal stress resistance in determining the required matrix volume. Should it be possible to substantially increase the slope of the temperature ramp, whether through improvement in material properties or through development of a matrix element geometry which reduces thermal stress, a further substantial reduction in matrix volume could be realized. Alternatively, increases in run time would be possible.

Without question, these data indicate that determination of material properties is essential before undertaking final design. Equally certainly, it is essential that manufacturers be encouraged to supply material of the highest feasible density.

Increasing the material density uniformly exerts a favorable effect on performance. Increase in density increases heat storage per unit volume, increases thermal conductivity (permitting a steeper temperature ramp for a given thermal stress), and increases allowable thermal stress (permitting a steeper temperature ramp). All of these trends tend to reduce matrix volume. Furthermore, the increased strength and tighter, firmer, smoother texture should minimize the tendency to form dust. Finally, creep strength and bearing strength are substantially improved, thereby holding forth the promise of operation at higher temperatures.

A representative arrangement of the heater for Triptee can now be developed. Fig. 30 shows such an arrangement, based on the 88% dense magnesia. As shown, the vessel would probably be field fabricated, although its outside dimensions are such that there is a possibility that it could be shipped by special rail car (see Section 2) or by a combination of barge and (special) highway transporter.

The arrangement of the dome was selected to minimize dome volume. This is desirable from the standpoint of

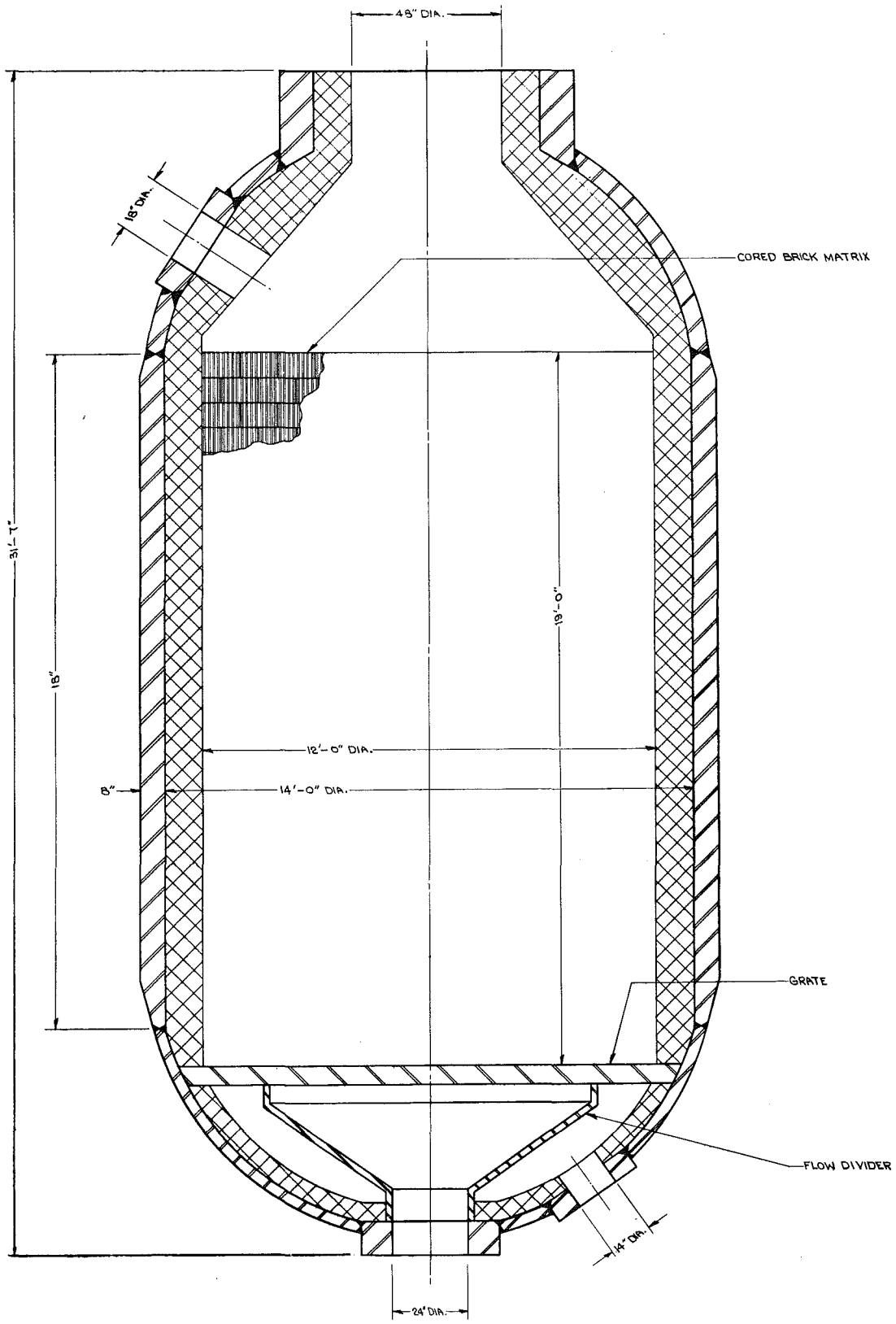

Fig. 30 General Arrangement of Heater

minimum loss of air during pressurization as well as from the standpoint of reduced cost. However, a bend in the discharge duct is required which would be undesirable. To eliminate this would require an arrangement of the dome such as shown in Fig. 31. The increase in dome volume would increase the cost of the vessel and refractories, and would increase the amount of air lost during pressurization.

If it should prove to be feasible to use a horizontal orientation of the vessel, the arrangement of the heater could be as shown in Fig. 30 and the discharge duct would then be straight. This would be both economical and desirable from the standpoint of small dome volume and simple arrangement of the discharge duct. The feasibility of such an arrangement depends on the characteristics (particularly bearing strength) of the insulation and the practical limits of matrix assembly. It also depends on the feasibility of restraining the matrix against the pressure drop forces. Because of these uncertainties, it can only be considered as a possible arrangement to be studied further if some serious deficiency developed in the vertically orientated arrangement.

At the bottom of the heater bed, regenerating gases will discharge into the exhaust stack through two concentric ducts controlled by individual valves. This arrangement, discussedin Section 6, permits a relatively small quantity of combustion gas, required during holding the heater in readiness, to be channeled through the matrix adjacent to the walls, insuring the maintenance of a flat radial temperature profile. The relative amount of reheat gases through the center and at the periphery of the matrix can similarly be adjusted.

Summarizing, one can state that it is feasible to construct a storage type air heater meeting the performance requirements of the Tripltee. It is likely that this heater can comprise a single vessel, and the general arrangement of this heater can be similar to extant heaters. By the selection of proper matrix element geometry, combined with achievable material properties, it is likely that no thermal stress cracking, creep or other forms of mechanical failure will be encountered for extended periods (perhaps 2 years) of operation. Freedom from dusting is at least possible; certainly dusting can be substantially reduced below that occurring in existing heaters.

The industry is prepared to produce the necessary refractory elements, the pressure vessel is well within current practice and the engineering understanding and analytic techniques required to design this heater are well developed.

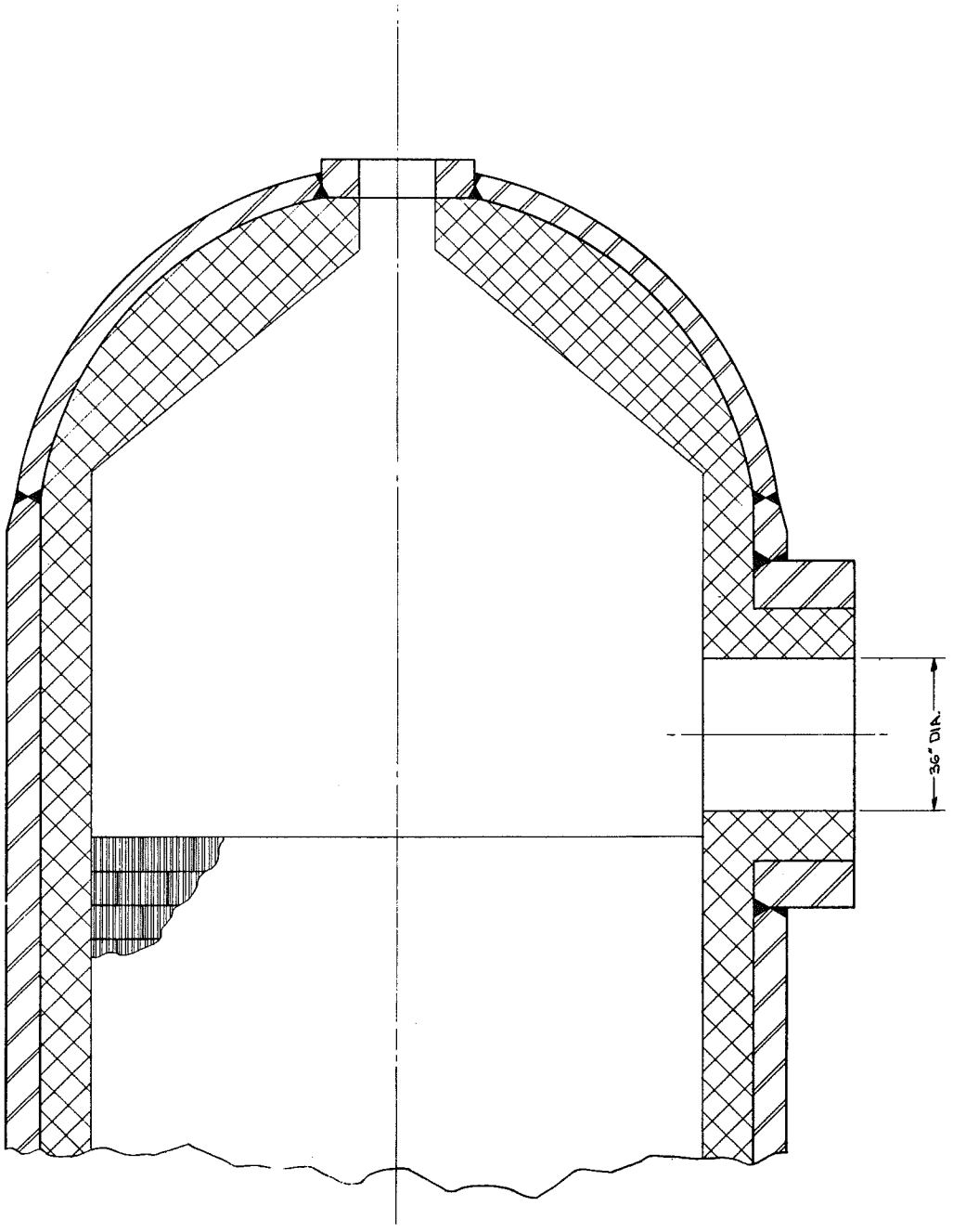

Fig. 31 General Arrangement of Heater, Alternate Discharge Duct

9. CONCLUSIONS

1. The use of refractory elements in the heater matrix that are specifically designed for this application results in large reductions in the heater volume requirements and an absolute minimum of dust carry-over.

2. The performance requirements can be met with a single heater, rather than multiple heaters, providing substantial reductions in system complexity and cost.

3. Within present knowledge, zirconia and magnesia are both satisfactory materials for the storage matrix and insulation. Eventual selection of a specific material will require property data not now available.

4. Dust carry-over from the heater can be minimized only through the prevention of dust production. This requires design for the elimination of thermal fractures. Thus, thermal stress becomes one of the controlling parameters in the heater design.

5. The preferred heater matrix geometry consists of a series of parallel holes, forming essentially a tubular regenerator.

6. Cooling of the heater vessel by free convection and radiation is adequate; water cooling is not necessary.

7. Significant reductions in vessel volume are possible through reduction of the insulation thickness between the bed and the vessel, with a corresponding increase in vessel wall temperature. This advantage can be gained with vessel temperatures about 500°F.

8. A feasible approach to the mixer design, for the Mach 4 nozzle, involves introducing the hot and cold air through a number of small streams, thereby reducing the length across which mixing must take place. A design concept based on this approach was examined and will provide adequate mixing within the 25 feet length available.

10. RECOMMENDATIONS

This study has shown that the geometry and thermo-physical and high temperature mechanical properties of the heat storage material are controlling in achieving the desired ends.

The influence of the properties of the heat storage material is so great that the use of material produced specifically for this application may very well reduce the cost of the heater installation by 50%. Also, the most suitable material promises long life, low maintenance and an extremely low level of dust formation.

A survey of the refractory ceramic industry has shown that several firms can produce a material which will closely approach, possibly achieve, the desired performance. These firms are unanimous in stating that the achievement of these material properties will require preliminary trials to determine the proper combination of processing variables.

A program is recommended to evaluate these improved refractories in terms of their application to the heater system and to proof-test selected materials in a pilot heater. This work should include refractories used in the heat storage matrix and in the insulation liners throughout the heater system.

Engineering properties necessary for design are not available for the materials under consideration, and furthermore, these properties are dependent upon the fabrication technique used to produce the desired shapes. Therefore, it would be necessary to measure certain properties in order to compare various materials and fabrication processes and to permit selection of the best materials. This selection would be based on an economic and performance analysis of the heater system.

The specific tasks which we believe to be desirable are listed below.

1. Prepare refractory specifications and procure preproduction qualification samples from refractory suppliers.

2. Have an independent laboratory test refractory samples to obtain thermal and mechanical properties at elevated temperature.

3. Design a test setup to thermally cycle sample quantities of refractories in a manner similar to that in which they would be cycled in a heater.

4. Evaluate the materials tests in terms of the large heater design.

5. Based on the information obtained from the refractories tests, design a pilot heater to be used for a final test of the refractories for the large heater to be designed.

6. Fabricate the pilot heater designed under 5 and install at AEDC.

7. Evaluate refractory performance in the pilot heater.

REFERENCES

1. Jacob, M., Heat Transfer, Vol. II, John Wiley and Sons, 1957. Chapter 35.

2. Carman, P.C., Fluid Flow Through Granular Beds, Trans. Inst. Chem. Engr. Vol. 15, 1937.

3. Ryshkewitch, E., Oxide Ceramics, Academic Press, 1960.

4. A Review of the Wisconsin Process for Nitrogen Fixation, Nitrogen Symposium Sponsored by Food Machinery and Chemical Corporation and Wisconsin Research Foundation, Nov. 21-22, 1955. Daniels, Dr. Farrington, Chairman.

5. Spalding, D. B., Some Fundamentals of Combustion, Butterworths, 1955.

6. Combustion Researches and Reviews 1957, Agardograph 15, Butterworths, 1957.

7. Smoot, T. W. and King, D. F., Permanence of Zirconia Stability, A Function of Purity. (In IEEE Trans. on Aerospace-Support Conference Procedure, p. 1192.1963)

8. Carslaw, H. S. and Jaeger, J. C., Conduction of Heat in Solids, Oxford, 2 ed 1959, pp 203 and 327-329.

APPENDIX A
COPY OF
EXHIBIT "A"
STATEMENT OF WORK

AF 40(600)-1039

FLUIDYNE ENGINEERING CORPORATION

A. Statement of the Problem and Objectives: Design criteria for a true temperature wind tunnel operating up to 2000 psia and 4000°R stagnation conditions is being prepared. Temperatures up to approximately 4000°R shall be provided by a storage heater system. A schematic of the proposed tunnel is shown in the attached Fig. I*. A storage heater system is tentatively required to provide true temperature air over the portion of the altitude-velocity envelope shown in the attached Fig. II*. The primary design points for the heater system will be for Mach 4 and Mach 7 operating conditions with air in the nozzle stagnation chamber at the following conditions:

	Mach 7	Mach 4
Stagnation Pressure p_t	2000 psia	400 psia
Stagnation Temperature T_t	3900°R	1600°R
Total Mass Flow $\dot{m}$	1500 lb/sec	5000 lb/sec

It is envisioned that the Mach 4 conditions may be produced by mixing hot storage heater air and ambient temperature air. Useful test times of at least 30 sec. are required with effluent temperature not varying more than ± 5% from the true stagnation temperature for a given run. True simulation of other portions of the performance envelope are desired but not at excessive increase in cost of simulating the primary design points. Consequently, a redefinition of the performance envelope probably will result from this study based on this criteria. Also, the heater size probably is not compatible between the Mach 4 and Mach 7 conditions. A redefinition of the Mach 4 conditions shall be considered if the technical and economical studies so suggest. It is also required that operation with temperatures below true stagnation temperatures be provided. Known problem areas for the storage heater and mixer systems are outlined below:

(1) Storage Heater System: The storage heater system is required to provide high pressure air to the nozzle stagnation chamber at a minimum of 3900°R. Higher temperatures up to 4300°R are desired to simulate "hot day" environments, however, this may be beyond the state of the art with storage heaters. The mass flows required probably dictate more than one storage heater and possibly different manifold requirements.

* Not included in this report.

The number and size of heaters will depend upon run time, mass flow rate and stagnation conditions as well as heater design and refractory materials used. A practical engineering and economic evaluation of all the parameters must be made to select the number and size of heaters. Others contributing analyses which must be made are:

(a) Selection of refractory material, including configuration, for heat storage elements and insulation.
(b) Refractory dusting must be kept below maximum acceptable levels in order to provide acceptable conditions for airbreathing propulsion testing.
(c) Regenerating techniques.
(d) Selection of a technique for rapidly bringing the heater system on and off line with a minimum depletion of air storage.
(e) Selection of a thermal and pressure control technique.

(2) Mixer: It is envisioned that the 5000lb/sec high mass flow will be obtained by mixing hot air from the storage heater with cooler ambient air, or by paralleling a number of lower temperature heaters. A mixer is also desirable for other secondary performance requirements. The best mixer configuration, or configurations, used must be determined based upon technical and economic evaluation. The mixer must be capable of handling a wide range of mass flows without an appreciable heat loss while maintaining adequate mixing.

B. Technical Approach: The Contractor shall conduct these research and engineering studies based primarily upon "state of the art" development of storage heaters and mixers.

(1) Storage Heater System: The Contractor shall select the refractory materials and configuration for the heat storage elements and insulation based upon the best available knowledge and experience with existing materials. The Contractor shall select the number, size, and arrangement of the storage heaters and associated components, such as manifolds and valves, based upon the operating requirements listed. The Contractor shall study and recommend a pressurization and thermal control system and operating technique for the heater system operation. The Contractor shall study and recommend a technique of regenerating the heater system assuming a maximum heat consumption run. Dusting of refractory material must be kept at a low level before airbreathing propulsion testing can be accomplished in a wind tunnel. The Contractor shall take this problem into account in the selection of a heater system configuration.

(2) Mixer: For the lower temperature high mass flow operation, the Contractor shall establish the most feasible method of mixing cold and hot air for the requirements listed. The selection of a mixer configuration requires that attention be given to minimizing heat loss while simultaneously providing adequate mixing. The Contractor shall consider using a mixer which may be an integral part of the manifold system plus any other feasible concepts.

APPENDIX B

SIMPLIFIED THERMAL ANALYSIS

As a first approximation to the problem of predicting the performance of the heater matrix as a function of various parameters, the Hausen results, Ref. 1, were used. The following assumptions are made:

a. The matrix temperature is initially uniform
b. The friction factor and heat transfer coefficients are those shown on the accompanying Figs. 1B and 3B
c. The pressure gradient at the top of the bed is equal to one half that required to float the bed, i.e.,

$$dp/dz = 1/2\,\rho(1-\sigma) = 1/2\,\rho_{bulk}$$

where:

ρ = density of matrix material
ρ_{bulk} = bulk density of matrix
σ = bed porosity

d. The matrix geometry is comprised of circular holes, parallel to the direction of flow, spaced uniformly:

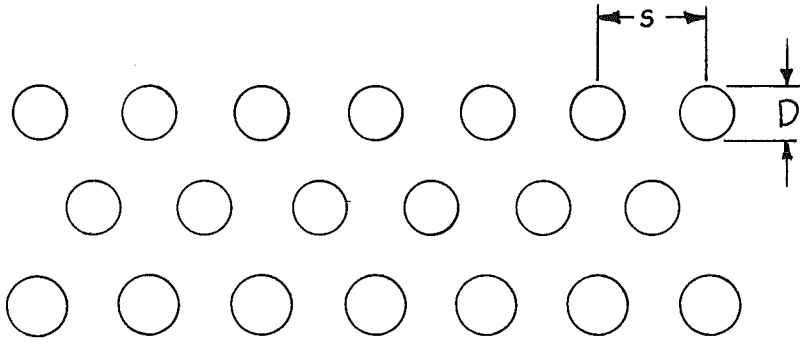

For this arrangement the porosity is

$$\sigma = \frac{0.908}{(s/D)^2}$$

and the surface area per unit volume is

$$\frac{A_{ht}}{V_{bed}} = \frac{P}{A_f} = \frac{3.624}{D\,(s/D)^2}$$

where:

A_{ht} = total heat transfer area
V_{bed} = total matrix volume
P = wetted perimeter
A_f = total face area

The parameters η and ξ are defined as:

$$\eta = \frac{hP}{CM}\theta \text{ , the limiting value being } \eta_f = \frac{hP}{CM}\theta_f$$

and

$$\xi = \frac{hP}{c_p \dot{m}} z \text{ , the limiting value being } \xi_\ell = \frac{hP}{c_p \dot{m}}\ell$$

where:

C = specific heat of matrix material
M = mass per unit length of matrix
θ = time elapsed, variable
θ_f = total run time
z = matrix length, variable
ℓ = total matrix length

We may write η_f and ξ_ℓ in terms of the matrix characteristics as follows.

$$\eta_f = 3.624 \quad \frac{h\theta_f}{C\rho\left\{1 - \frac{.908}{(s/D)^2}\right\}(s/D)^2 D}$$

and

$$\xi_\ell = 3.624 \quad \frac{hA_f\ell}{\dot{m}c_p(s/D)^2 D}$$

Dividing η_f by ξ_ℓ and rearranging we obtain an expression for gross matrix volume

$$V_{bed} = A_f\ell = \left[\frac{\dot{m}c_p\theta_f}{C\rho\left\{1 - \frac{.908}{(s/D)^2}\right\}}\right]\frac{\xi_\ell}{\eta_f}$$

The bracketed term is that volume of matrix which would have the same heat capacity as the fluid to be heated. This is therefore the lower limit to the matrix volume, if all the heat stored (relative to the gas inlet temperature), was extracted by gas leaving the matrix at the initial matrix temperature. The ratio ξ_ℓ / η_f thus can be thought of as an effectiveness factor. η_f is determined by matrix element

geometry, heat transfer coefficient, matrix material density, and run time.

The requirement that the gas discharge temperature not deviate from the specified value by more than ± 5% in conjunction with η_f results in a unique value for ξ_ℓ. In other words, any two quantities of the group η_f, ξ_ℓ, and T_{gf} determine the third as per Fig. 3a. The value of T_{gf} results from the ± 5% temperature tolerance specification.

$$T_{gf} = \frac{T_{gf} - T_c}{T_i - T_c} \simeq .9,$$

since $$T_{gi} = \frac{T_{gi} - T_c}{T_i - T_c} \simeq 1.0$$ for the range of ξ_ℓ's encountered.

The heat transfer coefficient used to determine a value of η_f depends on matrix geometry, mass velocity of the gas, and gas properties. More specifically the heat transfer coefficient is a function of Reynold's number, Prandtl number, mass velocity, and specific heat. The relationship is

$$\frac{h}{\rho_g u c_p} = \frac{Nu}{RePr} = St = .0231\ Re^{-.2}\ Pr^{-2/3}$$

Alternatively one can write h in the form

$$h = .0231\ (k_g/D)\ Re^{.8}\ Pr^{1/3}.$$

Friction factors depend on roughness and Reynolds number in the turbulent flow regime. Fig. 1B presents the estimated relationship between friction factor and Reynolds number. Figs. 2B-4B relate Reynolds number, heat transfer coefficient, and mass velocity to hole diameter and bulk density for the one-half bed flotation pressure gradient condition. Fig. 5B gives the relationship between η_f and ξ_ℓ for a value of T_{gf} equal to 0.9.

Calculations have been made to determine η_f, ξ_ℓ, and heater volume for a range of hole sizes and for two materials, magnesia and zirconia. Material densities of 197 lb/ft^3 and 263 lb/ft^3 were assumed for magnesia and zirconia, respectively. Once the material density is specified the bulk density depends only on bed porosity. Mean specific heats of 0.36 BTU/lb$^\circ$ R were selected for the magnesia and zirconia, respectively. The resulting values for η_f are shown in Fig. 6B, while corresponding volumes appear in Fig. 7B.

The net effect of increasing hole diameter at a constant

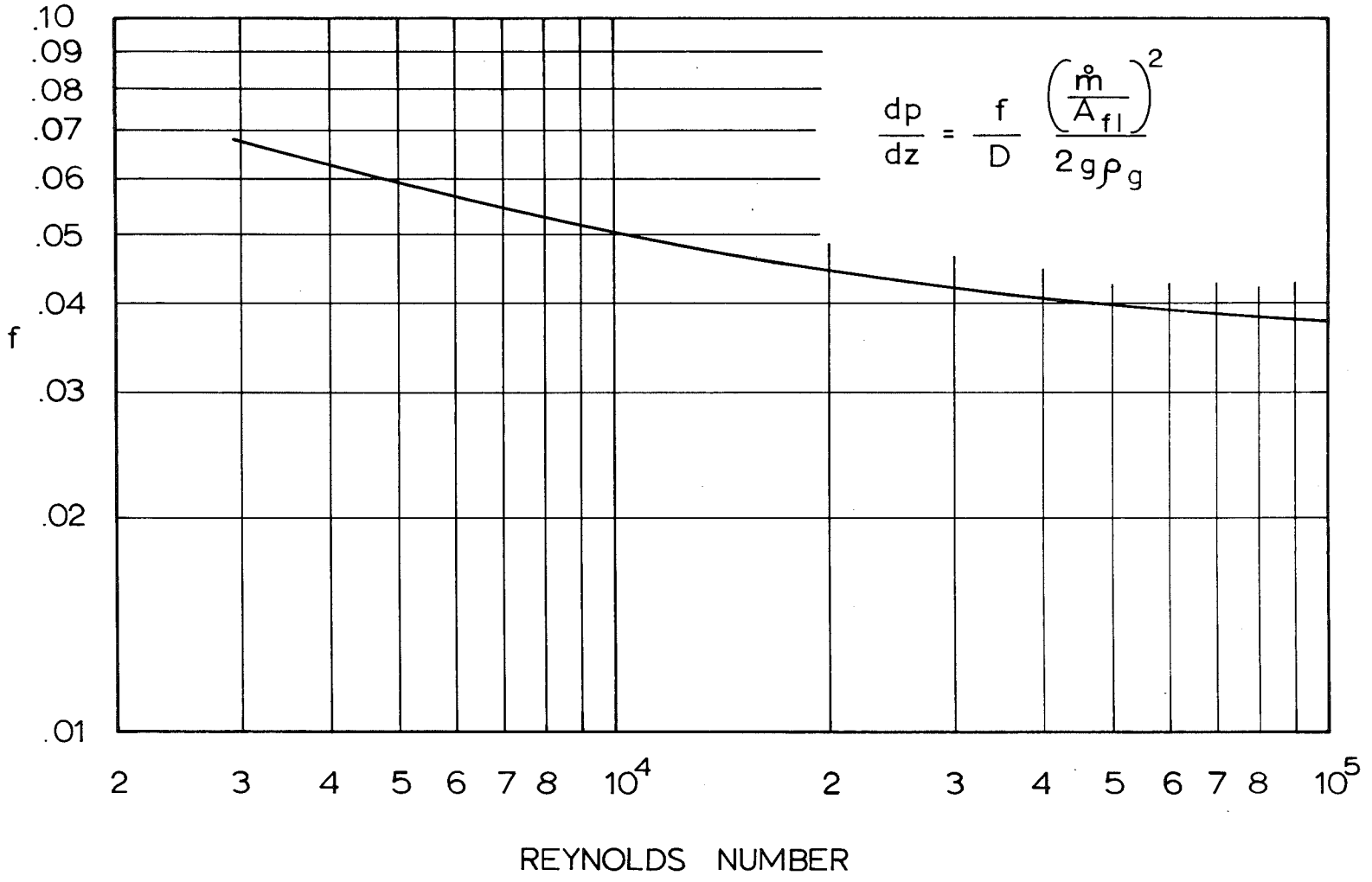

Fig. 1b Estimated Friction Factor for Circular Hole Matrix Elements

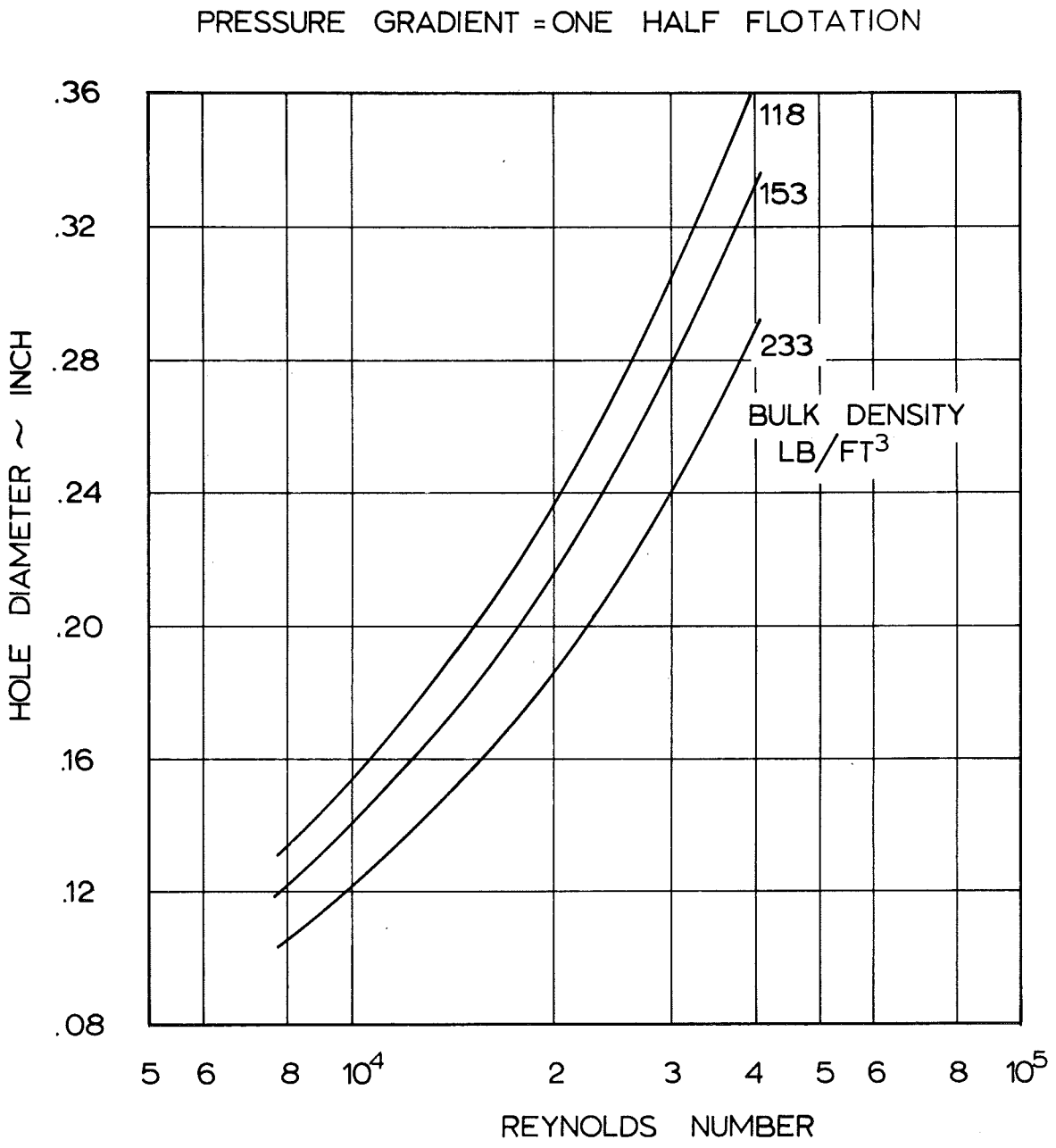

Fig. 2b Estimated Hole Diameter

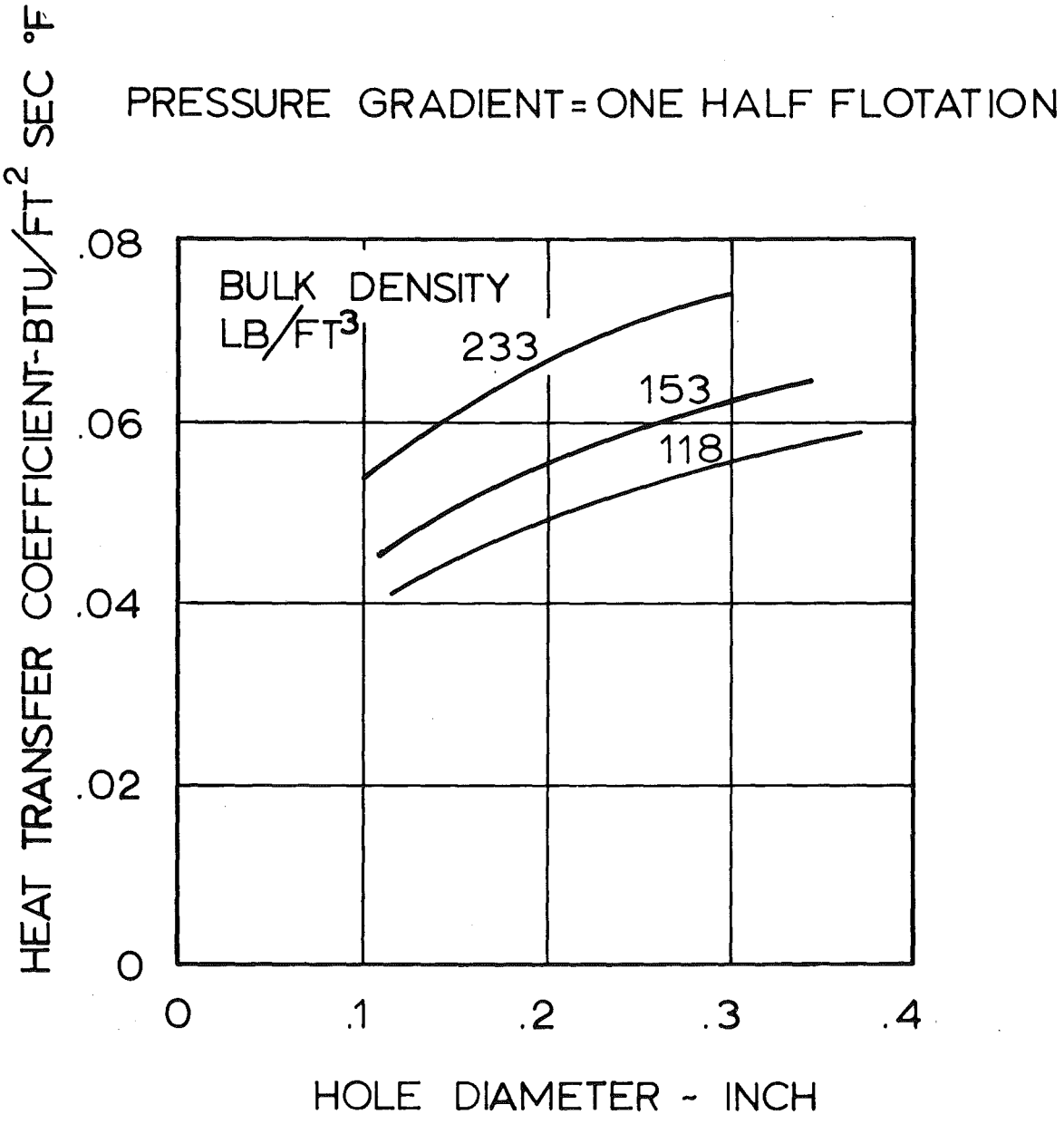

Fig. 3b Estimated Heat Transfer Coefficient for Circular Hole Matrix Elements

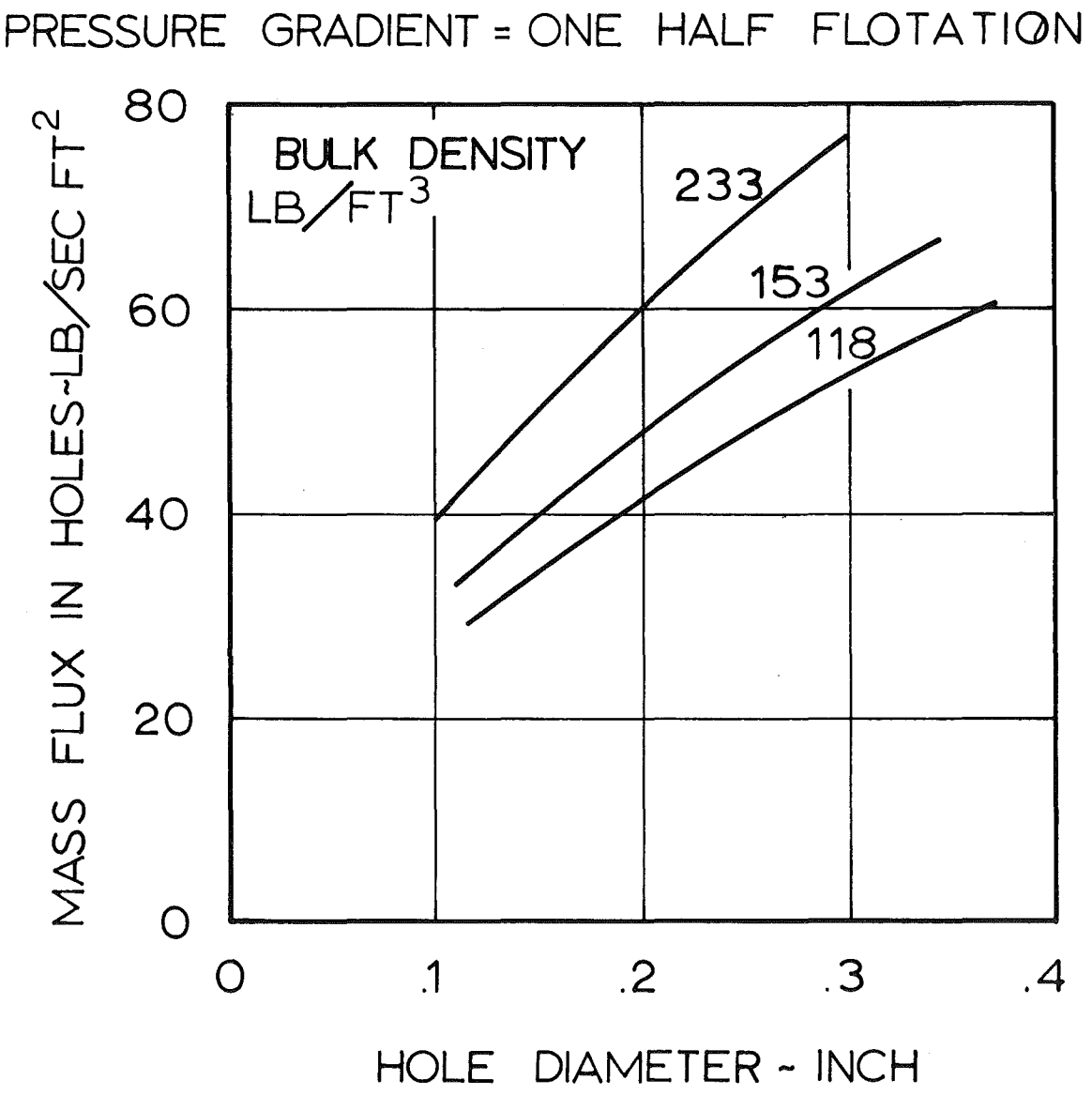

Fig. 4b Estimated Mass Flux in Holes

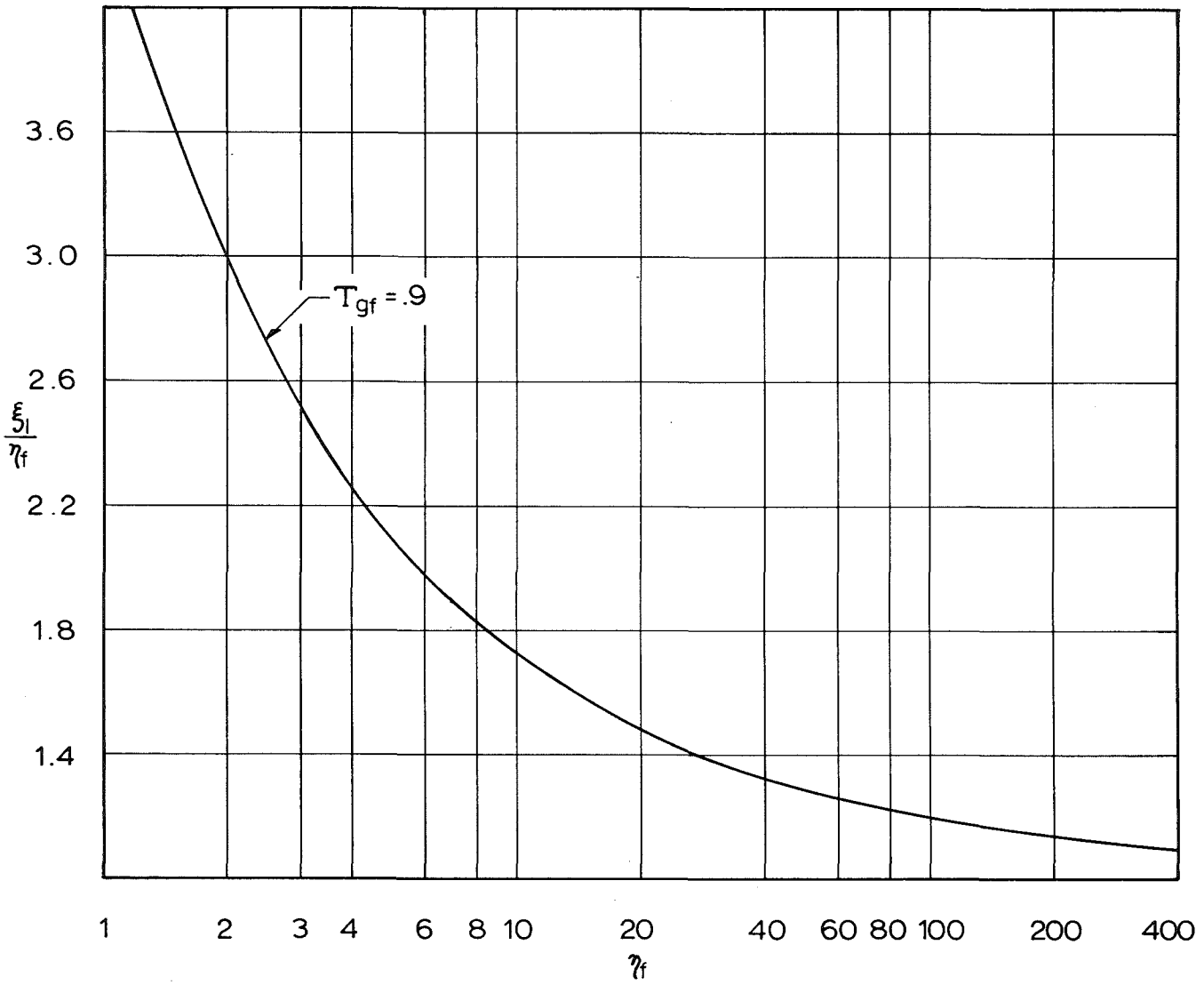

Fig. 5b Estimated Factor From Hausen Results

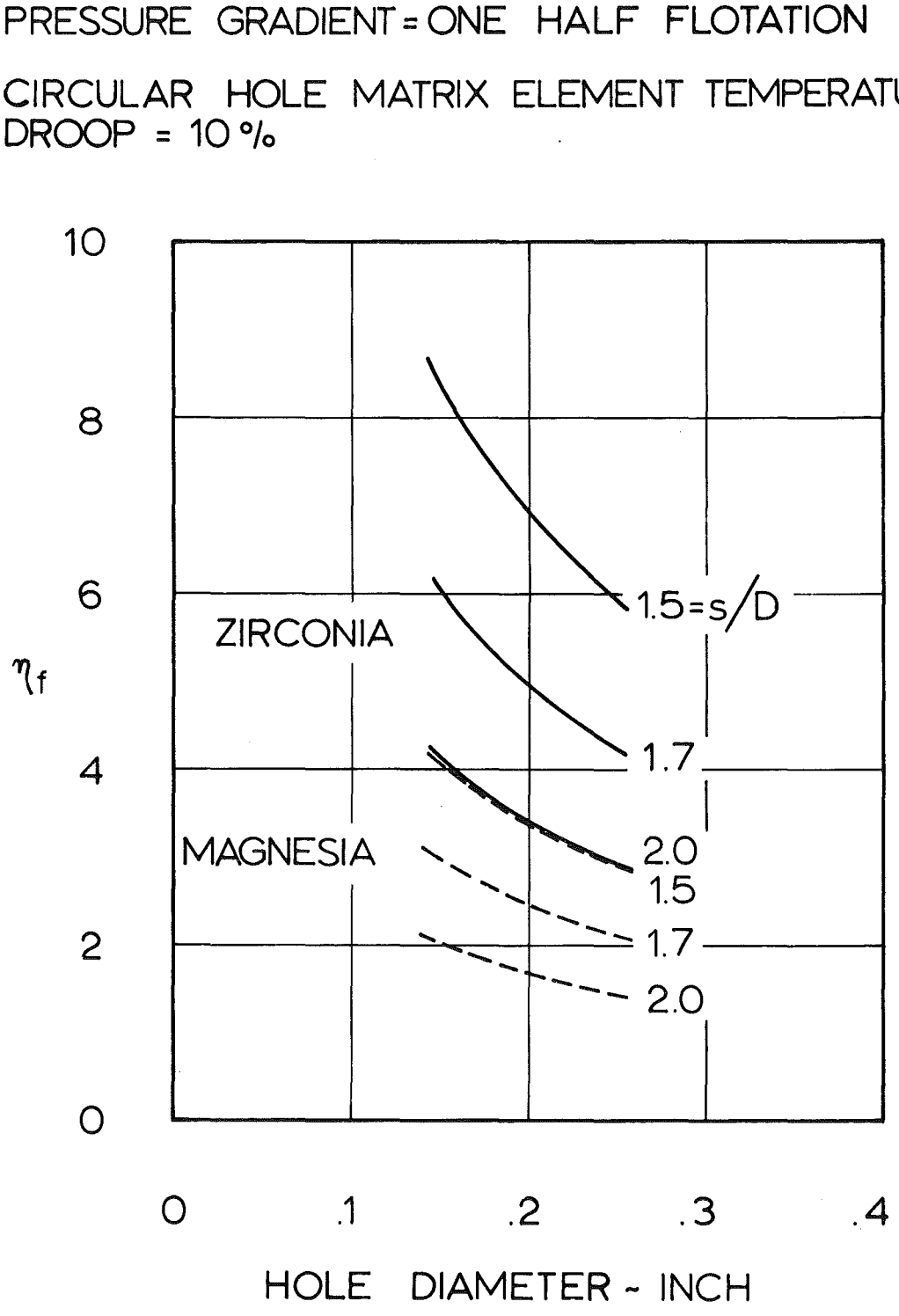

Fig. 6b Estimated Hausen η_f

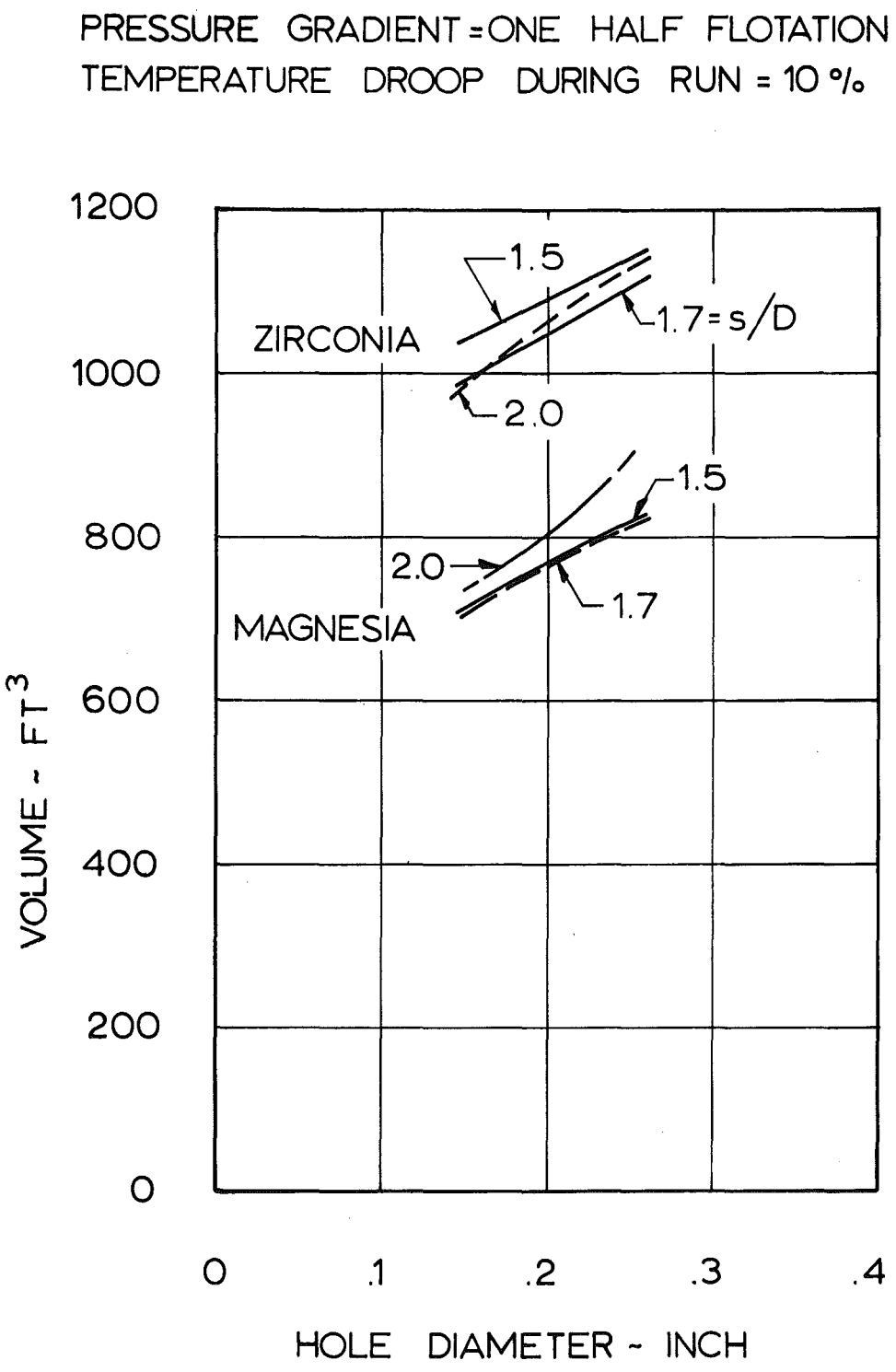

Fig. 7b Estimated Matrix Volume with Uniform Initial Temperature

spacing to diameter ratio (s/D) is a reduction in the value of η_f, the increase of heat transfer coefficient being dominated by the decrease in wetted perimeter (P). This reduction in the value of η_f results in a larger ξ_ℓ / η_f factor (see Fig. 5B) and therefore increased matrix volume. Comparison of the results for zirconia and magnesia, Fig. 7B, indicate the importance of the quantity $C\rho$ on matrix volume. Although lower values of $C\rho$ result in smaller ξ_ℓ / η_f values, the heat storage effect dominates. Hole spacing is seen to be of minor importance in the range of s/D's of interest.

The volumes indicated in Fig. 7B are clearly the least possible under the assumed conditions. However, if matrix element fracture is to be avoided, they are not realistic. A uniform initial matrix temperature would result in severe thermal stress conditions and fracture.

A more realistic assumption of initial matrix temperature distribution would be that corresponding to a value of η (see Fig. 3B) greater than zero. The starting rate of change of matrix temperature with length would then have a finite value. This starting temperature gradient of the matrix can be related to thermal stresses in the material as per Appendix H. On such a basis, and knowing material properties, an acceptable value of this gradient can be estimated for any particular matrix element design. Such a temperature gradient quantity can be related to the matrix characteristics curves of T versus ξ at constant η, (Fig. 3B). Recalling the definitions of T, ξ and η we can relate the quantities to the maximum initial matrix temperature gradient, $(\partial T/\partial z)_o$, as follows:

$$\left(\frac{\partial T}{\partial z}\right)_o = \frac{1}{T_i - T_c}\left(\frac{\partial T}{\partial z}\right)_o$$

and

$$\left(\frac{\partial T}{\partial \xi}\right)_o = \frac{dz}{d\xi}\left(\frac{\partial T}{\partial z}\right)_o = \frac{\dot{m} c_p}{h p}\,\frac{1}{T_i - T_c}\left(\frac{\partial T}{\partial z}\right)_o$$

or

$$\left(\frac{\partial T}{\partial \xi}\right)_o = \frac{\dot{m} c_p}{h A_f}\left(\frac{s}{D}\right)^2 \frac{D}{3.624}\,\frac{1}{T_i - T_c}\left(\frac{\partial T}{\partial z}\right)_o$$

For each value of $\left(\frac{\partial T}{\partial \xi}\right)_o$ there is an unique value of η_o corresponding to that characteristic curve which has as

its maximum slope that particular value. (See Fig. 8B). One can thus take an allowable $(\partial T/\partial z)_o$ number computed from thermal stress considerations, and, along with the geometric and flow conditions, compute a value for η_o. We now assume that η_o adequately represents the actual temperature distribution at the beginning of the run. η_f is computed as it was for the initially uniform temperature case. Adding η_o and η_f we obtain the value of η characterising the final temperature distribution in the matrix (Fig. 3b) and gas (Fig. 3a); call it η'. The temperature droop specification is used to determine the final T_g value (T_{gf}) desired, which for TTT will normally be about 0.9. Using Fig. 3a we now find the value of ξ corresponding to T_{gf} and η'; call it ξ'. At this point we can make the following observation. For most values of η the amount and temperature level of the heat stored near the upstream end of the bed (see Fig. 3b) is quite small. Clearly, this part of the heater matrix contributes little to the performance but significantly to the size of the matrix. In order to reduce the size of the heater, we draw a tangent to the η_o curve on Fig. 3b, at its maximum slope location. The curve formed by the tangent line from the $T = 0$ line (or ξ-axis) to the maximum slope location plus the η_o curve from there on is the one we now define as our initial temperature distribution. We shall call the value of ξ on Fig. 3b, where the tangent line crosses the ξ-axis, ξ_o, and assume that this temperature distribution gives us the same heater performance as the complete η_o curve. For reasons stated above and because of the preliminary nature of this analysis the assumption is justified. The difference between ξ' and ξ_o is ξ_ℓ and in conjunction with η_f enters directly into determining the necessary matrix volume as it did in the initially uniform temperature case. Thus we can write

$$V_{bed} = A_f \ell = \left[\frac{\dot{m} c_p \theta_f}{\rho\left\{1 - \frac{.908}{(s/D)^2}\right\}}\right] \xi_\ell / \eta_f$$

where

$$\xi_\ell = \xi' - \xi_o$$

and

$$\eta_f = \eta' - \eta_o$$

Numerical calculations were made for the case where the maximum initial temperature gradient was given the value 200°F/ft, a number typical of those based on thermal stress considerations although numbers appreciably larger and smaller also result. Values of $(\partial T/\partial \xi)_{max}$ and η_o are plotted vs. hole diameter in Fig. 9B. While hole spacing is a variable, the results with different s/D ratios don't differ enough to warrant consideration in this preliminary analysis. There is

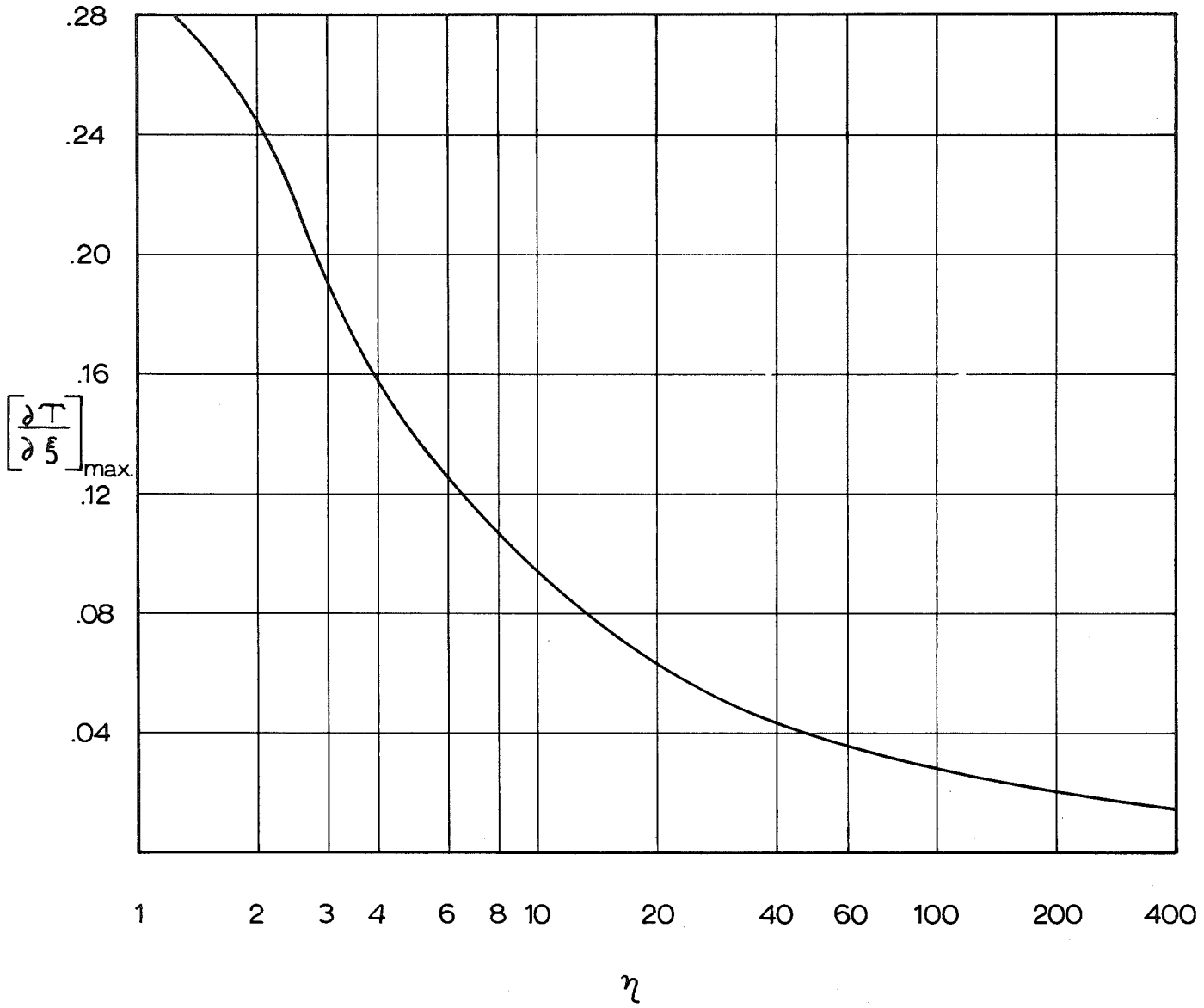

Fig. 8b Maximum Slope of T Versus ξ Curves

PRESSURE GRADIENT = ONE HALF FLOTATION
MATERIAL DENSITY FROM 190 TO 270 LB./FT.^{3}
RAMP TEMPERATURE GRADIENT = 200 °F PER FOOT
s/D FROM 1.5 TO 2.0

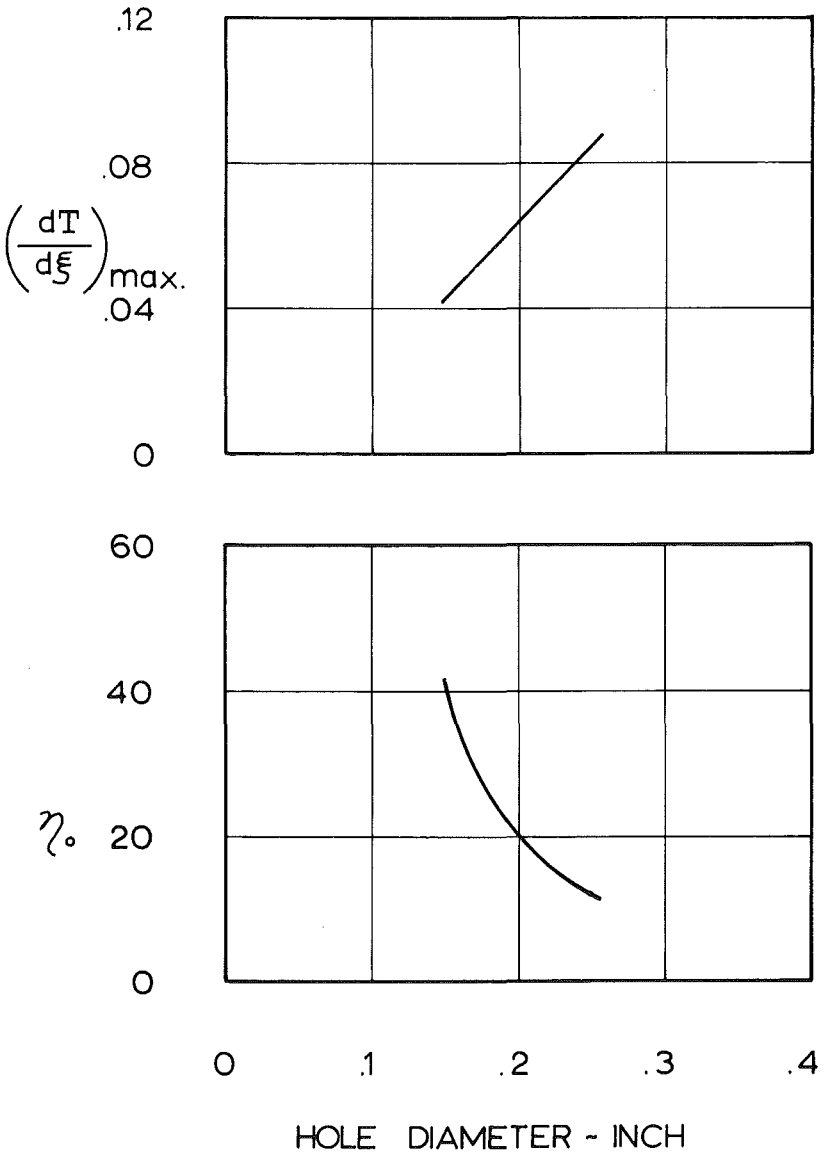

Fig. 9b Maximum Slope of T Versus ξ Curves and Corresponding Value of η_o

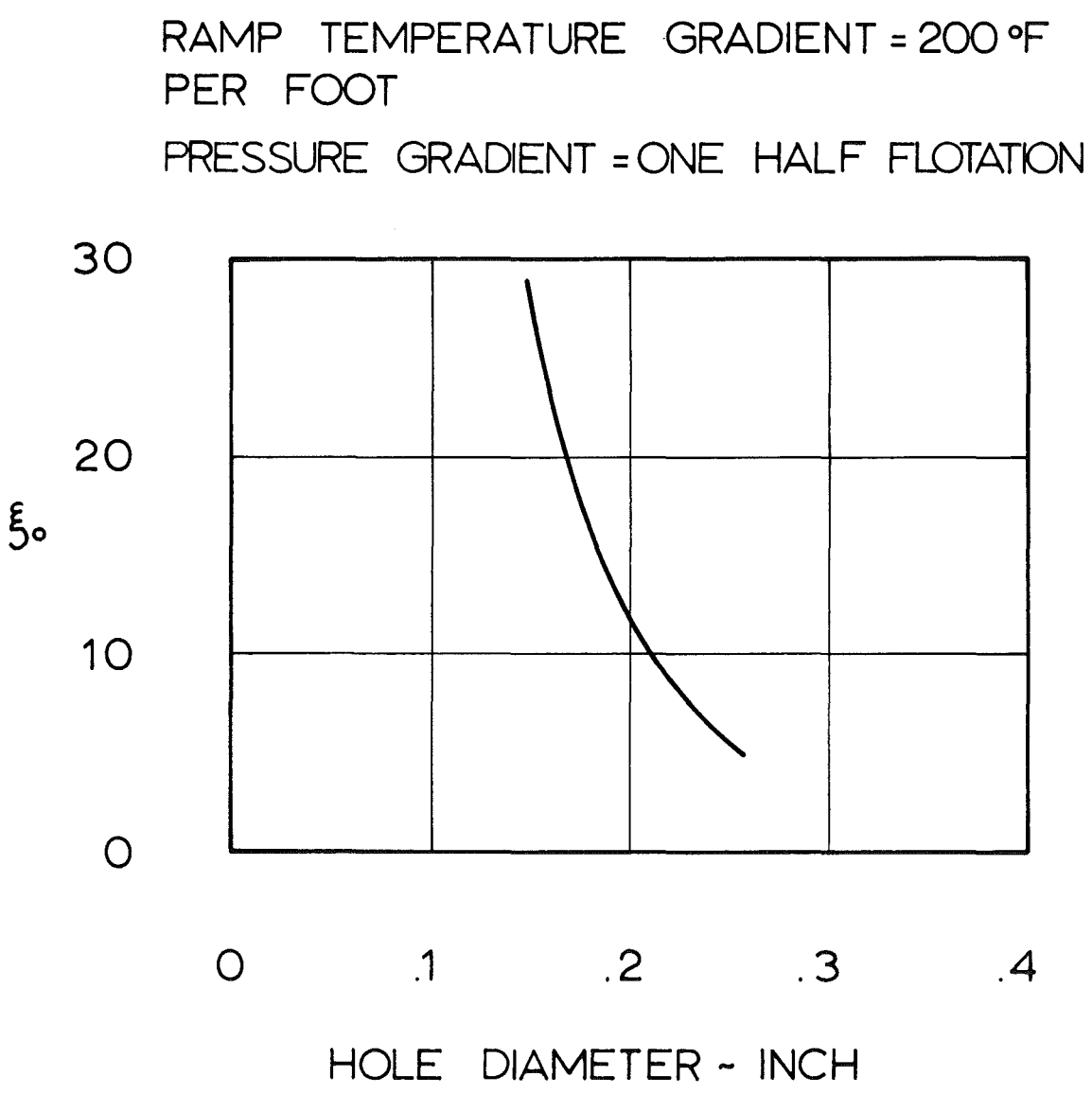

Fig. 10b Estimated Value of ξ_o

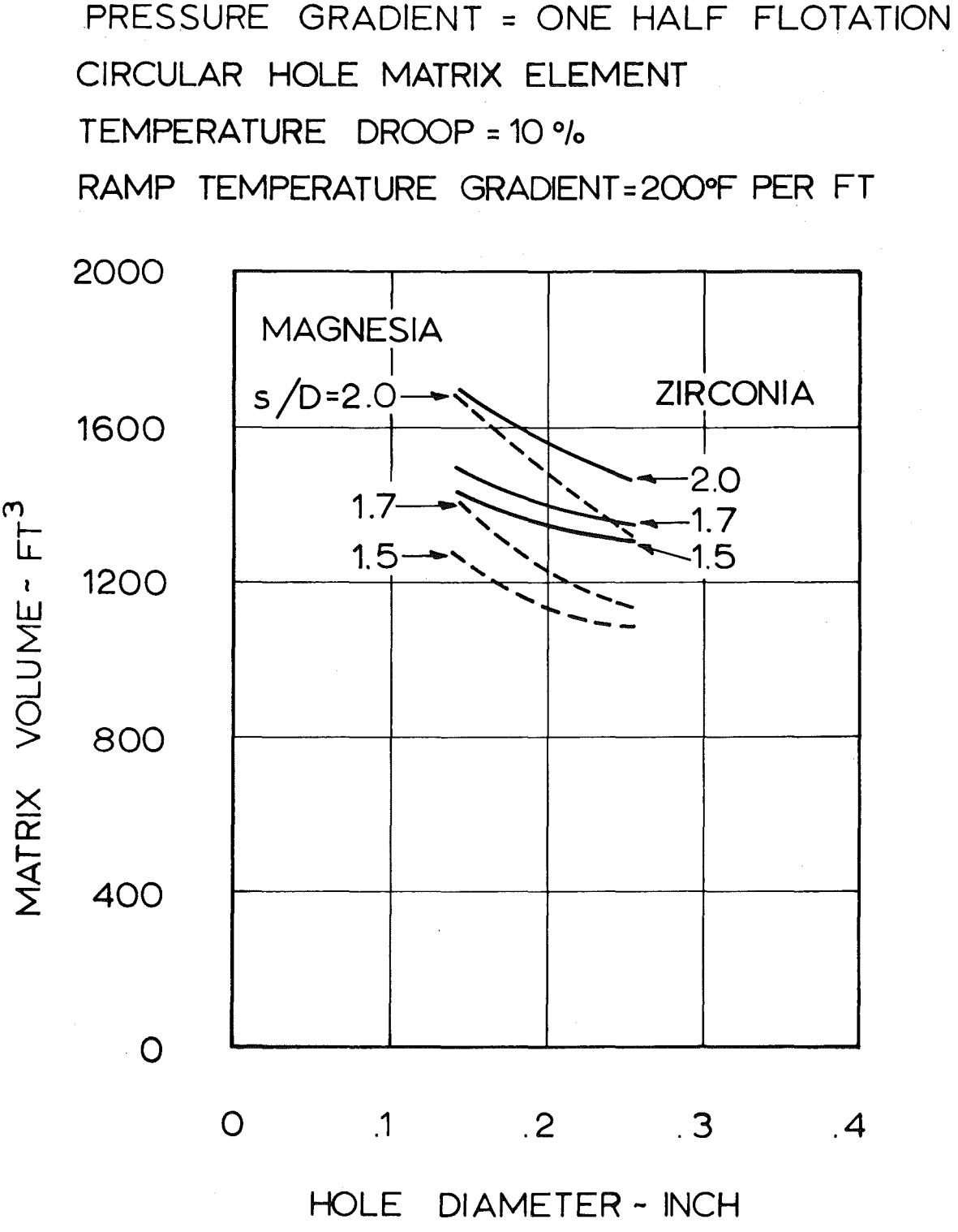

Fig. 11b Estimated Matrix Volume

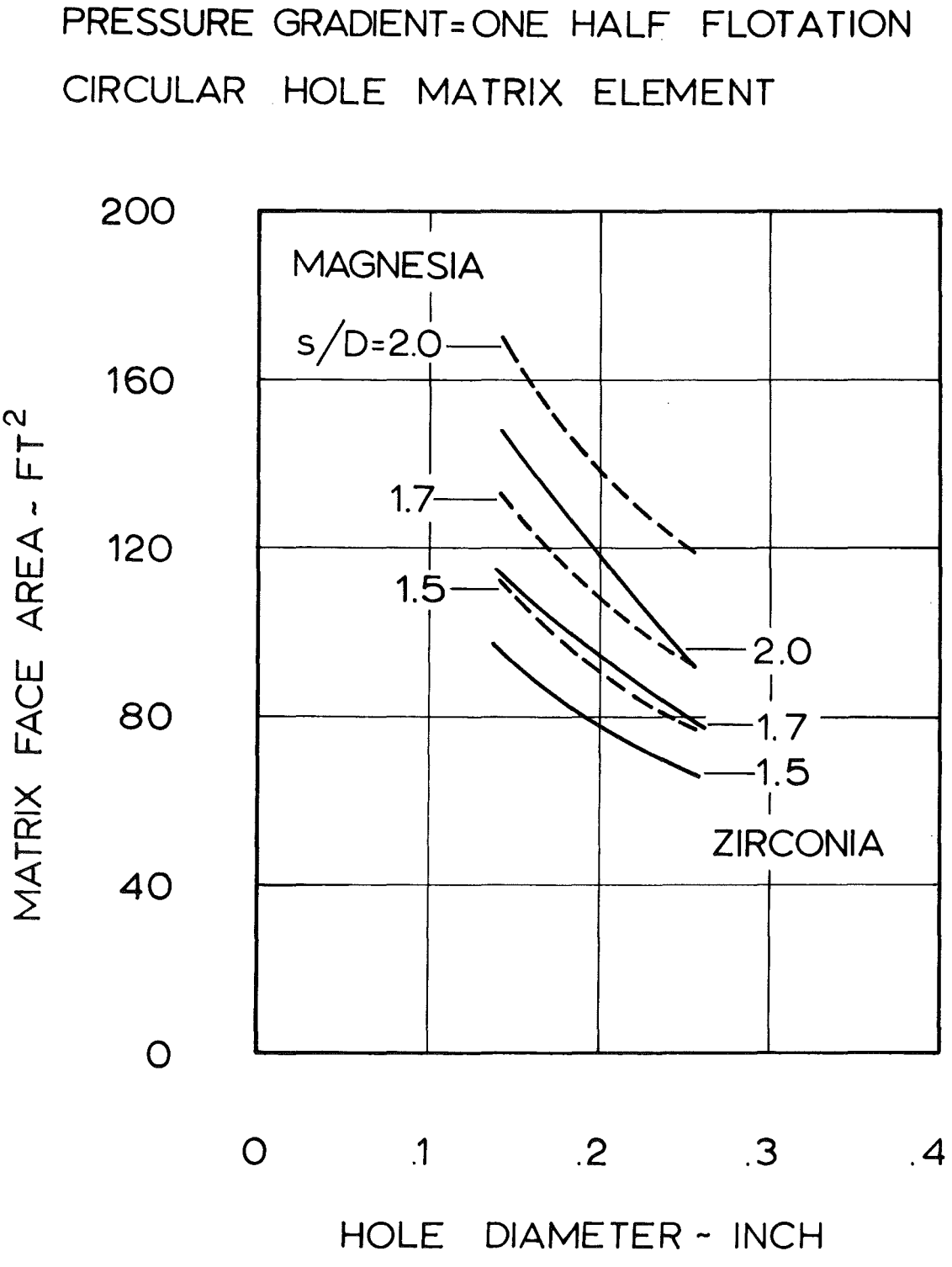

Fig. 12b Matrix Face Area

only a 2 to 3 percent difference in $(\partial T/\partial \xi)_{max}$ comparing s/D's of 1.5 and 2.0. Similarily, material density has little effect over the range of values to be considered. A density change of 50 percent changes $(\partial T/\partial \xi)_{max}$ by only 4 percent. Values of ξ_0 versus hole diameter are plotted in Fig. 10B. The matrix volumes predicted by this approach appear in Fig. 11B. As expected, this analytical model yields larger estimated matrix volumes than the initially uniform matrix temperature model. Trends with hole diameter are opposite and the effect of hole spacing is greater although qualitatively similar. However, one should not attach too much significance to these trends. The factors of major importance, which these curves ignore are the effects of geometry and material properties on the allowable value of $\partial T/\partial z$. However, these results serve to give us a more realistic preliminary matrix volume estimate than the uniform temperature case. Also, and perhaps more importantly, they imply that the initial temperature distribution and what specifies it are areas which deserve more detailed analysis. This they will receive in other sections of this report, primarily in Sections 6 and 8 and Appendices G and H.

The face area of the matrix is indicated in Fig. 12B. The effect of increasing hole diameter is to substantially reduce the face area. Larger holes reduce the friction by reducing wetted area which permits larger values of mass flow per unit area. Reductions in spacing ratio also substantially reduces the allowable face area because porosity is increased.

In conclusion, we may say that the volume of the Triplitee heater is likely to be on the order of 1500 ft^3 and the matrix face area about 100 ft^2. Also, for a matrix inlet temperature ramp slope of 200°F per foot, the effect of hole size, hole spacing, or material on volume is not large. The volume of the matrix is likely to be strongly influenced by the slope of the temperature ramp. Therefore thermal stresses, which will determine allowable values of temperature ramp slope, are likely to determine the matrix volume. These thermal stresses are reduced by closer hole spacing which also reduces the required face area.

APPENDIX C

REFRACTORY OXIDE PROPERTIES

The Tripltee Heater requires a matrix in which heat is to be stored. This matrix will be exposed to temperatures of approximately 4,200°R maximum. The material will be subjected to stresses due to pressure drop of the air passing through the material, and it will have to stand under its own weight for extended periods of time at very high temperatures. Because heat is being extracted from the material there will be a temperature gradient within the material. This temperature gradient that exists within the material causes thermal stresses. The material must be free from dust, and both mechanically and physically stable. Because the size of the heater depends directly upon the amount of heat that can be stored in the matrix, the heat capacity per unit volume of the material must be as high as possible. Also the material must be as reasonable in cost as possible and one which can be readily procured from commercial sources without requiring new facilities or extending the manufacturing state of the art.

Since the material must be held at high temperatures for long periods of time (one or two years) creep must be small for a period of about 10,000 hours. Considering manufacturing tolerances, a figure of 1% creep in 10,000 hours is probably reasonable. This creep resistance will depend upon the level of stress and temperature. Although the material will not be continuously held at maximum temperature, the above creep resistance should probably be specified at the maximum temperature. A minimum stress of 10 psi (more desirably 20 to 30 psi) at the specified value of creep would probably be required.

Heat is extracted from this matrix in a period of only 30 seconds. For minimal size the largest possible proportion of the stored heat should be extracted. For these conditions the rate of change of temperature within the matrix has been estimated at from 75 to 150°F per second. Resistance to thermal shock of this sort depends upon several material properties and also on geometry. A material experiences a stress whenever it is exposed to a temperature difference. The stress resulting from a given temperature difference can be simply expressed as the product of the strain due to the temperature difference and the modulus of elasticity. The temperature difference for a given rate of heat extraction will decrease with increasing conductivity. Since the strain is proportional to the temperature difference, the stress resulting from the given rate of heat extraction is proportional to the modulus of elasticity. Therefore, it is desired that the modulus of elasticity be small. Finally, the allowable rupture stress should be as large as possible.

The desired properties of the matrix material would be: high strength at the specified temperature, low modulus of elasticity, small values of linear thermal expansion, high conductivity, and large heat capacity per unit volume. Other desired properties would be resistance to oxidation, resistance to reduction by combustion gases, dimensional stability under conditions of thermal cycling, and ability to withstand a large number of cycles of heating and cooling without loss of strength. The oxidation resistance of refractory metals, e.g., molybdenum or tungsten at these temperatures, even with the best protective coatings, are inadequate. The carbides, nitrides, and borides are similarly lacking in chemical stability at elevated temperatures, particularly in the presence of oxygen. The only other suitable class of materials is the refractory oxides.

Of the several oxides that have high enough melting points (greater than 4500°F), only two are feasible considering cost, chemical stability, and operational suitability; these are zirconia and magnesia. Beryllia is excessively expensive; thoria also is expensive and both involve personnel hazards.

Zirconia has been used as a heater matrix material for some time. However, present commercial material is not satisfactory for this application. Commercial products are lacking in long time stability, perhaps due to loss of the calcia used to suppress a crystalline transformation that is accompanied by a volume change. The material is not able to withstand extended thermal cycling without deterioration. Its creep resistance at elevated temperatures appears to be inadequate. This experience is strange when one considers the basic characteristics of zirconia; its high melting point, its resistance to thermal shock, etc. It is important to understand why the presently available material is unsatisfactory.

One possible reason is the presence of impurities. Tests have been conducted which indicate that long term stability of the calcia-stabilized zirconia is possible for high-purity material (say less the 1/2% impurities). Creep strength is also greatly enhanced by high purity. Thus, the processing of the ores and the raw material up to the point of making the shape itself may strongly influence the properties of the finished product.

It is also true that the processing of the material into the finished shape can exert a very great influence on the final properties. An example of this would be a very high quality alumina brick which shows a modulus of rupture at 2500°F of a little over 2,000 pounds per square inch. In contrast, the same kind of material but somewhat purer and of higher density shows a rupture strength of more than 8,000 pounds per square inch at the same temperature. This is a

factor of four difference in strength. The major difference between the two materials is the fact the brick has a porosity of about 21% while the other alumina has a porosity of only about 5%. There was also some silica present in the brick. It has been demonstrated that silica in conjunction with many refractory oxides forms glassy phases which tend to accumulate at the grain boundaries and serve as a lubricant, promoting slippage of the grains past one another and consequently low strength and poor creep resistance.

The effect of material porosity has been quite extensively explored with regard to its effect on strength and on the modulus of elasticity. Ryshkewitch in Ref. 1 finds a clear relationship between strength and porosity for both alumina and zirconia in which the strength decreased by a factor of two for each ten percent increase in porosity. Other investigators have found similar effects and derived the general correlation that the ultimate stress at fracture for a porous material is equal to the ultimate stress of a nonporous material times $e^{-7\sigma}$ (where σ is material porosity). Investigations by others, for example Ref. 2, have shown a similar effect of porosity on the modulus of elasticity. In this case $e^{-4\sigma}$ is the factor accounting for the effect of porosity. The effect of porosity on the creep resistance of alumina is very great and adverse, as reported in Ref. 3.

Another processing variable would be grain size. A study by Spriggs & Vasilos, Ref. 4, shows that for alumina and magnesia the transverse bend strength, or rupture modulus, decreases with increasing grain size in a regular fashion which can be represented by the grain size in microns raised to a power. In the case of alumina the factor was a grain size to the $-1/3$; in the case of magnesia the factor was the grain size to the $-1/6$. This would indicate that serious losses in strength would occur should the grain size rise from a value on the order of 10 to 20 microns to a value of, say, 100 to 200 microns. The latter is fairly representative of what would be termed moderately fine grain brick and unfortunately is likely to be encountered in even an initially fine grained refractory oxide after it is held at high temperatures for extended periods of time.

It is certainly possible to reduce material porosity to very low values, of the order of 5% or less. Therefore, a quite appreciable proportion of the ultimate potential strength of the material can be realized as far as porosity is concerned, although the processing techniques may be somewhat different than those most commonly used in making brick shapes. In the case of grain size a degree of control is possible by using very finely divided material which is pressed and then sintered at high temperatures. As has been noted, grain growth occurs with extended periods of time at high temperatures.

However, Ryshkewitch has noted in his book "Oxide Ceramics" (Ref. 5) that additions of what he calls alloying elements to refractory oxides can control grain growth and also can increase the rupture strength and creep resistance at elevated temperatures. An example would be the addition of chromium oxide to alumina. Another example is the addition of small amounts of zirconia to magnesia. In the latter case the apparent effect seems to be similar to that of precipitation hardening of metals. That is, there is a hard and insoluble phase very finely divided and uniformly distributed throughout the primary material. This secondary insoluble phase appears to distort the lattice structure and to thereby increase its resistance to slip. It also decreases the rate of grain growth. The chromium oxide forms a solid solution with alumina which also hardens it, through distortion of the crystal lattice because of different ion radii. Although the literature pertaining to the addition of these alloying elements is not extensive, as far as we have been able to determine, it is clear that practice of the industry recognizes them and that they are commonly used, although perhaps in a largely empirical manner.

The literature clearly indicates that for refractory oxides to have the best high temperature properties it is necessary that they be of low porosity, small grain size, and very high purity. However, the general practice in the industry, in regard to producing brick shapes, is to make the brick porous, 20 to 22% is a typical value, and of a relatively coarse grain material which is sintered at a temperature somewhat below its ultimate use temperature. This appears to go in opposition to the previously stated effects of material porosity on mechanical and physical properties. The stated reason for the brick being made in this fashion is to increase what is sometimes called the thermal shock resistance but is more properly called spalling resistance. Since these two terms are frequently used interchangeably by people in the refractory business, it would be well to consider what the difference is.

As we use the word, thermal shock resistance refers to the ability to resist a fracture (even a micro crack) due to thermal stresses caused by a temperature difference within the material. Spalling refers to loss of material due to cracks under thermal cycling. The American Society for Testing Materials has a standardized test to determine spalling resistance of refractory shapes. This involves cycling from a relatively high temperature to a low temperature with a rapid cooling being effected by an air and water spray blast. The test is deliberately designed to create extremely severe thermal shock conditions to insure that fracture of the brick will occur. The measure of spalling resistance is not resistance to fracture per se. The measure of spalling resistance

is a loss in weight of the material under test due to fracture resulting from a specified number of such heating and cooling cycles (see Ref. 6). This test is meaningful in regard to the use of brick for liners in furnaces and other similar applications in which it cannot be anticipated that complete freedom from cracking would be achieved and where the criterion necessarily is: How long can the brick be used before it must be replaced? For the Tripltee Heater the criterion must be different. Since no dusting is to be encountered, if at all possible, it is clear that no fracture should be permitted. The material should be of such integrity that small particles would not be lost due to thermal cycling, thermal shock, abrasion or whatever.

The effect of increasing material porosity on thermal shock resistance is to lower it considerably (see Ref. 3). This comes about, although increasing the porosity decreases the modulus of elasticity of the material, because it reduces the strength. The modulus of elasticity is reduced at a lesser rate than is the strength. The effect of increasing porosity would be to increase thermal stresses resulting from a fixed value of temperature difference. What is more, porosity, particularly when its value is greater than, about 10 to 15%, decreases conductivity in the material at a rate much faster than the increase in porosity. Thereby the temperature difference existing within the material is increased considerably by increases in porosity for a given rate of heat transfer. So it is apparent that porosity in fact increases the probability of fracture of the material. Then why is porous material used when high spall resistance is needed? The apparent reason is that although cracks do occur, the pores tend to act as crack stoppers, and even when the material has been fractured through and through, the fracture does not form a smooth or regular surface but tends to be quite irregular. The surfaces which result from the irregular fracture may interlock and tend to retain pieces which are no longer structurally integral with the main body of the brick. Thus, it is possible that porosity is desirable in a situation where thermal shock is going to be so severe that fracture must be encountered, since it may substantially decrease the probability of material loss. However, in our case where we must avoid all fracture, any increase in material porosity beyond that which is the minimum readily and feasibily achieved in production, would be undesirable.

In summary, the desirable direction with regard to porosity and grain size is the same from the standpoint of strength, creep resistance, ability to withstand large pressure drop and the ability to withstand rapid changes in temperature without fracture or dusting. It is clear that it is desirable to have the lowest porosity material that is feasible, the smallest grain size that can be attained and maintained, and the highest purity that can readily be attained.

In view of the discussions which have preceded, the next question is: Can adequate properties be achieved in either zirconia or magnesia? A literature search has shown that the answer is yes, at least tentatively. It has been difficult to find properties taken under conditions which permit evaluation of the tests with some certainty, and to correlate these values with those obtained by others. However, it has been possible to find a limited amount of data from several different investigators which appears to be reliable and which correlates well. A body of data which appears to be reliable and covers the greater part of the temperature range of interest is that contained in Ref. 7. The author measured the properties of zirconia, magnesia, and alumina to temperatures above 2830°R. The author determined the ultimate bending stress, the modulus of elasticity, the linear coefficient of expansion, and Poisson's ratio. The purity of the materials was not clear, simply having been stated as less than 1% impurities. Zirconia was stabilized with approximately 4% of calcia. Materials were all prepared by hot pressing. The temperature level and the time for sintering were such as to insure that the grain size would be rather large. The porosities of the alumina, zirconia, and magnesia were 5%, 4%, and about 12%, respectively. These data have been compared with others and appear to be reliable and consistent. These data have been corrected to zero porosity and are presented in the accompanying curves, Fig. 5C and Fig. 6C. Schwartz's values of thermal coefficient of expansion do not appear to be quite as reliable as some others. Comparison of this data with other data recorded by Goldsmith et al. (Ref. 8) indicates that it lies appreciably below other values. Therefore, it is recommended to use the mean curve taken from Ref. 8 for the linear coefficient of expansion of both magnesia and alumina.

The coefficient of expansion of zirconia is of course anomalous since the material is subject to a change in crystalline form at a temperature of around 2000°F. In order to offset the deleterious effects of the resultant inversion in the coefficient of expansion, it is customary to stabilize the material with some calcia. Commonly the material that is supplied is (so called) partially stabilized zirconia. That is, it does not contain enough calcia to convert all of the zirconia to the stable cubic form; only a portion of it is so converted. The reason given for partial stabilization is greater thermal shock resistance, since the coefficient of expansion is lower when partially stabilized than when fully stabilized. Examination of the Norton curves of thermal expansion coefficient versus temperature indicates that the partially stabilized zirconia does possess a lower coefficient of expansion in the temperature range up to approximately 2200°F. However, at temperatures above 2200 to 2300°F the coefficient of expansion

equals that of the fully stabilized material. What is more, our experience, coupled with that of others, has indicated that the thermal cycling stability of partially stabilized, relatively impure zirconia of standard commercial quality is not adequate for heater use. Fully stabilized zirconia of a very high purity is desirable since it appears to possess much greater resistance to change due to thermal cycling. The most severe conditions of thermal shock occur at temperatures on the order of 2500°R where the partially stabilized material would have the same thermal coefficient of expansion as the fully stabilized material. It would appear then that the stated thermal shock advantage of the partially stabilized material depends upon tests conducted at temperatures less than about 2300°R. The coefficient of expansion values recommended are those given by Smoot and King in Ref. 9.

The values of thermal conductivity and specific heat for alumina should be taken from Goldsmith et al. It is recommended that the thermal diffusivity for alumina be calculated from the values of specific heat and conductivity. Values calculated in this manner agree well with measured values reported by Ryshkewitch in Ref. 5. Ryshkewitch reports only two points, which is not adequate for determining the variation of thermal diffusivity with temperature. For dense, stabilized, zirconia the conductivity and the specific heat should be taken from Goldsmith et al. Again the value of thermal diffusivity should be computed from these curves. Such data compares favorably with data reported by Ref. 5. The data from Ryshkewitch cannot be readily corrected to zero porosity since the value of the porosity was not known. Ryshkewitch's values of diffusivity are a little lower than the value indicated by the calculations, as expected, since some finite value of porosity certainly existed. Also included are the values of diffusivity calculated for Norton dense brick, based on Norton values of conductivity. For magnesia the data for linear coefficient of thermal expansion, thermal conductivity and specific heat from Goldsmith would probably be best. The values of thermal diffusivity should be computed from these values. Comparison with a few points reported by Ryshkewitch indicates satisfactory agreement. The properties of alumina, zirconia and magnesia from the sources just discussed are recorded in Figures 1C through 6C.

The best way to evaluate the reliability of the accumulated data would be to compare some characteristic which can be measured in another fashion with that indicated by this data. This can be done in the case of the thermal shock. Thermal shock involves the properties of rupture stress, modulus of elasticity, coefficient of expansion, conductivity, and specific heat. Therefore, a test to determine the thermal stress (or temperature difference) at fracture of a given

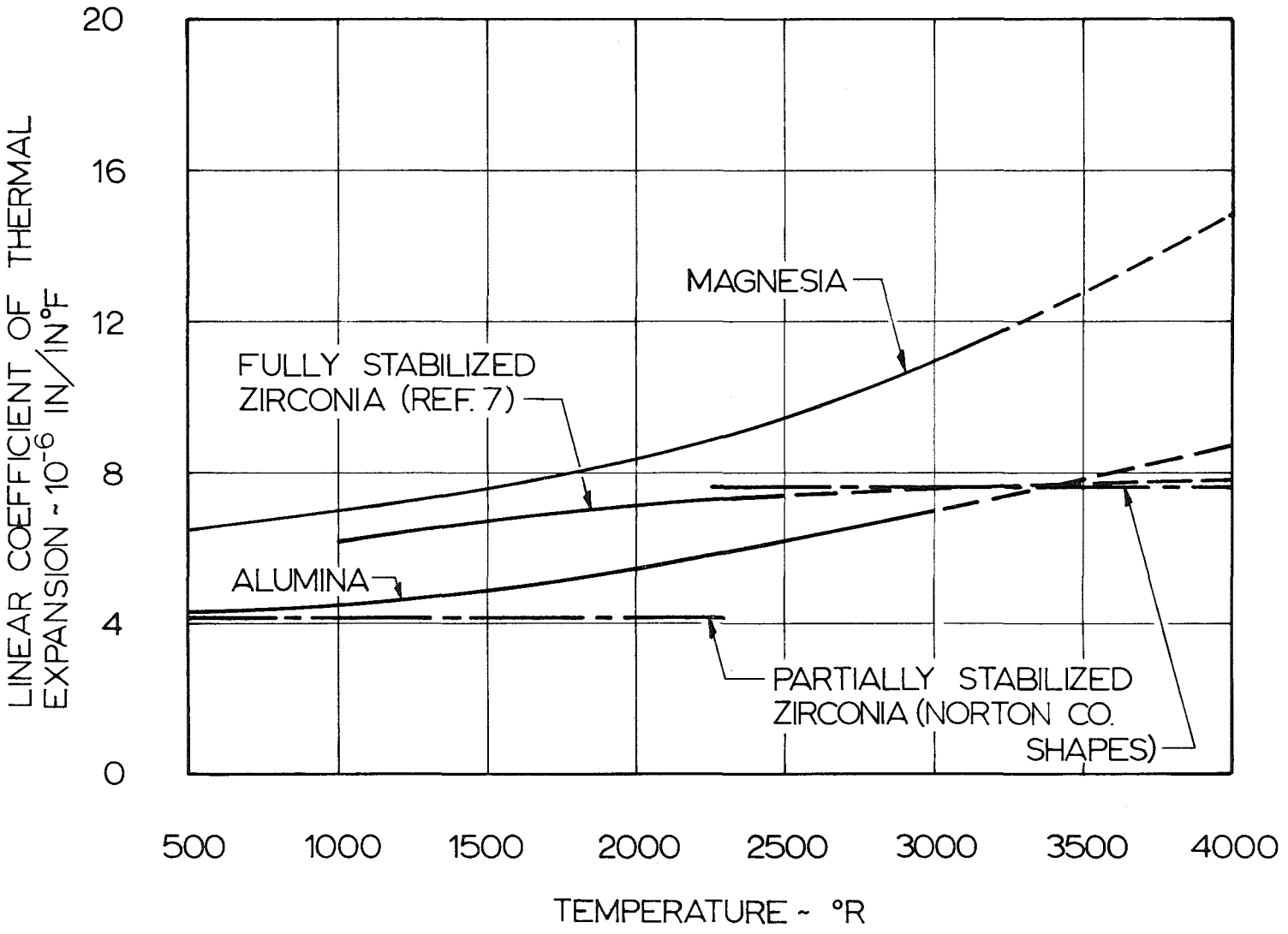

Fig. 1c Thermal Expansion Properties

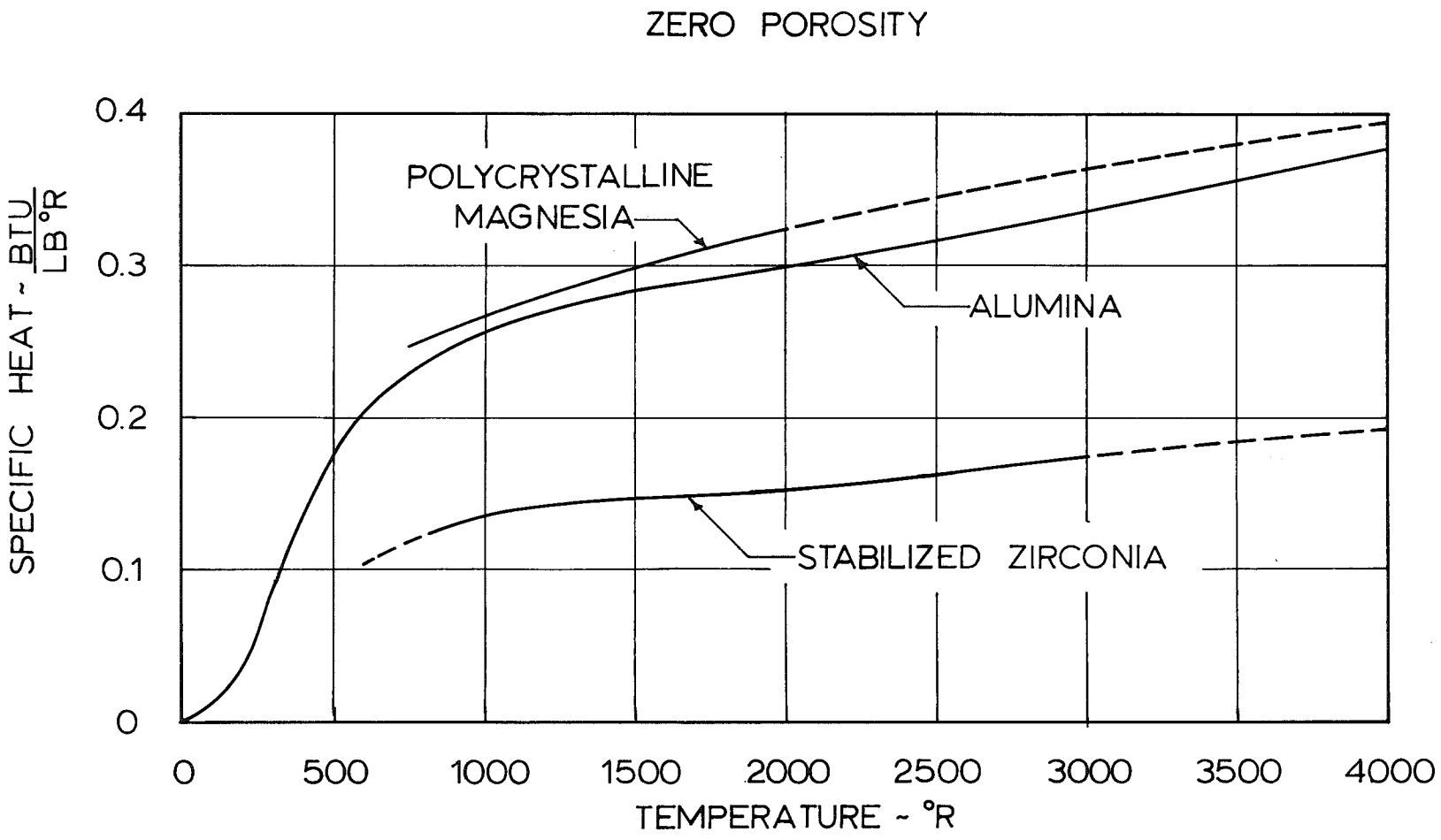

Fig. 2c Specific Heat

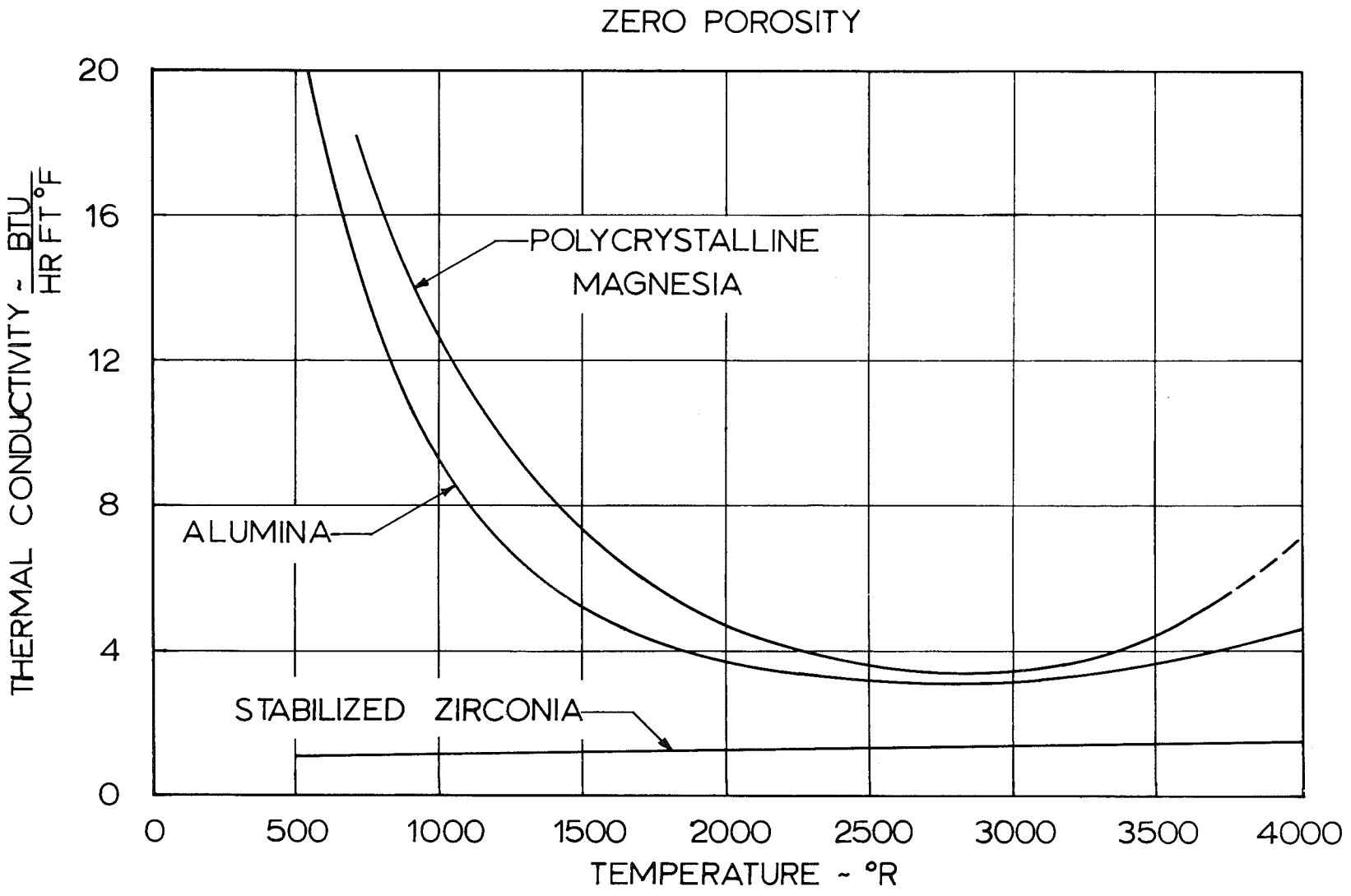

Fig. 3c Thermal Conductivity

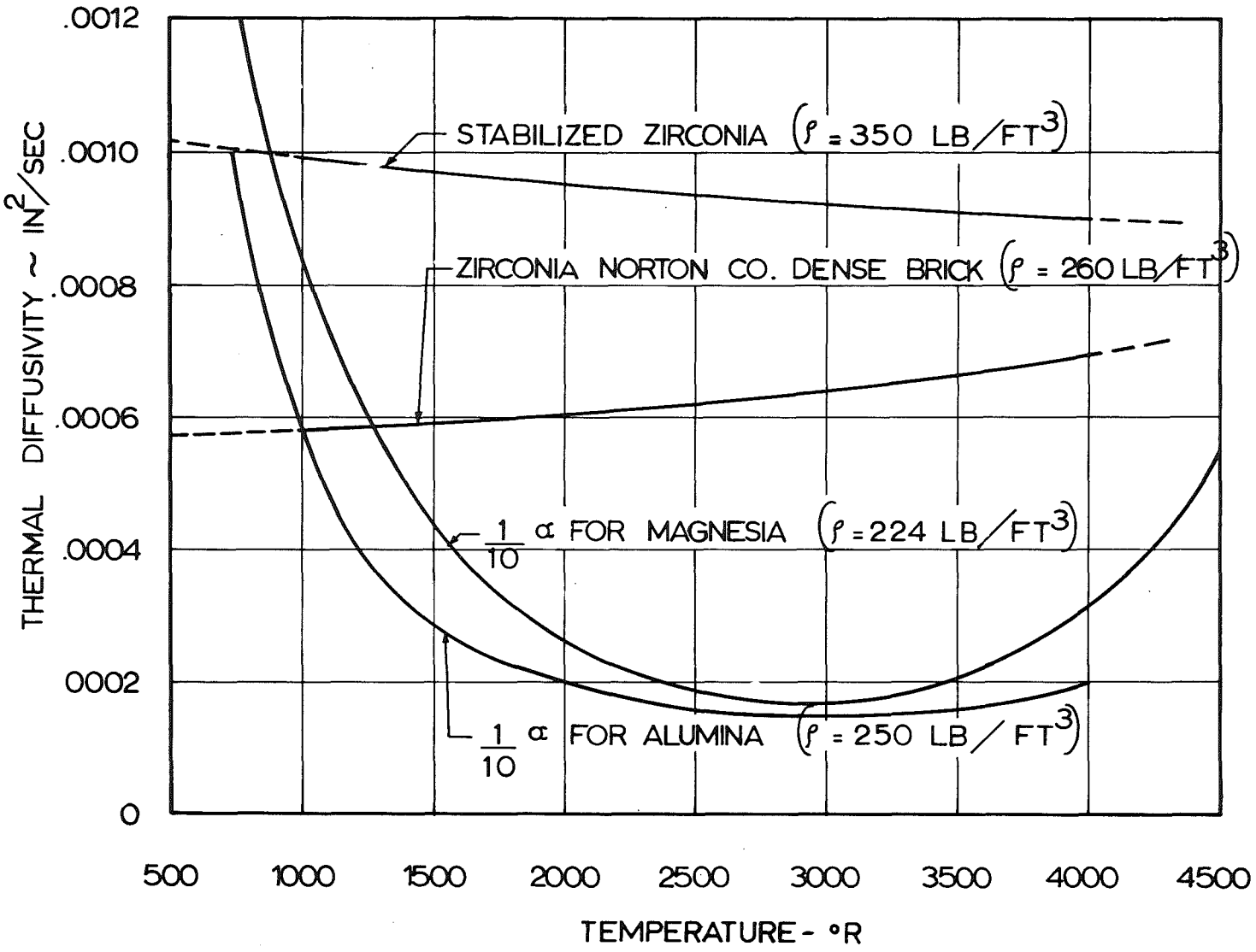

Fig. 4c Thermal Diffusivity

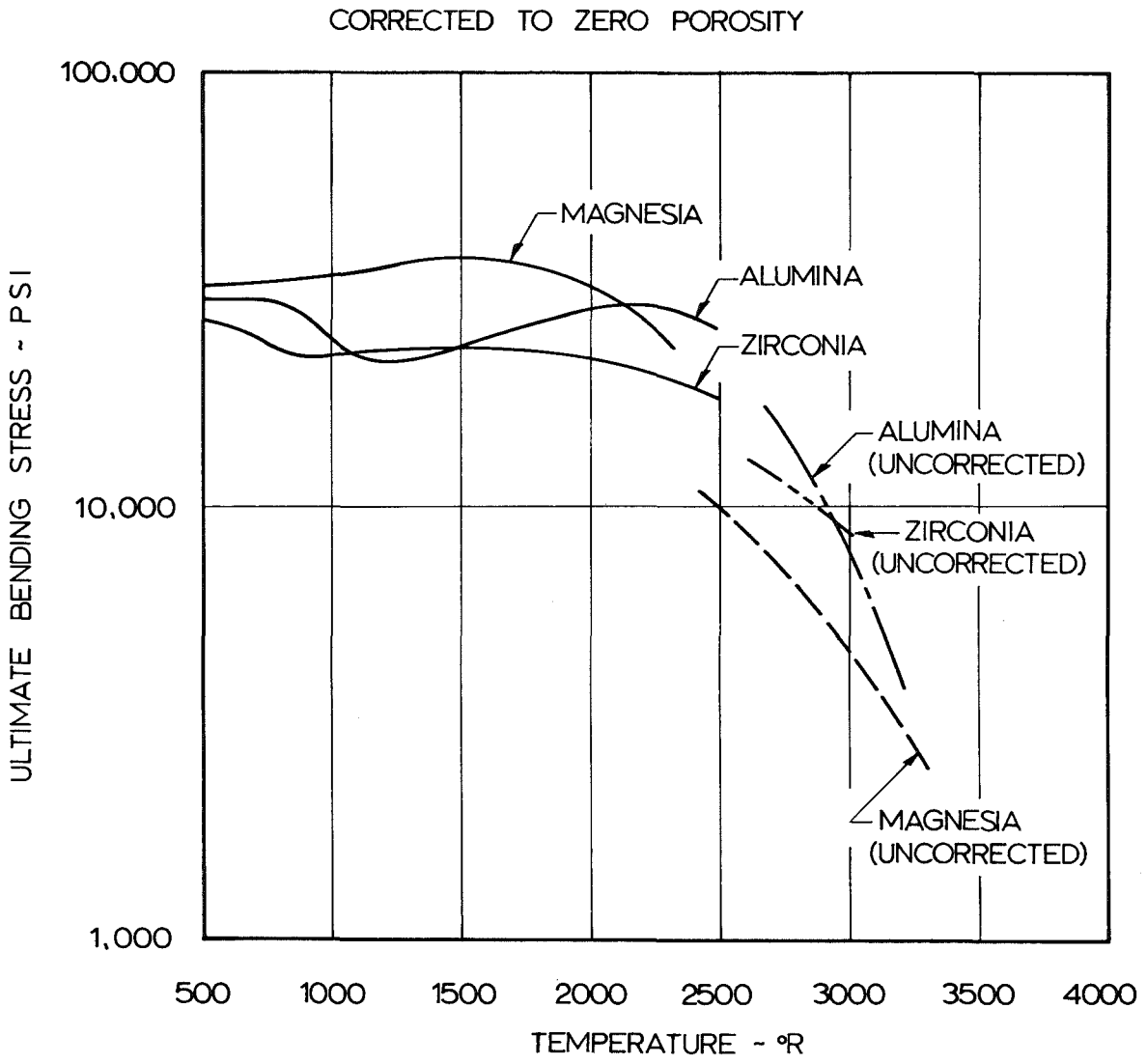

Fig. 5c Ultimate Bending Stress (Ref. 7)

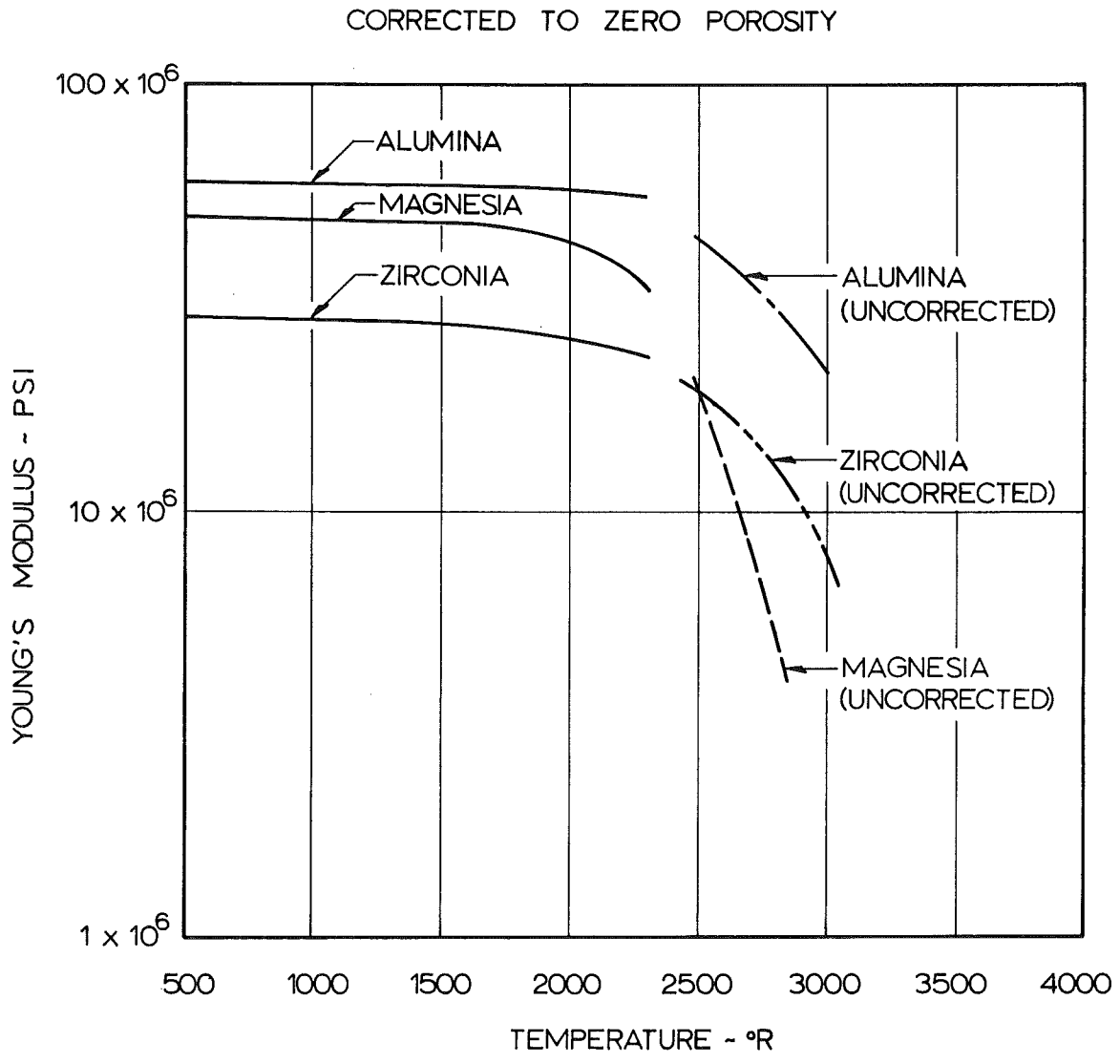

Fig. 6c Modulus of Elasticity (Ref. 7)

shape would provide a useful basis for checking the values of other measured properties. Schwartz in Ref. 7 did precisely this. Cylinders of alumina, zirconia, and magnesia were placed in a furnace and heated slowly. They were then heated further from the inside by a Globar inserted in the center of the hollow cylinder. Thus, the mean temperature was maintained at a fixed value and a temperature gradient was imposed upon the material. The temperature gradient could be controlled by controlling the temperature of the Globar. This was varied until the material cracked. The temperature difference across the material was measured with thermocouples. Property values of the test material were determined independently and used to calculate the values of the temperature difference at which the test cylinder would crack. The agreement between calculated and measured values was very good.

Since Schwartz demonstrated that the thermal shock resistance of a material can be estimated accurately from independent measurements of its properties, and since his property measurements were checked in this fashion, the values indicated by Schwartz should be adequate for our present purposes. Thermal shock resistance calculations have been carried out using the values corrected to a porosity of 3%. The value of the difference between the mean temperature and the surface temperature which would result in material fracture has been calculated for a range of temperatures. These data, which are presented in Fig. 7C, should be adequate for the heater evaluation. The physical property data used to calculate these curves are not necessarily the properties of the material best suited for use in a regenerative heater. Neither do they necessarily represent the properties of a final product which can be easily produced by industry. Eventually, data should be obtained for a sample which has been processed in a production type operation by a commercial supply of refractory oxides.

Referring to Fig. 7C it is apparent that below about 2700°R zirconia can withstand the greatest temperature difference. Since the maximum temperature difference is likely to exist at matrix temperatures of the order of 2500°R or less, zirconia would rate highly. However, this must be coupled with the thermal diffusivity which is proportional to the conductivity. In this respect, zirconia is not as good as magnesia. In terms of the maximum rate of change with time of the mean matrix temperature they will probably be comparable. Alumina, of course, is not suitable since it does not possess adequate strength at the required temperatures. Alumina has a melting point of about 4200°R.

With regard to creep resistance, very little work has been done for oxide ceramics. A correlation of creep

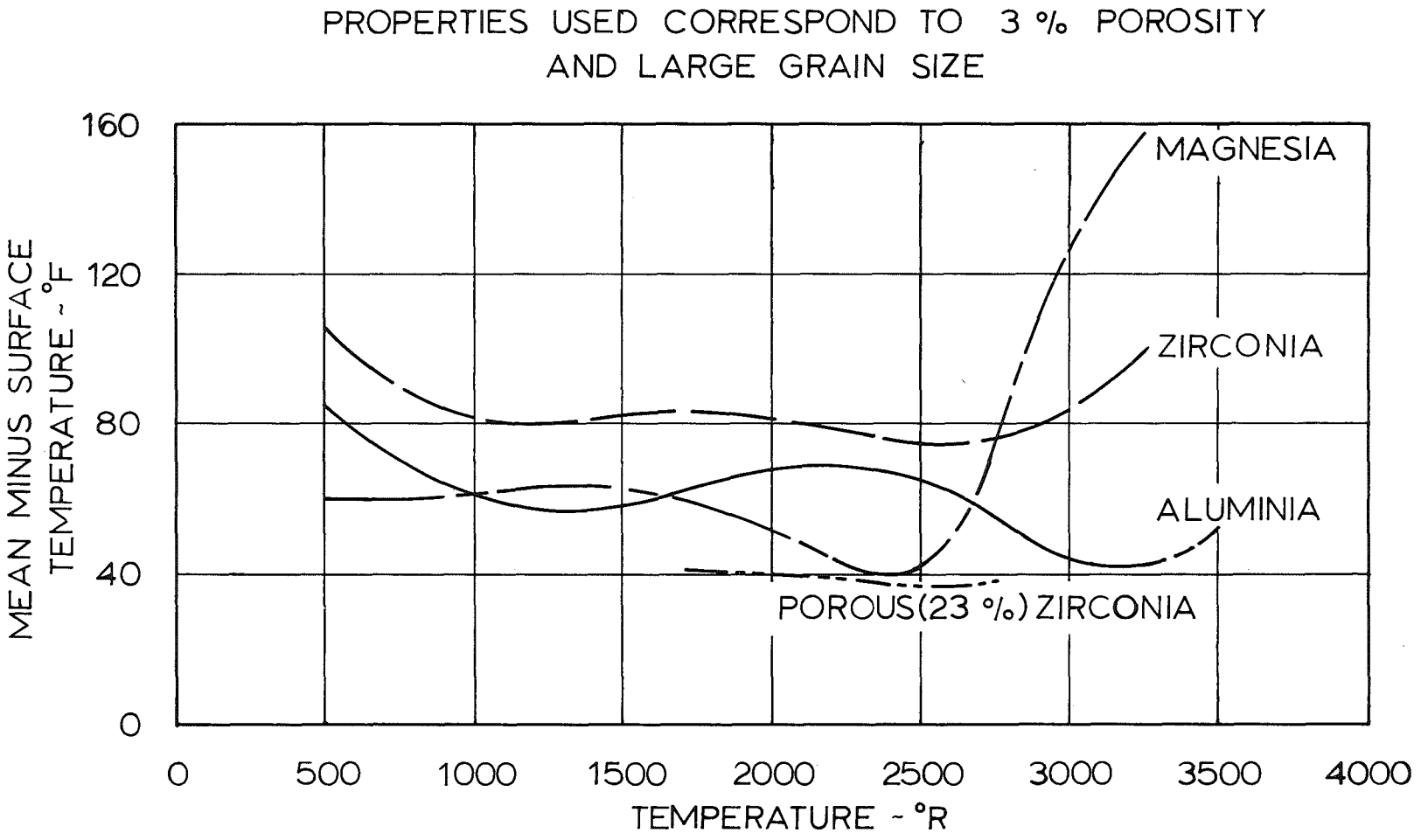

Fig. 7c Calculated Maximum Temperature Difference at Fracture Due to Cooling of Cylinder

properties with temperature and stress for magnesia is contained in a paper by Wygant (Ref. 10). A limited amount of creep data for alumina and one point for zirconia is reported by Stavrolakis and Norton, in Ref. 11. Unfortunately the Ref. 11 data cannot be compared directly with those reported by Wygant since one is reported in terms of twist (radians per inch per hour) whereas the other is reported in terms of elongation (inches per inch per hour). The size of the specimens was not indicated. Wygant, stated that the creep rate of magnesia was approximately 20 times that of alumina and 6 times that of zirconia. In the literature that we have been able to survey the data regarding the creep rate of zirconia is not adequate.

For 1% creep in 10,000 hours, using Wygant's correlation between stress level, temperature, and creep rate, the values of allowable stress as a function of temperature are shown in Fig. 8C for magnesia. These data have not been corrected for porosity, because adequate correlations are lacking. Therefore, they are likely to be conservative. For the maximum anticipated temperature of the matrix, about 4200°R, the allowable stress would be approximately 24 pounds per square inch. A value of this order was felt to be desirable. On the basis of statements made by Wygant and by Starolakis and Norton, zirconia is likely to be stronger. Since creep deformation of the bed would occur under its own weight, and since zirconia has a greater density than magnesia, zirconia would require a higher allowable stress than magnesia for a given creep rate and temperature. It is unlikely that the data in hand is adequate for design purposes. However, it is felt to be adequate for the purposes of the study.

In summary: (1) Values of thermal shock resistance have been calculated based on experimental data which indicate that both zirconia and magnesia in a dense high-purity form are probably suitable for the Tripltee Heater. (2) Data on dense, high-purity magnesia indicates sufficient creep resistance for the Tripltee Heater. The available data indicates that zirconia will be as strong as, if not stronger than, magnesia. (3) As long as the thermal shock limits of magnesia are not exceeded, thermal cycling should not have any deleterious effect on the magnesia. (4) If available, fully stabilized zirconia, which does not destabilize after a large number of thermal cycles, would probably be suitable as well as magnesia. (5) The deleterious effects of material porosity are so great that low porosity materials should be strongly considered for this application. (6) Low porosity materials, sintered at high temperature, should have a smooth, hard surface texture which will minimize dusting. This can be anticipated with either zirconia or magnesia with the qualification that zirconia should be fully stabilized and remain so after a large number of thermal cycles. (7) The achievement

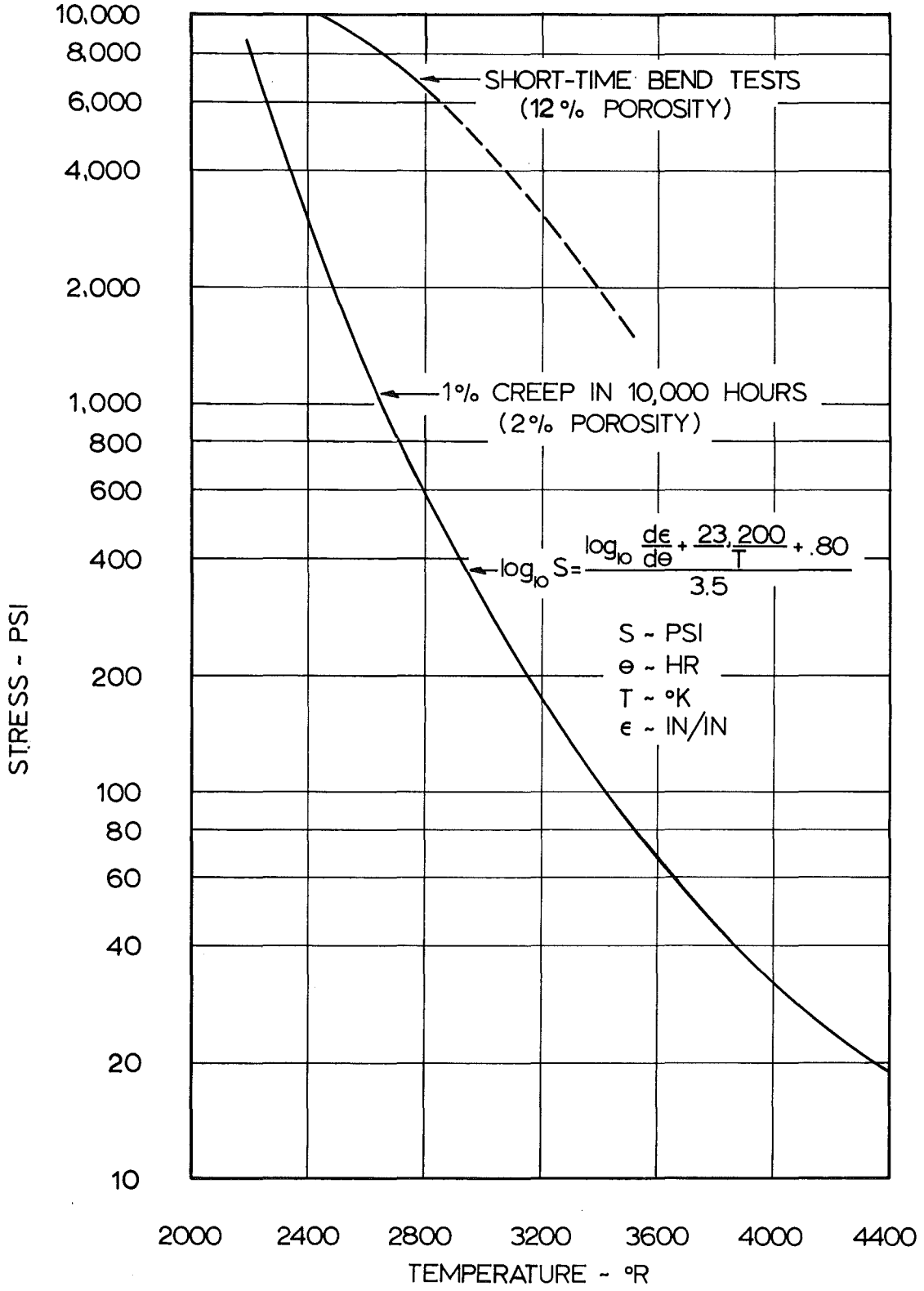

Fig. 8c Magnesia Creep Strength (Ref. 9)

of dense, fine grained material may require that the matrix forms be produced in a manner somewhat different from the brick shapes commonly made by the suppliers of refractory brick. Other techniques might include hot pressing, slip casting, and extrusion. (8) Nothing in the literature reviewed suggests that cored brick shapes would be unsuitable. (9) The data contained herein is limited in applicability for design purposes because of uncertainties as to the material, its source, the type and mode of fabrication, and many other factors which could affect it. There is no reason to believe that these data are unconservative; on the contrary. However, it would be unwise to use these data for basic design unless supported by, and preferably supplanted by, data obtained from tests of materials supplied by potential manufacturers of the matrix material. This data must include accurate determinations of: rupture strength, the modulus of elasticity, conductivity, and linear thermal expansion for the Tripltee temperature range. It must also include accurate determinations of creep resistance. Creep phenomena in refractory oxides appear to be basically similar to those in metals where data taken over a space of several hundred hours can be extrapolated by proper correlations. Thus, experimental creep data should not require test times approaching 10,000 hrs. (10) The material to be used should be qualified by thermal cycling in an atmosphere similar to that of the actual heater before its stability, both chemical and physical, can be established. (11) The required data probably cannot be obtained from industry without compensation. Therefore, we recommend that test lots of material be obtained from reliable potential suppliers at the earliest possible date. These should be subjected to thermal cycling under heater operating conditions. In addition, a qualified ceramic research establishment, such as Batelle Memorial Institute, should be asked to determine the properties of these materials. The industry would then be asked to supply material for the Tripltee heater to specifications based on such demonstrably attainable performance and properties.

APPENDIX C

REFERENCES

1. Ryshkewitch, E: Compression Strength of Porous Sintered Alumina and Zirconia. Jour. Am. Ceram. Soc. Vol 36, No. 2, 1953.

2. Knudsen, F. P. : Effect of Porosity on Young's Modulus of Alumina. Jour. Am. Ceram. Soc. Vol. 45, No. 2, 1962.

3. Cable, R. L. and Kingery, W. D.: Effect of Porosity on Physical Properties of Sintered Alumina Jour. Am. Ceram. Soc. Vol. 39, p. 377, 1956.

4. Spriggs, R. M. and Vasilos, T.: Effect of Grain Size on Tranverse Bend Strength of Alumina and Magnesia. Jour. Am. Ceram. Soc. Vol. 46, No. 5, 1963.

5. Ryshkewitch, E.: Oxide Ceramics. Academic Press, 1960.

6. Norton, F. H.: Refractories. McGraw-Hill Book Company Inc. 1949.

7. Schwarz, B.: Thermal Stress Failure of Pure Refractory Oxides. Jour. Am. Ceram. Soc. Vol 35, No 12. 1952.

8. Goldsmith, A., Waterman, T. E ., Hirschhorn, H J.: Handbook of Thermophysical Properties of Solid Materials. Macmillan Company, 1961.

9. Smoot, T. W. and King, D. F. Permanence of Zirconia Stability, A Function of Purity. (In IEEE Trans. on Aerospace-Support Conference Procedure.p. 1192 1963)

10. Wygant, J. F. : Elastic and Flow Properties of Dense, Pure Oxide Refractories. Jour. Am. Ceram. Soc. Vol. 34, No. 12, 1951.

11. Stavrolakis, J. A. and Norton, F. H.: Measurement of the Torsion Properties of Alumina and Zirconia at Elevated Temperatures. Jour. Am. Ceram. Soc. Vol. 33, No. 9, 1950.

INQUIRY TO REFRACTORY MANUFACTURERS

Gentlemen:

FluiDyne Engineering Corporation is carrying out an engineering analysis of a large capacity, storage heater under contract to the Arnold Engineering Development Center, contract number AF 40(600)-1039. This heater will be used to heat 1500 pounds of air per second to 3500°F for a large, air-breathing-engine (combustion) test facility.

The use of storage heaters for intermittently operating, aerodynamic test facilities is a well established practice. Also well established by universal experience are certain serious deficiencies of such heaters, as presently constructed, when used at high temperatures. Since the deficiencies commonly experienced would disqualify a conventional, high temperature storage heater, this analysis was undertaken with two objectives:

a. Establish what can be done by careful design and material selection to eliminate or minimize deficiencies of present heaters.
b. Establish design criteria for a complete heater system based on results of "a".

The characteristics of current high temperature storage heaters which are unacceptable in this application are:

a. Continuous formation of dust which is carried over into the test section. It is known that such particles can effect combustion, invalidating such tests.
b. Failure of refractory materials in heat storage matrix due to thermal cycling and/or creep. In addition to the expense of frequent matrix replacement, the resultant frequent unavailability of the facility is completely unacceptable.
c. Low efficiency of heat extraction. In the present instance, usual values of heat extraction per cubic foot would lead to a multiple vessel, manifolded heater complex. Such a configuration would aggravate the undesirable characteristics listed under "a" and "b". In addition, new and extremely difficult problems of valving, provision for thermal expansion, etc., would be introduced.

The analysis has been carried far enough to establish what is possible in the matter of increased efficiency of the heat extraction, and has indicated the probable resultant levels of matrix volume. It has also established the probable levels of rate of change of matrix temperature with time and resultant levels of temperature difference within

the matrix material corresponding to the matrix volumes that are possible. It now is necessary to determine the properties of materials which the industry can supply in appropriate forms. That is the substance of this inquiry.

Appended is a summary of the operating conditions and the desired properties of the matrix material. There is included a list of questions your reply to which we would greatly appreciate receiving.

Very truly yours,

FLUIDYNE ENGINEERING CORPORATION

W. S. Hedrick
Senior Engineer

WSH:ph

TRUE TEMPERATURE TEST FACILITY
HEATER
REFRACTORY SURVEY

The conditions of operation of the Tripltee heater and the desired characteristics of a refractory matrix for that heater are given in attached Tables I and II. The specification and final design of this heater must be realistic with regard to refractories, reflecting what now can be, or in the near future can be, procured from the industry. Your replies to the following questions will assist in the preparation of the specifications and design of this heater, and they will help to insure that the heater is realistic with regard to the refractories.

1. Do you now produce refractory material which might be suitable for this application?
2. If you do not at present produce such a material, will you be able to do so within, say, one year? Do you plan to do so? Would the demand represented by this job (perhaps 100 to 200 tons initially, with replacement orders of perhaps 25 to 50 tons at one to two year intervals) be sufficient to justify producing such a material?
3. If you produce such a refractory material, or will be able and willing to do so in the near future, can you produce the shape shown in attached figure 9C. Can you produce this in the entire range of hole sizes and spacings indicated in Table II?
4. Could you indicate the probable level of price of shapes such as figure 9C in a material suitable for this application?
5. If you would prefer for any reason to produce a different shape from that shown, please so indicate. However, the shape should be one with thermal shock resistance at least equal to that of the shape shown.
6. Assuming that you are able and willing to produce, in shapes of interest, a material which you feel is suitable for this application, can you supply test results which will qualify the material and shape for the thermal shock and thermal cycling requirements?

Please note the requirements for thermal shock resistance and thermal cycling given in Table II. ASTM Spalling Test (panel test of fireclay brick) results will not be applicable, because, among other things, it relates the resistance to spalling to the amount of damage to the brick. Note that the requirements of this application involve no damage. In general, two types of test will be acceptable to qualify a material. One would be laboratory tests of a small number of small specimens with at least one dimension

comparable to the mean web thickness of cored brick shape. The specimens would be subjected to the type of thermal cycling and cooling rates specified. At the present time this is considered a satisfactory, in fact preferred, test. Another type of test would involve the production of a small number of matrix units of the actual shape which would be installed in an existing storage air-heater and subjected to a period of actual operation. Although this test is more meaningful, and it must be conducted eventually, it is less useful at this time. This is because it is more difficult to separate the effect of variables and to gain insight into the phenomena observed.

7. Can you supply test results that will qualify the material for the load bearing requirements? The same comments relative to test procedures apply as were made under 6 above. In addition, since secondary creep is usually regular in its behavior, extrapolation of the test results to 10,000 hours would be acceptable if it could be shown that the secondary creep rate has been well established. Further, if the test results can show a time-temperature-stress interdependence in a single parameter which correlates creep rate, then short time, high stress and/or high temperature results covering the necessary range of this parameter would be acceptable evidence of long term creep performance for preliminary qualification.
8. Both zirconia and magnesia will be considered for this application. In the case of magnesia, additional test data must be supplied. It must be demonstrated (possibly from data obtained during thermal cycling tests) that the loss in weight of the MgO due to vaporization is small, say less than 5%, over a period of 10,000 hours. Extrapolation of data taken over a shorter time is acceptable. If it is necessary to specify an excess of air (or oxygen) for the heating phase so as to insure an oxidizing atmosphere at all times, this is acceptable.
9. Since the anticipated use temperature is greater than the usual firing temperature of refractory shapes, and since a regular geometric arrangement of these matrix elements (rather than random, as with spheres) is necessary, it will be necessary that the dimensions of the matrix elements remain within fairly close limits after thermal cycling to the anticipated operational temperatures. If you do not believe that such dimensional stability is possible at usual firing temperatures, can you supply shapes fired at operational temperatures?

TABLE I

TRUE TEMPERATURE TEST FACILITY
HEATER
OPERATING CONDITIONS

Gas to be heated	air
Temperature, inlet,	ambient
Temperature, outlet,	3500°F
Temperature cycle,	Heating, 5 hours
	Cooling, 30 seconds to 100 seconds
Number of cycles required without degradation of matrix*	500
Method of heating	combustion products
Fuel	natural gas (Texas origin)
Maximum temperature change at any point in matrix	1800°F
Maximum rate of change of temperature at any point	75° F/sec.
Maximum temperature of matrix	3700°F

NOTE: *Heating-5 hours; cooling -100 seconds.

TABLE II

TRUE TEMPERATURE TEST FACILITY
HEATER MATRIX
DESIRED PROPERTIES AND GEOMETRY

Geometric form		cored brick
Note: This is a hexagonal shape with a large number of holes as shown in attached figure 9C.		
Hole size		minimum 1/16 inch maximum 1/4 inch
Hole spacing	(about)	1. 6 x hole diameter
Thickness		open
Size		open
Material		open
Strength		total creep of 1% in 10,000 hours at 10 psi and 3000°F
Thermal shock resistance		
Note: This is the minimum acceptable temperature difference within a matrix element due to rapid cooling at which no fracture is to occur		$T_{min.} = 60^{\circ}F$
Thermal cycling resistance		100 cycles
1900°F to 3700°F, heating		1 hour
3700°F to 1900°F, cooling		30 seconds
ΔT not less than 60°F for 20 seconds		
or		500 cycles

1900°F to 3700°F, heating	1 hour
3700°F to 1900°F, cooling	90 seconds
ΔT not less than 20° for 60 seconds	

NOTE: Heating by combustion of natural gas-air-oxygen; cooling by air

SUPPLEMENT

TO REFRACTORY SURVEY

Continuing analysis of the thermal shock requirements of this heater, together with literature surveys on the subjet, have led to the following tentative conclusions. We should greatly appreciate your reactions to these ideas.

The thermal shock criterion for this heater has been established as no fracture or cracks, so as to minimize the likelihood of dusting. We have determined that the likelihood of making adequate engineering calculations to define probability of fracture is great (see reference 1, for example). Preliminary calculations have been carried out to determine the effect of various factors on conditions for fracture. These calculations have emphasized the desirability of the highest possible values of strength and conductivity to resist thermal stress fracture. They have also shown that increasing porosity, even though favorable in its effect on modulus of elasticity (reference 2) is ultimately unfavorable through its excessively unfavorable effect on strength (reference 3), and for larger values of porosity, an excessively unfavorable effect on thermal conductivity (reference 4). Since other considerations also emphasize the desirability of minimum porosity (e.g., compare creep values for low and high density MgO in reference 5), we now wish to emphasize the desirability of the lowest possible porosity. Considering what density has been demonstrated as attainable in the literature (e.g., reference 1, 5 and 6), it appears that density value of, say, 95% of theoretical is attainable. Also, it appears that, while hot pressing is certainly able to produce such densities in materials of interest, hydrostatically pressed and slip cast specimens can also be sintered to similar densities when the particle size is small. By the use of rubber inserts, cored articles may be made to close tolerances by a closed die pressing technique that approximates hydrostatic (isostatic) pressing effects (reference 7).

Grain size has also been demonstrated to exert a substantial influence on mechanical properties (reference 8). Since extended time at elevated temperatures usually causes grain growth to large sizes (detrimental), means for minimizing grain growth are needed. Ryshkewitch (reference 9) indicates that for some refractory oxides (e.g. alumina and magnesia) additions of certain other oxides can control grain growth. What is more, there can be an effect of hardening and strengthening due to such additions (through solution or precipitation hardening mechanisms). Creep resistance can be enhanced. Therefore we should appreciate knowing whether you can supply such modified (alloyed) oxide

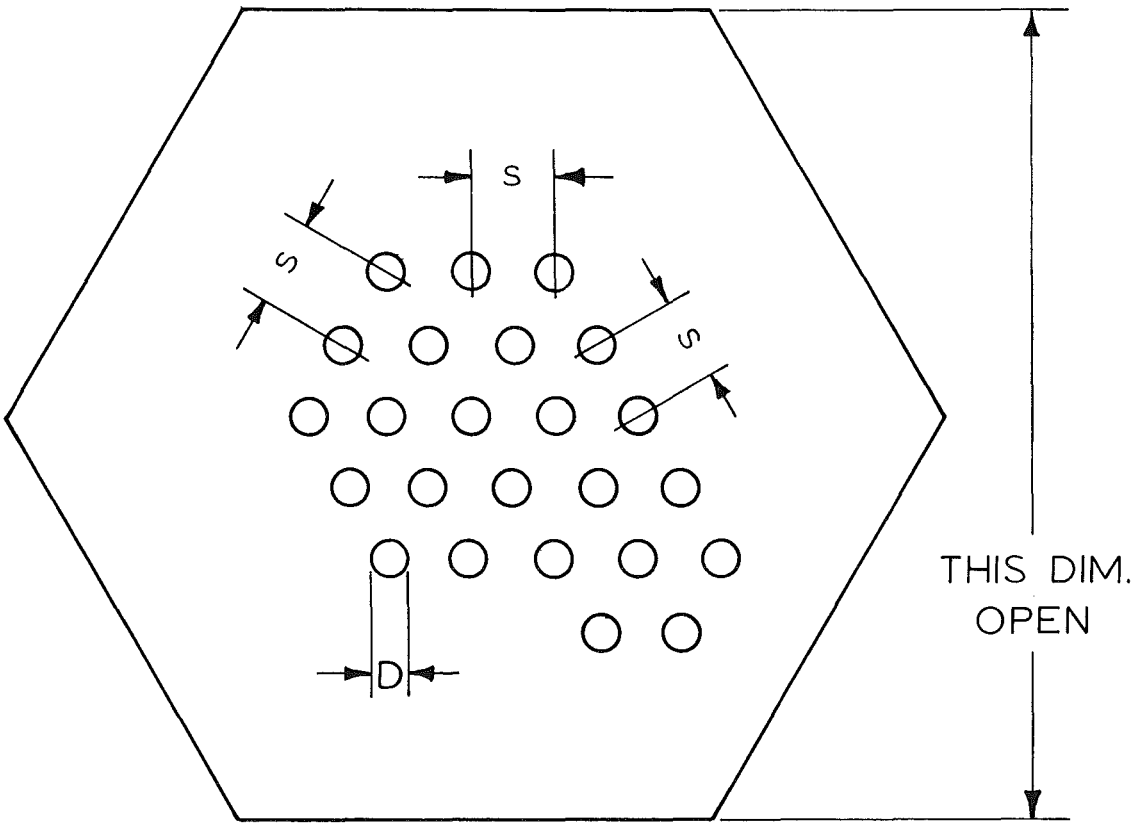

$\frac{S}{D}$ IS ABOUT 1.6
D WILL LIE BETWEEN $\frac{1''}{16}$ AND $\frac{1''}{4}$
THICKNESS IS OPEN

Fig. 9c Cored Brick Configuration for TTT

ceramics.

An alternative shape to the cored brick appears suitable for this application. It is shown in figure 10C. The length should be, say, at least 12 inches. It appears that long, very straight tubes can be sintered (see reference 10). Please indicate whether you can produce this shape and what your preference would be.

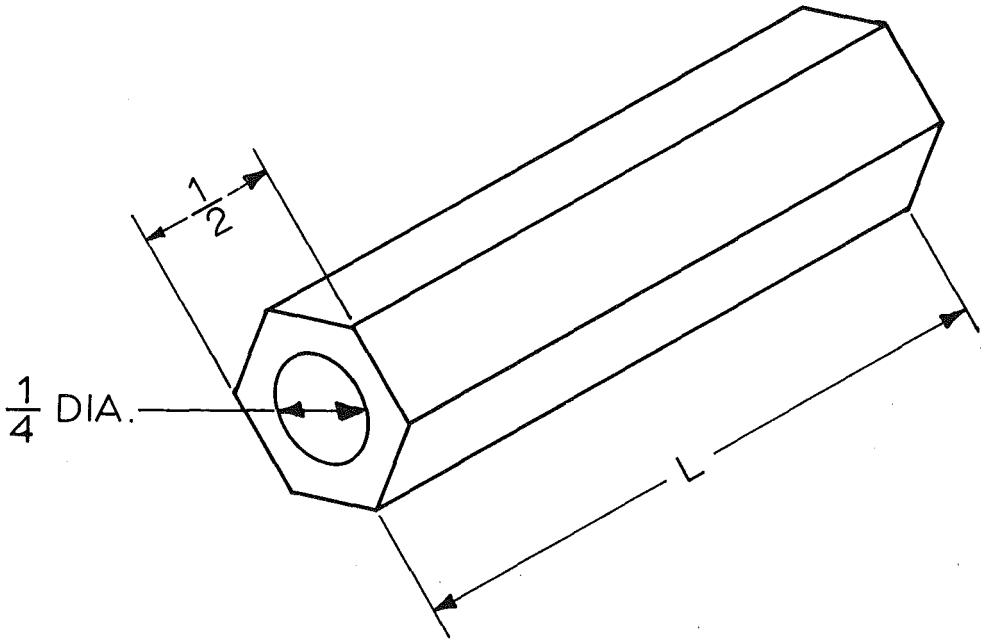

DESIRED THAT L BE AT LEAST 6 INCHES AND PREFERRED THAT L BE LONGER, UP TO 24 INCHES

Fig. 10c Tubular Shape for TTT

REFERENCES

1. Schwartz, Bernard: Thermal Stress Failure of Pure Refractory Oxides. Jour. Am. Ceram. Soc., Vol. 35, 35, No. 12.

2. Knudsen, F.P.: Effect of Porosity on Young's Modulus of Alumina. Jour. Am. Ceram. Soc. Vol. 45, No. 2.

3. Ryshekewitch, Eugene: Compression Strength of Porous Sintered Alumina and Zirconia, and Duckworth, Winston: Discussion of Ryshkewitch Paper. Jour. Am. Ceram. Soc. Vol. 36, No. 2.

4. Kingery, W. D.: Introduction to Ceramics. John Wiley & Sons, Inc. 1960

5. Wygant, J. F.: Elastic and Flow Properties of Dense, Pure Oxide Refractories. Jour. Am. Ceram. Soc., Vol. 34, No. 12.

6. Whiteway, S. G.: Density and Permeability of Sintered Slip Cast Magnesia. Jour. Am. Ceram. Soc. Vol. 46, No. 5.

7. Weber, Thompson, Bielstein and Schwartz: Ceramic Crucible for Melting Titanium. Jour. Am. Ceram. Soc. Vol. 40, No. 11.

8. Spriggs & Vasilos: Effect of Grain Size on Transverse Band Strength of Alumina and Magnesia. Jour. Am. Ceram. Soc. Vol. 46, No. 5.

9. Ryshkewitch, Eugene: Oxide Ceramics. Academic Press. 1960.

10. Whiteway, S.G.: Sintering Long Thermocouple Sheaths Without Warping. Bull. Am. Ceram. Soc. Vol. 41, No. 2.

REFRACTORY MANUFACTURERS CONTACTED

Allis Chalmers
New Products Department
Box 512
Milwaukee, Wisconsin
Attn: Dr. Ervin Colton

American Lava Corporation
219 Kruesi Building
Chattanooga, Tennessee
Attn: Mr. J. S. McFarland

Carborundum Company
New Products Branch
Niagara Falls, New York
Attn: Mr. Paul Braas

Coors Porcelain Company
Golden, Colorado
Attn: Mr. M. Simons

Corhart Refractories Co.
944 Commonwealth
Louisville, Kentucky
Attn: Mr. John Rauscher

Corning Glass Works
Development Laboratory
Ceramics and Refractories
Corning, New York
Attn: Dr. Gale Smith

Corning Glass Works
New Products Division
Corning, New York
Attn: Mr. Charles L. Goss

Diamonite Products Mfg. Co.
P. O. Box 581
Shreve, Ohio
Attn: Mr. Ken Alexander

Gladding McBean & Co.
2901 Los Feliz Boulevard
Los Angeles 39, California
Attn: Mr. S. V. Saginor

Harbison-Walker Refractories Co.
Garber Research Center
P. O. Box 98037
Pittsburgh 27, Pennsylvania
Attn: Mr. T. W. Smoot
Sr. Research Engineer

International Pipe & Ceramics Corporation
Glendale Research Center
2901 Los Feliz Boulevard
Los Angeles 39, California
Attn: G. M. Butler
Director of Research

Kaiser Refractories
300 Lakeside Drive
Oakland 12, California
Attn: Mr. J. C. Hicks

Laboratory Equipment Corp.
Hilltop Road & Leco Ave.
St. Joseph, Michigan
Attn: Mr. H. C. Wagner

McDonel Refractory Porcelain Co.
510 Ninth Avenue
Beaver Falls, Pennsylvania
Attn: Mr. Mitchell

Minneapolis-Honeywell Research Center
500 Washington Avenue So.
Hopkins, Minnesota
Attn: Mr. R. D. Fenity

Minnesota Mining & Manufacturing Company
St. Paul, Minnesota
Attn: Mr. Ward Sanford, Mgr.
Ceramics Project

National Beryllia Corporation
Haskell, New Jersey
Attn: Mr. Phillip S. Hessinger

Norton Company
50 Bond Street
Worchester, Massachusetts
Attn: Mr. G. W. Barnes

Remmy Division
A. P. Green Firebrick Co.
Hedley Street & Delaware River
Philadelphia, Pennsylvania
Attn: Mr. K. K. Breit

Silk City Ceramics & Tool Mfg. Inc.
222 Seventh Avenue
Hawthorne, New Jersey
Attn: Mr. K. P. Doerseln

Zirconium Corporation of America
P. O. Box 9583
Solon 39, Ohio
Attn: Mr. E. C. Sargent, President

APPENDIX D

INSULATION ANALYSIS

Radiation and Free Convection Coefficients

The analysis considers primarily the case of the heater vessel cooled by free convection and radiation from its exterior. The radiation heat transfer coefficient was based on an environment temperature of 90°F and an emissivity of 0.6, thus,

$$h_{rad} = \sigma \epsilon \frac{T_{ex}^4 - T_{amb}^4}{T_{ex} - T_{amb}}$$

where $\sigma = 0.173 \times 10^{-8}$ BTU/hr ft^2 °R^4

Free convection was calculated from the following turbulent flow equation given in Ref. 1:

$$Nu = .10\ Pr^{1/3}\ Gr^{1/3}$$

Substitution of property values corresponding to 680° R reduces this equation to the working form:

$$h_{conv} = .85\ (\Delta T/210)^{1/3}\ \text{BTU/hr ft}^2\ ^\circ\text{F}$$

ΔT is the difference between the shell temperature and the environment temperature (90°F).

It may be noted that McAdams (Ref. 2) gives an empirical formula for turbulent free convection as

$$h_{conv} = .19\ \Delta T^{1/3}$$

which is equivalent to

$$h_{conv} = 1.13\ (\Delta T/210)^{1/3}$$

Thus the equation used is the more conservative of the two, giving lower values of heat transfer coefficient and consequently thicker insulation requirements, (for any pressure vessel temperature limit).

Insulation Properties

The results presented here are based on a thermal conductivity for the insulation of 0.375 BTU/hr ft°F. This value corresponds to commercially available insulating zirconia of 150 lb/ft^3 density at a temperature of 2100°F, approximately the mean temperature of the insulation for a pressure vessel

temperature of 300°F. Increasing the pressure vessel temperature to 600°F gives a mean temperature of 2250°F and a thermal conductivity of 0.40, an increase of only 7%. Therefore, the influence of heater vessel temperature on the insulation conductivity is negligible for the present discussion.

An insulation liner composed of layers of materials of different individual thermal conductivities is a likely configuration. The use of Fiberfrax in the cool zone (below 2000°F) or the use of corrugated ceramic materials would give an effective conductivity less than the chosen value. Thus, in these cases the required insulation thickness would be reduced.

The situation with respect to insulation for a magnesia bed is not as clear because of the lack of thermal conductivity data for this material in low density (insulating) form. At high densities, the thermal conductivity of magnesia is more than twice that of zirconia. However, this does not imply that more than twice the insulation thickness is required. If magnesia were used for the high temperature insulation the outer layer of insulation could be a lower conductivity material such as zirconia, foam alumina, or Fiberfrax. The interface temperature between the magnesia and the second material will be limited by reactions between the materials. Corrugated ceramics may also be used to advantage here. We currently estimate that a magnesia bed will require 50% greater insulation thickness than the values presented in this appendix for the insulating zirconia case.

Heat Flow Analysis

We are concerned only with the insulation required at the location in the pressure vessel where the bed temperature is at its assumed maximum, $T_h = 3900°F$. At all other locations the requirement for insulation will be less severe. The insulation liner and the steel vessel comprise two concentric cylinders. Thus, the heat conduction equation may be written

$$T_h - T_{amb} = q_{loss}\left[\frac{t_{ins}}{k_{ins}}\frac{\ln\frac{D_2}{D_1}}{1-\frac{D_1}{D_2}} + \frac{t_{shell}}{k_{shell}}\frac{\ln\frac{D_3}{D_2}}{\frac{D_3}{D_2}-1} + \frac{1}{h}\frac{D_2}{D_3}\right]$$

where

t_{ins} = insulation thickness

t_{shell} = pressure vessel wall thickness

k = thermal conductivity

h = sum of radiation and convection coefficients

D_1 = inner diameter of insulation

D_2 = outer diameter of insulation (I.D. of vessel)

D_3 = outer diameter of vessel

q_{1oss} = heat flux based on inner diameter of vessel

No allowance has been made for thermal resistance due to air gaps. The three terms in the brackets are the thermal resistances of the insulation, vessel, and outer surface, respectively.

The thermal resistance of the vessel contributes typically 8% to the total resistance. Therefore this term was assumed constant at 0.028 hr ft^2 ^oR/BTU, corresponding to 7 inches of carbon steel with k_{shell} = 21 BTU/ft hr ^oF and D_2 = 12 feet. In the third term, D_2/D_3 was taken equal to one, introducing an error of less than 1%.

Insulation Analysis Results

Results of the insulation calculations are presented in Figs. 1D through 4D and Fig. 9 in Section 4. The latter figure demonstrates the advantage of thin insulation in reducing the heater vessel volume.

The influence of uncertainties in the insulation thermal conductivity and the heat transfer coefficient is shown in Fig. 1D. Obviously an increase in conductivity and a reduction in heat transfer from the vessel will cause the vessel temperature to rise. For example, 25% errors in each, with 1 foot of insulation in a 12 foot I.D. vessel will increase its temperature from 500°F to 640°F. Alternately, the insulation required for a 500°F temperature would change from 12 to 19 inches. This points to the need for accurate information if the design is not to be unduly conservative.

Bearing on this problem of uncertainty in conductivity and heat transfer are the results plotted in Fig. 3D. Here the effect of increasing the heat transfer rate above that estimated for free convection and radiation is shown. An increase in heat transfer coefficient by a factor of two, gives a substantial reduction in vessel temperature, for example, from 500°F to near 300°F with 1 foot of insulation. Such an increase in heat transfer could be provided by a forced draft around the heater.

The temperature difference across the pressure vessel wall is plotted in Fig. 4D for a 7 inch wall thickness. These results apply to a thermal resistance, t_{shell}/k_{shell}, = .028 hr ft^2 ^oF/BTU and can be scaled to other values by the

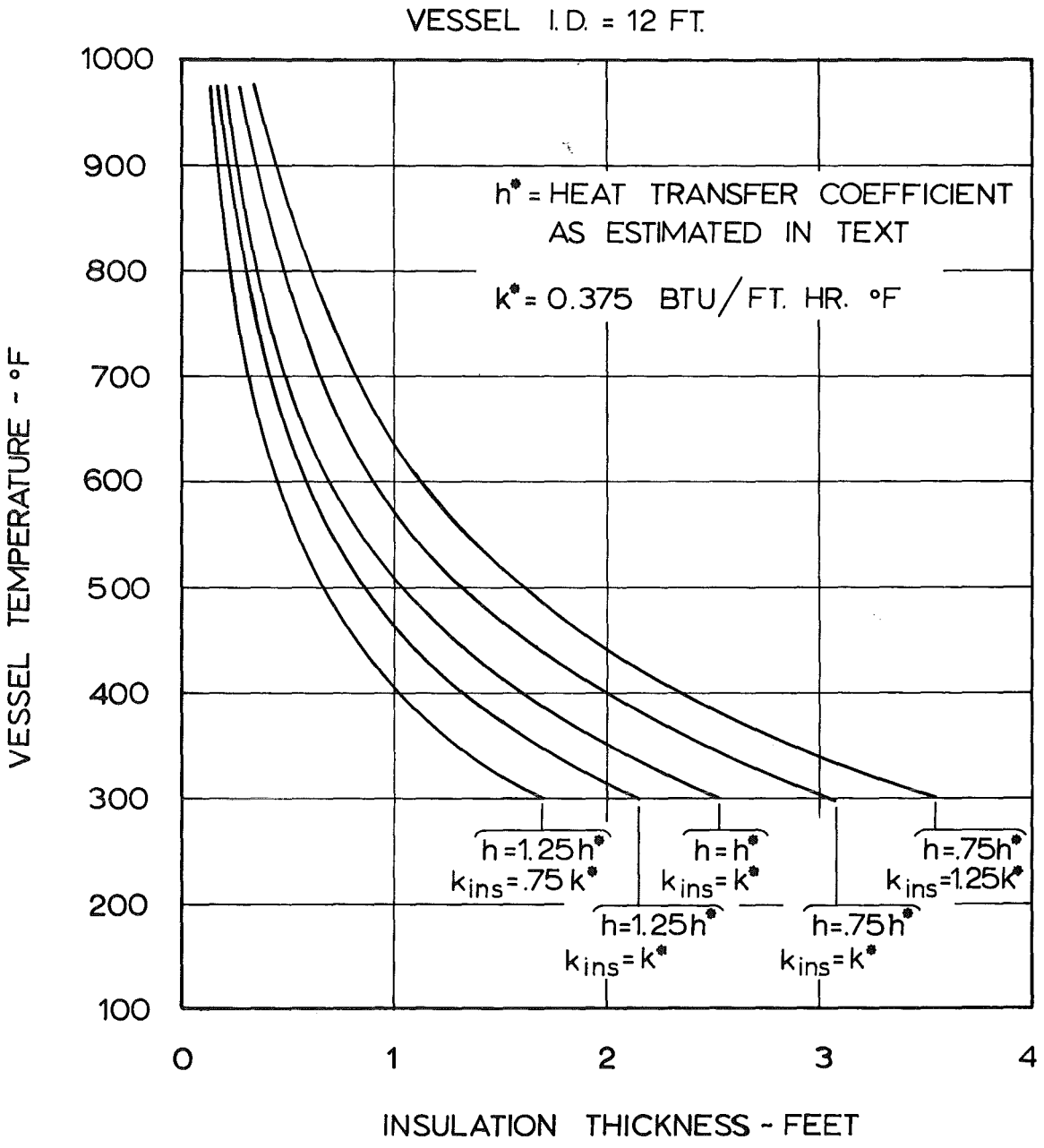

Fig. 1d Heater Vessel Temperature

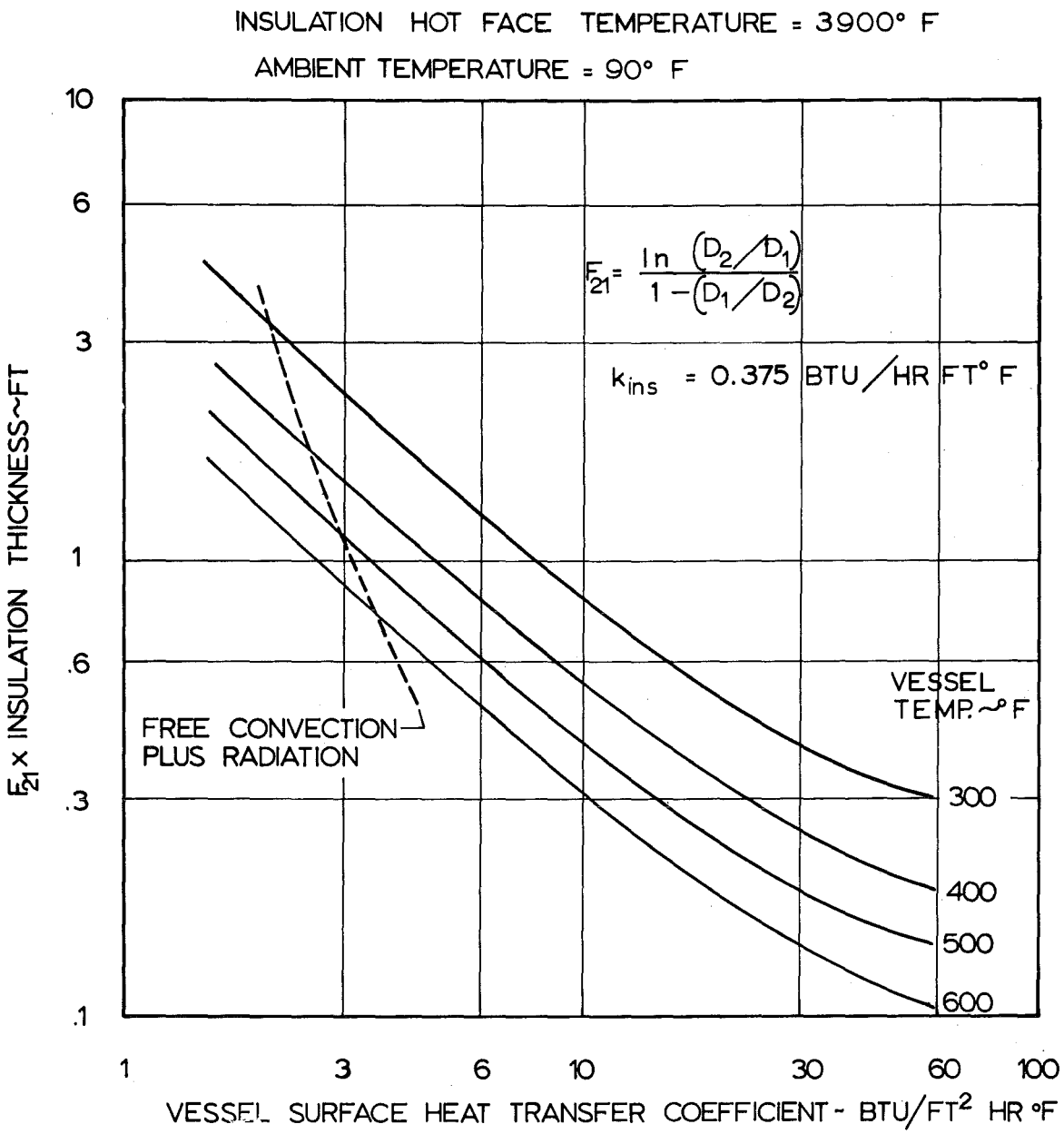

Fig. 2d Insulation Thickness

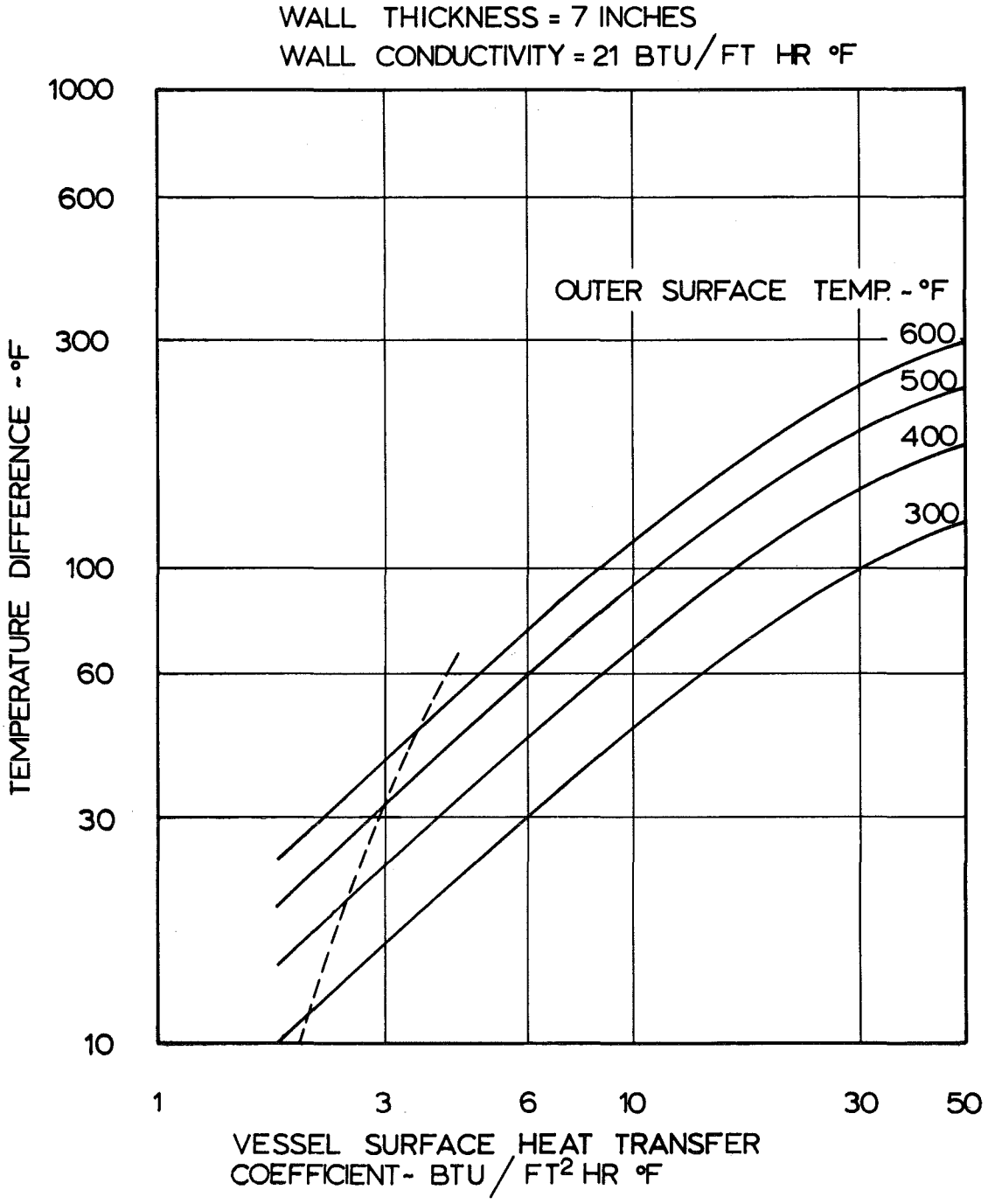

Fig. 3d Temperature Difference Across Heater Vessel Wall

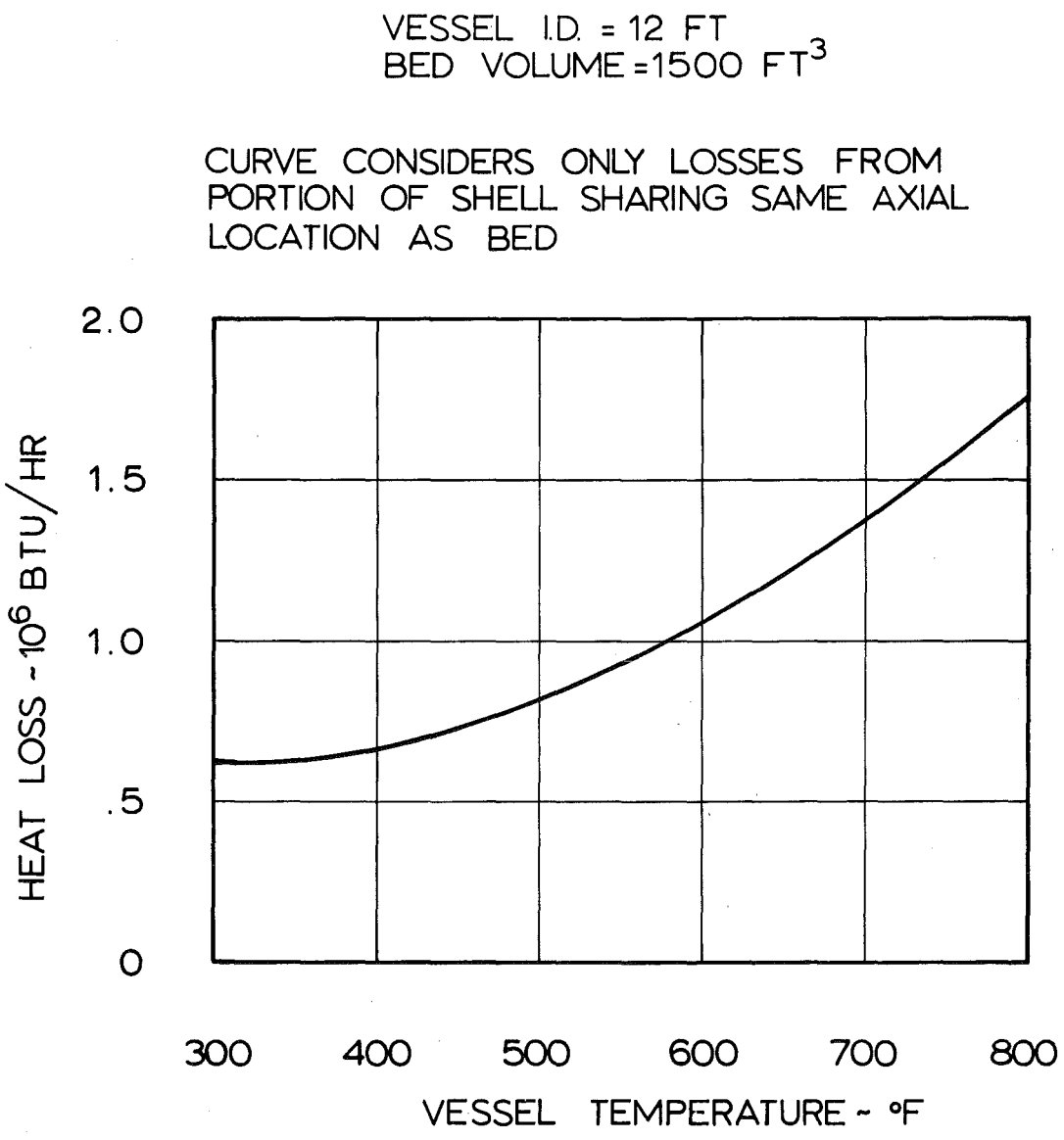

Fig. 4d Effect of Vessel Temperature on Heat Loss

relation

$$\Delta T_{shell} = \Delta T_{.028} \frac{(t/k)_{shell}}{.028}$$

The corresponding thermal stress is

$$S = \frac{\alpha_{ex} E}{2(1-\nu)} \Delta T_{shell}$$

$$= 127 \Delta T_{shell} \quad \text{(steel)}$$

With cooling by free convection and radiation only, the temperature difference and thermal stresses are low, e.g., 30°F and 3900 psi at a 500°F outer surface temperature. Increased cooling by use of forced air flow will cause higher values, but not high enough to create a design problem.

Heat loss from the heater for a particular case is plotted in Figure 4D. In the range of vessel temperatures of interest the heat loss is about 1 million BTU/hr.

Air Flow Through Insulation

There are two possible sources of insulation layer air flow:

1. The cracks between the various pieces of the insulating layer, between insulating layer and vessel wall, and those between heater bed and insulating layer, and
2. The permeability of the insulating material itself.

Flow Through Cracks

For turbulent flow:

$$\Delta p = f \frac{\dot{m}_{cr}^2}{A_{cr}^2} \frac{K_{cr}}{2\rho_g} \frac{\ell}{D_h}$$

where
- A_{cr} = crack flow area
- f = friction factor
- $\dot{m}_{cr}$ = mass flow in cracks
- K_{cr} = ratio of effective crack length to bed length
- ℓ = bed length
- ρ = gas density

D_h = hydraulic diameter = 2 crack widths

therefore

$$\dot{m}_{cr} = \left[\frac{\Delta p}{l}\,\frac{2 g D_h \rho}{K_{cr} f}\right] A_{cr}$$

In applying this equation the following assumptions were made.

1. crack width = 0.03 inches
2. f = 0.08
3. ρ = 1.99 lb/ft^3 (2000 psi, 2250°F)
4. K_{cr} = 1.5
5. crack length = 0.8 in per in^2 of insulation
   = 9.6 ft/ft^2

The assumption that K_{cr} = 1.5 accounts for brick staggering as one horizontal layer is laid upon another. Assumption 5 gives the crack length in a cross section plane normal to the heater axis, based on construction with standard size bricks. The calculated results confirm the assumption of turbulent flow for the range of bed parameters of interest.

Permeability

This source of bypass flow was investigated without benefit of permeability data for the insulating materials which appear desirable for Tripltee. However, data for: alumina filter plates, a range of ceramic bricks, and Fiberfrax were examined. Among these data, the alumina filter plates had the highest permeability, which is reasonable since they are designed to pass flow. Chogsing a value for the least permeable plates gave 4 SCFM/ft^{2}min for 2 inches water pressure drop across a 1 inch thick plate. This value is equivalent to a hydraulic diameter D_h of 1/1000 inch where the entire face area of the insulation is considered flow area. The mass flow through the insulation material itself can then be calculated from

$$\dot{m}_{ins} = \frac{\Delta p}{l}\,\frac{g \rho D_h^2}{32 \mu} A_{ins}$$

A calculation was made for 7 inch thick insulation in a 12 foot I.D. vessel with a 36% porosity bed of 1/16 inch

holes. Flow through the insulation material was only 0.03% of the bed flow. The conclusion is, therefore, that bypass flow due to the permeability of the insulation can be neglected. Only the flow through the cracks need be considered.

Bypass Flow Results

Bypass mass flow rates are plotted in Fig. 5D. The insulation face area for each value of vessel I.D. was based on a vessel outer surface temperature of 600°F and cooling by free convection and radiation (see Fig. 9 in Section 4). Lower vessel temperatures would give higher flow rates. The results of Fig. 5D are applied to a cored brick bed in Fig. 10 of Section 4.

REFERENCES

1. Eckert, E. R. G. and Drake, R. M., Jr., Heat and Mass Transfer, McGraw - Hill, 1959, 2nd Edition.

2. McAdams, W. H., Heat Transmission, McGraw - Hill, 1954, 3rd Edition.

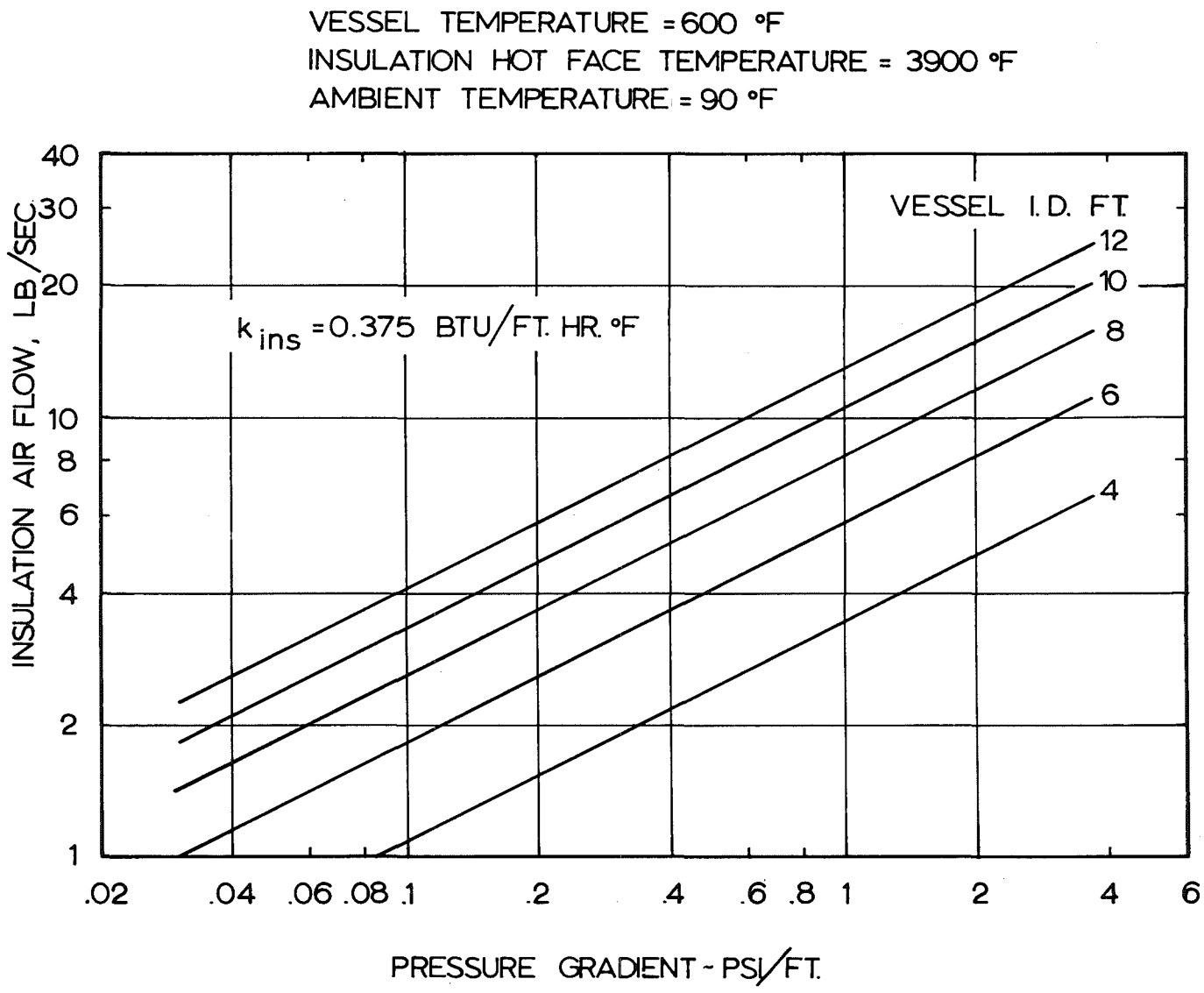

Fig. 5d Air Flow Through Insulation

APPENDIX E

MIXER ANALYSIS

Mixer Requirements

In order to meet the Mach 4 nozzle requirements of 5000 lb/sec, 400 psia, and 1600°R for mass flow, total pressure, and total temperature respectively, the use of a thermal mixer appears attractive. The basic idea would be to take high temperature air from the heater and mix it with low temperature air directly from storage.

Requirements for Mach 7 operation are 1500 lb/sec, 2000 psia, and 3900°R for mass flow, total pressure, and total temperature, respectively. The Mach 4 specification corresponds closely to mixing the Mach 7 heater output with 3500 lb/sec of cold air.

In addition to this favorable energy situation, the difference in the length of the Mach 4 and Mach 7 nozzles allows about 25 feet for the installation of a mixing section which also becomes the stilling chamber for the Mach 4 nozzle.

Coaxial Mixer Concept

The Mach 4 nozzle will have a throat diameter of about 3 feet. In order to provide an area ratio of at least 4, the mixer clear inside dimension will have to be at least 6 feet. Because of its inherent simplicity, a coaxial mixer was the first concept investigated. In order to aid in the application of experimental data to this particular problem, a mathematical mixing model was evolved. A steady state heat balance in cylindrical coordinates is made; assuming axisymmetric flow, the sum of axial convection and radial heat flow terms is set equal to zero. The following partial differential equation results.

$$\frac{\epsilon_t}{r}\,\frac{\partial}{\partial r}\left(r\,\frac{\partial T}{\partial r}\right) - u\,\frac{\partial T}{\partial x} = 0$$

where T = temperature

x = distance in axial direction

r = radius

u = velocity

ϵ_t = a coefficient describing the radial flow of energy (thermal eddy diffusion coefficient).

The lower bound for ϵ_t is $k_g/\rho c_p$, the thermal diffusivity.

The following boundary conditions were assumed.

$$T = T_h \text{ at } x = 0 \text{ for } r < r_j$$

$$\frac{\partial T}{\partial r} = 0 \text{ at } r = 0$$

$$T = T_{mix} \text{ at } r = r_j, \text{ for } x \geq 0.$$

This model deals with a circular jet initially at a uniform temperature for $r \leq r_j$, where r_j is the radius of the jet. Beyond r_j there is initially ($x = 0$) flow at a lower temperature.

T_{mix} = the enthalpy average temperature of the two streams (that temperature obtained if all the flow is mixed perfectly).

Defining the following new variables,

$$\phi = \frac{T - T_{mix}}{T_h - T_{mix}}$$

$$\eta = \frac{r}{r_j}$$

$$\xi = \frac{\epsilon_t x}{u r_j^2}$$

the solution is (for ϵ_t = constant),

$$\phi(\xi, \eta) = 2 \sum_{i=1}^{\infty} e^{-\beta_i^2 \xi} \frac{J_0(\beta_i \eta)}{\beta_i J_1(\beta_i)}$$

where the β_i's are zeros of the Bessel Function of the first kind, zero order, i.e. $J_0(\beta_i) = 0$. This model leaves much to be desired but gives one a basis upon which to examine the experimental data and apply it to other situations. The first term of the solution ($i = 1$) is generally the largest and the one upon which attention was focused. This first term suggests that a relatively simple representation of coaxial mixing might be.

$$\phi \propto e^{-5.79 \frac{\epsilon_t x}{u r_j^2}} J_0\left(2.405 \frac{r}{r_j}\right)$$

Experimental data from Ref. 1 was plotted on semilog paper as

ϕ_{ϵ} vs x/D_j; where $x/D_j = x/2r_j$. ϕ_{ϵ} is the temperature decay function at $r = 0$. Some of this data is shown in Fig. 1E. The data beyond an x/D_j of about 4 validates the exponential decay hypothesis. The initial centerline temperature inertia is to be expected, as it takes some time (i.e. x/u) for the thermal diffusion process to make itself felt on the centerline. It would appear that more terms of the series solution would better represent reality at low x/D_j's. The data in Ref. 1 was used to determine values for ϵ_t based on the assumed mathematical model. Semilog slope values for the data beyond the low x/D_j stage imply ϵ_t's of about 1 ft^2/sec.

The solution suggests that mixing length requirements for a circular jet are established by the volume flow, if ϵ_t is fixed, since ur_j^2 is proportional to the volume flow rate (ft^3/sec). Information found in Ref. 2 indicates that ϵ_t varies with Reynolds number to the 1.29 power. In applying Ref. 2 data to the Tripltee situation, the ϵ_t values should probably be increased because of the higher Reynolds numbers involved. The equation given in Ref. 2 is:

$$\epsilon_{t\,max} = 29 \times 10^{-6}\ Re^{1.29} \qquad \left(\frac{Ft^2}{Hr.}\right)$$

For a case where the Ref. 1 data implies an effective ϵ_t of 1.0, the above formula predicts an $\epsilon_{t\ max}$ of 2.0. Since ϵ_t generally varies across a tube, the overall value would be less than $\epsilon_{t\ max}$ and therefore the experimental value of 1.0 seems to agree quite well with the Ref. 2 equation.

If one uses an ϵ_t for Tripltee of 1/2 $\epsilon_{t\ max} = 27\ ft^2/sec$ the distance required to mix to a $\pm$ 5 percent uniformity of temperature is about twice the 25 feet available. This number is based on the Tripltee mixed flow Reynolds number.

Improved Mixer Concepts

It is now apparent that a more sophisticated mixer than the simple coaxial stream arrangement will be needed. Basically what must be done is to eitherincrease the thermal eddy diffusivity and/or break up the hot and cold streams into a number of substreams where the dimension across which mixing must take place is significantly reduced. In order to minimize the storage heater size it is advisable to run a high mass velocity (lb/ft^2sec) through the heater bed. A limit on the mass velocity is set by bed flotation. Because of the starting process etc., the heater bed will likely be designed to provide a flow pressure drop of 1/3 to 1/2 that required to float the bed for the maximum pressure gradient steady state condition. Excluding the Mach 4 specification, the

worst steady state condition is the one at Mach 7 and 2000 psia. The Mach 4 hot flow requirement is nearly 1500 lb/sec, the exact value depending on ducting losses and the temperature of the cold flow. If this hot flow is to be introduced into the mixing chamber at a pressure much less than 2000 psia, it will become the critical heater design condition and will increase the size of the heater above that required for Mach 7 operation. In order to avoid this undesirable situation, a flow restriction is provided before the mixing section which forces the pressure in the heater to be the same as with Mach 7 conditions. This restriction would have approximately the same minimum area as the Mach 7 tunnel nozzle. Without any flow restriction, the pressure in the heater would run about 400 psia, the required Mach 4 total pressure.

A mixer concept, Fig. 11, was developed to suggest how one might provide adequate mixing in the 25 feet available. The main function of this mixer is to break the stream into many substreams, whereupon mixing can take place in the remaining 19 to 20 feet. The mixer separates the flow into 10 hot and 11 cold rectangular streams. An integral part of this mixer is a nozzle which serves to backpressure the heater as per the previous discussion.

Because of the high temperature of the hot stream (3900°R), it is necessary to either cool the nozzle - mixer device or to make it of heat and oxidation resistant materials. Since possible disturbance of the flow field is of little concern in a mixing device, and probably an advantage, it was decided to use transpiration cooling and introduce a portion of the cool flow through the nozzle - mixer walls. It is desirable, from an air storage viewpoint, to be able to introduce cold flow at a low pressure level. The design concept presented permits exhausting the air storage to a pressure level in the neighborhood of 500 psia.

As shown in Fig. 11, high pressure cold air is provided to transpiration cool that portion of the nozzle from the upstream end to about two inches past the throat section exit. From about two inches past the throat to the mixer exit a static pressure difference in favor of the low pressure cold air will exist. Approximately 16 inches downstream from the throat, the supersonic flow in the nozzle will shock down and become subsonic. At this point the hot flow enters a wedge shaped chamber where the only exits are provided by 10 rectangular passages. The cold flow (about 3500 lb/sec) enters from one or more sides and discharges into the open mixing duct through 11 rectangular passages (oriented vertically in Fig. 10) plus 2 horizontal passages (top and bottom). Cold flow is thus discharged completely around the periphery of the mixer exit plane in order to cool the metal walls

enclosing the mixer during its square to circular transition. A restriction in the cold flow area provided at the mixer exit plane causes the static pressure in the cold stream to drop as it enters the open mixing duct. There is no similar restriction in the hot flow slots. Thus because the flow area in each hot passage increases as one moves toward the exit plane, the static pressure also tends to increase. At the exit plane, equality of static pressure across the duct should nearly be obtained. Upstream of the exit plane, the static pressure in the cold stream will therefore be greater than that in the hot flow. Porous plate construction of the mixer and nozzle will permit the flow of cold air from the cold to the hot side, thereby cooling the walls without any heat losses.

The amount of flow necessary to cool the nozzle - mixer device was calculated on the basis of the following equation for the ratio of heat transfer with transpiration cooling to that without.

$$\frac{h}{h_o} = \frac{\alpha}{e^{\alpha}-1} \qquad \text{(from Ref. 3)}$$

where

$$\alpha = \frac{(\rho u c_p)_{inj}}{h_o}$$

h_o was computed by using the Bartz correlation, Ref. 4, for heat transfer at the throat, and then modifying this result by a multiplicative factor of 2/3 to bring it into agreement with experimental results for air. The appropriate h_o at other locations was computed assuming an inverse proportionality with flow area. For purposes of establishing cooling requirements, hot flow and wall temperatures of 4000°R and 1000°R, respectively, were assumed. The results of the cooling calculations indicate that from 60 to perhaps a 100 lb/sec of high pressure (2000 psia) air will be required for the higher static pressure regions of the nozzle. A constant flow permeability wall would require about 100 lb/sec while with a variable permeability wall the lower figure would be adequate. Similarly, to cool the low pressure regions of the device, about 300 lb/sec of low pressure air should flow through the separating walls.

The choice of 10 hot channels, and the specific geometry shown in Fig. 10, was made on the basis of the Ref. 1 data from which a thermal eddy diffusion coefficient of value 1 ft^2/sec was estimated. The circular jet radius r_j was taken equivalent to 1/2 the channel width. On the basis of Ref. 2

the diffusivity probably is much higher than this for the Tripltee conditions. If such is actually the case, the design as shown is conservative.

REFERENCES

1. Burley, R. R. and Bryant, L., Experimental Investigation of Coaxial Jet Mixing of Two Subsonic Streams at Various Temperatures, Mach Numbers, and Diameter Ratios for Three Configurations. NASA Memo 12-21-58E, February 1959.

2. Jakob, Max, Heat Transfer, Vol. 2, Wiley, 1957, p. 527.

3. Eckert, E. R. G. and Drake, R. H., Jr., Heat and Mass Transfer, 2nd Ed., McGraw-Hill, 1959, p. 305.

4. Bartz, D. R., A Simple Equation for Rapid Estimation of Rocket Nozzle Convective Heat Transfer Coefficients, Jet Propulsion, Vol. 27, No. 1, January 1957.

(REF. 1)	□	△	○
JET DIA., D_j (IN.)	10.0	3.6	3.6
TOTAL DIA. (IN.)	14.3	21.0	21.0
JET MACH NO.	.3	.3	.3
ANNULUS MACH NO.	.3	.3	.1
TEMP. RATIO $\frac{T_h}{T_c}$	1.55	2.44	1.93

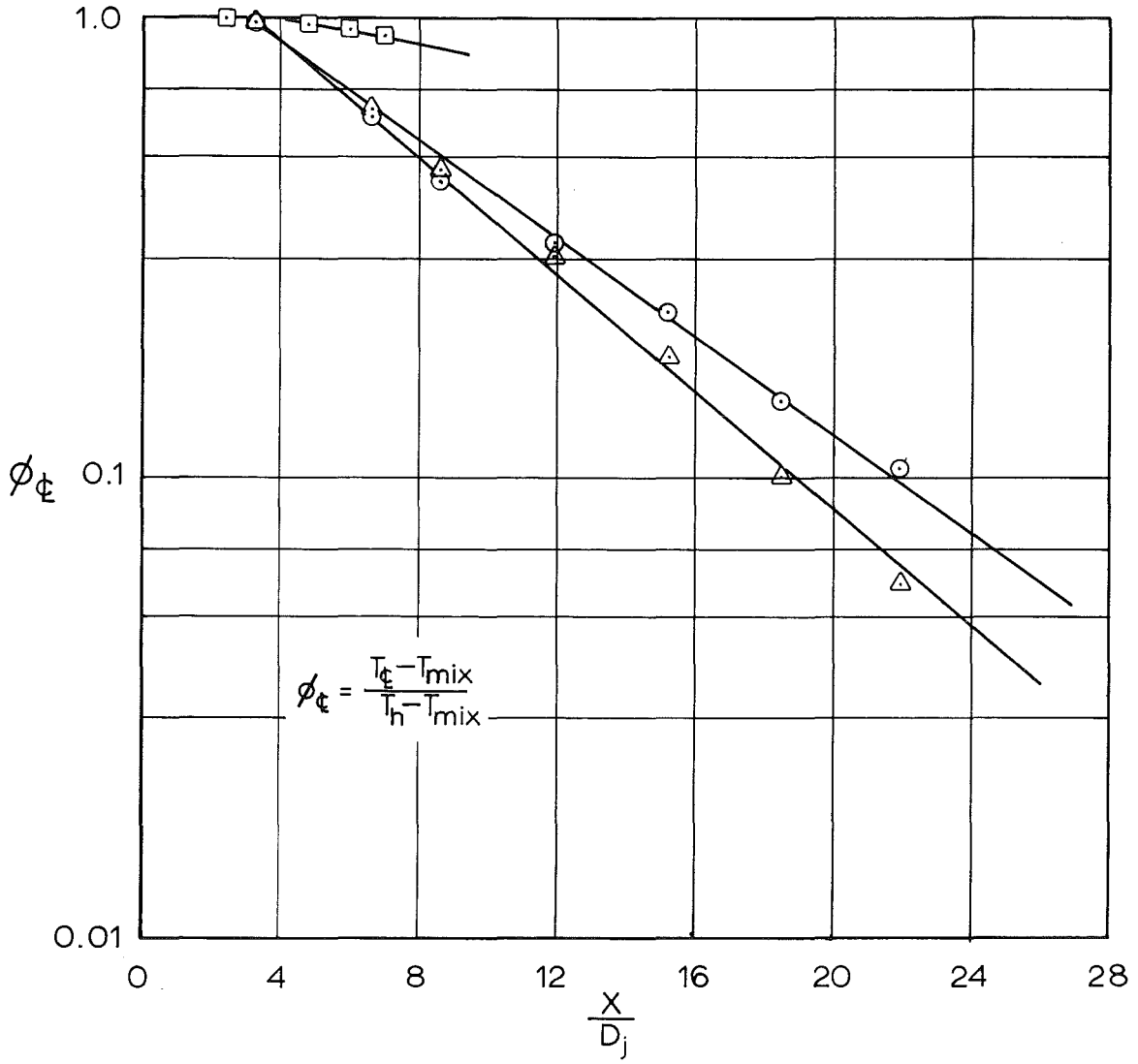

Fig. 1e Coaxial Jet Mixing

APPENDIX F

START-STOP ANALYSIS

This appendix presents some of the mathematical analyses made in studying the start-stop phase of heater operation. Of the specific cases covered, the following are most relevant: Cases A-1, A-4, B-1, B-2, C, D, and E.

The model used for most of the analyses was that of an insulated control volume receiving and losing energy only by the mechanism of mass crossing its boundaries. This control volume is sketched below.

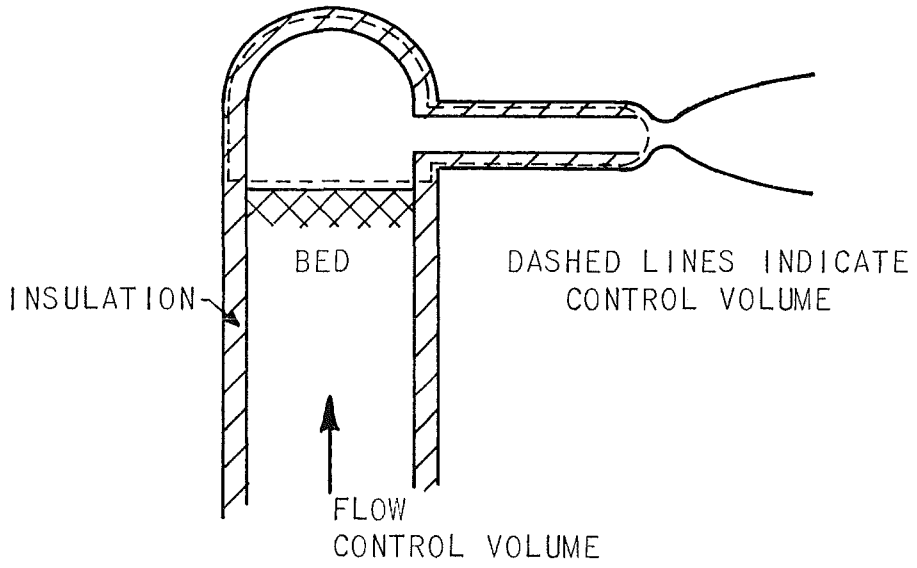

The following equations describe conditions in the control volume.

1. Conservation of mass

$$\oint d\dot{m} = \frac{dm}{d\theta}$$

where m = mass in control volume
$\dot{m}$ = mass flow rate
θ = time

2. Conservation of energy

$$\oint c_p T \, d\dot{m} = \int \frac{d}{d\theta}(c_v T)\, dm \qquad \text{(neglecting velocity terms) etc.}$$

In this analysis flow crossing the control volume boundaries is either that coming in from the top of the heater bed or that leaving through the nozzle throat. The equations can then be written as: (with usual assumptions - adiabatic, ideal gas, etc.)

$$\dot{m}_h - \dot{m}_{noz} = \frac{dm}{d\theta} \qquad (1)$$

$$\dot{m}_h c_p T_h - \dot{m}_{noz} c_p T_{noz} = \frac{d}{d\theta}(m c_v T) \qquad (2)$$

where subscript h = flow crossing heater bed boundary
subscript noz = flow crossing nozzle boundary

The c_v value used to describe the internal energy of the mass within the control volume is subject to some uncertainty as is the appropriate temperature T for the control volume as a whole. The control volume contains both gas and solids (refractory liner) and thus its mc_v in reality is higher than that for the gas alone. Also the temperature is not uniform. Heat losses by conduction have the same effect as increasing mc_v. If we write the previous equations, letting m be the mass of the gas, which is the only component of the mass in the control volume which changes, the effective specific heat we use should be greater than that for the gas alone. This implies an effective γ for the process somewhat less than c_p/c_v for the gas involved.

Let us now consider some of the cases where an analysis has been carried out.

A. Compressive Heating

During the pressurization process compression of the control volume gas by the incoming flow tends to raise the gas temperature above that which obtains during steady flow conditions. This rise could result in material problems.

Case A-1

This case is the hot valve situation where flow enters the control volume after flowing through the heater bed. The nozzle is plugged and therefore $\dot{m}_{noz} = 0$. Equations 1 and 2 become

$$\dot{m}_h = \frac{dm}{d\theta}$$

$$\dot{m}_h c_p T_h = c_v \frac{d}{d\theta}(mT)$$

Substituting γ for c_p/c_v and solving the two equations simultaneously we obtain

$$\gamma T_h = \frac{d(mT)}{dm} = m\frac{dT}{dm} + T$$

Solving this differential equation and evaluating the constant gives:

$$T_2 = \left(T_1 - \gamma T_h\right)\frac{m_1}{m_2} + \gamma T_h$$

where the subscript 1 represents an initial state in the control volume and 2 a later state. Since T_h, the temperature of the fluid leaving the bed, should be very nearly the same as that in the control volume during steady state design conditions (i.e., $T_h \approx T_d$), we can write the result as

$$T_2 = \left(T_1 - \gamma T_d\right)\frac{m_1}{m_2} + \gamma T_d$$

Now the initial mass in the control volume is often small compared to the mass at later states of interest; we note for those cases that

$$T_2 = \gamma T_d$$

As mentioned before the effective γ is less than c_p/c_v of the gas. To decide what the effective γ is, a detailed analysis of a particular design and operational situation would have to be made. Even for the same geometry this number might vary from run to run depending to some extent on such things as the rate of pressurization and dome refractory temperatures.

Case A-2

This is the case where the pressure gradient at the top of the bed is kept the same as during steady state operation. (Subscript d refers to steady state, i.e., design conditions).

$$\left(\frac{dp}{dz}\right)_h \propto f \rho_h u_h^2 \propto \dot{m}_h^2 \frac{T_h}{\rho_h} = \dot{m}_d^2 \frac{T_d}{\rho_d}$$

where we have assumed or noted that the friction factor is the same for all conditions of interest, and

$$\rho_h u_h^2 = \frac{\dot{m}_h^2}{A_{fl}^2 \rho_h}$$

$$\rho_h = \frac{p_h}{R_g T_h}$$

Therefore

$$\dot{m}_h = \dot{m}_d \left[\frac{p_h}{p_d} \frac{T_d}{T_h} \right]^{\frac{1}{2}}$$

Let us use T, m, V, and p when referring to conditions in the control volume. The above equation with $p_h = p$, $T_h = T_d$ and $pV = mR_g T$, becomes

$$\dot{m}_h = \dot{m}_d \left(\frac{p}{p_d} \right)^{\frac{1}{2}} = \dot{m}_d \left(\frac{mT}{m_d T_d} \right)^{\frac{1}{2}} \tag{3}$$

since

$$\frac{p}{p_d} = \frac{m R_g T V}{m_d R_g T_d V} = \frac{m}{m_d} \frac{T}{T_d}$$

For a choked nozzle, $\dot{m}_{noz} = (\text{const}) \frac{p}{T_{noz}^{1/2}}$ and therefore

$$\dot{m}_d = (\text{const.}) \frac{p_d}{T_d^{1/2}}$$

assuming that $T_{noz} = T$ we obtain

$$\frac{\dot{m}_{noz}}{\dot{m}_d} = \frac{P}{P_d}\left(\frac{T_d}{T}\right)^{\frac{1}{2}} = \frac{m}{m_d}\left(\frac{T}{T_d}\right)^{\frac{1}{2}} \tag{4}$$

Combining equations 1 and 2,

$$\gamma \frac{(\dot{m}_h T_h - \dot{m}_{noz} T_{noz})}{\dot{m}_h - \dot{m}_{noz}} = \frac{d(mT)}{dm} \tag{5}$$

Combining equations 3, 4, 5 we obtain the differential equation

$$\frac{dT}{dm} = \frac{\gamma T_d - T\left[1 + (\gamma - 1)\sqrt{m/m_d}\right]}{m\left(1 - \sqrt{m/m_d}\right)}$$

The solution to this differential equation is

$$\frac{mT}{m_d} = T_d\left[\frac{2\gamma\sqrt{m/m_d} - 1}{2\gamma - 1} + \text{const}\left(1 - \sqrt{m/m_d}\right)^{2\gamma}\right] \tag{6}$$

Prescribing initial conditions, which we denote by the subscript i, the above equation becomes

$$\frac{T}{T_d} = \frac{m_d}{m}\left[\frac{2\gamma\sqrt{m/m_d} - 1}{2\gamma - 1} + \left(\frac{1 - \sqrt{m/m_d}}{1 - \sqrt{m_i/m_d}}\right)^{2\gamma}\left\{\frac{m_i}{m_d} - \left(\frac{2\gamma\sqrt{m_i/m_d} - 1}{2\gamma - 1}\right)\right\}\right]$$

If $m_i/m_d = 0$, the solution reduces to

$$\frac{T}{T_d} = \frac{m_d}{(2\gamma - 1)m}\left[2\gamma\sqrt{\frac{m}{m_d}} - 1 + \left(1 - \sqrt{\frac{m}{m_d}}\right)^{2\gamma}\right] \tag{7}$$

Case A-3

In this case the flow into the control volume is kept a constant proportion of the flow out of the control volume.

Define $$A = \frac{\dot{m}_{noz}}{\dot{m}_h}$$

using this with equation 5, we obtain

$$\frac{dT}{dm} = \frac{\gamma T_d - T\{1+(\gamma-1)A\}}{m(1-A)}$$

The solution to this differential equation is:

$$T = \frac{\gamma T_d}{1+(\gamma-1)A} - \left[\frac{\gamma}{1+(\gamma-1)A} - T_i\right]\left(\frac{m_i}{m}\right)^{\frac{1+(\gamma-1)A}{1-A}} \qquad (8)$$

where T_i, m_i are the initial gas temperature and mass quantities in the control volume.

If we assume that $T_i = T_d$ (the steady state value) the solution becomes

$$\frac{T}{T_d} = \frac{\gamma}{1+(\gamma-1)A} - \left[\frac{\gamma}{1+(\gamma-1)A} - 1\right]\left(\frac{m_i}{m}\right)^{\frac{1+(\gamma-1)A}{1-A}} \qquad (9)$$

With a negligible initial mass in the control volume the equation reduces to

$$\frac{T}{T_d} = \frac{\gamma}{1+(\gamma-1)A}$$

Case A-4

In this case the pressure gradient at the top of the bed is some multiple of the steady state pressure gradient and there is nozzle flow out of the control volume.

Now $$\left(\frac{dp}{dz}\right)_h = f_h \frac{\dot{m}_h^2 T_h R_g}{A_{fl}^2 p_d}$$

and $$\left(\frac{dp}{dz}\right)_d = f_d \frac{\dot{m}_d T_h R_g}{A_{fl}^2 p_d} \qquad \text{(at top of bed)}$$

We assume that the friction factor at the top of the bed is independent of flow conditions, and we thus can combine the above two equations to obtain

$$\dot{m}_h = \dot{m}_d \left(\frac{p_h}{p_d}\right)^{\frac{1}{2}} \left[\left(\frac{dp}{dz}\right)_h \Big/ \left(\frac{dp}{dz}\right)_d\right]$$

Now $\frac{p}{p_d} = \frac{mT}{m_d T_d}$ and we define C_1 by

$$C_1^2 = \left(\frac{dp}{dz}\right)_h \Big/ \left(\frac{dp}{dz}\right)_d$$

We can then write

$$\dot{m}_h = \dot{m}_d \left(\frac{mT}{m_d T_d}\right)^{\frac{1}{2}}$$

Recalling equation 5, i.e.

$$\gamma \frac{\dot{m}_h T_h - \dot{m}_{noz} T_{noz}}{\dot{m}_h - \dot{m}_{noz}} = \frac{d(mT)}{dm} \qquad (5)$$

and equation 4, i.e.

$$\dot{m}_{noz} = \dot{m}_d \frac{m}{m_d} \left(\frac{T}{T_d}\right)^{\frac{1}{2}} \qquad (4)$$

We combine the past three equations to obtain

$$\frac{dT}{dm} = \frac{\gamma T_d C_1 - T\left\{C_1 + (\gamma-1)\sqrt{m/m_d}\right\}}{m\left(C_1 - \sqrt{m/m_d}\right)} \tag{10}$$

The solution to this differential equation for any γ is

$$\frac{T}{T_d} = \frac{m_d}{m} C_1^2 \left[\frac{2\frac{\gamma}{C_1}\sqrt{\frac{m}{m_d}} - 1}{2\gamma - 1} + \left(\frac{1 - \frac{1}{C_1}\sqrt{\frac{m}{m_d}}}{1 - \frac{1}{C_1}\sqrt{\frac{m_i}{m_d}}} \right)^{2\gamma} \left(\frac{m_i}{m_d C_1^2} - \frac{2\frac{\gamma}{C_1}\sqrt{\frac{m_i}{m_d}} - 1}{2\gamma - 1} \right) \right] \tag{11}$$

For $\gamma = 1.0$, T/Td = 1.0
For $\gamma = 1.25$, the solution is:

$$\frac{T}{T_d} = 2.5 C_1 \left\{ \frac{C_1}{2.5\frac{m}{m_d}} - \frac{\left(C_1 - \sqrt{\frac{m}{m_d}}\right)}{1.5\frac{m}{m_d}} \right\} + \text{const} \; \frac{\left(C_1 - \sqrt{\frac{m}{m_d}}\right)^{2.5}}{\frac{m}{m_d}}$$

where const =

$$\frac{m_i/m_d}{\left(C_1 - \sqrt{m_i/m_d}\right)^{2.5}} + \frac{5C_1}{3\left(C_1 - \sqrt{m_i/m_d}\right)^{1.5}} - \frac{C_1^2}{\left(C_1 - \sqrt{m_i/m_d}\right)^{2.5}}$$

This const for $\gamma = 1.25$ assumes $T_i = T_d$.
For $m_i/m_d = 0$ this reduces to

$$\frac{T}{T_d} = 2.5 C_1 \left\{ \frac{C_1}{2.5\,(m/m_d)} - \frac{C_1 - \sqrt{\frac{m}{m_d}}}{1.5\,(m/m_d)} \right\} + \frac{2}{3} \frac{\left(C_1 - \sqrt{\frac{m}{m_d}}\right)^{2.5}}{C_1^{.5}\,(m/m_d)}$$

B. Pressurization Times and Gas Mass Expended During Process

B-1 Time to Pressurize

Conservation of mass:

$$\dot{m}_h - \dot{m}_{noz} = \frac{dm}{d\theta} \qquad (1)$$

Now as shown under section A-4 we have

$$\dot{m}_h = C_1 \dot{m}_d \sqrt{\frac{p}{p_d}}$$

For a choked nozzle

$$\dot{m}_{noz} \propto \frac{p}{T_{noz}^{1/2}} \qquad \text{therefore} \qquad \dot{m}_{noz} = \dot{m}_d \frac{p}{p_d} \sqrt{\frac{T_d}{T_{noz}}}$$

Note that we have assumed that pressure differences existing in the heater are small compared to the absolute pressure level in the heater.

By the perfect gas law and a constant control volume we have

$$m = m_d \frac{T_d p}{T p_d}$$

Differentiating the above expression with respect to time, and substituting the expressions given for $\dot{m}_h$ and $\dot{m}_{noz}$ into equation 1, and assuming $T_{noz} = T$, the effective control volume gas temperature, we obtain the differential equation

$$\frac{\dot{m}_d p_d}{m_d T_d} \left(C_1 \sqrt{\frac{p}{p_d}} - \frac{p}{p_d} \sqrt{\frac{T_d}{T}} \right) = \frac{d}{d\theta} (p/T)$$

In order to simplify the solution, T was eliminated as a variable by using a mean value for T and treating it as a constant in solving the previous differential equation,

$$\frac{\dot{m}_d}{m_d}\left\{C_1\sqrt{\frac{P}{P_d}}-\frac{P}{P_d}\sqrt{\left(\frac{T_d}{T}\right)_{mean}}\right\}=\left(\frac{T_d}{T}\right)_{mean}\frac{d(P/P_d)}{d\theta} \tag{13}$$

The solution is:

$$\frac{\dot{m}_d\theta}{m_d}=2\sqrt{\left(\frac{T_d}{T}\right)_{mean}}\ \ln\frac{C_1\sqrt{\left(\frac{T_d}{T}\right)_{mean}}\sqrt{\frac{P_i}{P_d}}}{C_1\sqrt{\left(\frac{T_d}{T}\right)_{mean}}\sqrt{\frac{P}{P_d}}} \tag{14}$$

where p_i is the initial pressure and p is the pressure corresponding to the time θ .

As T_{mean} decreases, i.e., T_d/T_{mean} increases, the dimensionless time $\dot{m}_d\,\theta\,/m_d$ increases. For $\gamma = 1$, T_d/T_{mean} is essentially unity and the solution becomes

$$\frac{\dot{m}_d\theta}{m_d}=2\ln\frac{C_1-\sqrt{P_i/P_d}}{C_1-\sqrt{P/P_d}}$$

This is the upper bound to the time required to pressurize with respect to the assumptions used. However, the assumption that pressure differences in the heater are small compared to the absolute pressure level is not valid initially, when the pressure level is low. Thus actual pressurization times will in general be larger than those calculated. With regards to the total mass expended through the nozzle during pressurization, a more important quantity, this assumption is very good.

B-2 Mass Expended During Pressurization

The mass leaving the nozzle during each increment of pressurization time is

$$dm_{noz}=\dot{m}_{noz}\,d\theta$$

For a choked nozzle

$$\dot{m}_{noz} \propto \frac{P}{T_{noz}} \qquad \text{therefore} \qquad \dot{m}_{noz} = \dot{m}_d \frac{P}{P_d}\sqrt{\frac{T_d}{T}}\, d\theta$$

assuming $T_{noz} = T$, the effective control volume gas temperature. Utilizing this last equation we can write an expression for $\dot{m}_d$ in terms of $\dot{m}_{noz}$. Substituting this into equation 13 (again using a T_{mean}) we obtain

$$\frac{dm_{noz}}{m_d} = -\sqrt{\left(\frac{T_d}{T}\right)_{mean}} \; \frac{(P/P_d)\;\; d(P/P_d)}{C_1\sqrt{P/P_d} - (P/P_d)\sqrt{(T_d/T)_{mean}}}$$

The solution to this differential equation is

$$\frac{m_{noz}}{m_d} = -2C_1\sqrt{\left(\frac{T_d}{T}\right)_{mean}} \left(\sqrt{\frac{P}{P_d}} - \sqrt{\frac{P_i}{P_d}}\right) - \left(\frac{T_d}{T}\right)_{mean}\left(\frac{P}{P_d} - \frac{P_i}{P_d}\right)$$

$$+ 2C_1^2 \;\ln \frac{C_1 - \sqrt{(T_d/T)_{mean}}\;\sqrt{P_i/P_d}}{C_1 - \sqrt{(T_d/T)_{mean}}\;\sqrt{P/P_d}}$$

C. Time and Mass Losses Involved in Decaying the Compression Temperature Rise to Acceptable Levels

During the pressurization process the temperature of the gas in the control volume tends to rise, due to compression by the incoming gas. After the desired pressure is reached the incoming flow is reduced and the conditions tend toward the quasi-steady values desired. We here consider the case where once having reached the design pressure p_d, the incoming flow is varied in a manner which holds the heater pressure constant. We start with the perfect gas law, i.e.,

$$mT = \frac{pV}{R_g}$$

differentiating with respect to time we obtain

$$\frac{d(mT)}{d\theta} = \frac{d(pV/R_g)}{d\theta} = 0$$

since p, V, and R_g are constant during this process. Again, for choked nozzle flow with $p = p_d$ we have

$$\dot{m}_{noz} = \dot{m}_d \sqrt{\frac{T_d}{T}} \qquad \text{(assume } T_{noz}=T\text{)}$$

Also, from the perfect gas law for these circumstances

$$m = \frac{m_d T_d}{T}$$

Recalling equation (2), i.e.,

$$\dot{m}_h c_p T_h - \dot{m}_{noz} c_p T_{noz} = \frac{d}{d\theta}(mc_v T) \qquad (2)$$

and assuming constant specific heats and $T_{noz} = T$, we note that

$$\frac{d(mT)}{d\theta} = 0 \qquad \textit{implies} \qquad \dot{m}_h T_h = \dot{m}_{noz} T$$

Recall equation (1), i.e.,

$$\dot{m}_h - \dot{m}_{noz} = \frac{dm}{d\theta} \qquad (1)$$

Differentiating the expression for m_{cv} we obtain

$$\frac{dm}{d\theta} = -m_d \left(\frac{T_d}{T}\right)^2 \frac{d}{d\theta}\left(\frac{T}{T_d}\right)$$

Assuming $T = T_h$, using the expression for $\dot{m}_h T_h$, and the

above expression we can write equation (1) as

$$\frac{\dot{m}_d}{m_d} = \left(\frac{T_d}{T}\right)^2 \frac{\frac{d}{d\theta}\left(\frac{T}{T_d}\right)}{\left(1-\frac{T}{T_d}\right)\sqrt{\frac{T_d}{T}}} \tag{16}$$

The solution to this differential equation is

$$\frac{\dot{m}_d \theta}{m_d} = -2\left(\sqrt{\frac{T_d}{T}} - \sqrt{\frac{T_d}{T_i}}\right) + \ln\left\{\frac{\left(1+\sqrt{\frac{T}{T_d}}\right)\left(1-\sqrt{\frac{T_i}{T_d}}\right)}{\left(1+\sqrt{\frac{T_i}{T_d}}\right)\left(1-\sqrt{\frac{T}{T_d}}\right)}\right\} \tag{17}$$

The subscript i refers to the initial ($\theta = 0$) conditions which correspond to the time at which the pressure first reaches p_d. The mass expended is $\int \dot{m}_{noz} d\theta$; and using equation 16 in conjunction with $\dot{m}_{noz} = \dot{m}_d \sqrt{T_d/T_{noz}}$ and assuming $T_{noz} = T$ we obtain

$$\frac{m_{noz}}{m_d} = -\left(\frac{T_d}{T} - \frac{T_d}{T_i}\right) + \ln\left\{\left(\frac{T}{T_i}\right)^2 \frac{1-(T_i/T_d)}{1-(T/T_d)}\right\} \tag{18}$$

D. Flow Distribution Through Heater Bed During Pressurization

Gas is stored in the heater during the pressurization process. This storage of mass causes a difference in flow rate as one moves axially through the bed. The analysis of this process is based on the following equations and assumptions.

For any control volume, (m is the mass of gas in the control volume)

$$\frac{dm}{d\theta} = \dot{m}_{in} - \dot{m}_{out}$$

The pressure is assumed uniform throughout the heater and thus $dp/d\theta$ is independent of location. The perfect gas law is assumed to hold and thus for any control volume,

$$\dot{m}_{in} - \dot{m}_{out} = \frac{V}{R_g T}\frac{dp}{d\theta}$$

Thus, for any two control volumes,

$$\frac{(\dot{m}_{in} - \dot{m}_{out})_1}{(\dot{m}_{in} - \dot{m}_{out})_2} = \frac{V_1}{V_2}\frac{\bar{\bar{T}}_2}{\bar{\bar{T}}_1} \tag{19}$$

where $\bar{T}$ is the effective temperature in a control volume, i.e.,

$$\frac{1}{\bar{\bar{T}}} = \frac{1}{V}\int \frac{dV}{T}$$

Relating the flow at the bottom of the storage heater bed to that at the top of the bed we obtain the following formula from equation 19

$$\left(\frac{\dot{m}_c}{\dot{m}_h}\right)_{max} = \frac{1}{\alpha}\left(1 - \frac{\dot{m}_{noz}}{\dot{m}_h}\right) + 1 \tag{20}$$

Subscript max refers to the bed entrance since the flow is a maximum here.

$$\alpha = \frac{V_{cv}}{V_b}\frac{\bar{\bar{T}}_b}{\bar{\bar{T}}_{cv}}$$

V_{cv} = void volume between top of bed and nozzle throat

V_b = void volume in bed and adjacent insulation

For any axial location in the bed we can similarly write

$$\frac{\dot{m}_z}{\dot{m}_{noz}} = \frac{1}{\alpha}\left(1 - \frac{\dot{m}_{noz}}{\dot{m}_h}\right)\frac{V_z}{V_b}\frac{\bar{\bar{T}}_b}{\bar{\bar{T}}_z} + 1 \tag{21}$$

where V_z/V_b = the gas volume between a given bed location and the top of the bed divided by V_b.

This quantity is normally just the distance from the top of the bed, z, divided by the total bed length ℓ , or z/ℓ .

Related to the flow distribution through the bed are the dynamic pressure and pressure gradient quantities. These parameters can be related to values at the top of the bed (bed exit).

$$\frac{dp}{dz} = f\, q / D_h$$

where q = dynamic pressure
f = friction factor
D_h = hydraulic diameter

$$q = \frac{\rho u^2}{2g} = \frac{1}{2}\left(\frac{\dot{m}}{A_{fl}}\right)^2 \frac{R_g T}{\rho g}$$

Thus

$$\frac{(dp/dz)_z}{(dp/dz)_h} = \frac{\dot{m}_z}{\dot{m}_h} \frac{T_z}{T_h}$$

if f and A_{fl} do not vary along the length of the bed.

E. The Stopping Process Analysis

After a tunnel run has been completed, the pressure in the heater will be returned to near atmospheric. During this process, flow of the heater will be regulated by the tunnel nozzle which will be choked for most of the process. The equations describing this process are:

$$dm = -\dot{m}_{noz}\, d\theta \qquad (22)$$

where m = mass of air in the heater, stilling chamber, etc.

Now

$$dm = \frac{V}{R_g T}\, dp \qquad (23)$$

(from the perfect gas law)

where V = free volume

p = pressure in heater

$\bar{T}$ = mean gas temperature in heater, stilling chamber, etc.

$$\frac{V}{\bar{T}} = \int_V \frac{dV}{T}$$

also

$$\dot{m}_{noz} = \frac{m^* p A^*}{\sqrt{T_{noz}}} \qquad (24)$$

where T_{noz} = total temperature at nozzle

and $$m^* = \frac{\sqrt{\frac{\gamma g}{R_g}}}{\left(\frac{\gamma+1}{2}\right)^{\frac{\gamma}{\gamma-1}-\frac{1}{2}}}$$ = choked flow parameter.

Combining equations 22, 23, and 24 we obtain

$$\frac{dp}{p} = \frac{R_g \bar{T}}{V} \frac{A^* m^*}{\sqrt{T_{noz}}} d\theta$$

$$\theta = \ln \frac{p}{p_i} \left\{ \frac{V\sqrt{T_{noz}}}{R_g \bar{T} A^* m^*} \right\}$$

Assuming T_{noz} equals the steady state temperature T_d while:

$$\frac{V}{\bar{T}} = \left(1 + \frac{1}{\alpha}\right) \frac{V_{cv}}{T_d}$$

where α is defined in section D.

Then

$$\theta = -\left(1 + \frac{1}{\alpha}\right) \frac{V_{cv} \ln(p/p_i)}{R_g \sqrt{T_d} A^* m^*}$$

where p_i is the heater pressure at the start of depressurization.

The total mass lost is

$$m_{lost} = -\left(1+\frac{1}{\alpha}\right)\frac{V_{cv}(p-p_i)}{R_g T_d}$$

The energy lost is:

$$E_{lost} = m_{lost}\, c_p\, T_d$$

F. Discussion of Figures

The following paragraphs discuss Figs. 1F through 4F and their application. These figures were drawn from results of the proceding analyses.

Fig. 1F

This graph illustrates the effect of several factors on the temperature rise experienced by the gas in the heater dome-nozzle inlet volume (i.e., the control volume) for case A-4 (equation 11).

The parameter C_1 relates to the rapidity with which the heater is pressurized. The flow rate for a given heater pressure and bed top temperature is directly proportional to C_1. For a finite heater pressure at the start of pressurization, we note that the peak temperature and the temperature when $p = p_d$ both increase with rate of pressurization as characterized by C_1.

The curve for zero initial pressure is not shown, but at $p_i/p_d = 0$ has the value $T/T_d = \gamma$, (1.25 assumed for graph). This curve for $p/p_d > .3$ becomes essentially the same as the plotted curves with the same C_1 value.

p_i/p_d is seen to have its major effect in modifying the peak temperature experienced during startup.

There is some question as to the appropriate γ to use for the pressurization process. Because of heat losses from the control volume gases to the surrounding refractories, it is clear that the γ best describing the process is less than c_p/c_v for the gas. How much less depends on the particular geometry and process rate. The gas γ for $4000^{\circ}R$ is

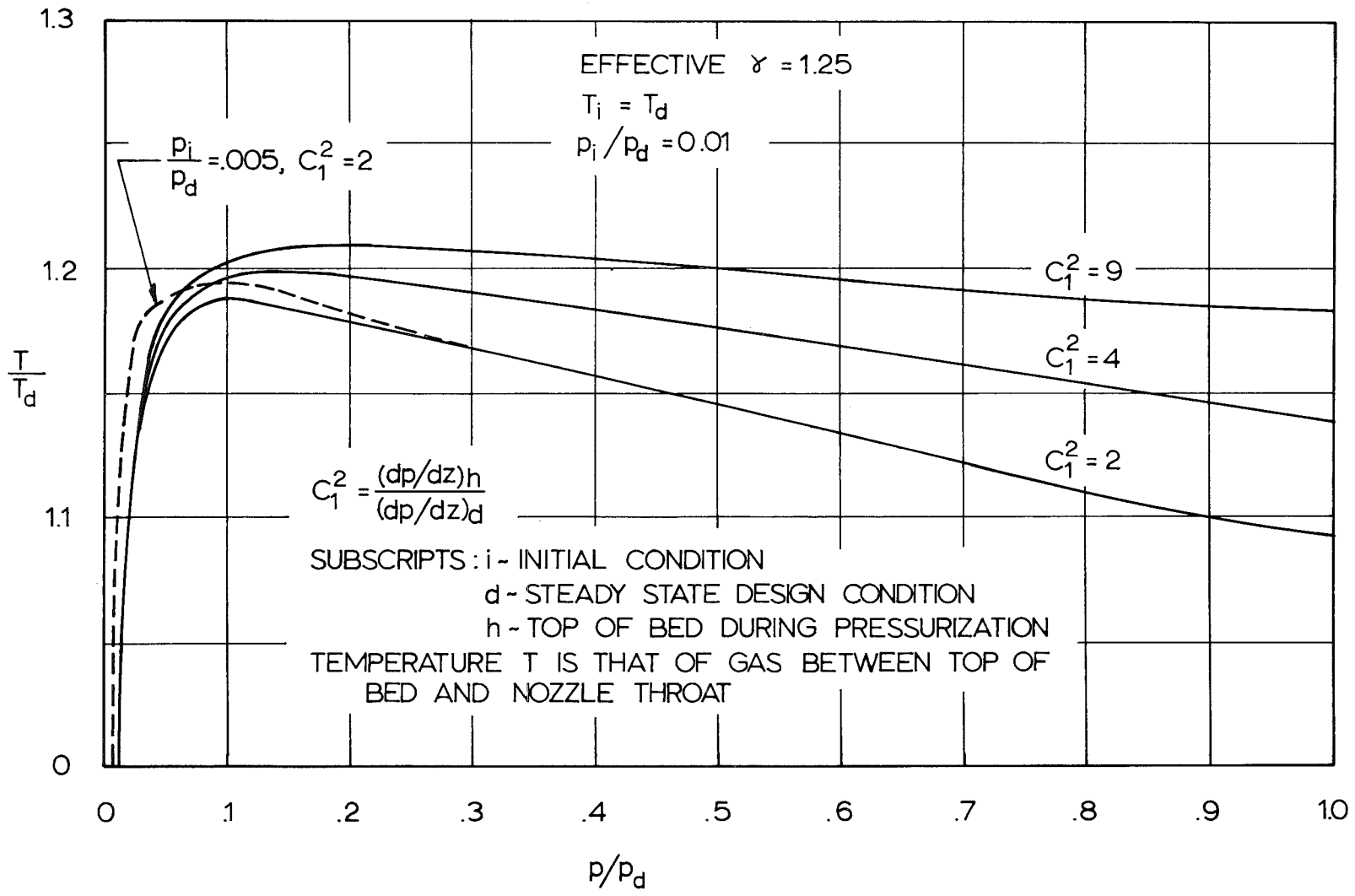

Fig. 1f Pressure-Temperature Variation During Heater Pressurization

about 1.28, so the value 1.25 used for Fig. 1F implies some allowance for such losses, etc.

Fig. 2F

The figure shows the relationship between pressurization rate, as described by C_1, the average control volume gas temperature, and the amount of time and mass expended in reaching the desired steady state pressure (p_d) from equations 14 and 15.

We see from this graph that there is an appreciable advantage, from a lost mass standpoint, in more rapid pressurization. This is particularly true when one is operating with a nearly steady state pressure gradient limitation on the top of the bed, i.e., the slope of the curve approaches ∞ as $C_1^2 \rightarrow 1$.

The average control volume temperature appears to have a significant effect on the mass lost with a somewhat lesser effect on time expended. This temperature is, recalling Fig. 1F, also a function of pressurization rate.

Fig. 3F

During the pressurization process, mass is stored throughout the heater. This storage of mass causes a flow rate reduction in the heater as one moves towards the heater exit. The flow rate is a maximum at the heater entrance and a minimum at the nozzle. Quantitatively, the flow variation through the heater depends on the void volume and temperature distributions in the heater.

Fig. 3F relates the ratio of flow rate at the bottom of the storage bed to that at the top of the bed, as a function of the void volume ratio , (void volume above the bed divided by void volume in the bed and its associated insulation), and a mean temperature ratio. This plot relies simply on the perfect gas law and the assumption that $dp/d\theta$ is nearly uniform throughout the heater (equation 19).

The flow rate and dynamic pressure at any bed location can be related to this maximum flow rate by the simple equations given on the figure. A knowledge of the dynamic pressure distribution throughout the bed is essential in determining operation procedures and limitations.

Fig. 4F

During the pressurization process, the temperature in the gas above the bed tends to rise above that obtained during steady state operation and is still above the steady state (quasi-steady) value when the pressure reaches the

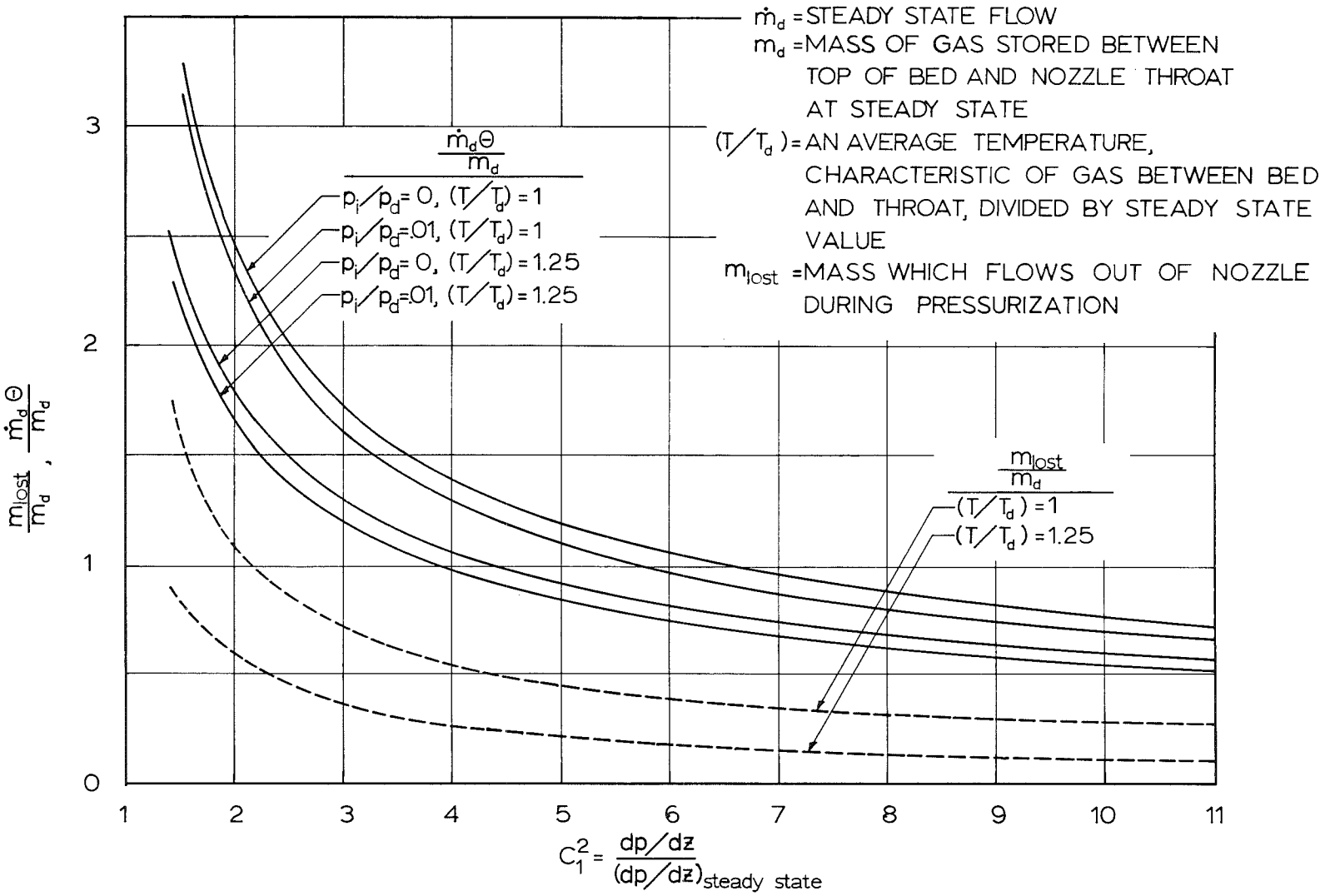

Fig. 2f Time and Mass Expended During Pressurization of Heater

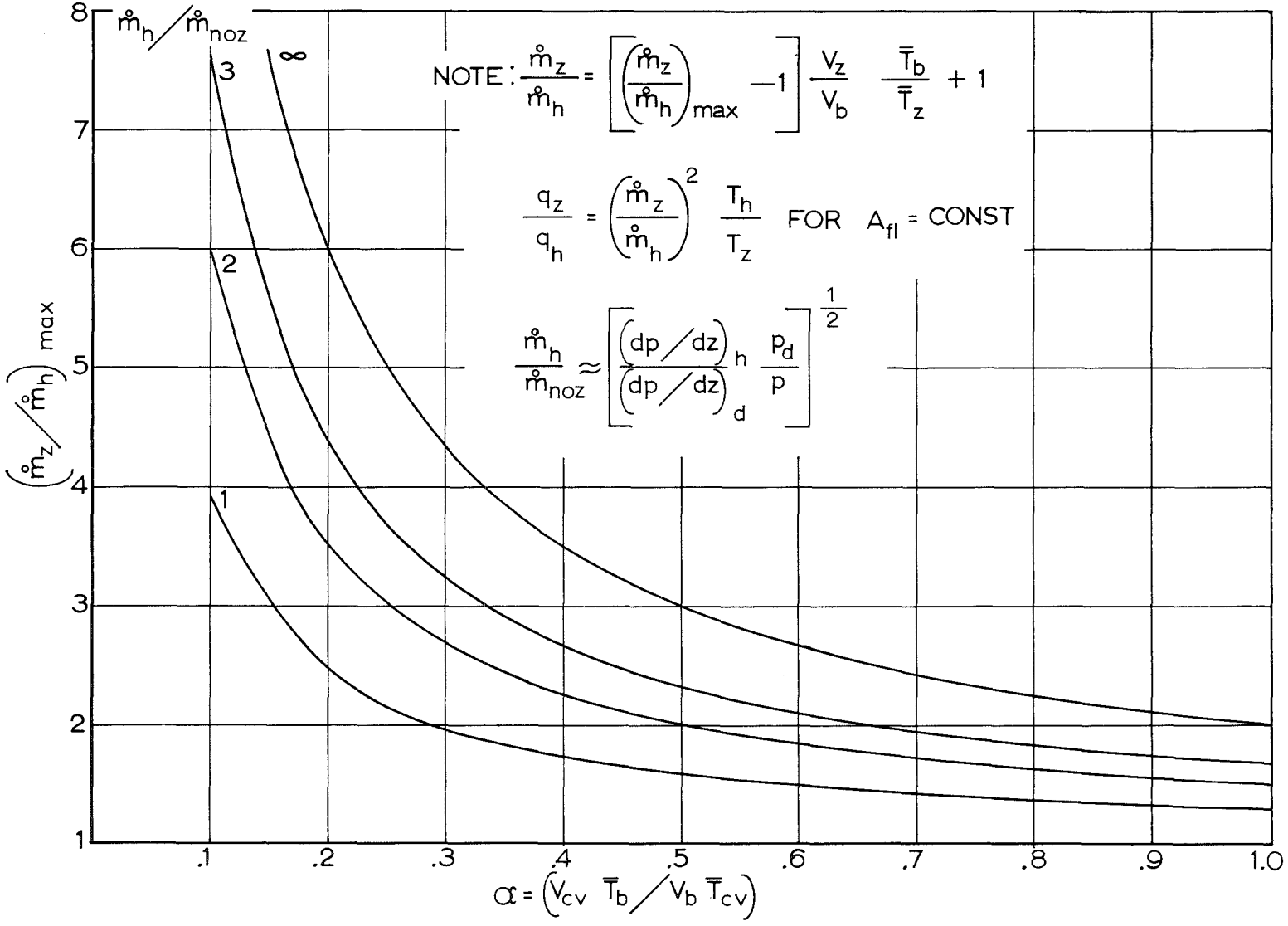

Fig. 3f Mass Flow in Heater During Pressurization

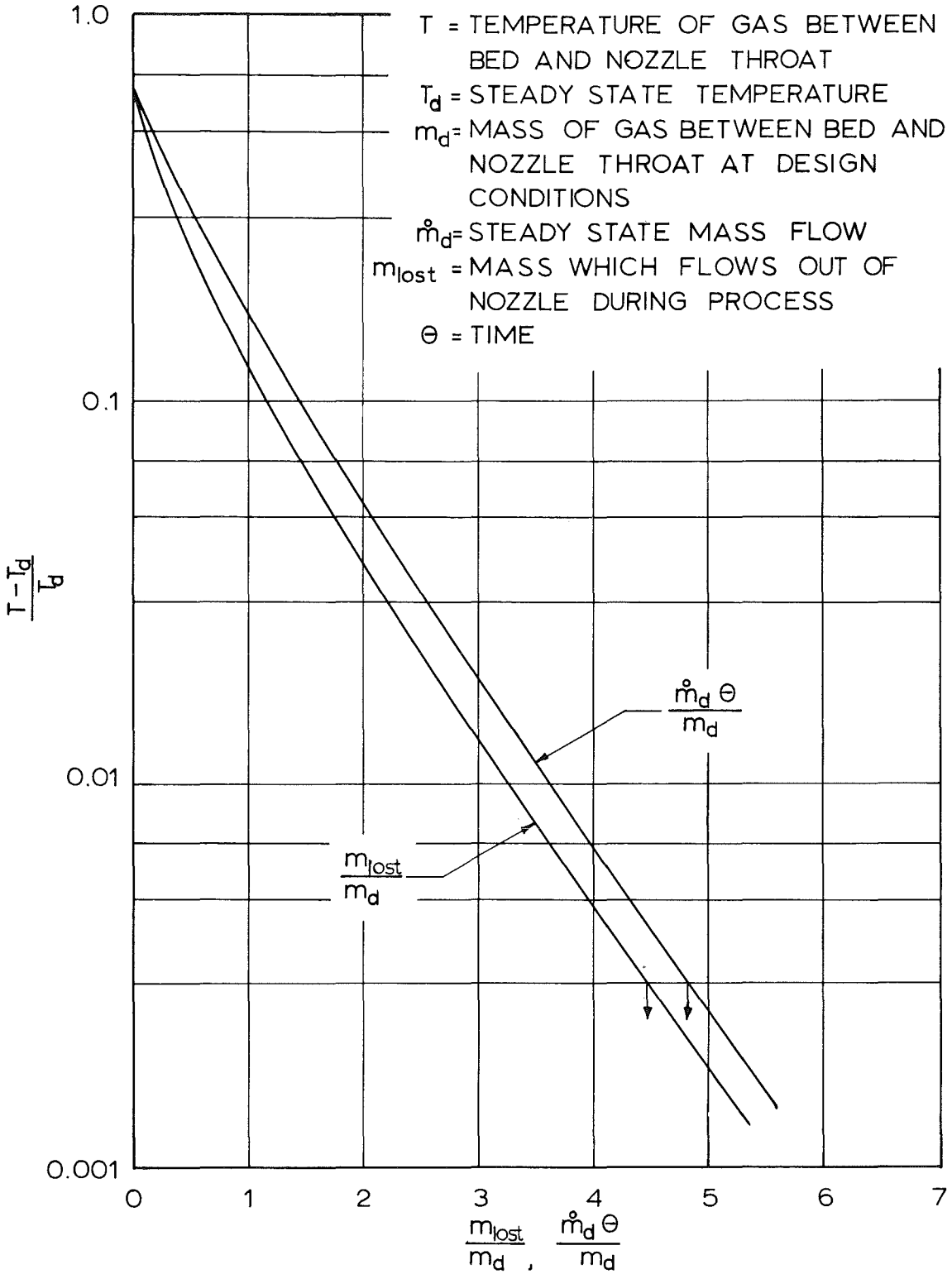

Fig. 4f Time and Mass Lost in Decay of Compression Temperature Rise

desired steady state pressure. In order to obtain a relatively flat temperature-time curve during the data taking phase of wind tunnel operation, it will be necessary to let this compression temperature rise decay to some acceptable level. Fig. 4F relates decay of this temperature excess under constant pressure conditions to time and mass expended.

General Discussion

Within the limitations of the assumptions implicit in their construction, Figs. 1F - 4F can be applied in optimizing heater design and/or heater operation procedures.

Pressurization rate, for instance, has conflicting effects on various phases of the starting process. In order to reach the desired steady state pressure with as little wasted mass as is possible, requires rapid pressurization. Conversely, this rapid pressurization results in more compression temperature buildup, requiring longer times to decay this excess after steady state pressure is reached. Also, too rapid pressurization may result in excessive thermal shock to the bed material.

Hot Valve

A hot valve appears to be an attractive concept, for no mass is expended through the nozzle in reaching steady state pressure. However, during the pressurization process the gas temperature between the bed and nozzle throat rises to perhaps 25% above its steady state value. It is this closed hot valve situation which results in the maximum compression temperature rise. In order to decay the excess temperature to an acceptable level, enough mass may be expended through the nozzle to largely offset the advantage of reduced mass loss during the pressurization process. These factors would have to be studied quantitatively to assess the value of a hot valve. The analyses presented here do permit such an evaluation to a first approximation. These analyses can be carried further to consider in greater detail the real situation. The actual heat transfer and flow absorption characteristics of dome insulation, for example, could be analysed and a better mathematical model generated. However, the analyses presented here should permit satisfactory initial evaluation of the various start-stop effects for heater design purposes.

APPENDIX G

HEATER BED THERMAL PERFORMANCE

The preliminary analysis of the heat storage bed was based on Hausen's solution (see Section 1 and Appendix B). This solution assumes infinite thermal conductivity normal to the flow, zero conductivity parallel to the flow, and an initially uniform temperature distribution or a distribution which matches one of the ξ , η family of curves.

The present analysis was undertaken to determine the influence of finite thermal conductivity in the storage matrix and to provide a method applicable to an arbitrary initial temperature distribution.

Two cases are considered.

1. a. infinite conductivity normal to flow
   b. zero conductivity parallel to flow
   c. arbitrary initial temperature distribution
2. a. finite conductivity normal to flow
   b. zero conductivity parallel to flow
   c. arbitrary initial temperature distribution

Both cases assume that flow and heat transfer in all holes are identical. This means that case 2 considers a finite conductivity normal to flow only as it affects temperature variations in the webs between holes. It does not provide for any effects of temperature level variation from hole to hole; (i.e., the center of the bed has the same temperature as the edge of the bed at a given cross section).

Case 1

The time rate of change of local solid temperature is

$$\frac{\partial T}{\partial \theta} = \frac{h P}{MC} (T_g - T) \qquad (1')$$

Writing a heat balance in the flow channel, the instantaneous longitudinal rate of change of fluid temperature is

$$\frac{\partial T}{\partial z} = \frac{h P}{\dot{m} c_p} (T - T_g) - \frac{1}{u} \frac{\partial T_g}{\partial \theta}$$

If we assume $\partial T_g / \partial \theta = \partial T / \partial \theta$, this equation reduces to

$$\frac{\partial T_g}{\partial z} = \frac{hP}{\dot{m} c_p}\left(1+\frac{\dot{m} c_p}{MCu}\right)(T-T_g)$$

Now, the ratio $\frac{\dot{m} c_p}{MCu}$ can be written as

$$\frac{\dot{m} c_p}{MCu} = \frac{\rho_g c_p \sigma}{\rho C(1-\sigma)} \approx \frac{\rho_g}{\rho}$$

which is seen to be of the order 10^{-2} for the present analysis; therefore we will neglect it and write

$$\frac{\partial T_g}{\partial z} = \frac{hP}{\dot{m} c_p}(T-T_g) \qquad (2')$$

Converting equations (1') and (2') into difference equations we obtain

$$\Delta_\theta T = \frac{hP}{MC}\overline{(T_g-T)}_{\Delta\theta}\Delta\theta \qquad (1)$$

and

$$\Delta_z T_g = \frac{hP}{\dot{m} c_p}\overline{(T-T_g)}_{\Delta z}\Delta z \qquad (2)$$

where the $\overline{(T_g - T)}_{\Delta\theta}$ difference is the mean value over the time interval $\Delta\theta$ and the $\overline{(T - T_g)}_{\Delta z}$ difference is the mean value over the length interval Δz.

Now, introduce subscripts on temperatures

$T_{\substack{o \\ m \\ p}}$ = solid temperature

and $T_{\substack{g \\ m \\ p}}$ = fluid (gas) temperature

where m refers to the time interval such that $\theta = m\Delta\theta$, and p refers to the length interval such that $z = p\Delta z$. Also define

$$E \equiv \frac{hP}{2MC}\Delta\theta$$

and

$$F \equiv \frac{hP}{2\dot{m}c_p}\Delta z$$

The mean temperature differences in equations 1 and 2 are

$$\overline{(T_g - T)}_{\Delta\theta} = \frac{1}{2}\left[\left(T^{g}_{m_p} + T^{g}_{m_{p-1}}\right) - \left(T^{o}_{m_p} + T^{o}_{m_{p-1}}\right)\right]$$

and

$$\overline{(T - T_g)}_{\Delta z} = \frac{1}{2}\left[\left(T^{o}_{m_p} + T^{o}_{m_{p-1}}\right) - \left(T^{g}_{m_p} + T^{g}_{m_{p-1}}\right)\right]$$

The temperature changes are

$$\Delta_\theta T = T^{o}_{m_p} - T^{o}_{m_{p-1}}$$

and

$$\Delta_z T_g = T^{g}_{m_p} - T^{g}_{m_{p-1}}$$

Now we can rewrite equations 1 and 2

$$T^{o}_{m_p} - T^{o}_{m_{p-1}} = E\left(T^{g}_{m_p} + T^{g}_{m_{p-1}} - T^{o}_{m_p} - T^{o}_{m_{p-1}}\right)$$

and

$$T^{g}_{m_p} - T^{g}_{m_{p-1}} = F\left(T^{o}_{m_p} + T^{o}_{m_{p-1}} - T^{g}_{m_p} - T^{g}_{m_{p-1}}\right)$$

Solving each for $T_{o_{m_p}}$ and $T_{g_{m_p}}$ respectively, gives

$$T^{o}_{m_p} = \frac{E}{1+E}\left(T^{g}_{m_p} + T^{g}_{p_{m-1}}\right) + \frac{1-E}{1+E}\,T^{o}_{p_{m-1}} \tag{3}$$

and

$$T^{g}_{m_p} = \frac{F}{1+F}\left(T^{o}_{m_p} + T^{o}_{m_{p-1}}\right) + \frac{1-F}{1+F}\,T^{g}_{m_{p-1}} \tag{4}$$

To use these equations one must use a "marching" technique. That is, to find a temperature at time m and position p one must use the temperatures of the preceding interval.

Suppose the temperatures

$$T^{o}_{p_{m-1}},\ T^{o}_{m_{p-1}},\ T^{g}_{p_{m-1}},\ \text{and}\ T^{g}_{m_{p-1}}$$

are known. Then, the temperatures $T_{o_{m_p}}$ and $T_{g_{m_p}}$ are uniquely determined by equations 3 and 4. One finds however, that in addition to the known temperatures above, one needs the result of equation 4 to use 3 and vice versa. This difficulty was eliminated by solving equations 3 and 4 simultaneously for $T_{o_{m_p}}$. That is

$$T^{o}_{m_p} = \frac{(1-E)(1+F)}{1+E+F}\,T^{o}_{p_{m-1}} + \frac{E(1+F)}{1+E+F}\,T^{g}_{m_{p-1}}$$

$$+\frac{E(1-F)}{1+E+F}\,T^{g}_{m_{p-1}} + \frac{EF}{1+E+F}\,T^{o}_{m_{p-1}} \tag{5}$$

(5)

The temperature history for this problem can now be worked out by machine using the following procedure.

(1) Initial solid temperature (m = 0), given
(2) Entering fluid temperature (p = 0), given
(3) Initial fluid temperature (m = 0), Eq. 4
(4) Solid temperature at m = 1, p = 0, Eq. 3
(5) Solid temperature at m = 1, p = 1, Eq. 5
(6) Fluid temperatures at m = 1, p = 1, Eq. 4
(7) Continue (5) and (6) at m = 1, p = 2,3,4,5, etc.
(8) Repeat (4), (5), (6), and (7) at m = 2,3,4 etc.

Case 2

In the cored brick matrix the fluid channels are circular holes arranged in the equilateral triangular array.

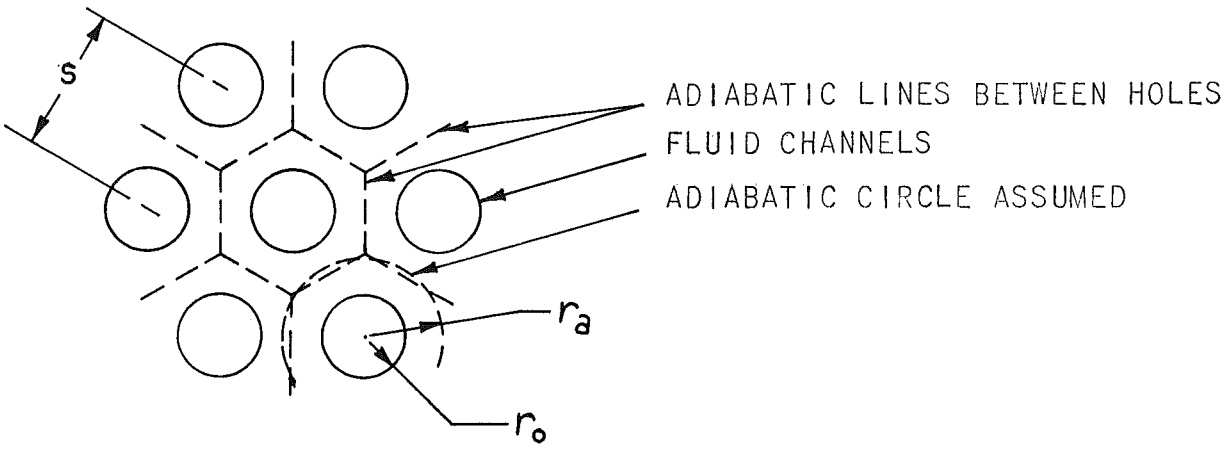

CORED BRICK CROSS SECTION

The heat storage matrix was assumed to consist of cylindrical walls of inside radius r_o and outside radius r_a. The outside radius was defined as the radius of a circle having an area equal to that of the adiabatic hexagon around each hole as illustrated in the sketch on the preceding page. The radius of this circle is such that

$$R_a = \frac{r_a}{r_o} = 1.05 \frac{s}{D} .$$

The differential equation for radial heat conduction in the cylinder is

$$\frac{\partial T}{\partial \theta} = \alpha\left(\frac{\partial^2 T}{\partial r^2} + \frac{1}{r}\frac{\partial T}{\partial r}\right) \qquad (6)$$

The heat transfer boundary condition in the hole is

$$\frac{\partial T}{\partial r} = \frac{h}{k}(T - T_g) \qquad \text{at} \quad r = r_o \qquad (7)$$

The adiabatic boundary condition at the outside surface is

$$\frac{\partial T}{\partial r} = 0 \qquad \text{at} \quad r = r_a$$

Certain substitutions make the equations dimensionless; they are:

$$R = \frac{r}{r_o} \quad \Rightarrow \quad R_a \frac{r_a}{r_o} \qquad \text{and} \qquad \Delta R = \frac{\Delta r}{r_o}$$

$$\tau = \frac{\alpha \theta}{r_o^2} \quad \Rightarrow \quad \Delta\tau = \frac{\alpha \Delta\theta}{r_o^2}$$

$$H = \frac{h r_o}{k}$$

$$a = \frac{\Delta R^2}{2\Delta\tau} , \quad (a \geq 1, \quad \text{and} \quad a \geq \frac{1 + H\Delta R}{2}$$

must be satisfied for stability). Introduce the following subscripts on temperatures, n, m, and p,
(i.e., $T_{\substack{n\\m\\p}}$ = solid temperature at radius $r = r_o + n\,\Delta r$

and $T_{\substack{g\\m\\p}}$ = fluid (gas) temperature)

where n refers to radius increment, m refers to time increment, and p refers to length increment.

The conversion of Eq. 6 into a difference equation was found in NASA TR R56, giving

$$T_{\substack{n\\m\\p}} = \left(1 - \frac{1}{a}\right) T_{\substack{n\\m-1\\p}} + \frac{1}{2a}\left\{1 - \frac{\Delta R}{2(1+n\Delta R)}\right\} T_{\substack{n-1\\m-1\\p}}$$

$$+ \frac{1}{2a}\left\{1 + \frac{\Delta R}{2(1+n\Delta R)}\right\} \tag{8}$$

Now, to make the computations economically feasible, a reasonable number of radius increments is required. This is because the total number of computations varies with the cube of the number of radius increments used (see definition and requirements of a above). The number of radius increments chosen for use with this program was five.

The radius ratios R_a, (or hole spacings $s/D = R_a/1.05$), contemplated are such that a considerable fraction of the heat will be stored in the outer and inner volume elements. For this reason it seemed unrealistic to set up difference equations which would take into account only the temperature gradients at $r = r_o$, and would be independent of the heat capacity of the material in these elements.

Equation 8 is essentially a balance of the heat flowing through the interfaces midway between r and $r - \Delta r$, and r and $r + \Delta r$, the difference resulting in a change in temperature at r. This same type of heat balance can be done for the outside element. Assume the temperature gradient at the interface midway between $r = r_a$ and $r_a - \Delta r$ is $(T_{\substack{n_a\\m\\p}} - T_{\substack{n_a-1\\m\\p}})/\Delta r$.

The thickness of the element between this interface and the outside is $\Delta r/2$. We can now write

$$\left(T_{\substack{n_a \\ m \\ p}} - T_{\substack{n_a \\ m-1 \\ p}}\right) \frac{\Delta r}{2} C\rho = -\frac{K\Delta\theta}{\Delta r}\left(T_{\substack{n_a \\ m-1 \\ p}} - T_{\substack{n_a-1 \\ m-1 \\ p}}\right)$$

This can be converted to

$$T_{\substack{n_a \\ m_a \\ p}} = \left(1 - \frac{1}{a}\right) T_{\substack{n_a \\ m-1 \\ p}} + \frac{1}{a} T_{\substack{n_a-1 \\ m_a-1 \\ p}} \qquad (9)$$

Consider finally, the heat flowing into the cylindrical element of volume bounded by the inside surface of a hole, $r = r_0$, and the surface $r = r_0 + \Delta r/2$. Assume that the rate of heat flow per unit length into this volume element is

$$\frac{\Delta Q}{\Delta z} = 2\frac{\pi(T_i - T_0)K}{\ln \frac{r_0+\Delta r}{r_0}} + 2\pi r_0 h(T_g - T_0)$$

and the average over the interval $\Delta\theta$ is

$$\frac{\Delta Q}{\Delta z} = \pi\frac{\left(T_m + T_{m-1} - T_{0m} - T_{0_{m-1}}\right)K}{\ln \frac{r_0+\Delta r}{r_0}} + \pi h r_0\left(T_{g_m} + T_{g_{m-1}} - T_{0_m} - T_{0_{m-1}}\right)$$

The rate of temperature rise of this element is related to heat input as

$$\frac{\Delta Q}{\Delta z} = \rho C\pi\left[\left(r_0 + \frac{\Delta r}{2}\right)^2 - r_0^2\right]\frac{\Delta T_0}{\Delta\theta}$$

Equating the righthand sides and substituting

$$H = \frac{hr_0}{K}, \quad \Delta R = \frac{\Delta r}{r_0}, \quad \Delta\tau = \frac{\alpha\Delta\theta}{r_0^2},$$

$$A = a\left(\frac{2}{\Delta R} + \frac{1}{2}\right), \quad \text{AND} \quad B = \frac{1}{\ln(1+\Delta R)}$$

and introducing p subscripts and solving for $T_{o_{m_p}}$, we obtain

$$T_{o_{m_p}} = \frac{B}{A+B+H}\left(T_{1_{m_p}} + T_{1_{m-1_p}}\right) + \frac{H}{A+B+H}\left(T_{g_{m_p}} - T_{g_{m-1_p}}\right)$$

$$+ \frac{A-B-H}{A+B+H} T_{o_{m-1_p}} \qquad (10)$$

Solving this equation simultaneously with equation 4 for $T_{g_{m_p}}$ gives

$$T_{g_{m_p}} = \frac{F(A+B+H)}{\{(A+B)(1+F)+H\}} T_{o_{m_{p-1}}} + \frac{(1-F)(A+B+H)}{\{(A+B)(1+F)+H\}} T_{g_{m_{p-1}}}$$

$$+ \frac{FB}{\{(A+B)(1+F)+H\}}\left(T_{1_{m_p}} + T_{1_{m-1_p}}\right) + \frac{FH}{\{(A+B)(1+F)+H\}} T_{g_{m-1_p}}$$

$$+ \frac{F(A-B-H)}{\{(A+B)(1+F)+H\}} T_{o_{m-1_p}} \qquad (11)$$

Temperatures for this problem can be computed by a machine using the following procedure.

(1) Initial solid temperature (m = 0)
given
(2) Entering fluid temperature (p = 0)
given
(3) Outside solid temperature for m = 1, n = n_a,
all p, Eq. 9
(4) Intermediate solid temperature for m = 1,
$1 \leq n \leq n_a - 1$,
all p, Eq. 8
(5) Inside surface temperature for m = 1, n = 0,
for p = 0,
Eq. 10
(6) Fluid temperature for m = 1, p = 1,
Eq. 11

(7) Inside surface temperature for m = 1, n = 0, p = 1, Eq. 10

(8) Repeat (6) and (7) for m = 1, p = 2,3, etc.

(9) Repeat (3) through (8) for m = 2,3,4, etc.

When a high conductivity material is to be used in the upstream portion of the bed it is possible to make computations assuming the combination case 1 and case 2 problem. The procedure follows.

(1) Initial solid temperature (m = 0, all $p \geq 0$), given

(2) Entering fluid temperature (p = 0, all $m \geq 0$), given

(3) Initial fluid temperature for all m = 0, all $p > 0$, Eq. 4

(4) Solid temperature for m = 1, p = 0, Eq. 3

(5) Solid temperature for m = 1, p = 1, Eq. 5

(6) Fluid temperature for m = 1, p = 1, Eq. 4

(7) Repeat (5) and (6) for m = 1, p = 2,3,$\cdots\cdots$ $p_{L1} - 1$,

(8) Intermediate solid temperature for m = 1, n = 1, $p = p_{L1}$ Eq. 8

(9) Fluid temperature for m = 1, $p = p_{L1}$, Eq. 11

(10) Inside surface temperature for m = 1, $p = p_{L1}$ Eq. 10

(11) Repeat (8), (9), (10), for m = 1 and all $p > p_{L1}$

(12) Intermediate solid temperature for m = 1, n = 2, all $p \geq p_{L1}$ Eq. 8

(13) Repeat (12) for n = 3,4,....n_a-1

(14) Outside solid temperature for m = 1, $n = n_a$, all $p \geq p_{L1}$, Eq. 9

(15) Repeat (4) through (14) for m = 2,3,4.... lim m.

These procedures were programmed for calculation by a digital computer. The results reported in the text, (Section 8), were obtained in this way. The physical properties of the heat storage materials were evaluated at the arithmetic mean of maximum and minimum initial bed temperatures. The fluid properties were evaluated at the arithmetic mean of inlet and outlet air temperatures.

APPENDIX H

HEATER BED THERMAL STRESSES

The thermal stresses under consideration here are those due to temperature variation in the heat storage material in the direction normal to the heat transfer surfaces. During heat extraction, the heat transfer surfaces will be the coldest areas at any given station along the heater matrix. Therefore, these areas will be in tension, and fracture will result if ultimate strength is exceeded. While all cracks are potential sources of dust, those open to air flow are particularly bad.

The heat storage matrix has numerous parallel circular channels for the air flow, in an equilateral triangular arrangement. As was done in the analysis of thermal performance in Appendix G, this geometry has been approximated by a circular tube with purely radial temperature gradients. This model neglects the nonuniform wall thickness around the hole in a cored brick but compensates in part since it employs a mean wall thickness. Results with this model should be quite accurate for cored bricks with hole spacing ratios, s/D, greater than 1.2. Thermal stresses in the infinitely long cylindrical wall are given by the relations:

$$S_r = \frac{\alpha_{ex} E}{1-\nu} \frac{1}{r^2}\left[\frac{r^2-r_o^2}{2} T_m - \int_{r_o}^{r} Tr\, dr\right] \qquad (1)$$

radial,

$$S_t = \frac{\alpha_{ex} E}{1-\nu} \frac{1}{r^2}\left[\frac{r^2-r_o}{2} T_m + \int_{r_o}^{r} Tr\, dr - Tr^2\right] \qquad (2)$$

tangential, and

$$S_z = S_r + S_t \qquad (3)$$

longitudinal (Ref. 1). The mean temperature T_m is defined by

$$T_m = \frac{2}{r_a^2 - r_o^2} \int_{r_o}^{r_a} Tr\, dr$$

The maximum stress during heat extraction will be tension at the hole surface ($r = r_o$). Here the radial stress equation reduces to zero, and the tangential and longitudinal stresses become

$$S_t = S_z = \frac{\alpha_{ex} E}{1-\nu} (T_m - T_o) \tag{4}$$

Introducing the tensile strength of a material into equation (4) gives $(T_m - T_o)$ allowable as a material property. Elimination of thermal stress fracture therefore requires designing so that the allowable mean-to-hole surface temperature difference is not exceeded. To do this requires relating this temperature difference to the matrix element dimensions and the heater operating conditions. These relations are developed in the following discussion.

The conduction equation for purely radial heat flow in cylindrical coordinates is

$$\frac{\partial}{\partial R} \left(R \frac{\partial T}{\partial R} \right) = R \frac{\partial T}{\partial \tau} ,$$

in dimensionless form. (The dimensionless variables used here are defined in Appendix G). Except for a very short period at the beginning of a run $\partial T/\partial \tau$ is constant across the wall thickness. Setting $\partial T/\partial \tau = \dot{T}$ and holding it fixed we obtain a quasi-steady temperature distribution shape which is independent of τ . The boundary conditions are:

$$\frac{\partial T}{\partial R} = 0 \quad \text{at } R = R_a,$$

and

$$T = T_o \quad \text{at } R = 1.$$

The solution is

$$T = T_o + \frac{1}{2} \dot{T} \left\{ \frac{R^2 - 1}{2} - R_a^2 \ln R \right\} \tag{5}$$

Now, the mean-to-hole surface temperature difference becomes

$$T_m - T_o = \frac{2}{R_a^2 - 1} \int_1^{R_a} T R \, dR - T_o$$

$$T_m - T_o = -\frac{1}{2} \dot{T} R_{a1} \tag{6}$$

where:

$$R_{a1} = \frac{R_a^4 \left(\ln R_a - \frac{3}{4}\right) + R_a^2 - \frac{1}{4}}{R_a^2 - 1}$$

Equating the cooling of the solid to the convective heat transfer per unit length we obtain:

$$-\pi (r_a^2 - r_o^2) \rho C \frac{\partial T}{\partial \theta} = 2\pi r_o h (T_o - T_g)$$

and substituting the dimensionless variables and solving for $\dot{T}$, there results

$$\dot{T} = -2 \frac{H}{R_a^2 - 1} (T_o - T_g) \tag{7}$$

Substituting this into the righthand side of equation 6 yields a convenient relationship for mean-to-hole surface temperature difference;

$$T_m - T_o = H (T_o - T_g) R_{a2} \tag{8}$$

where $R_{a2} = \frac{R_a^4 \left(\ln R_a - \frac{3}{4}\right) + R_a^2 - \frac{1}{4}}{(R_a^2 - 1)^2}$

Similarly, equating the cooling of the solid to the heating of the fluid per unit length we obtain:

$$-\pi (r_a^2 - r_o^2) \rho C \frac{\partial T}{\partial \theta} = \dot{m}_{hole} C_p \frac{\partial T_g}{\partial z}$$

and substituting the dimensionless variables and solving for $\dot{T}$, there results

$$\dot{T} = -\frac{1}{2} \frac{k_a}{k} \frac{Re\, Pr}{(R_a^2 - 1)} \frac{\partial T_g}{\partial Z} \tag{9}$$

Substituting this into the righthand side of equation 6 yields a second convenient relationship for mean-to-hole surface temperature difference.

$$T_m - T_o = \frac{1}{4} \frac{k_g}{k} Re\, Pr \frac{\partial T_g}{\partial Z} R_{a2} \tag{10}$$

This relationship with dimensional notation is

$$T_m - T_o = \frac{D^2}{8} \frac{c_p}{k} \left(\frac{\dot{m}}{A_f}\right) \frac{\partial T_g}{\partial z} R_{a3} \tag{11}$$

where

$$R_{a3} = R_a^2 \left\{ \frac{R_a^4 (\ln R_a - 3/4) + R_a^2 - 1/4}{(R_a^2 - 1)^2} \right\}$$

The functions R_{a1}, R_{a2}, and R_{a3} are plotted versus R_a in Fig. 1-H.

Having these relationships, it is possible to set up allowable initial bed temperature distributions. We shall assume that $\partial T_g / \partial z = \partial T / \partial z$. If the shape of the matrix longitudinal temperature distribution is linear there is a value of entrance temperature which makes this assumption valid for the complete matrix ramp section of the heater. At other matrix entrance temperatures this assumption, while not valid near the entrance, will improve as one moves away from the entrance.

The assumption that $\dot{T}$ does not vary with R is quite valid. At the matrix entrance, variation of $\dot{T}$ is negligible during most of a run. Higher in the matrix, it is constant with both time and radius for a linear ramp. In each case the assumptions lead to predicted $T_m - T_o$ values which are conservatively high.

An optimum longitudinal initial bed temperature distribution for a given matrix material and geometry which will be allowable from the thermal stress standpoint is therefore one having the maximum allowable $T_m - T_o$. This is one having a solid to fluid temperature difference at the bottom in accordance with equation 8 and a straight ramp with an allowable slope as per equation 11.

A typical radial temperature distribution calculated

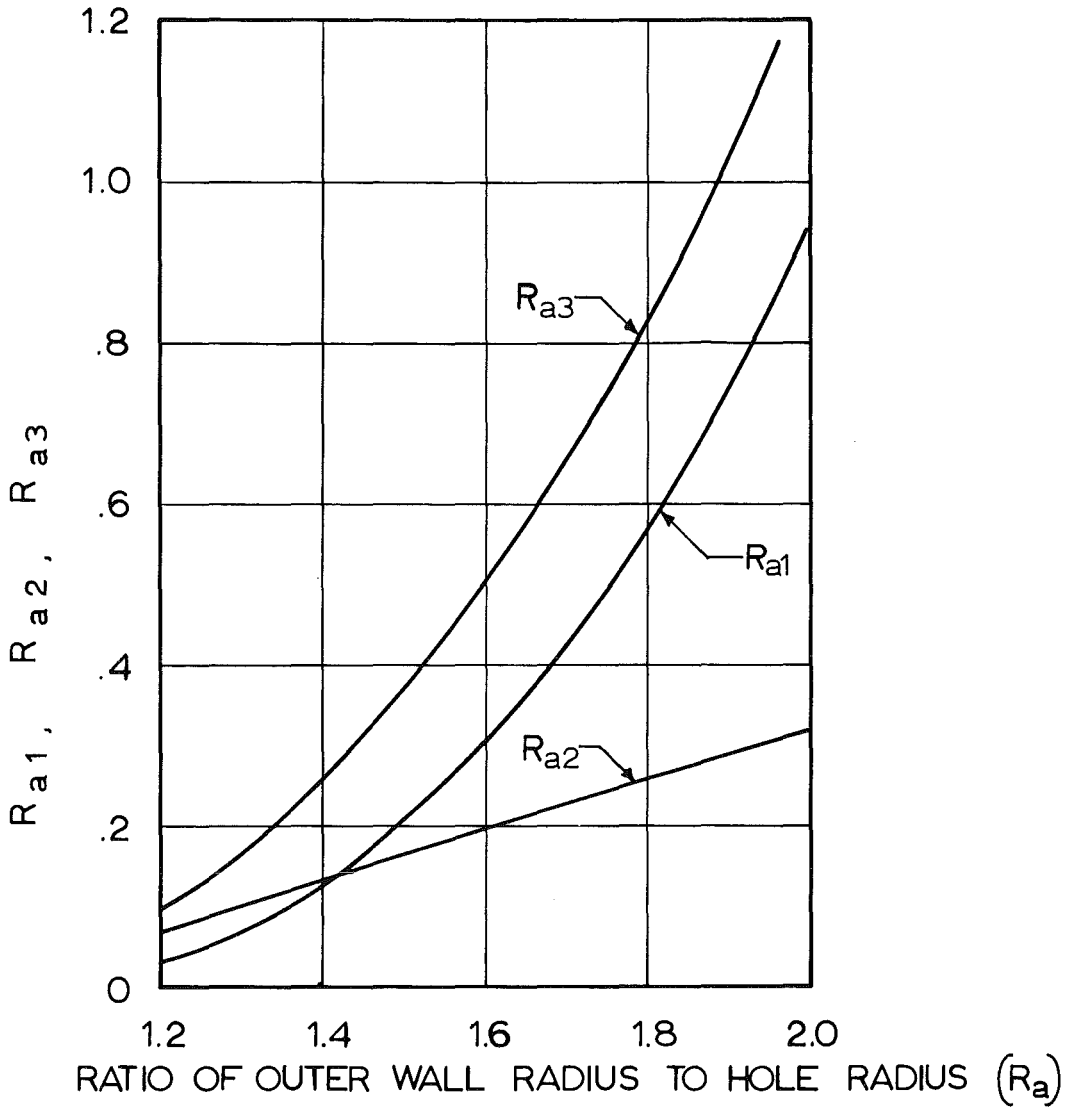

Fig. 1h Hole Geometry Functions for Quasi Steady Temperature Distributions in Cylindrical Wall

from equation 5 is shown on Fig. 2H. Thermal stresses calculated from equation 1, 2, and 3 using this temperature distribution are given on Fig. 3H.

REFERENCES

1. B. A. Boley and J. H. Weiner, "Theory of Thermal Stresses" John Wiley and Sons Inc., New York, London, 1960, pp 290-291.

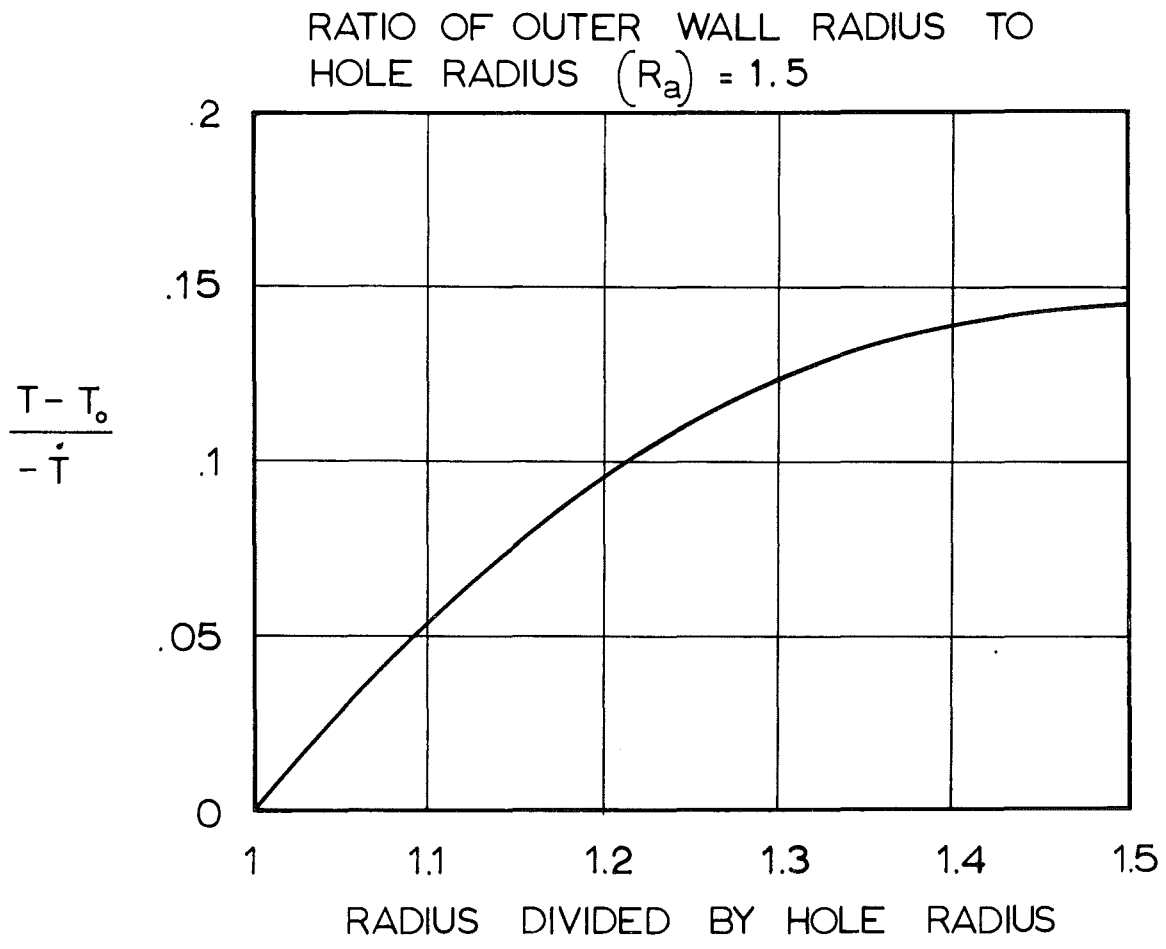

Fig. 2h Quasi Steady Temperature Distribution in Cylindrical Wall

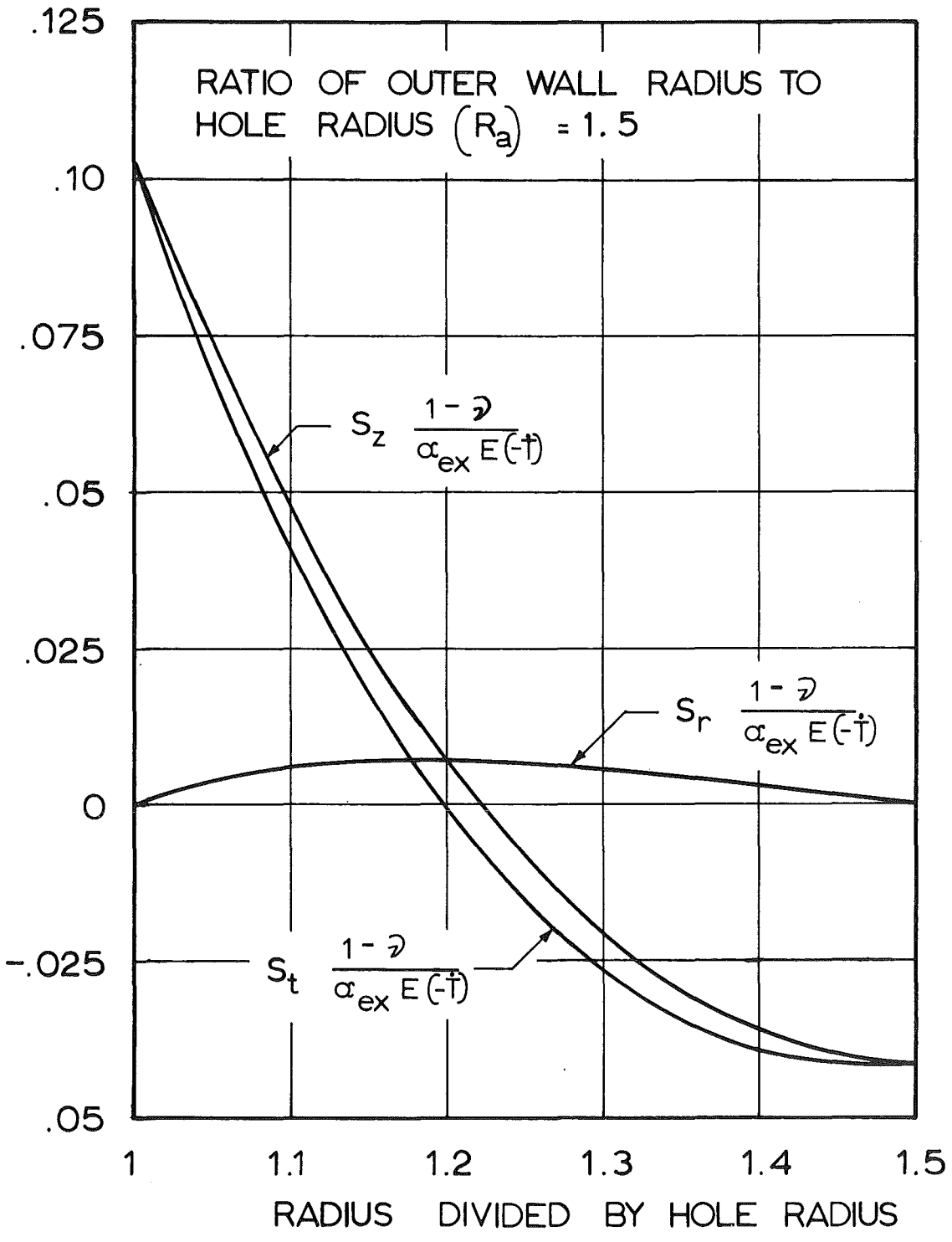

Fig. 3h Thermal Stresses in Long Cylindrical Wall with Constant Cooling Rate